Organotypic Human Skin Disease Models for the Assessment of Novel Therapeutic Approaches

Benjamin Fell

Supervisor: Prof David Kelsell

Co-Supervisor: Prof Edel O'Toole

A thesis submitted for the degree of PhD

Centre for Cutaneous and Cell Biology

The Blizard Institute

Barts and the London School of Medicine and Dentistry

Queen Mary University London

Statement of Originality

I, Benjamin Fell, confirm that the research included within this thesis is my own work or that where it has been carried out in collaboration with, or supported by others, that this is duly acknowledged below and my contribution indicated. Previously published material is also acknowledged below.

I attest that I have exercised reasonable care to ensure that the work is original, and does not to the best of my knowledge break any UK law, infringe any third party's copyright or other Intellectual Property Right, or contain any confidential material.

I accept that the College has the right to use plagiarism detection software to check the electronic version of the thesis.

I confirm that this thesis has not been previously submitted for the award of a degree by this or any other university.

28th August 2016

Abstract

Comprehensive *in vitro* modelling of inflammatory human skin conditions is an essential first step in the development and assessment of potential therapeutic approaches. Mouse models or monolayer keratinocyte cultures come with distinct limitations which might be complimented or overcome by the use of human-specific organotypic 3D culture models.

Over the course of this thesis, an organotypic culture system, based on patient-derived immortalised keratinocyte cell lines on a dermal equivalent collagen 1 gel, was established and used to recapitulate phenotypical features for two hereditary skin diseases, Harlequin ichthyosis and Tylosis with oesophageal cancer. Small molecular compounds, supplied via the medium, or RNA interference were used to modulate disease-specific changes in histology and marker expression of the skin equivalent.

Since hyperproliferative skin conditions can be associated with an aberrant wound healing phenotype, the organotypic system was manipulated to obtain a basic *in vitro* wound healing model. This model displays typical features of re-epithelialisation over time (both normal and disease-specific) which can further be manipulated via shRNA-mediated knockdown or the exogenous supply of compounds.

In parallel, a non-disease model was used to assess the topical application of novel nanopolymeric drug delivery systems in regard to their ability to penetrate across the permeability barrier. Penetrance profiles for the organotypic model (in dependence of co-application with chemical enhancers) showed a similar pattern as for topical applications performed in parallel on explant skin.

In conclusion, a highly adaptable human organotypic keratinocyte culture model was developed and used to recapitulate (and manipulate) skin disease phenotypes and epidermal wound healing *in vitro*, as well as perform first essential assessments of novel drug delivery systems.

Publications, Presentations and Awards arising from this Work

Publications

Maruthappu T, Chikh A, Fell B, Delaney PJ, Brooke M, Levet C, Moncada-Pazos A, Ishida-Yamamoto A, Blaydon D, Waseem A, Leigh IM, Freeman M, Kelsell DP. (2016) *iRHOM2 Regulates Keratin 16, a Major Cytoskeletal Stress Keratin.*
Nature Communications. (under Revision)

Poster Presentations

In vitro Model for Tylosis: Dysregulation of ADAM17 in the Epidermis
Fell B, Brooke M, Etheridge S, Getsios S, Kelsell DP
Annual ESDR Meeting 2014 (10^{th} – 13^{th} September 2014, Copenhagen)

In vitro Organotypic Wound Healing Model: the role of iRHOM2 in Tylosis
Fell B, Maruthappu T, Chikh A, Kelsell DP
Annual ESDR Meeting 2015 (9^{th} – 12^{th} September 2015, Rotterdam)

Awards

Best Poster Prize at the Annual ESDR Meeting 2015 for the poster
"In vitro Organotypic Wound Healing Model: the role of iRHOM2 in Tylosis"

Acknowledgments

I would like to thank and acknowledge my supervisor Prof David Kelsell for the opportunity to undertake this exciting project as part of his research group and the constant help and supervision. This also applies equally to my secondary supervisor Prof Edel O'Toole, who was always present and of utmost help when needed.

I thank the European Commission for funding my PhD project as part of the Marie-Curie ITN (FP7) *NANODRUG*.

Many thanks to all members of Cutaneous in the Blizard but especially to the Kelsell Group and Dr Rosalind Hannen. Further thanks to the members of Resmini Group (SBCS, QMUL) for their help regarding everything nanochemical.

Even more thanks (and eternal gratefulness) to my family and friends, without whom none of this would have been possible!

Oh, and Emy of course...

Table of Content

List of Figures and Tables

Abbreviations

BA	benzylic alcohol	ICC	immunocytochemistry
CK1	cytokeratin 1	IHC	immunohistochemistry
CK10	cytokeratin 10	Li's ICQ	Li's intensity correlation quotient
CK14	cytokeratin 14	LY	lucifer yellow
CK16	cytokeratin 16	NGS	normal goat serum
CK5	cytokeratin 5	PBS	phosphate buffered saline
Cx26	connexin 26	PC	Pachyonychia congenita
DED	de-epidermalised dermis	PDM	product of the differences from the mean
DMSO	dimethylsulphoxide	PET	polyethylene terephthalate
EGF	epidermal growth factor	PFA	paraformaldehyde
EGFR	epidermal growth factor receptor	PolyNIPAm	poly(N-isopropyl acrylamide)
FFA	flufenamic acid	PsCo	Pearson coefficient
H&E	haematoxylin & eosin	RT	room temperature
HI	Harlequin ichthyosis	shRNA	small-hairpin RNA
HPV	human papilloma virus	TGM1	transglutaminase 1
HRP	horseradish peroxidase	TOC	Tylosis with oesophageal cancer
hTERT	human telomerase reverse transcriptase		

1. Introduction

1.1. Structure and Function of the Human Skin

The skin is not just the largest organ in the human body but also its protection against external assaults of different biological, chemical and physical varieties as well as water loss from the inside (Figure 1) (Proksch et al. 2008). In order to sustain this function, it is comprised of an outer epidermal layer, a stratified assembly of keratinocytes in varying stages of differentiation, which is in turn structurally supported and supplied with nutrients by the underlying dermis, a mechanically strong and flexible matrix arrangement containing further neural, vascular, glandular as well as immune system components. Underneath epidermis and dermis, a subcutaneous connective and adipose tissue layer serves as additional thermal and mechanical insulation as well as attachment to the muscular tissue (Figure 2) (Jakubovic and Ackerman 1992; Montagna 2012).

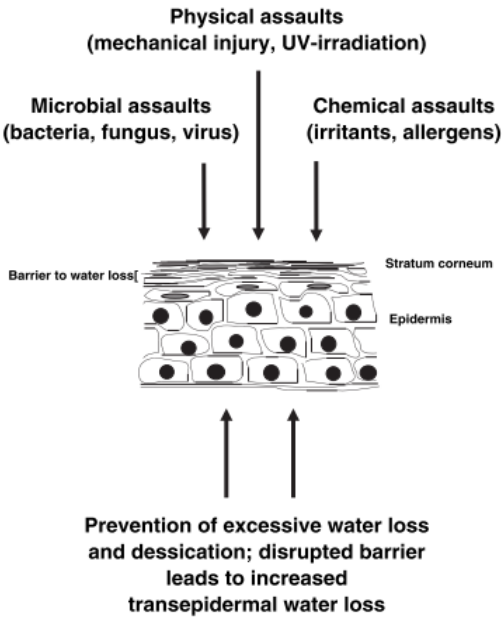

Figure 1: Human skin barrier function
The human skin in general and the epidermis in specific serve as barrier against diverse environmental assaults as well as protection against excessive trans-epidermal water loss and subsequently dehydration of the body. (Proksch et al. 2008)

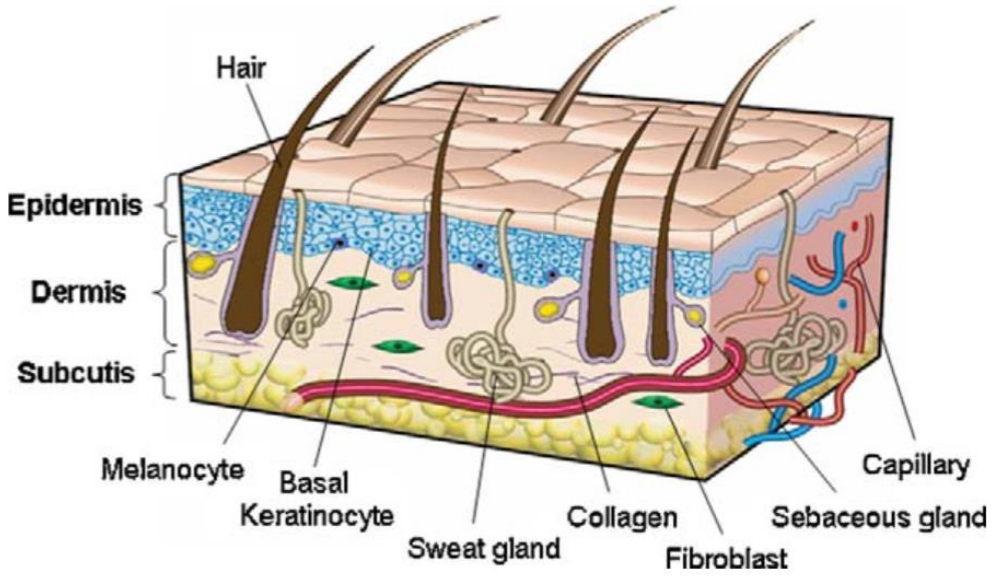

Figure 2: Structure of the human skin

Human skin is comprised of several distinct layers: epidermis, dermis and subcutis. The epidermis as the outermost layer is the major factor in the barrier function of the skin whereas the mostly collagen-based dermis lends structural support by being tightly connected to the epidermis via the basement membrane. In addition, it anchors a variety of glands, hair follicles and contains blood vessels for nutrient supply. The subcutaneous adipose tissue serves as insulation, padding and attachment to the underlying subdermal muscle tissue. (Bannasch et al. 2010)

1.1.1. Dermis

The dermis is a fibrous connective tissue component of the skin that lends tensile and elastic properties to the tissue while also retaining water and harbouring skin appendages (Jepps et al. 2013). Its two layers, the relatively thin papillary region and the underlying thick reticular region, are defined by different extracellular matrix compositions as well as cellular content and demarcated by the presence of a horizontal plane of capillaries, the subpapillary plexus. Intertwining with the epidermis through epidermal rete ridges and dermal papillae, the 100 – 200 µm thick papillary region is mostly comprised of a relatively loose network of thin collagen 1 fibres surrounded by glycosaminoglycans (mostly hyaluronan) and proteoglycans. It contains most of the dermal cells which are predominantly fibroblasts and cells of the innate immune system (macrophages, mast cells, dermal dendrocytes) in

addition to tactile and thermosensitive nerve endings. In contrast, the reticular dermis is comprised of a tightly interwoven network of large-diameter collagen, elastic and reticular fibres, which is mainly responsible for the mechanical strength of the skin. It is also in this part where the majority of blood vessels, hair follicles, sweat and sebaceous glands are found. (Freinkel and Woodley 2001; Montagna 2012)

1.1.2. Epidermis

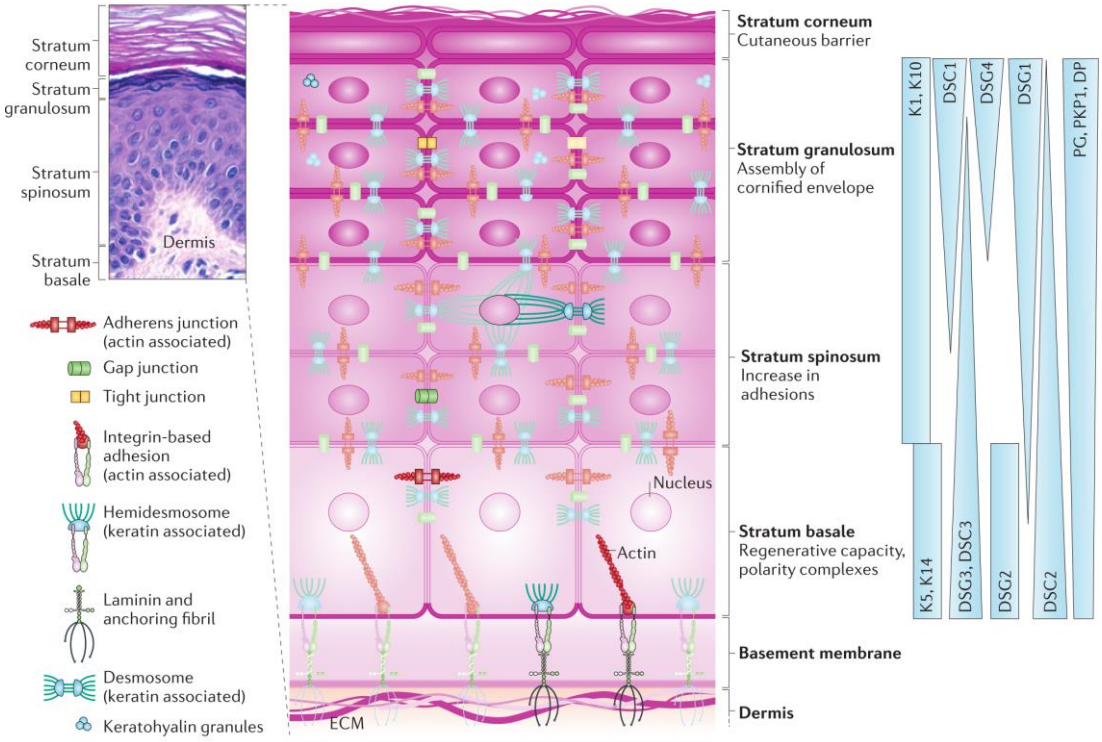

Figure 3: Stratification and functional layering of the epidermis

The epidermis is structured into several distinct layers (“strata”) of keratinocytes in progressing states of terminal differentiation, each layer being characterised by a defining set of functional features (morphology, intercellular contacts, protein and lipid synthesis). (Simpson et al. 2011)

Being structurally supported and supplied with nutrients by the underlying, vascularised dermis, the epidermis is comprised of a layered assembly of keratinocytes undergoing terminal differentiation while migrating in an outwards direction (Figure 3) (Fuchs 1990; Simpson et al. 2011). The lowermost layer is referred

to as the stratum basale. It is separated from the dermis by the collagen 4 and laminin-rich basal lamina on which it is tightly anchored by hemidesmosomes, comprised of integrins (Paulsson 1992; Margadant et al. 2010). Epidermal stem cells, thought to reside in the bulge region of hair follicles outer root sheaths as well as 'epidermal proliferative units' in the basal layer of the interfollicular epidermis, provide a continuous supply of keratinocytes for tissue homeostasis and regeneration in case of wounding (Cotsarelis 2006; Strachan and Ghadially 2008; Blanpain and Fuchs 2009). From this basal layer of mitotically active cells asymmetric cell division, driven by a perpendicular orientation of the spindle apparatus, gives rise to suprabasal keratinocytes (Lechler and Fuchs 2005; Fuchs 2008). These cells cease their mitotic activity and commit to a terminal differentiation program when entering the stratum spinosum, due to the aforementioned asymmetrical, perpendicular cell division or, in early stages of development, delamination. (Williams et al. 2014). In addition, the Notch-dependent downregulation of the transcription factor p63 is indicated to be an essential regulator in the switch from proliferation to differentiation (Nguyen et al. 2006; Senoo et al. 2007; Estrach et al. 2008). With the commitment to stratification and the concomitant onset of differentiation several distinct changes occur in the keratinocytes of the stratum spinosum. For one, the cytoskeletal composition changes, with the basal cytokeratins 5 (CK5) and 14 (CK14) being replaced by cytokeratin 1 (CK1) and 10 (CK10) (Eichner et al. 1986). Furthermore, desmosomes exhibit a change in individual subunits accompanied by an increase in size and number, facilitating stronger intercellular contacts and affecting cell morphology from a cubic to a more elongated shape (Mcmillan et al. 2003; Brandner et al. 2010).

A distinct feature of the next layer of the epidermis, the stratum granulosum, is the increased production of keratohyalin granules and lamellar bodies. Keratohyalin granules contain predominantly profillagrin and loricrin, two important structural components for the formation of the cornified envelope in subsequent layers (Watt 1983). Lamellar bodies serve as storage / transport compartment for a multitude of lipids and enzymes/proteases, the secretion of which in the upper stratum granulosum is of equal importance for the establishment of a functional barrier in the next layer, the stratum corneum (Feingold 2012). Contributing to the barrier

function of the skin in the upper epidermis, tight junctions are formed in the apical parts of the stratum granulosum (Kirschner et al. 2010).

The outermost layer of the epidermis, the stratum corneum, is comprised of by now terminally differentiated corneocytes. Undergoing apoptosis, they expel their intracellular contents, in addition to the exocytosis of keratohyalin and lamellar granules at the transition from stratum granulosum to corneum, and change into a tightly packed, flattened morphology. This change is facilitated through the collapse and aggregation of intermediated filaments (mostly CK1 and CK10), whereby this process is supposed to be promoted by the proteolytically cleaved filaggrin (Dale and Presland 1997). Further crosslinking of the filament bundles with additional structure proteins loricrin and involucrin as well as fully matured corneodesmosomes into a tightly knit submembraneous matrix by transglutaminase 1 (TGM1) gives mechanical support to the cornified envelope (Candi et al. 2005). Lipid lamellae are being formed by cholesterol, ceramides and free fatty acids, which surround the protein components of the cornified envelope, and are key to the epidermal permeability barrier function (Feingold and Elias 2014). The incorporation of antimicrobial peptides, such as beta-defensins and cathelicidins, provide a microbial barrier (Elias and Choi 2005). In the course of skin homeostasis dead corneocytes are then continuously shed of the skin through desquamation; a process that is facilitated by the degradation of corneodesmosomal components, namely desmoglein 1 and corneodesmosin, by serine proteases (Caubet et al. 2004).

In addition to keratinocytes, which make up 95% of epidermal cells, various other cell types can be found throughout the epidermis (Figure 4) (Burns et al. 2008). Melanocytes are specialised cells in the stratum basale, producing pigment-containing melanosome and transporting them via dendrites to the surrounding basal and suprabasal keratinocytes. Once there, the melanosomes localise around the nucleus and protect its DNA from UV radiation-induced mutagenesis (Agar and Young 2005; Nissan et al. 2011). Also located in the basal layer of the epidermis are the so-called Merkel cells. Associated with somatosensory afferent nerve fibres these receptor cells have recently been proved to be essential for light-touch sensation (Halata et al. 2003; Maricich et al. 2009). As epidermal part of the immune system, Langerhans cells on the other hand are predominantly found in the stratum

spinosum. Classified as professional antigen-presenting cells, these dendritic cells are a crucial component in the adaptive immune response to skin-resident pathogens (Langerhans 1868; Clausen and Kel 2010).

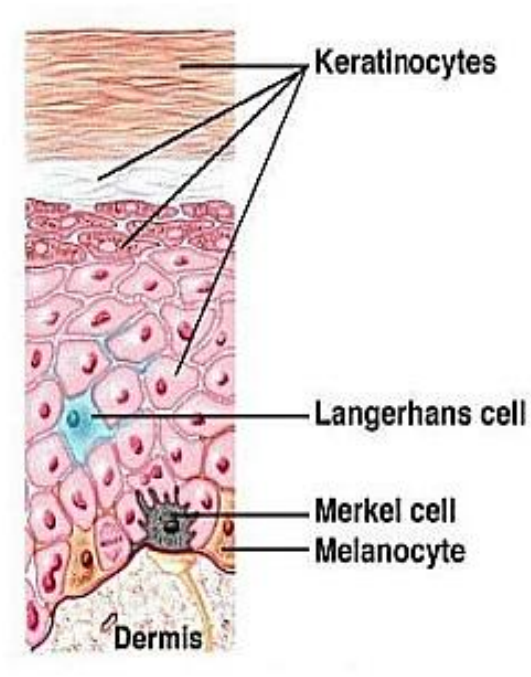

Figure 4: Non-keratinocyte cells of the epidermis
Apart from keratinocytes the epidermis is comprised of several other cell types. In the basal layer are melanocytes, that protect surrounding cells from phototoxicity, as well as somatosensory Merkel cells. Antigen-presenting Langerhans cells can be found suprabasally but predominantly in the stratum spinosum.

While the epidermis is dependent on dermal blood vessels for the diffusion-based supply of nutrients, it has been shown that epidermal oxygen supply happens almost exclusively through the uptake of external atmospheric oxygen, creating a reverse gradient to the basally supplied nutrients (Stücker et al. 2002). Another important gradient in the epidermis is based on the concentration of extracellular calcium ions (Menon et al. 1992). Calcium is an important regulator of keratinocyte differentiation and cell-cell adhesion (Elsholz et al. 2014); it is therefore no surprise that calcium concentrations can be found to increase in suprabasal layers, with the highest concentration in the stratum granulosum . Upwards of this layer, the relative dryness of the stratum corneum results in a distinct drop in extracellular calcium, which further regulates the exocytosis of lamellar and keratohyalin granules (Lee et al. 1992). In addition, calcium was found to be an important regulator of protein synthesis in the epidermis and essential for the activity of transglutaminases (Hitomi 2005).

1.2. Hereditary Skin Disorders

The World Health Organisation provides a comprehensive listing for diseases of the skin and subcutaneous tissue in Chapter 12 of the ICD-10. The classified types of disorders are hereby divided into eight different classes, dependent on localisation and cause of the individual disease (Table 1).

Table 1: Diseases of the skin and subcutaneous tissue according to ICD-10

	CLASS	**EXAMPLES**
L00 – L08	Infections of the skin and subcutaneous tissue	Cutaneous abscess (L02), Cellulitis (L03)
L10 – L14	Bullous disorders	Pemphigus (L10), Acquired epidermolysis bullosa (L12.3)
L20 – L30	Dermatitis and eczema	Atopic dermatitis (L20), Exfoliative dermatitis (L26)
L40 – L45	Papulosquamous disorders	Psoriasis vulgaris (L40.0), Lichen planus (L43)
L50 – L54	Urticaria and erythema	Allergic urticaria (L50.0), Bullous erythema mulitforme (L51.1)
L55 – L59	Radiation-related disorders of the skin and subcutaneous tissue	Sunburn (L55), Radiodermatitis (L58)
L60 – L75	Disorders of skin appendages	Hypertrichosis (L68), Acne vulgaris (L70.0)
L80 – L99	Other disorders of the skin and subcutaneous tissue	Acquired ichthyosis (L85.0), Keloid scarring (L91.0)

While Chapter 12 only lists acquired disorders, hereditary skin defects can be found in ICD-10 Chapter 17: Congenital malformations, deformations and chromosomal abnormalities (Q80-82: Other) (Table 2).

Table 2: Congenital malformations, deformations and chromosomal abnormalities according to ICD-10 (excerpt for the skin-specific sections Q80-82)

	CLASS	EXAMPLES
Q80	Congenital ichthyosis	Ichthyosis vulgaris (Q80.0), Harlequin ichthyosis (Q80.4)
Q81	Epidermolysis bullosa	Epidermolysis bullosa simplex (Q81.0)
Q82	Other congenital malformations	Xeroderma pigmentosum (Q82.1)

Since the functional homeostasis of the epidermis and especially stratification towards a viable permeability barrier is dependent on a tightly regulated network of protein expression across all stages of keratinocyte differentiation, disease phenotypes such as the ones listed in the ICD-10 can often be traced back to originate in loss- or gain-of-function mutations in single genes encoding essential epidermal proteins. Simpson et al. provided a comprehensive list of mutations and associated disorders, a selection of which is presented here (Table 3) (Simpson et al. 2011).

Congenital disorders (of the skin as well as other organs) have the distinct advantage of being very suitable for disease modelling. Animal models such as mouse or zebra fish can be modified via mutagenesis or more recently CRISPR/Cas9 methodology to recapitulate human monogenic disease phenotypes (Rossant and McKerlie 2001; Lieschke and Currie 2007; Platt et al. 2014). Further on, human cell-based *in vitro* models can be generated, even for more complex polygenic disorders, by using patient-derived and tissue-specific cell lines or reprogrammed induced pluripotent stem cells (Tiscornia et al. 2011; Soldner and Jaenisch 2012; Robin et al. 2015). These human cell models would then further allow for the genomic manipulation (e.g. functional repair) of disease-causing mutations (Cong et al. 2013; Schwank et al. 2013; Cai and Yang 2014).

Table 3: Mutations in epidermal proteins and associated diseases
(excerpt from a table originally published by Simpson et al. 2011)

PROTEIN	DISEASE	REFERENCE
Gap junctions		
Cx26	Keratitis ichthyosis deafness syndrome	(Richard et al. 2002)
Cx30	Hidrotic ectodermal dysplasia	(Lamartine et al. 2000)
Keratin filaments		
K16, K17	Pachyonychia congenita	(McLean et al. 1995)
K5, K14	Epidermolysis bullosa simplex	(Bonifas et al. 1991)
Desmosomes		
DSG3	Pemphigus vulgaris	(Amagai et al. 1991)
DP, DSG1	Striate palmoplantar keratoderma	(Norgett et al. 2000)
Hemidesmosomes		
Laminin 5	Junctional epidermolysis bullosa	(Pulkkinen et al. 1994)
Stratum corneum		
ABCA12	Harlequin ichthyosis	(Kelsell et al. 2005)
TGM1	Lamellar ichthyosis	(Russell et al. 1995)

1.2.1. Harlequin Ichthyosis

Harlequin Ichthyosis (HI; OMIM #242500; ICD-10 Q80.4) is a rare form of congenital ichthyosis, a family of genetic skin disorders being generally characterised by dry, scaly, thickened skin and varying widely in severity from mild types such as ichthyosis vulgaris to the far more severe Harlequin Ichthyosis, which can be fatal shortly after birth. It features a severely thickened skin with ‘armour-like’ scales being separated by deep fissures, which leaves the newly born with a high risk of dehydration,

impaired thermoregulation and infection (Figure 5). Preliminary data suggests that early-on treatment with oral retinoids greatly increases the chance of survival, with older children changing to a phenotype resembling severe nonbullous congenital ichthyosiform erythroderma (Rajpopat et al. 2011).

Figure 5: Clinical presentation of HI at birth
New-borns display a severely thickened and deeply fissured skin that results in a heightened risk of dehydration and infection and subsequently death, if left untreated. (Kelsell et al. 2005)

The molecular basis for HI is a recessive loss-of-function mutation in the ABCA12 gene (Akiyama 2005; Kelsell et al. 2005). ABCA12 encodes for a transmembranous lipid transporter found localised in lamellar granules of the stratum granulosum where it is proposed to be involved into the packaging of glycosylceramides into the lamellar bodies. Those glycosylceramides are then, together with other lipids and enzymes, transported to the apical plasma membrane of granular keratinocytes, released into the intercellular space and consequently contribute to the proper formation and processing of the cornified envelope in the stratum corneum (Ishida-Yamamoto et al. 2004). Due to the loss of transport function and impaired loading of lipids, lamellar bodies are found to be abnormally shaped, reduced in size and number in affected epidermis. The resulting lipid imbalance in the stratum corneum (Figure 6a) is thought to affect the tightly regulated differentiation program in the epidermis, leading to a premature terminal differentiation phenotype (Figure 6b) (Thomas et al. 2009). Furthermore, with proteases such as kallikrein 5 and cathepsin D not being properly transported to the stratum corneum (Figure 6b), formation of the permeability barrier and later desquamation of apical corneocytes

are severely impaired, leading to the distinct phenotype of HI (Figure 6c) (Ishida-Yamamoto and Kishibe 2011; Scott et al. 2013).

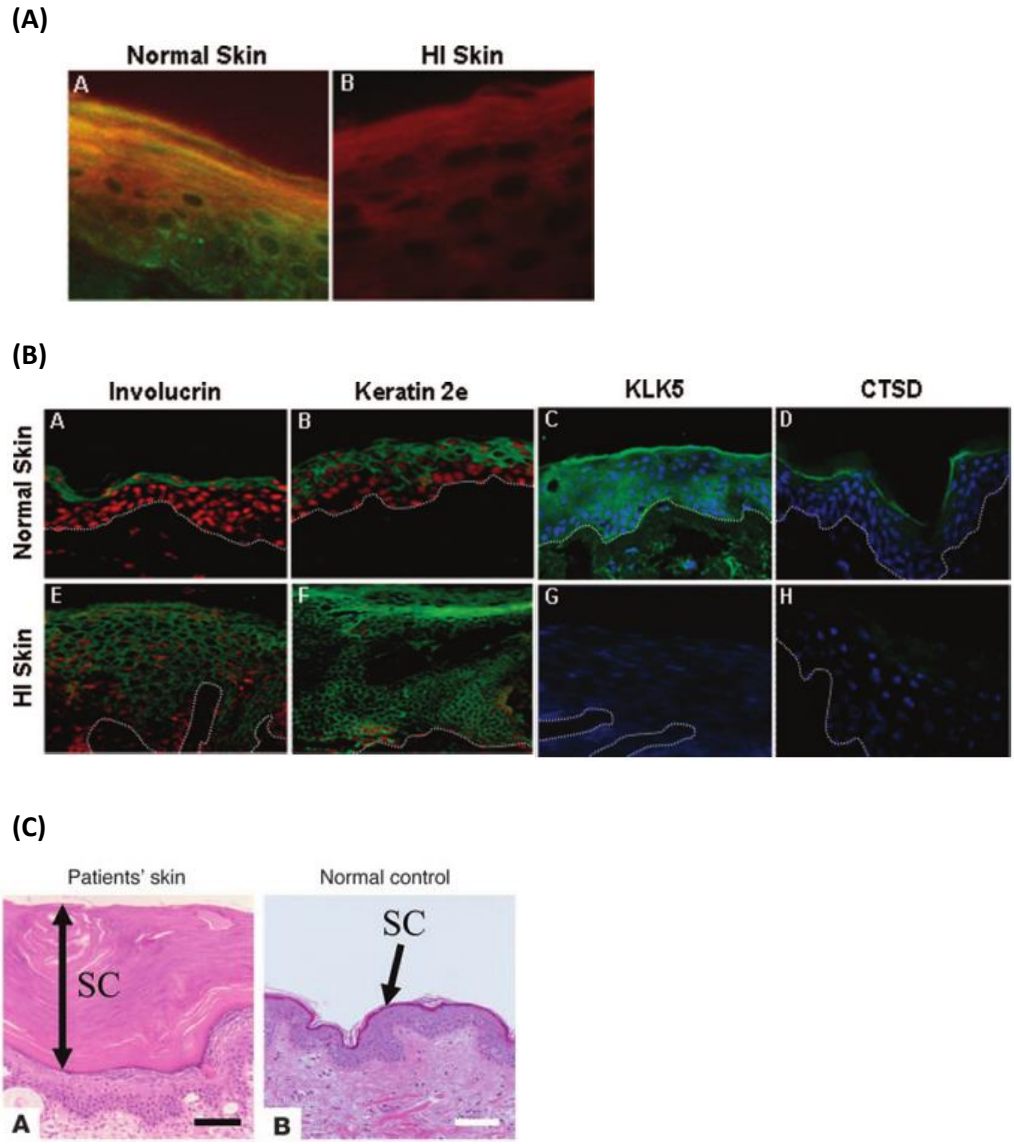

Figure 6: Phenotypical features of HI

Epidermis of HI patients displays a striking lipid imbalance, with in this case green-fluorescent non-polar lipids being completely absent from suprabasal layers. (Thomas et al. 2009) (A). Staining of protein markers in HI skin reveals an increased expression of differentiation markers (involucrin, cytokeratin 2e) in lower layers of the epidermis and complete absence of specific proteases such as kallikrein 5 and cathepsin D (Thomas et al. 2009) (B). As a result of dysregulated differentiation and impaired desquamation the stratum corneum is severely thickened in patients with HI (Akiyama 2005) (C).

1.2.2. Tylosis

Tylosis with oesophageal cancer (TOC; OMIM #148500, ICD-10 Q82.8) is a dominantly inherited syndrome of focal palmoplantar keratoderma. Affected individuals typically display thickened skin on palm and soles, oral leukokeratosis (Figure 7) and have a heightened susceptibility for oesophageal squamous cell carcinoma (up to 95% by the age of 65) (Ellis et al. 1994).

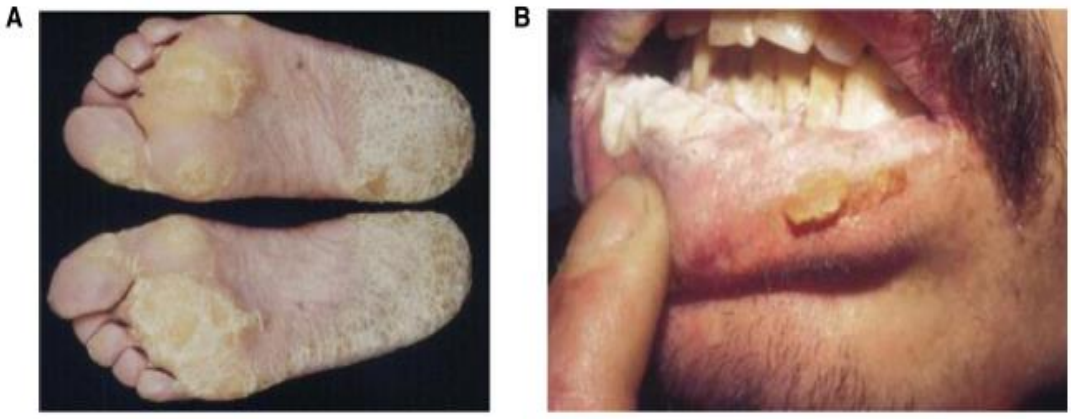

Figure 7: Clinical presentation of TOC
Patients with TOC typically display palmoplantar keratoderma (A) and oral leukokeratosis (B). (Blaydon et al. 2012)

The underlying cause for this syndrome was discovered to be an autosomal-dominant mutation in the RHBDF2 gene encoding iRHOM2 (Blaydon et al. 2012). iRHOM2 belongs to a family of inactive rhomboid serine proteases and is involved in the epidermal growth factor receptor (EGFR)-signalling pathway via one of its substrates, the sheddase ADAM17. Hereby, the gain-of-function mutation in iRhom2 leads to a heightened rate of maturation of ADAM17, accompanied by a translocation from the trans-Golgi to the plasma membrane, and consequently an increased shedding of epidermal growth factor receptor (EGFR) ligands and other cytokines (Figure 8) (Brooke et al. 2014). The resulting upregulation in EGF-mediated signalling is presumed to be the cause for the hyperproliferative keratoderma phenotype and the susceptibility for oesophageal cancer (Blaydon et al. 2012) and was furthermore indicated to lead to an increased permeability and microbial barrier function in the epidermis (Brooke et al. 2014). In addition, ADAM17 is describe to be

widely involved in processes associated with inflammation and tissue regeneration (Arribas and Esselens 2009; Scheller et al. 2011), for example via its substrates Interleukin 6 and 8 which have been shown to exhibit positive effects on epidermal wound healing (McKay and Leigh 1991; Gallucci et al. 2000; Rennekampff et al. 2000). Subsequently, TOC keratinocyte have recently been described to possess features of "constitutive wound healing" (Brooke et al. 2014; Ellis et al. 2015).

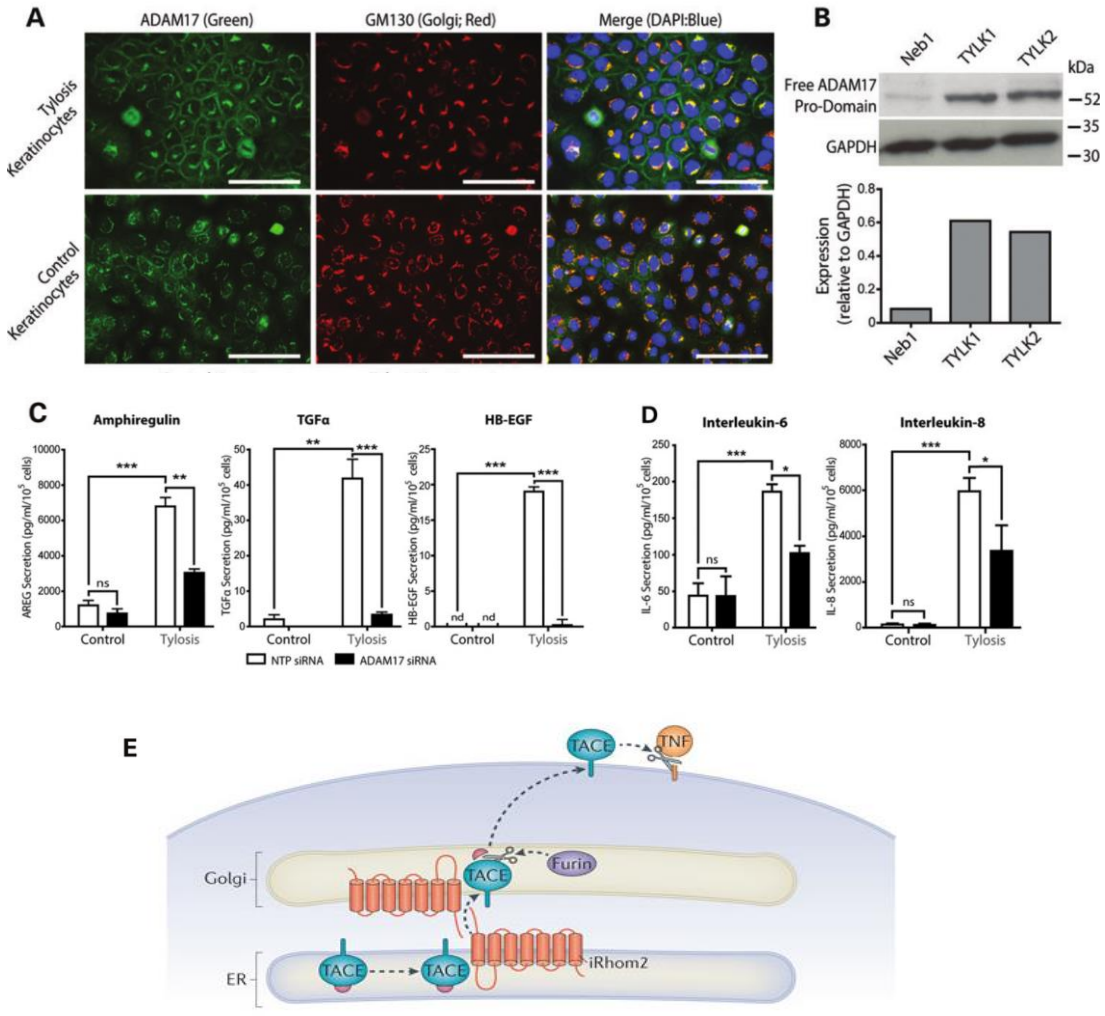

Figure 8: Phenotypical features of TOC keratinocytes

TOC keratinocytes display an increased plasma membrane localisation of the sheddase ADAM17 (TACE) (A) which is accompanied by an upregulated iRHOM2-driven maturation, visible by a stronger presence of the free pro-domain of the enzyme (B). As a result TOC keratinocytes secret a higher amount of EGF-family growth factors such as Amphiregulin, TGFα and HB-EGF (C) as well as certain cytokines, e.g. Interleukin 6 and Interleukin 8 (D). The underlying steps of ADAM17 maturation and activity are tied to several subcellular compartments (E). (modified from Adrain and Freeman 2012; Brooke et al. 2014)

1.2.3. Pachyonychia Congenita

Pachyonychia congenita (PC; OMIM #167200; ICD-10 Q84.5) is autosomal dominantly inherited form of palmoplantar keratoderma (Leachman et al. 2005), presenting itself in a clinical phenotype that involves painful keratoderma of the palms and soles, nail deformities, epidermal cysts and oral leukokeratosis (Figure 9) (Smith et al. 1993). The underlying molecular cause was found to be missense mutations in genes for several intermediate filaments, whereas mutations in Keratin 6a and 16 (CK16) are responsible for Type 1 PC and Keratin 6b and 17 lead to Type 2 PC (Bowden et al. 1995; McLean et al. 1995). Further details about the specific disease-causing mechanism are so far unknown but almost all PC-related mutations occur in the conserved 1A helical domain for each of the affected keratins (Terrinoni et al. 2001). These helix boundary motifs have also previously been described as mutational hotspot for most of the characterised keratin disorders (Fuchs and Cleveland 1998; Irvine and Mclean 1999). Possible treatment options for PC include the post-transcriptional downregulation of Keratin 6a through mTOR inhibitors such as Rapamycin (Hickerson et al. 2009).

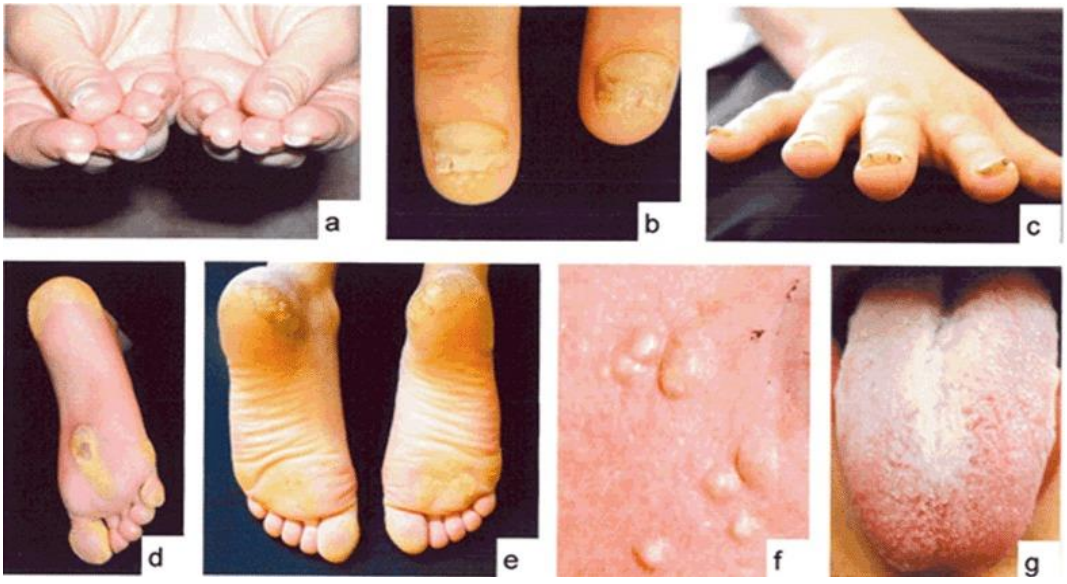

Figure 9: Clinical presentation of Pachyonychia congenita

Typical symptoms of PC are thickened and/or dystrophic finger and toe nails (a-c), painful plantar keratoderma including calluses and underlying blisters (d-e), epidermal cysts (f) and oral leukokeratosis (g). (Smith et al. 1993)

1.3. Cutaneous Wound Healing

1.3.1. Physiological Process of Cutaneous Wound Healing

The repair of acute cutaneous wounds is a well-orchestrated process involving a variety of cellular components from the epidermis, dermis, immune system and vasculature (Singer and Clark 1999). This process is classically divided in three distinct but overlapping phases over time: inflammatory phase, proliferative phase and remodelling phase (Figure 10) (Gurtner et al. 2008).

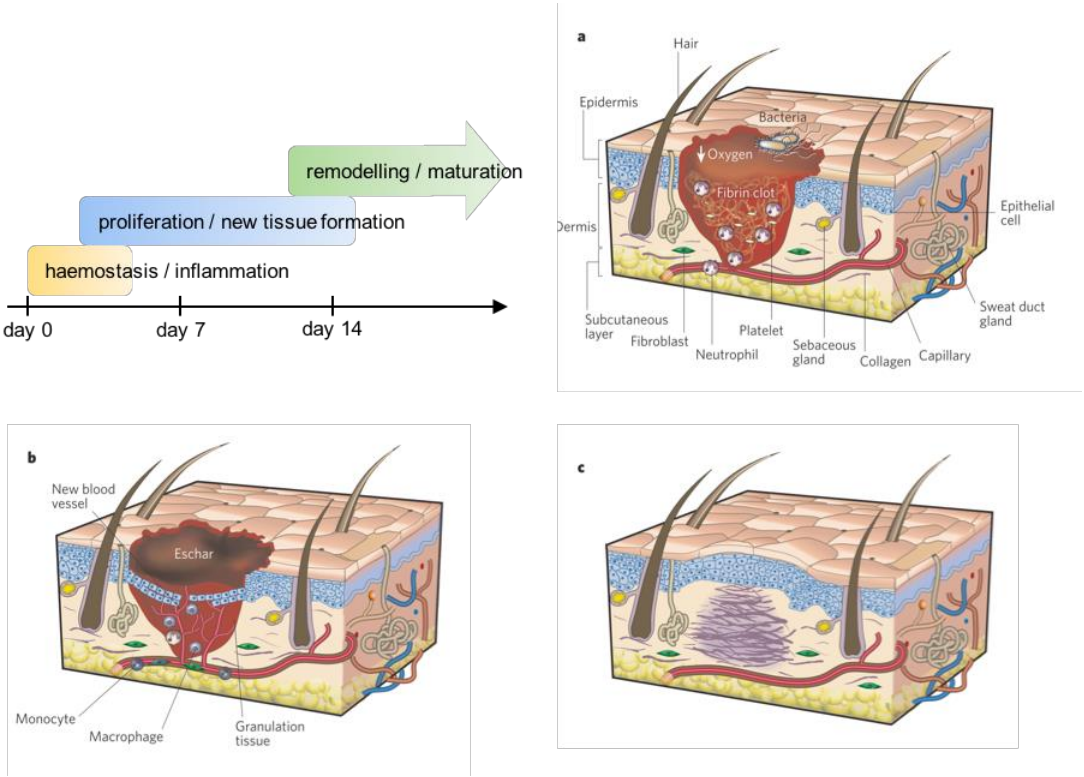

Figure 10: Stages of cutaneous wound repair

The classical description of cutaneous wound healing is based on three sequential but overlapping phases. The first phase, lasting up to three days from injury, is the inflammatory phase and involves an initial haemostasis followed by immune-mediated clearance of the wound (a). Subsequently, during the up to two weeks long proliferative phase, newly formed granulation tissue forms the basis for re-epithelialisation from the wound edge (b). The remodelling phase can last up to a year and ends with mature, structurally strong scar tissue replacing the granulation tissue and lending support for the fully functional, reformed epidermis (c). (modified from Gurtner et al. 2008)

The inflammatory phase happens in the immediate aftermath of an injury and involves the initial stabilisation and clearance of the wound area (Martin and

Leibovich 2005). As a first step in this haemostasis is established through the formation of a plug by extravasated platelets and fibrin, whereby this haemostatic plug also serves as a matrix for the migration of infiltrating immune cells. Neutrophils are recruited into the wound by platelet degranulation and activation of the complement system via bacteria and clean the wound via proteolytic breakdown and phagocytosis of debris as well as antibacterial activity. In conclusion to this action and subsequent apoptosis they are either extruded with the eschar or themselves phagocytised by macrophages. The macrophages are thought to be crucial in setting up the next stage of the healing process by secreting a multitude of cytokines and growth factors essential for the initiation and propagation of new epithelial tissue formation and neovascularisation after the initial few days of inflammation (Figure 11), though recent studies suggest that redundancies in the inflammatory response can mitigate missing (cellular) factors (Martin and Leibovich 2005). Among the newly formed structures is the granulation tissue, being made up of sprouting capillaries, remaining macrophages and recruited fibroblasts. Replacing the fibrin clot, it is mainly composed of fibronectin, hyaluronan and in increasing parts collagen 3 in order to provide a scaffold for migration of endothelial and epithelial cells. Even during the inflammatory phase keratinocytes from the wound edge, or alternatively from potential appendageal remainders inside the dermis, start to migrate into the wound, degrading hemidesmosomal contacts with the basement membrane and upregulating the expression of several integrins and matrix-metalloproteases to allow for the lateral migration from the injured dermis and unto the newly formed granulation tissue (Larjava et al. 1993; Pilcher et al. 1997). This mechanism of migration and proliferation and maturation, leading in the end to a fully functional epidermis, is hereby thought to be driven by growth factors derived from the macrophages and fibroblasts inside the underlying tissue (Figure 11), in addition to the loss of contact inhibition and certain wound-specific chemicals such as nitric oxide (Witte and Barbul 2002; Zegers et al. 2003). Myofibroblasts, which are contractile cells derived from triggered differentiation of dermal fibroblasts inside the granulation tissue, help with this re-epithelialisation process by contracting the wound and bringing the edges closer together (Werner et al. 2007). During the last phase, which normally starts around two weeks after injury and can last up to a year,

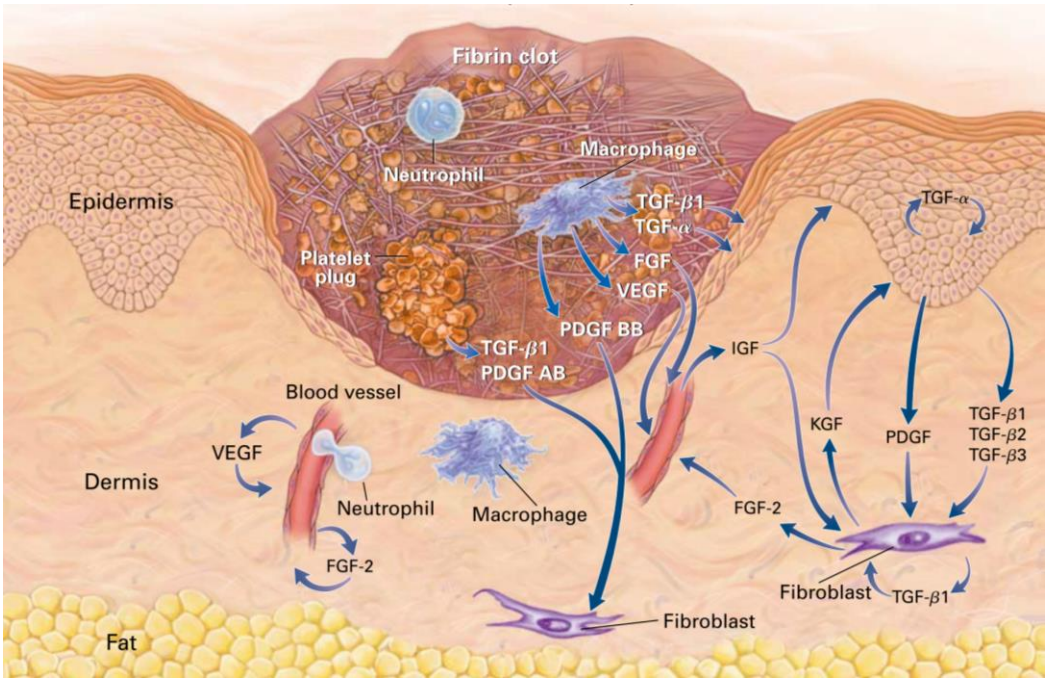

Figure 11: Cellular crosstalk during cutaneous wound healing

Proper progression through the stages of cutaneous wound repair and subsequent re-establishment of a functional epidermis is dependent on a well-coordinated interplay of cellular components from the immune system (neutrophils and macrophages), endothelial cells, dermal fibroblasts and re-epithelialising keratinocytes. Most of this interaction is regulated by the timed secretion of growth factors leading to recruitment and/or functional activation of receipting cells. (modified from Singer and Clark 1999)

the provisional, collagen 3-containing granulation tissue is gradually remodelled into a collagen 1-rich, crosslinked and aligned tissue by the incorporated fibroblasts, potentially triggered in this by epidermally secreted TGF-b (Clark et al. 1995). In the end, the majority of remaining endothelial cell, macrophages and fibroblast undergo apoptosis or exit the wound, leaving a most acellular, structurally strong scar tissue underneath the newly formed epidermis (Desmoulière et al. 1995).

1.3.2. Aberrant Wound Healing and Therapeutic Approaches

Cutaneous wound healing is a complex process and can therefore be impaired by various factors. These can be either local, for example ischemia or excessive dryness of the wound, or especially systemic factors, such as age, nutrition, diabetes or inflammation (Guo and Dipietro 2010). In contrast, hypertrophic scarring and keloid formation are prominent examples of excessive healing, either due to external or genetic factors, and consequently characterised by unusually upregulated vascularisation and cell proliferation as well as subsequent aberrant deposition of extracellular matrix (Robles and Berg 2007; van der Veer et al. 2009). The understanding of underlying mechanisms allows for the possibility of therapeutic intervention, potentially through external stimulation of angiogenesis in diabetic wounds or the inhibition of TGF-b in hypertrophic scar formation (Figure 12) (Ferguson et al. 2004; Galiano et al. 2004).

Another important to consider in terms of cutaneous wound healing is the difference between tissue repair and regeneration: while *repair* refers to the physiological adaption and re-establishment of continuity after a tissue injury, *regeneration* means a complete morphological and functional restoration of the tissue (Orgill and Blanco 2009). While the former is the case with normal wound healing, the latter is under ongoing investigation, with the idea being that the right combination of stem cell-based tissue engineering approaches and instructive scaffolds could results in the fully functional reconstruction of dermal appendages such as sweat glands (Figure 12) (Lutolf and Hubbell 2005; Huang et al. 2012). These considerations become especially important in the context of bioengineered wound covers and skin substitutes, which are crucial in the treatment of large-area (burn) wounds and will be mentioned again later on in Chapter 1.5.1 (Matoušková and Mestak 2014; Nicholas et al. 2016).

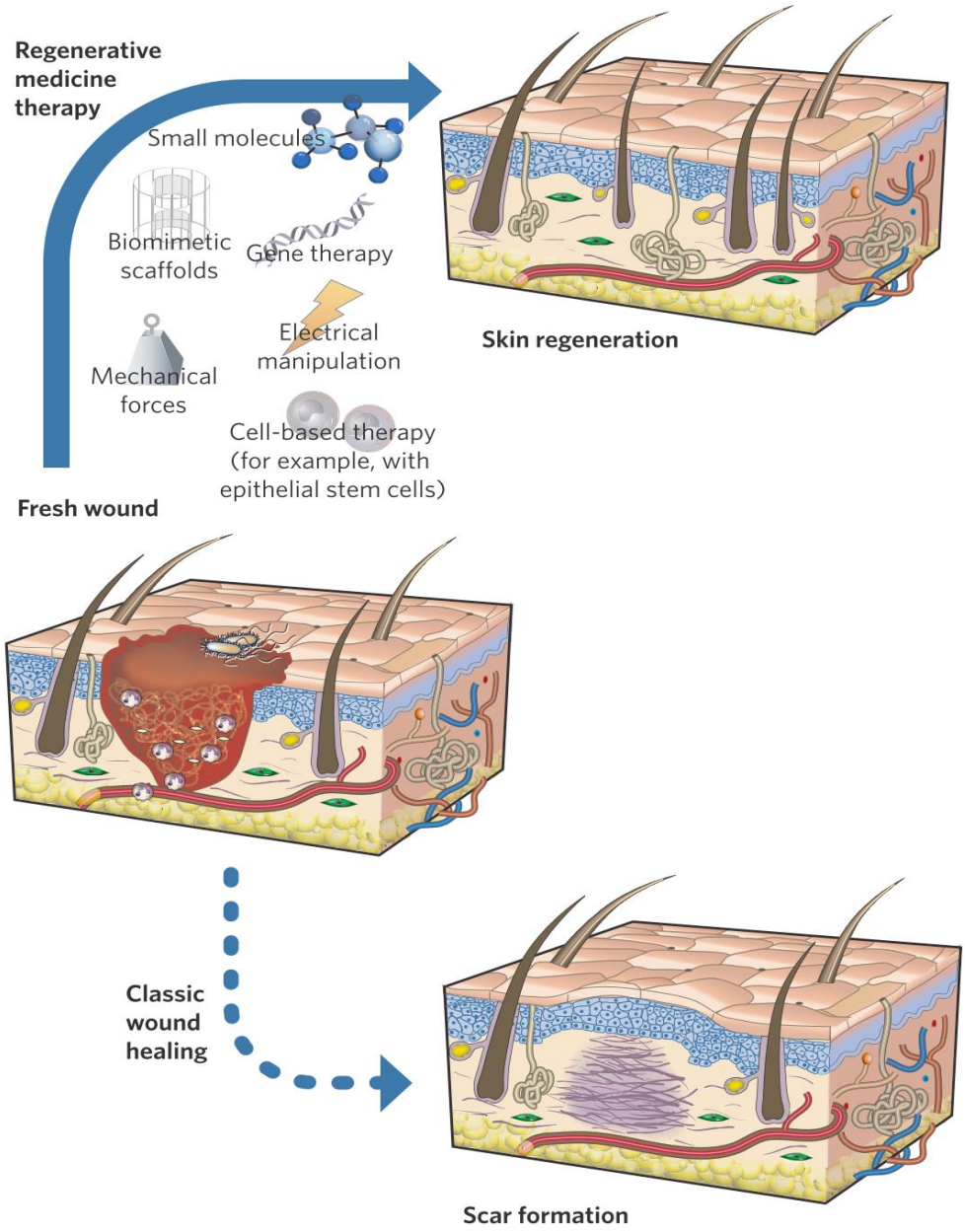

Figure 12: Artificially improved cutaneous regeneration

While normal (and especially aberrant) wound healing results in acellular dermal scar tissue, advances in growth factor-based treatment in combination with tissue engineering approaches might result in the regeneration of fully functional skin, including normal dermis and appendages. (Gurtner et al. 2008)

1.4. Epidermal and Transdermal Drug Delivery

1.4.1. Caveats of Percutaneous Transport

Hereditary skin conditions offer the possibility of disease phenotype alleviation via systemic application of drugs, for example retinoids in case of Harlequin ichthyosis or mTOR inhibitors for the treatment of Pachyonychia congenita (Warren and Khanderia 1989; Hickerson et al. 2009; Rajpopat et al. 2011; Nguyen and Zuniga 2013). Oral administration of these drugs is known though to lead to, partially severe, systemic side effects (Gollnick 1996; Salmon 2015). Local administration, which in case of skin disorders means external application of a topical formulation, is therefore a preferable administration route and consequently the focus of ongoing development (Falke et al. 2015; Feely et al. 2015; van de Kerkhof 2015). In addition, the transdermal administration of systemically active drugs has several advantages over oral or injection-based routes, for example in terms of pharmacodynamics and users acceptance (Prausnitz and Langer 2008).

When it comes to the epidermal and transdermal delivery of substances across the upper layers of the epidermis several possible pathways are considered to be feasible (Figure 13). Transappendageal transport relies on the presence of hair shafts and glandular ducts in order to reach lower epidermal layers and is therefore considered a preferential pathway but nonetheless insignificant for overall transport since follicles and glands make up only 0.1% of the skin surface (Blank et al. 1967; Schaefer and Lademann 2001). In contrast, interfollicular transport (trans- and predominantly intercellular) is far more likely but severely hindered by the by the native barrier function of the epidermis where penetration across stratum corneum and upper stratum granulosum is highly limited and dependent on a multitude of factors, like molecular weight and partition coefficient (Pouillot et al. 2008; Proksch et al. 2008; Andrews et al. 2013).

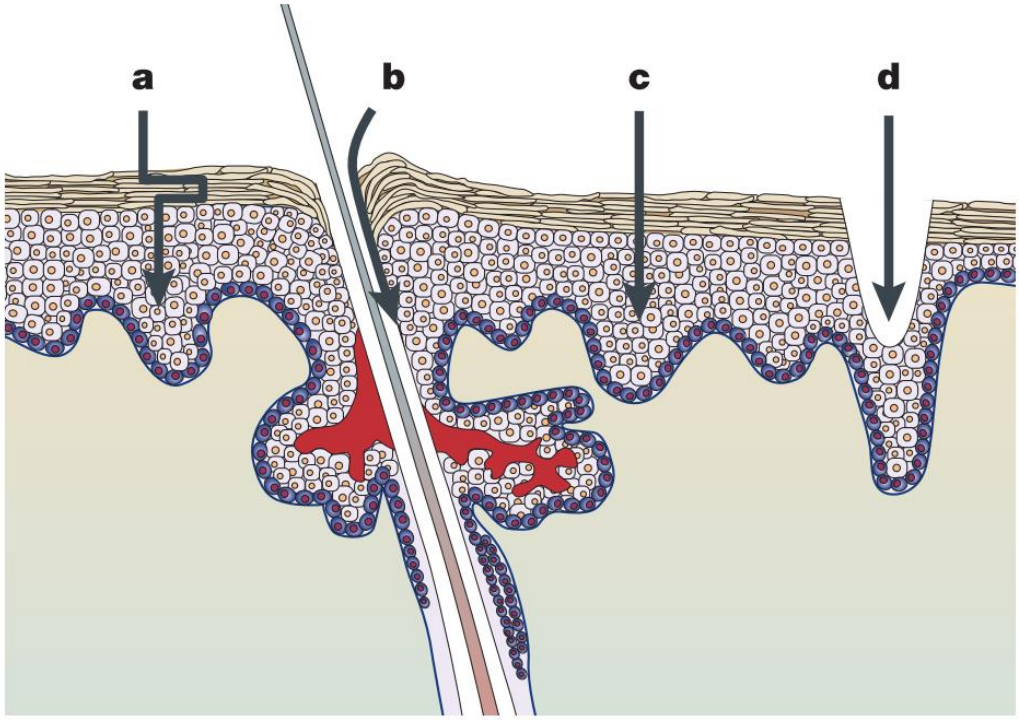

Figure 13: Epidermal permeation pathways of topically applied substances

Topically applied substances are thought to be transported across the epidermis in a variety of possible ways. Intercellular transport happens in between the corneo- and keratinocytes, across the lipid lamellae (a), whereas transcellular transport relies on the temporary internalisation and excretion of the permeating substances (c). Transappendageal transport uses hair follicles or glands to reach lower epidermal layers (b) and microlesions across upper layers of the epidermis would also allow for a similar permeation (d). (Prausnitz et al. 2004)

Building on the consideration of more complex biochemical / biophysical properties of applied substances and formulations, a considerably more complex picture regarding the restricting factors of (trans-)epidermal delivery emerges (Figure 14). These models not only take into account size-dependent exclusion, partition and diffusion of particles after release from a formulation and across the different layers of the epidermis (all of which can be described as mathematical models) but also more broader, physiological aspects such as binding and metabolisation in addition to vascular and immune clearance as soon as substances reach the dermis (Jepps et al. 2013; Lane 2013).

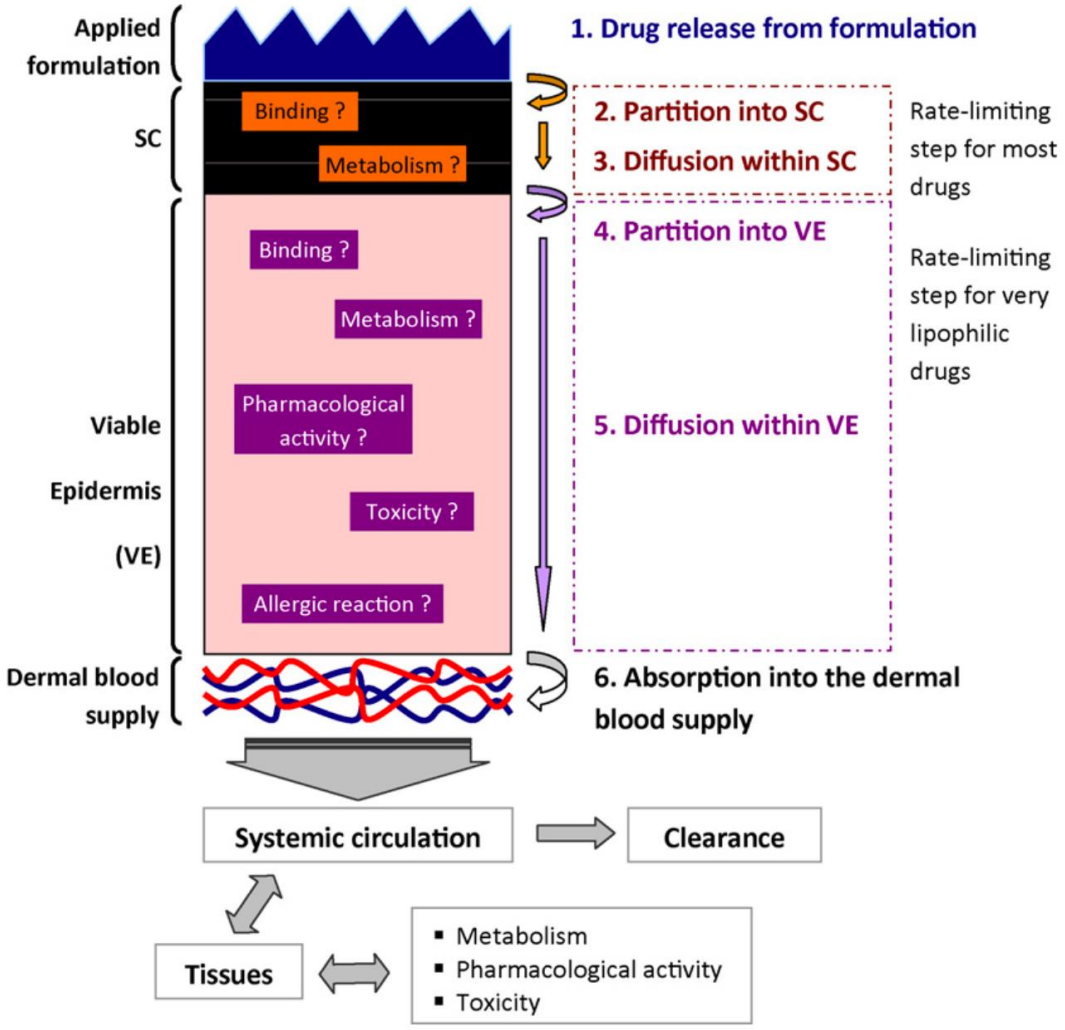

Figure 14: Factors influencing transdermal transport of topically applied substances

After the release of a drug from the applied formulation a variety of factors influence its permeation into and across the skin. Size- and concentration-dependent diffusion (described by Fick's first and second law) as well as the partition, determined by the hydro- and lipophilicity of the substance, are important biophysical factors in the initial transport across the upper layers of the epidermis. These get complemented by more complex interactions with the tissue, such as binding to biological structure, internalisation and metabolisation through cells. Once the substance reaches the dermal layer, clearance via the immune system and vasculature play an important role in the withdrawal of the substance from the skin and its systemic distribution. (Lane 2013)

1.4.2. Facilitation of Percutaneous Drug Delivery

In parallel to working on more refined methods of understanding and modelling the barrier function of the skin, a variety of approaches and techniques have been developed to facilitate percutaneous drug delivery. These different approaches are hereby based on physical as well as (nano-) chemical applications (Trommer and Neubert 2006; Prausnitz and Langer 2008; Alexander et al. 2012; Wong 2014; Schmieder et al. 2015).

1.4.3. Physical Methods of Enhancing Percutaneous Delivery

Examples for the physical enhancement of transdermal delivery of drugs are iontophoresis, electroporation, sonophoresis, microneedles and jet injection (Raphael et al. 2015).

Iontophoresis is based on the application of a small electrical current across the treated skin region (maximum of 0.5mA/cm^2) which, instead of disrupting the skin structure, provides an adaptable electrical driving force. This force leads to the electrophoretic movement of small, charged drugs whereas uncharged compounds can also exhibit a limited degree of movement through electroosmotic water flow (Kalia et al. 2004; Dhote et al. 2012).

Electroporation also works with the applications of an electrical current but instead of a continuous small current repeated high-voltage pulses (50-1500V for microseconds to milliseconds per interval) are used. As a consequence, in addition to a short-lived electrophoretic field during each pulse interval longer-lasting lipid bilayer disruptions and electropores are generated across the upper layers of the epidermis, which allow for an enhanced diffusion of low and high molecular weight substances (Charoo et al. 2010; Ita 2016).

Sonophoresis includes the application of ultrasound (20 kHz to 16 MHz depending on application) to the skin which is thought to increase drug permeation mostly through thermal effects as well as acoustic cavitation, leading to the disruption of lipid structures via oscillating small gaseous bubbles (Azagury et al. 2014; Park et al. 2014).

Microneedles are usually comprised of an array of microscopic needles that, when applied as a patch on the skin, penetrate between 100 and 300 µm into the epidermis and superficial dermis. This creates temporary micro-fissures along which topically applied substances can diffuse in the tissue. Furthermore, microneedles can be coated with a drug and thereby used to directly delivery it or alternatively biodegradable microneedles can encapsulate a substance and subsequently act as a reservoir, slowly releasing it through degradation of the actual needle (Prausnitz 2004; Gonzalez-Gonzalez et al. 2010).

Jet injection involves the painless application of high pressure and velocity in order to force a liquid or powder across the epidermis and is therefore a popular alternative to traditional needle-based, transdermal injections (Hogan et al. 2015).

Naturally, over time combinatorial approaches emerged as well in the attempt to further the efficiency of existing methods, for example through the combination of microneedles and ultrasound (Chen et al. 2010) or electroporation and iontophoresis (Tokumoto et al. 2006).

1.4.4. Chemical Methods of Enhancing Percutaneous Delivery

Chemical penetration enhancers are varied in nature and possible mechanism of action (Figure 15). Aiming primarily on the disruption of intercellular lipid bilayers in the stratum corneum, several categories of chemicals have been used to-date (Williams and Barry 2012; Lane 2013). Several properties for the ideal penetration enhancer have hereby been defined early on and include, among others, non-toxicity and –irritancy, rapid and quickly reversible effect on permeation and the absence of pharmacological activity (Barry 1983). A few examples of investigated types of chemicals for enhanced cutaneous penetration (though far from a comprehensive listing) are alcohols, azones, fatty acids, surfactants and sulphoxides. Alcohols such as ethanol, isopropyl and benzyl alcohol (BA) are commonly used in aqueous solutions as solvents for drugs, increasing their solubility (and consequently the drug's partitioning in the lipophilic phases) and further destabilising the lipid bilayers of the stratum corneum through lipid extraction and lipid fluidisation (Berner et al.

1989; Nanayakkara et al. 2005; Engelbrecht et al. 2012). Azone was the first specifically designed penetration enhancer (Stoughton and McClure 1983). Strongly lipophilic and with a relatively large polar head group, this non-irritant, non-toxic compound is thought to intercalate into lipid bilayers and increase their fluidity. Fatty acids and especially unsaturated, cis-configured varieties such as oleic acids have been found to be viable penetration enhancers as well, presumably though incorporation and subsequent perturbation of the lipid lamellae (Jiang and Zhou 2003; Van Zyl et al. 2016). Surfactants (preferentially non-ionic for increased biosafety) are another commonly used class of penetration enhancers, being able to solubilise lipophilic active compounds as well as lipids of the stratum corneum and also form micelles for the phase separation of lipid bilayers (Sarpotdar and Zatz 1986; Palma et al. 2006). Dimethylsulphoxide (DSMO) has been widely published and used as especially potent solvent and is in consequence also applicable as penetration enhancer. The enhancing effect is hereby attributed to several mechanisms: interaction with lipids and generation of solvent-filled spaces inside the bilayers, extraction of lipids and also changes in keratin conformation due to water displacement (Rammler 1967; Anigbogu et al. 1995). One problem that arises in parallel to the potency of DMSO is its well-known range of side effects from skin irritation to systemic metabolisation (Kligman 1965; Iliev et al. 1997).

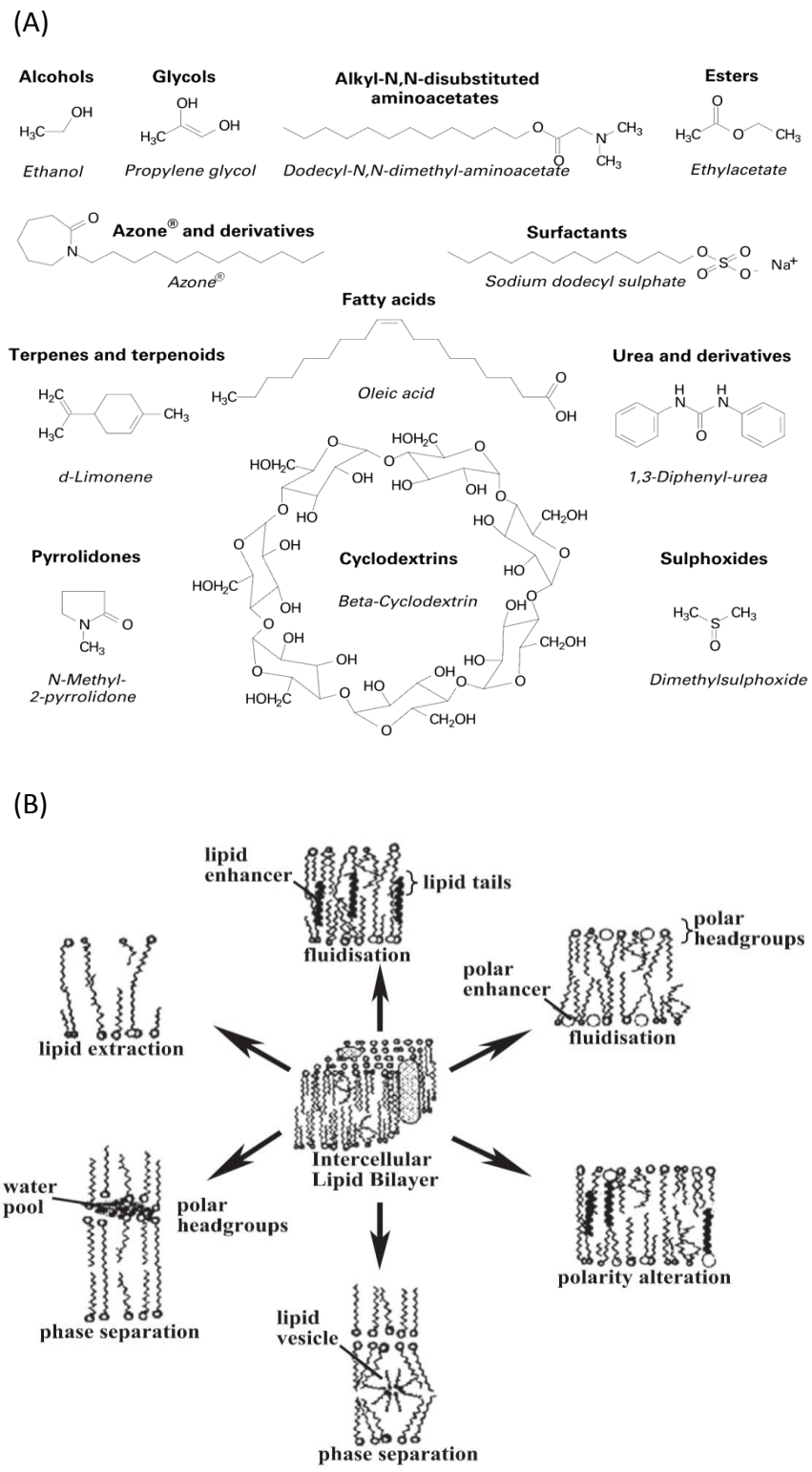

Figure 15: Categorisation and possible action of penetration enhancers at intercellular lipids
Chemical penetration enhancers can be classified in several categories (A) and interact with and consequently disrupt the lipid lamellae of the stratum corneum in variety of ways, dependent on the chemical properties of the specific enhancer category (B). (modified from Trommer and Neubert 2006 / Roberts and Walters 2008)

1.4.5. Nanochemical Methods of Enhancing Percutaneous Delivery

With the advance of nanotechnology the idea of using chemical adjuvants to transport small molecular compounds across the epidermis has been further developed into a variety of different nanomaterial-based approaches for (trans-) dermal delivery (Prow et al. 2011; Delouise 2012; Antonio et al. 2014; Arif et al. 2015). Nanomaterials, which depending on the definition should not exceed 100-200 nm in dimension, are of special interest for emerging technologies due to their different physicochemical properties in comparison with macroscale materials of the same composition, which is mostly based on the drastically increased surface-to-volume ratio (Figure 16) (Nel et al. 2006; Misra et al. 2008).

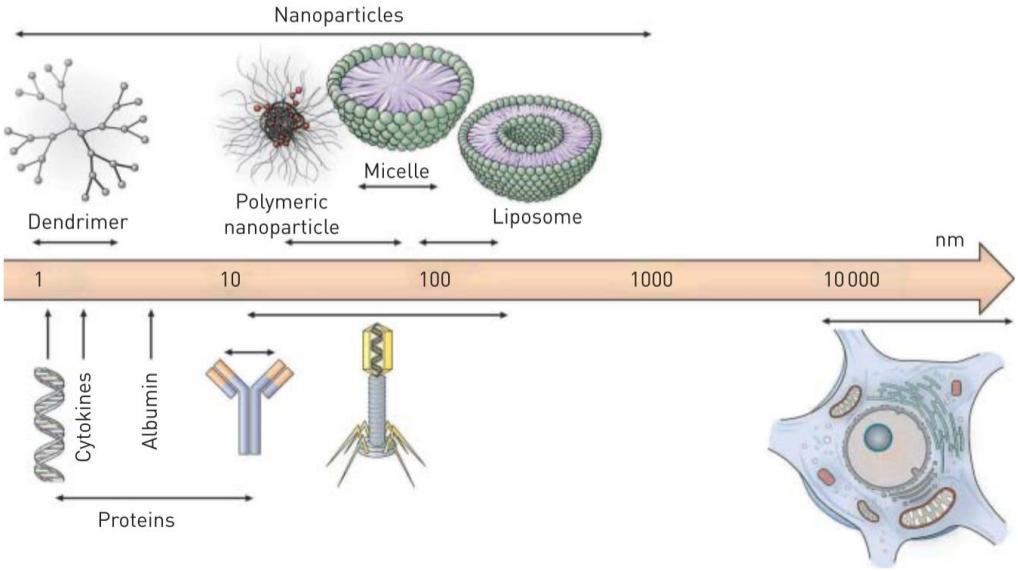

Figure 16: Comparative size of various nanoparticles

Nanoparticles vary in size but should not exceed 200nm, which puts them in the same dimension as phage viruses and enables them to readily interact with considerably larger cell structures. (Van Rijt et al. 2014)

Subsequently, over the years different types of specifically designed nanomaterials, varying hugely in composition and properties, have been applied in a variety of fields (Figure 17). Metal core particles, based for example on oxidized titan or silver molecules, are increasingly used in consumer products such as sunscreens or deodorants (Contado 2015). Medical diagnostic applications make use of superior *in*

vivo contrast imaging that can be achieved with tumour-specific fluorescent quantum dots or superparamagnetic iron particles (Padmanabhan et al. 2016). Furthermore, several therapeutic approaches are based on the application of nanoparticles, for example by utilising them as antimicrobial agents (Rudramurthy et al. 2016), in physical tumour therapy (Zhang et al. 2016) or as drug carrier system (Cho et al. 2008), whereby in those last two cases the ability to functionalise nanoparticles and make them specifically bind to certain molecular targets is of special importance (Liu et al. 2014; Adebowale et al. 2015).

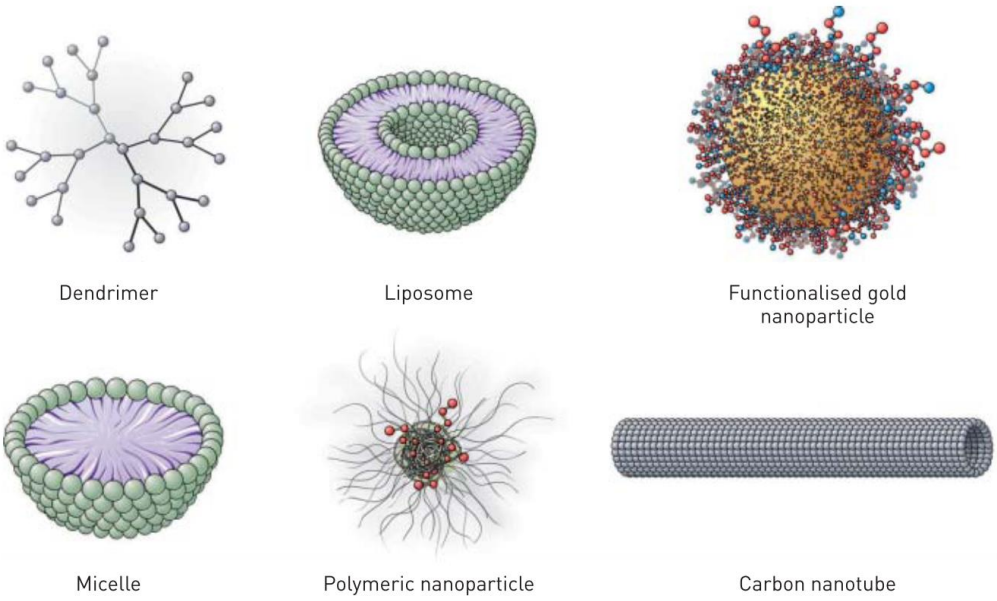

Figure 17: Selection of different nanoparticle types

Different types of nanoparticles are varied in their chemical composition, ranging from lipid complexes over polymeric structures to metal and carbon complexes, and subsequently in their physicochemical properties. (Van Rijt et al. 2014)

As mentioned above, nanoparticles as drug delivery vehicles are also of particular interest in the field of dermatology and different nanomaterials have been utilised in the past in order to optimise dermal and transdermal delivery of compounds. In this context, the ability of different nanoparticle types to effectively cross the epidermal permeability barrier is an on-going matter of debate, with potential permeation being seemingly very dependent on size, composition and application of the specific nanoparticle (Baroli 2010; Lademann et al. 2013; Watkinson et al. 2013; Larese Filon

et al. 2015). Flexible, lipophilic nanopolymers such as micelles have been well demonstrated to permeate along the intercellular spaces of the stratum corneum (Cevc 2004; Sinico and Fadda 2009). Solid nanoparticles, especially when approaching a size of 40nm and above, on the other hand appear to be generally hindered in their penetration and rely on the co-administration of chemical penetration enhancers (Smijs and Bouwstra 2010; Campbell et al. 2012). Alternatively, most nanoparticles seem to show significant advantages in terms of transappendageal transport, being able to deeply penetrate along hair follicles and form drug releasing reservoirs (Lademann et al. 2007; Fang et al. 2014). Subsequently, even though solid nanoparticles do not necessarily facilitate epidermal permeation by themselves they might still be of interest for drug delivery, especially when taking into account other properties specific to certain types of nanomaterials that allow for a targeted or triggered release of a drug, for example in response to changes in pH or temperature (Cheng et al. 2013; Karimi et al. 2016).

One interesting option would hereby the application of thermoresponsive nanogels (Molina et al. 2014; Bergueiro and Calderõn 2015). Poly(N-isopropylacrylamide) (PolyNIPAm) forms a thermosensitive hydrogel when chemically crosslinked, undergoing a reversible phase transition at 32°C; above this temperature the nanogel changes into a dehydrated state, shrinking to approximately 10% of its initial volume and expelling its content (Yan and Tsujii 2005; Cuggino et al. 2011). Since this conformational change happens at a temperature close to body temperature, it has already been investigated for its potential in controlled transdermal drug delivery (Singka et al. 2010; Witting et al. 2015).

The potentially harmful effects of naturally occurring and man-made nanoparticulates, for example as part of industrial exhaust, have been under investigation for some time and the rise of nanomaterial-based applications further presses the need for comprehensive studies of cytotoxicity and systemic effects for biomedically or cosmetically applied nanoparticles (Dowling et al. 2004; Buzea et al. 2007; Kennedy 2014). In this regard, suitable *in vitro* models are of special importance for initial safety assessments but also to gain further insight into mechanisms of action for nanoparticles once applied to the tissue (Tsuji et al. 2006; Sayes et al. 2007).

1.5. *In vitro*-generated Skin Equivalents

The generation of *in vitro* skin equivalents can be broadly divided into two potential applications: the creation of skin substitutes for therapeutic purposes and cutaneous models for *in vitro* test assays as well as discovery science (Figure 18) (Groeber et al. 2011).

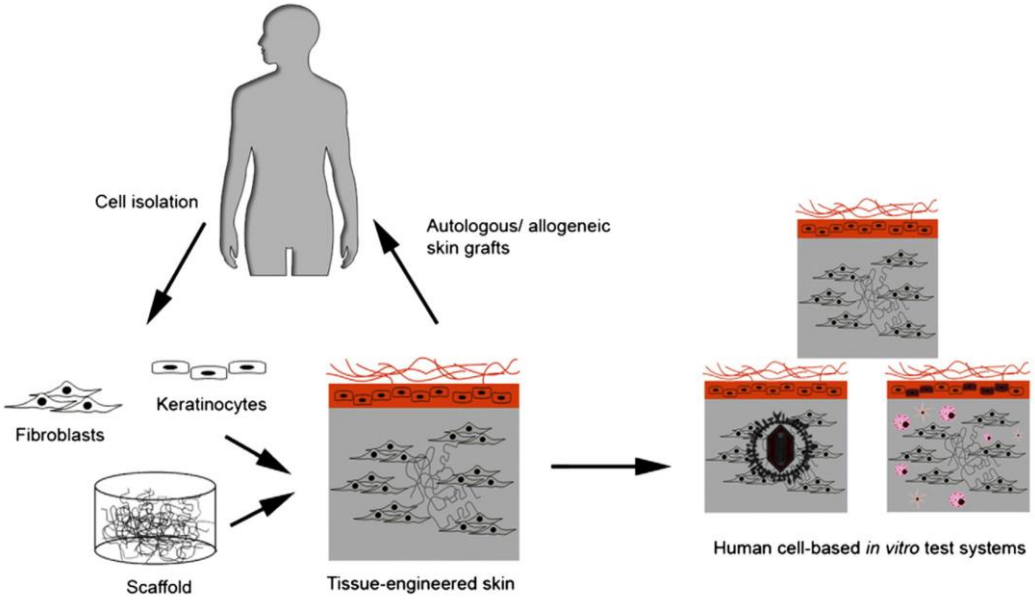

Figure 18: *In vivo* and *in vitro* application of skin equivalents
In vitro tissue-engineered skin equivalents can be generated by the combination of human-derived cells and suitable biomimetic scaffolds and subsequently used either for *in vivo* application as therapeutic skin substitute or for *in vitro* test models. (Groeber et al. 2011)

1.5.1. Therapeutic Application of Tissue-engineered Skin Substitutes

Skin substitutes are a promising treatment option for large-scale wound (for example from extensive burns), where autologous skin grafts are no longer viable due to limited availability (Shahrokhi et al. 2014). While momentary skin covers are predominantly acellular matrices (either of biological or synthetic origin) that allow for a facilitated migration of cells into the wound area and subsequently improved re-epithelialisation, it has been shown that the incorporation of (autologous) cells of different origins can greatly improve the outcome (Nicholas et al. 2016).

Furthermore, recent advances in tissue engineering lead to the potential addition of functional appendages such as sweat glands into the newly generated skin tissue (Huang et al. 2010). An important aspect in the development of these advanced skin substitutes are the high requirements in regard to quality control, safety assessments and commercialisation, that have to be taken into account when aiming for a viable therapeutic product and create additional, specific demands for the generation of this kind of skin equivalents (Bannasch et al. 2010).

1.5.2. Use of Human Skin Equivalents as *in vitro* Models

In regard to the second potential field of application, human skin equivalents become an increasingly essential tool in industrial research in order to accommodate progressively thorough regulatory requirements for the hazard assessment of novel substances (e.g. REACH Regulation [EC] 1907/2006). The use of animal models in pharmaceutical and especially cosmetic industry was a long-standing standard (Phillips et al. 1972) but has been drastically scaled down recently due to decreasing social acceptance and legislative support; with the 3Rs-principle finding itself increasingly included in regulatory policies across the EU (e.g. EU Directive 2010/63/EU; 7th Amendment EU Cosmetics Directive 76/78/EEC) and United States (Schechtman 2002; Becker et al. 2006). Furthermore, enzymes responsible for drug-metabolism can differ widely in between species; rendering the transfer of cytotoxicity results from animal to human difficult (Martignoni et al. 2006). Thus, there is a necessity for the development of suitable, human-specific *in vitro* test systems (Astashkina et al. 2012; Vellonen et al. 2014). Monolayer cell cultures are hereby a good first approximation but lack the three-dimensional cell-cell and cell-matrix interactions of the native tissue as well as proper metabolisation characteristics, therefore necessitating more complex, *in vivo*-like models (Figure 19) (Sun et al. 2006; Götz et al. 2012a). In case of assessing epidermal interactions of novel compounds and carriers, using skin explant cultures, for example obtained as surplus material from plastic surgeries or as patient samples, delivers a most *in vivo*-like setting but is severely limited in regard to availability and reproducibility due to biological variation in between samples; reconstructed skin equivalents have

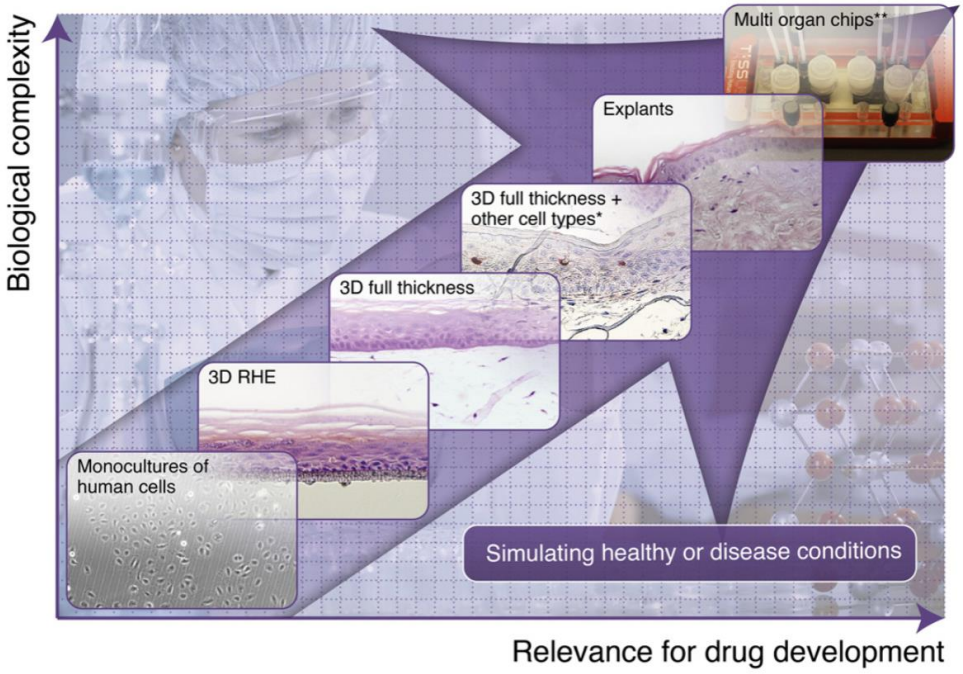

Figure 19: Complexity and relevance of various *in vitro* models

In vitro skin models show a general correlation in between their complexity and relevance for test systems, ranging from simple monolayer to 3D culture (both epidermal and full-thickness) and explant cultures as most in vivo-like option. Multi-organ chips, which combine several reconstructed tissues in one system, provide a further step in complexity due to 'system-wide' assessments. (Mathes et al. 2014)

therefore to be considered as an alternative (Ponec 2002). Recreating skin biology in a sufficient but scalable manner, those models could then be used as extension for initial assessments of basic parameters in monolayer cultures (Poumay and Coquette 2007; Pappinen et al. 2012; Rimann and Graf-Hausner 2012). By applying cultured keratinocytes in a standardised setting, batch-to-batch variety can be kept comparatively low and the possibility of up-scaling is only limited by cell culture facilities and the available budget (Lotte et al. 2002). Correspondingly, various commercially available skin equivalents have been made available over the last two decades and used to for the assessment of skin corrosion and irritancy of novel products, adhering hereby to guidelines established by the OECD (OECD TG 431 / 439) regarding for example the viability, morphology and reproducibility of a specific test system. Existing products can hereby be divided into two categories: epidermal models, which consist of epidermal keratinocytes on a synthetic membrane (e.g. Episkin™ by L'Oréal or EpiDerm™ by MatTek Corporation), and full-thickness models,

which include an additional cellularised dermal component (e.g. EpiDermFT™ by MatTek Corporation or the Phenion® FT Model by Henkel AG). In general, it can hereby be said that the full-thickness models are closer to native skin in several biological parameters, for example lipid composition and barrier function, than the epidermal models but conversely require more effort in regard to standardisation and reliable readout due to the increased complexity (Mathes et al. 2014). This has to be taken into consideration when expanding the use of a model to address more complex questions such as permeation of topically applied substances for intended transdermal delivery or localisation and effect inside the epidermis (Gabbanini et al. 2009; Ackermann et al. 2010). For academic research full-thickness models are also the more preferential option since the increased complexity is essential in the study of physiological and aberrant skin biology.

1.5.3. Matrix and Cellular Components of Skin Equivalents

The first concern when it comes to three-dimensional cell culture in general is the choice of the right scaffolding. While epidermal models can be achieved by culturing keratinocytes on simple synthetic membranes in airlift, more complex models (and most commercially available ones) have an additional collagen coating for better cell adhesion (Frankart et al. 2012; Pendaries et al. 2014). In contrast, full-thickness models require a dermal component as well and provide thereby the chance for more variation in the choice of material. De-epidermalised dermis (DED), mostly acquired from cadaver skin, is a commonly used support for the reconstruction of full skin (Tjabringa et al. 2008; Bogaard et al. 2013). Close in morphology to actual skin once supplied with keratinocytes, it comes with mostly the same advantages and disadvantages as skin explants, namely availability but especially biological variability. Similar de-cellularised scaffolds can also be generated from animal tissue such as porcine intestines (Jannasch et al. 2015; Lindberg and Badylak 2015). Reducing the dermal support structure to simplified extracellular matrix protein gels, collagen 1 as major constituent of the dermis being hereby a preferred candidate, makes for a more reproducible and scalable model and has therefore become a widely used method (Mildner et al. 2010; Eckl et al. 2011; Gschwandtner et al. 2013).

Instead of using single protein gels, different proteins can furthermore be combined to mimic a biologically more relevant composition, for example by applying collagens 1;3 and 5 in conjunction with elastin (Reijnders et al. 2015). Conversely and in order to counteract biological variability even further the protein matrix can be (partially) substituted by synthetic polymers like polycarbonate, polystyrene or polycaprolactone (Dai et al. 2004; Sun et al. 2005; Poumay and Coquette 2007). Another approach works entirely without an artificially created scaffold, instead relying on high-density fibroblast sheets to self-assembly an extracellular matrix to seed the keratinocytes on (Cvetkovska et al. 2009; Jean et al. 2009).

Regarding the choice of keratinocytes for the epidermal portion of the organotypic culture, several alternative types of cell supply have to be considered. While the majority of the literature describes the successful generation of *in vitro* skin models based on primary keratinocytes and fibroblasts (Mildner et al. 2006; Bogaard et al. 2013; Alnasif et al. 2014) and all commercially available models are based them as well, using immortalised cell lines has certain advantages over the use of primary cells (Reijnders et al. 2015). By applying a continuously self-renewing supply of cells, experiments can be conducted over a long time frame without risking variability in results due to aging or having to replace cell supplies (Schoop et al. 1999; Kolditz et al. 2014; Skazik et al. 2014). Furthermore, in case of rare genetic disorders transforming a small pool of primary cells, yielded from a singular skin sample, is the only possibility to achieve a sufficient supply of cells for *in vitro* studies without having to rely on artificial, transient or permanent knockdown models (Blaydon et al. 2012, 2013) which becomes even more prevalent when dealing polygenic disorders. On the other hand, the quality of immortalised skin equivalents does appear to be hugely dependent on the specific setup and especially the source of the used cell line. While for example successful models, including proliferation and differentiation similar to primary keratinocytes, based on human telomerase reverse transcriptase (hTERT) and spontaneously immortalised keratinocytes have been previously published (Allen-Hoffmann et al. 2000; Dickson et al. 2000; van Drongelen et al. 2014), other groups described insufficient barrier properties and lack of typical metabolic redox activity in HaCaT-based organotypics (Boelsma et al. 1999; Götz et al. 2012b) or premalignant, hyperproliferative phenotypes with human papilloma

virus (HPV)-immortalised keratinocyte organotypic cultures (Blanton et al. 1991; Delvenne et al. 1995, 2001). In regard to organotypic disease modelling, if patient-derived cells are not available, stable knockdown models for disease-specific genes using either primary or immortalised cells, are a viable option and have been described extensively in the literature (Mildner et al. 2010; Eckl et al. 2011; Pendaries et al. 2014; Skazik et al. 2014). Furthermore, novel TALEN- and CRISPR/Cas9-based approaches make it possible to introduce sequence-specific mutations into cultured cells and by that reproduce disease-related gene defects (Gaj et al. 2013; Wei et al. 2013). Another intriguing alternative is made possible by the rather recent advance of somatic cell reprogramming, with skin equivalents being based on keratinocytes derived from patient-specific, induced-pluripotent stem cells (Itoh et al. 2013; Petrova et al. 2014). Having established an (disease-based) organotypic culture model, it can then be used to further elucidate disease mechanisms and/or assess the effect of potentially therapeutic compounds in a more skin-like, three-dimensional setting (Bogaard et al. 2013; Alnasif et al. 2014; Eckl et al. 2014).

In addition to keratinocytes and fibroblasts, as minimal essential components of a dermal/epidermal model, other cell types and constructs can be introduced to the skin equivalent. Different kinds of melanocytes can be added in order to investigate pigmentation or melanoma formation (Duval et al. 2012; Hill et al. 2015), the addition of Langerhans cell or macrophages can introduce an immunological component to the model (Linde et al. 2012; Ouwehand et al. 2012) and endothelial cells, alternatively re-differentiated from adult stem cells first, allow for capillary formation in the dermal portion of the skin equivalent (Black et al. 1998; Auxenfans et al. 2012). Of similar importance for the potential application in therapeutic skin equivalents is the possibility to transplant or de novo-reconstruct appendages like hair follicles and sweat glands, which is also interesting for *in vitro* permeation models due to the preferential transappendageal transport route of some topically applied substances (Michel et al. 1999; Huang et al. 2010; Lindner et al. 2011).

1.5.4. Skin Equivalents in Disease, Wound and Infection Models

With the right choice of cells (either patient-derived, genetically manipulated or biochemically triggered) skin equivalents can be used for the complex *in vitro*-modelling of disease phenotypes. Consequently, over the course of the last decade numerous disease models have been published. Some examples are hereby based on keratinocyte-specific disorders, such as psoriasis (Tjabringa et al. 2008; Krajewska et al. 2011), chloracne (Forrester et al. 2014), atopic dermatitis (Bogaard et al. 2013), recessive congenital ichthyosis (Eckl et al. 2011) and exfoliative ichthyosis (Blaydon et al. 2011). Other models concentrate on dermal fibroblasts instead, in order to investigate for example mechanisms of hypertrophic scarring (van den Broek et al. 2012, 2014). Combinatorial approaches can involve disease-related changes in both keratinocytes and fibroblasts, which would for example cause basement membrane abnormalities in models for dystrophic epidermolysis bullosa (Itoh et al. 2011, 2013). Furthermore, additional cell types can be included into the model to create specific phenotypes, like the addition of activated T cells for eczematous dermatitis (Engelhart et al. 2005) or aberrant melanocytes for the generation of an organotypic melanoma model (Hill et al. 2015).

In addition to disease models, skin equivalents can also be used to model and characterise simple wound healing processes. Several models have hereby been used to investigate basic keratinocyte (and fibroblast) behaviour during re-epithelialisation in response to burn or cold wounds, superficial incisions or full-thickness punch wounds (El Ghalbzouri et al. 2004; Breetveld et al. 2006; Safferling et al. 2013).

Regarding the use of functional skin equivalents for the *in vitro* investigation of infections, models have been developed including all major types of pathogens: bacteria such as Staphylococcus aureus (Popov et al. 2014), fungi like Candida albicans (Schaller et al. 2002), a variety of relevant viruses (Andrei et al. 2010) and also worm larvae (Jannasch et al. 2015). Bacterial infection models have recently been further combined with thermal wounding of the skin equivalent in order to have a more specific look at the interaction of S. aureus with the wound milieu and the potential of therapeutic intervention (Haisma et al. 2014).

1.6. Aims of the Thesis

Combining various aspects of *in vitro* skin modelling, the overall aim of this thesis is the establishment of an adaptable protocol for the generation of organotypic skin disease model and its application in the characterisation of hyperproliferative disease phenotypes, the modulation of said phenotypes through potential therapeutic approaches and the parallel use of the functional organotypic for the assessment of topically applied nanopolymeric drug delivery. The thesis has therefore the following aims (Figure 20):

- ✓ Establishment of an organotypic culture model for HPV16-immortalised keratinocyte cell lines (normal phenotype and patient-derived)

- ✓ Application of the organotypic culture protocol for the generation of phenotypic models for Harlequin ichthyosis, Tylosis and Pachyonychia congenita

- ✓ Modulation of modelled disease phenotypes through the application of appropriate, potentially therapeutic compounds

- ✓ Establishment of an organotypic epidermal wound model and its combination with the TOC disease model

- ✓ Use of the normal phenotype model for the assessment of topically applied nanopolymers in regard to (assisted) permeation in addition to general characterisation of the nanopolymer-keratinocyte interaction

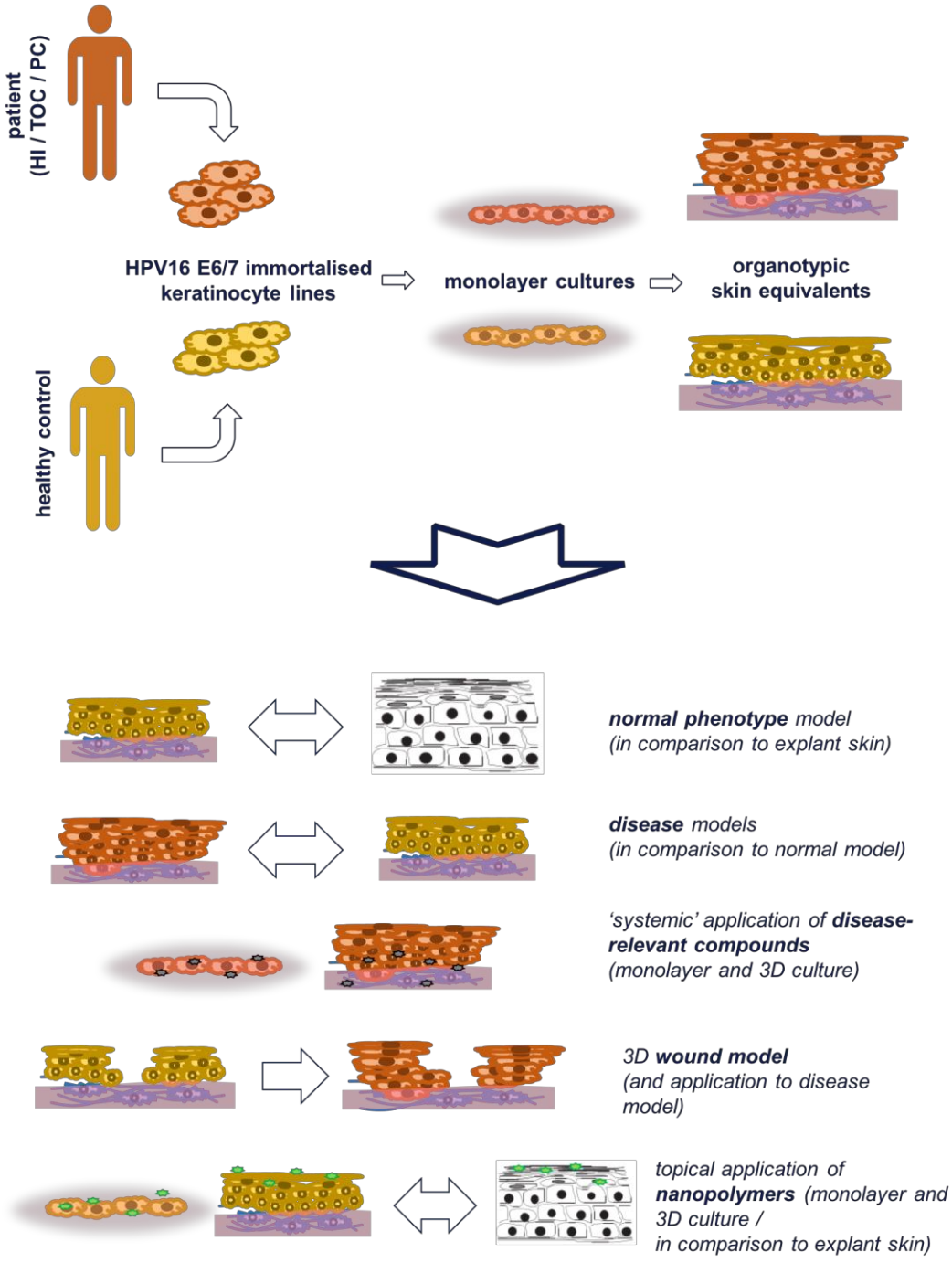

Figure 20: Principle and aims of the thesis

Patient-derived and normal phenotype keratinocytes are immortalised, expanded and subsequently used to establish a 3D organotypic model. The model is then characterised both for the normal phenotype (in comparison to explant skin) and disease phenotypes (in comparison to the normal phenotype). In conclusion to this, compounds are used to modulate the specific disease phenotypes, an organotypic wound model is established and combined with certain disease models and the normal phenotype model is used to assess nanopolymer interaction and permeation (again in comparison to explant skin).

2. Materials and Methods

2.1. Tissue- and Cell Culture

2.1.1. Maintenance Culture of Immortalised and Primary Keratinocytes

Patient-derived and normal control keratinocytes were initially isolated from skin biopsies using established protocols (Blaydon et al. 2012). In short, freshly explanted skin biopsies (2mm diameter) were cleaned from excess fat tissue, washed in phosphate buffered saline (PBS) and transferred to 2.5 mg/ml Dispase 1 (Roche) for overnight incubation at 4°C. The next day, dermis and epidermis were pulled apart via tweezers and the epidermis treated separately from here on. The tissue was washed several times in Versene solution containing 0.2 g/l EDTA in PBS (Thermo Fisher Scientific) and then chopped with a scalpel before being transferred to a trypsin-EDTA solution (0.5 g/l trypsin and 0.2 g/l EDTA in PBS; Sigma-Aldrich) for 2h at 37°C. After further dissociation of the tissue pieces through up- and down suction in increasingly smaller volume pipettes, the now cloudy cell suspension was pelleted (0.2g for 5 minutes), resuspended (in differentiation medium without the addition of Ham's F12; see Table 5) and added unto a semi-confluent layer of pre-seeded NIH-3T3 immortalised and growth-arrested feeder fibroblasts. After an initial culture period of 48 hours (at 37°C and 10% CO_2 in a humidified incubator), half of the medium was changed every other day and additional feeder cells added if necessary. The cells were passaged when keratinocyte colonies reached about 50% confluency. For this, feeder fibroblasts were washed off through a 5 minutes' incubation period in Versene and then keratinocytes detached via 5 to 10 minutes in trypsin-EDTA. After pelleting and resuspending, the cells were then either seeded unto a new batch of feeder fibroblasts or alternatively cultured on their own in serum-free maintenance medium (Table 5).

Established keratinocyte cultures, as well as previously immortalised cell lines (Table 4), were kept in maintenance medium (at 37°C and 10% CO_2); medium was changed

every other day and the cells passaged when reaching 80% confluency. In order to passage the keratinocytes, cells were washed once in PBS and incubated in trypsin-EDTA for 5 to 10 minutes. When the cells were detached, the suspension was neutralised via adding equal volume Trypsin Neutralizer Solution (Thermo Fisher Scientific) and then pelleted (0.2g for 5 minutes) and resuspended in maintenance medium before seeded into a new culture flask. If necessary, cells were counted before the pelleting using a NucleoCounter NC-100 (Chemometec).

Assessment of viability in (treated) monolayer cells was determined via an Alamar Blue Viability assay (Thermo Fisher Scientific) according to the manufacturer's instructions. Cells were incubated with the assay solution for 3-4 hours at 37°C to assure good conversion of the dye and for the final readout the red fluorescence (585 nm) per well was determined with an automated plate reader.

Table 4: Keratinocyte cell lines
Control or disease-specific cell lines were immortalised from primary keratinocyte cultures either spontaneously (Boukamp et al. 1988) or through introduction of genes for hTERT (Lee et al. 2004) or HPV16 E6/7 (Storey et al. 1988).

	Immortalisation	**Source**
HaCaT	spontaneous	healthy control skin
nTERT	hTERT	
K17	HPV16 E6/7	
NEB1		
HI		skin from patient with Harlequin ichthyosis with recessive mutation for ABCA12 (p.Glu2264X)
TOC		skin from patient with Tylosis with dominant mutation for iRHOM2 (p.Ile186Thr)
PC		skin from patient with Pachyonychia congenita with dominant mutation for CK16 (p.Leu128Glu)

2.1.2. Maintenance Culture of Primary Dermal Fibroblasts

In order to isolate and culture dermal fibroblast from healthy skin biopsies first steps were done in parallel to the isolation of epidermal keratinocytes (see above). Subsequently to the Dispase 1 digestion and separation of the dermis and epidermis,

the dermis was washed in PBS and cut with a scalpel in 1 cm^2 pieces before evenly distributed in a fresh culture plate. The plate was kept at 37°C for 1 hour in order to allow for the tissue pieces to dry and adhere unto the plastic surface. Fibroblast medium (Table 5) was slowly added from the side of the dish and the tissue kept at 37°C (10% CO_2) for at least 48 hours without movement. Medium was changed carefully in accordance with phenol red-based discoloration and the tissue pieces observed for eventual outgrowing of fibroblast cells. After obtaining sizeable fibroblast colonies through outgrowth, cells were then passaged through trypsinisation and reseeding into fresh culture dishes (see above for details).

Table 5: Media compositions

Ingredient	**Supplier**	**Product no.**	**Final concentration**
Fibroblast medium			
DMEM	Sigma-Aldrich	D5671	
FCS	life technologies	16000044	10%
L-Glutamine	Sigma-Aldrich	G7513	2 mM
Pen/Strep	Sigma-Aldrich	P0781	100 units/ml (Pen) 100 µg/ml (Strep)
Maintenance medium (0.06 mM Ca^{2+})			
Epilife	life technologies	M-EPI-500CA	
HKGS	life technologies	S-0015	1%
Pen/Strep	Sigma-Aldrich	P0781	100 units/ml (Pen) 100 µg/ml (Strep)
Differentiation medium (1.5 mM Ca^{2+})			
DMEM	Sigma-Aldrich	D5671	
Ham's F12	Sigma-Aldrich	51651C	25%
FCS	life technologies	16000044	10%
L-Glutamine	Sigma-Aldrich	G7513	2 mM
Pen/Strep	Sigma-Aldrich	P0781	100 units/ml (Pen) 100 µg/ml (Strep)
RM+	in-house formulation (see Table 6)		

Table 6: Composition of RM+

Ingredient	**Supplier**	**Product no.**	**Final concentration**
Choleratoxin	Sigma-Aldrich	C8052	$1x10^{-10}$ M
EGF	Serotec	EGF-1	10 ng/ml
Hydrocortisone	Sigma-Aldrich	H4881	0.4 µg/ml
Insulin	Sigma-Aldrich	I5500	5 µg/ml
Transferrin	Sigma-Aldrich	T2252	5 µg/ml
L-Thyronin	Sigma-Aldrich	T6397	$2x10^{-11}$ M

Established primary fibroblast cultures were kept in fibroblast medium at 37°C and 10% CO_2 in humidified incubators. Medium was changed every other day and cells were passaged when reaching 100% confluency.

2.1.3. shRNA-mediated Protein Knockdown in Keratinocytes

Selected keratinocyte cell lines were treated with small hairpin-RNA (shRNA) lentiviral particles in order to silence iRHOM2 protein expression. Transduction-ready particle mixtures (Santa-Cruz) contained hereby three individual constructs encoding a target-specific 19-25 nucleotide sequence (plus hairpin) and puromycin resistance cassette. For the transduction, cells were grown in 6well plates to 60% confluency before being treated with 5 µg/ml polybrene (in maintenance medium) for 20 minutes at 37°C and then incubated with the lentiviral particles (either specific for iRHOM2 or scrambled shRNA negative control) overnight at 37°C. The following day transduced cells were positively selected by using medium containing 2µg/ml puromycin for another three days before being switched back to normal maintenance medium. The degree of iRHOM2 knockdown was confirmed by using Western Blotting (Chapter 2.7).

2.1.4. Generation of Organotypic Keratinocyte Cultures – Alvetex Model

A first protocol for the generation of organotypic skin models was based on the application of Alvetex polystyrene scaffolds (Reinnervate). The highly porous, 200µm thick scaffolds (Figure 21 a) were hereby first rehydrated in 70% ethanol and washed twice in fibroblast medium before being placed in a 6well via the attached hanging culture insert (Figure 21 b). Primary dermal fibroblasts were seeded directly into the rehydrated scaffold (1 million cells in 100µl fibroblast medium) and incubated for 1 hour at 37°C before being cultured for up to three weeks under submerged conditions (fibroblast medium from underneath and inside the culture insert) at 37°C (10% CO_2) with medium changes every two to three days. Following this first culture period all the medium was removed and immortalised keratinocytes seeded directly on top of the cellularised scaffold (1 million cells in 100µl differentiation medium) or alternatively on a freshly prepared uncellularised scaffold. After incubating the cells on the scaffold for 1 hour at 37°C the complete scaffolds were submerged in differentiation medium and cultured like this for 2 days before being put in airlift culture condition (differentiation medium only from underneath the culture insert, Figure 21 c). The organotypics were cultured for up to an additional 3 weeks in airlift (at 37°C and 10% CO_2, with medium changes every other day) before being harvested and processed for imaging.

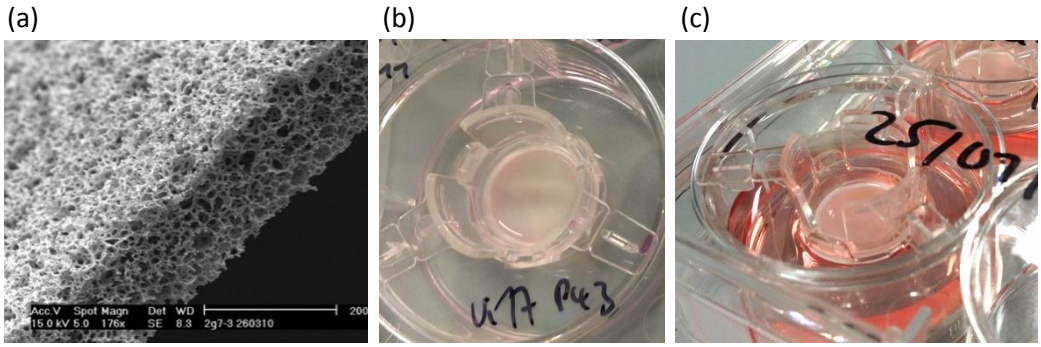

Figure 21: Preparation of Alvetex-based organotypics

The Alvetex culture system consists of a highly porous, 200µm thick polystyrene scaffold (a; image provided by Reinnervate) that is incorporated into a hanging insert for mid-air positioning in 6well culture plates (b). For the essential airlift culture conditions medium levels in the 6well are adjusted to only reach the bottom of the culture insert, leaving the interior scaffold dry and air-exposed (c).

2.1.5. Generation of Organotypic Keratinocyte Cultures – Collagen Model

The protocol for the generation of collagen-based organotypics was based on published procedures (Mildner et al. 2006) and optimised for the use with in-house keratinocyte cell lines (Figure 22). As a first step, a 4 mg/ml collagen 1 solution was set up on ice by mixing a high-concentration (ranging from 8 to 9 mg/ml depending on batch) rat tail collagen 1 solution in acetic acid (VWR) with an according volume of cold fibroblast medium. The solution was then further neutralised with 0.1M sodium hydroxide, using the phenol red of the fibroblast medium as indicator. Primary human fibroblasts were resuspended in the neutralised collagen solution at a concentration of 250,000 cell per ml and the mixture pipetted into hanging culture inserts (Millicell 0.4µm polyethylene terephthalate (PET) 12well inserts, Millipore) with 350 µl per inserts. The inserts were then kept at 37°C for 30 minutes to allow for the collagen-fibroblast gels to completely polymerise. Polymerised gels were cultured submerged in fibroblast medium and cultured for 24 hours at 37 °C and 10% CO_2. The next day, medium was aspirated and sterile plastic cloning rings (9.5mm inner diameter, Sigma-Aldrich) placed on top of the gels in order to account for the partial contraction of the gel and reseal the inner part for the following keratinocyte application. Keratinocytes were resuspended in differentiation medium (Table 5) and pipetted unto the resealed gels (100,000 cells per gel). The gels were kept in submerged conditions for another 24 hours, using the differentiation medium, to allow for the keratinocytes to settle unto the gel. After this last incubation time, the cloning rings were removed, all the medium aspirated and only replaced underneath the insert in order to create airlift culture conditions. From this point the organotypics were cultured in airlift for up to two weeks (in a humidified incubator with 37 °C and 10% CO_2) with medium changes every other day. For selected experiments, organotypics were treated with additional compounds (Table 7) by adding them to the normal differentiation medium and refreshing them every other day (adding DMSO to control organotypics as appropriate).

Unless specifically stated otherwise, this protocol was used by default for the generation of all organotypics.

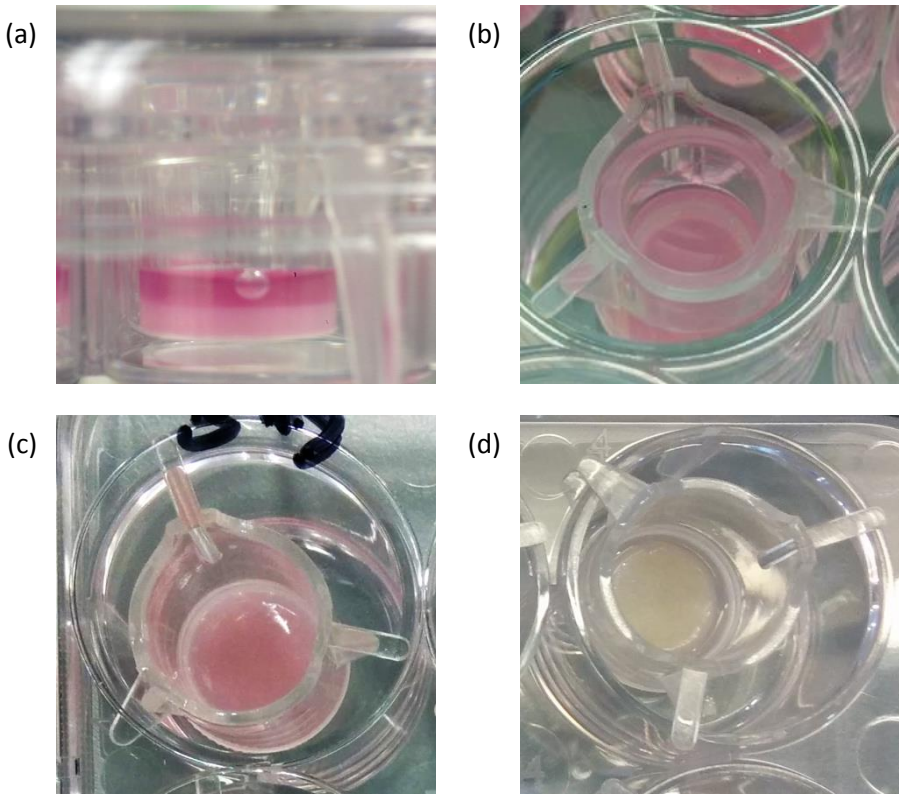

Figure 22: Preparation of collagen-based organotypics

As a first step in the preparation of collagen-based organotypics a fibroblast containing collagen 1 gel is cast into a hanging insert and initially kept in submerged conditions (a; shown here with medium only on top of the collagen gel inside the insert). A plastic cloning ring is used to 'reseal' the organotypic before the application of keratinocytes on top of the gel (b). The next day the cloning ring is removed and the freshly prepared organotypic (c) put into airlift conditions for up to two weeks, during which its appearance distinctly changes to a flattened, dried out form (d).

Table 7: Compounds for the addition to organotypic and monolayer cultures

Compound	**Description**	**Concentration**	**Supplier**
GW 0742	small-molecular PPARβ/δ agonist	10 µM	Sigma-Aldrich
TO 901317	small-molecular LXR agonist	8 µM	Sigma-Aldrich
Cetuximab	therapeutic antibody against EGFR	1 µg/ml	Merck
TMI-005	small-molecular ADAM17 inhibitor	500 nM	Sigma-Aldrich

2.1.6. Generation of Organotypic Wound Models

For the first step in the generation of *in vitro* wound models, collagen 1 gels were cast in 6well hanging culture inserts (Millipore) (Figure 23 a). Gels were prepared as described above, with the optional omission of fibroblast or addition of 30 ng/ml EGF (Serotec). After culturing the fresh collagen gels for two days under submerged conditions, fibroblast medium was aspirated and the gels used as wound scaffold. For this, two weeks-old, fully differentiated organotypics were cut out of their culture inserts (but kept on the underlying PET membranes) and subjected to full-thickness punches through epidermal and dermal portion as well as the membrane, using a sterile 2mm biopsy punch (Stiefel). The punched organotypics were then transferred unto the wound scaffold collagen gels and the whole setup cultured in airlift conditions for an additional time period of up to five days, allowing the epidermal keratinocytes to migrate / proliferate along the scaffold collagen gel into the wound area (Figure 23 b). After the completed culture period, the wound organotypics were paraformaldehyde(PFA)-fixed and processed for paraffin sectioning (Chapter 2.4).

(a) (b)

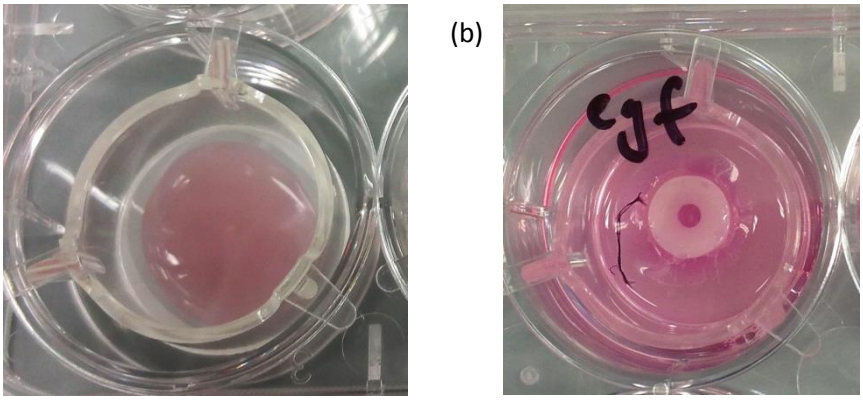

Figure 23: Preparation of an organotypic wound model
Collagen 1 gels were cast into 6well culture inserts and pre-cultured as wound scaffolds (a). Fully differentiated organotypics were then punched and transferred unto the wound scaffold to allow for wound healing processes to take place (b).

2.2. Preparation and Application of Fluorescent Nanopolymers

PolyNIPAm-based nanopolymers (intended for the encapsulation and temperature-dependent release of drug compounds) were synthesised and chemically characterised by Dr Dolca Fabregat-Montfort (School for Biological and Chemical Science, Queen Mary University London) (Figure 24). The crosslinking of NIPAm via MBA and incorporation of fluorescent probes resulted hereby in globular polymers with an average diameter of 10 nm (Figure 25 a). Different surface charges for the nanopolymers was further achieved through the addition of either acrylic acid (negative surface charge) or N-(2-aminoethyl)acrylamide hydrochloride (positive surface charge). For one subset of experiments Flufenamic acid (FFA) was added to the nanopolymers in order to test for a triggered release of the model drug.

The nanopolymers were obtained in freeze-dried form (stored in the dark an at RT) and reconstituted for application purpose by solubilising them in maintenance medium (for application on monolayer cells) or water (for topical application on skin or organotypics) at varying concentrations (ranging from 0.1 mg/ml to 10 mg/ml). To assure a homogenous single-polymer solution, the reconstituted polymers were sonicated (10 seconds at 3 Watt) and filtrated (0.4µm pore size) directly before use. The fluorescently labelled nanopolymers were applied on monolayer keratinocytes in 96well format for viability assessment and in 12well format on cover slips for imaging (λ_{Ex}= 395 nm / λ_{Ex}= 530 nm; Figure 25 b) .

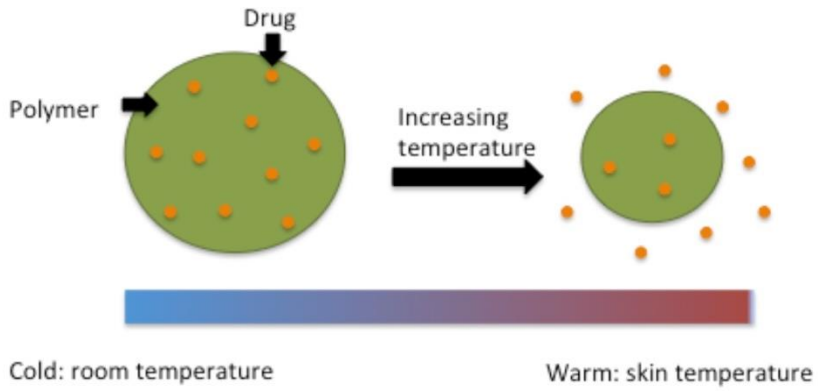

Figure 24: Drug release from thermo-responsive nanopolymers

The encapsulated drug gets expelled from the nanopolymer as consequence from the volume decrease that take place above a certain temperature threshold (around 32 °C for the applied PolyNIPAm-based polymers). Figure provided by Dr Dolca Fabregat-Montfort (SBCS, QMUL).

(a)

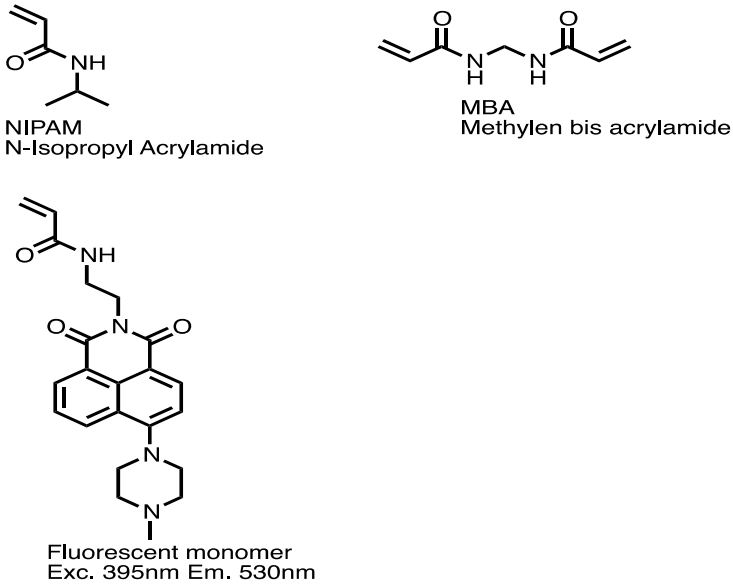

(b)

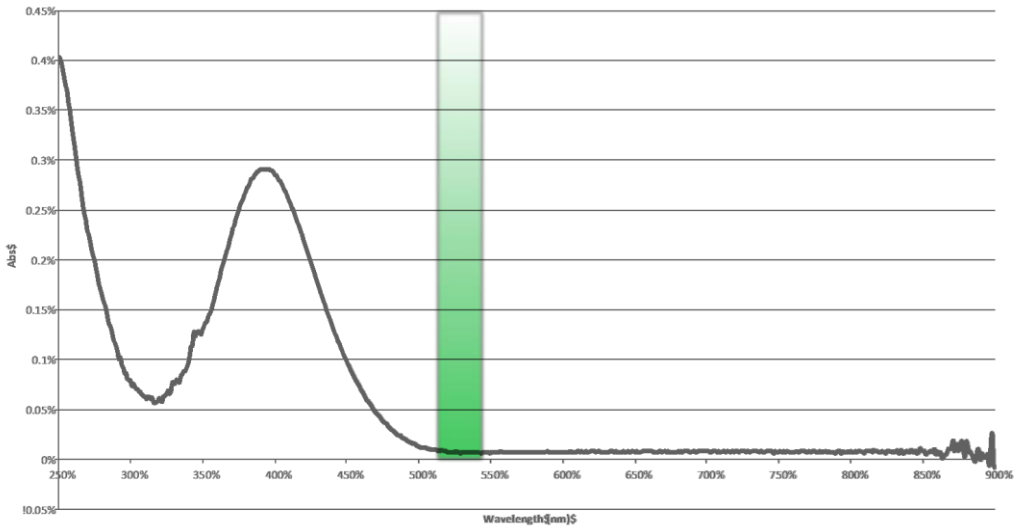

Figure 25: Composition of fluorescently labelled nanopolymers

Fluorescent nanopolymers were synthesised by crosslinking NIPAM monomers with MBA and the covalent linkage of fluorescent monomers (a). For imaging purposes, the nanopolymers displayed an excitation peak at 395nm, resulting in green fluorescence at around 530nm (b). Data provided by Dr Dolca Fabregat-Montfort (SBCS, QMUL).

2.3. Using Explant Skin and Organotypics for Topical Particle Application

For the topical application of nanopolymer solutions normal skin was obtained as surplus material from plastic surgeries, transported in saline solution and processed under sterile conditions no later than 6 hours after surgery. Whole skin was separated from subcutaneous fat tissue and divided into 4cm^2 pieces (Figure 26a). These pieces were either placed in a PBS-containing 6well plate for direct application or flash frozen on dry ice and stored at -80°C for later experiments. Sterile metal rings were used to create a reservoir for the applied solution. In addition to firmly pressing them unto the tissue the bottom edge was also coated with high-vacuum silicon grease (Dow Corning) in order to stick the components together and create a biologically inert and hydrophobic seal against leakage of the applied solution over time (Figure 26b). Organotypics were prepared in a similar fashion: after two-weeks culture, 4m plastic cloning rings were pressed into the organotypic with silicon grease acting as adhesive sealant (Figure 26c).

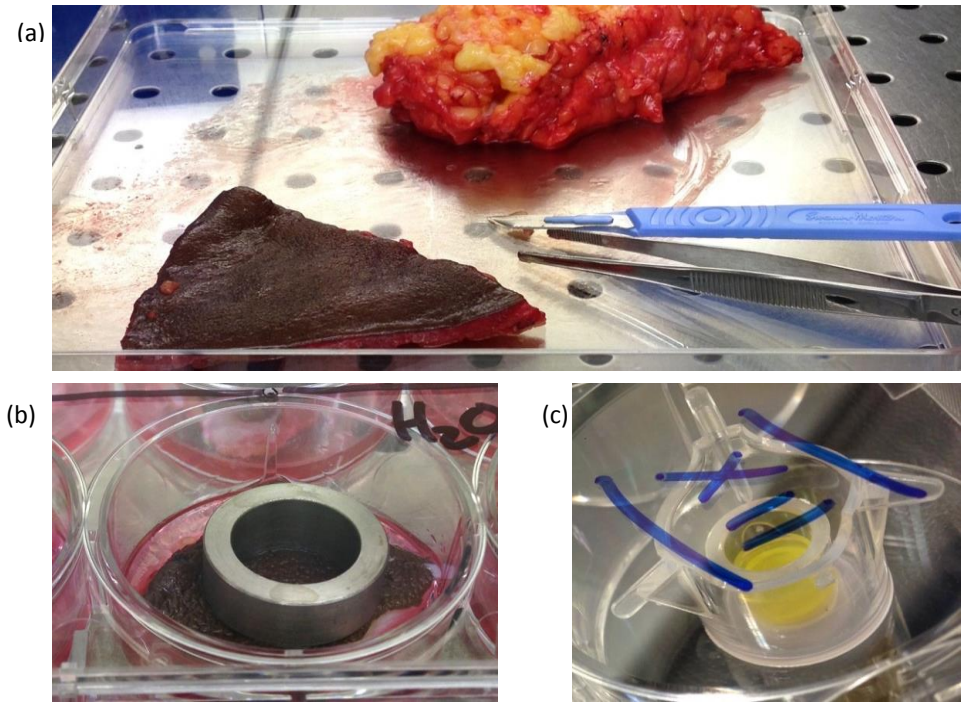

Figure 26: Topical application of polymer solutions on explant skin and organotypics
Fresh explant skin, received from plastic surgery, was cleaned from subcutaneous fat (a), divided into 4cm^2 pieces and placed in a 6well plate with PBS. A metal ring (with silicon grease applied to the bottom edge) was then pressed unto it in order to form a reservoir for the topically applied solution (b). Similarly, fully differentiated organotypics were kept in their culture inserts and a small-diameter plastic ring (again with silicon grease applied to the bottom edge) placed on top to allow for the topical application of polymer solutions (c).

The fluorescently labelled nanopolymers were prepared as described above and reconstituted for this application's purpose by solubilising them in an aqueous solution, containing 2% DMSO or BA for selected samples at 1 mg/ml. Polymer solutions were kept on the samples for up to 48 hours at 37°C and humidified conditions in a warm room before being discarded and the tissue samples being washed in PBS and processed for cryo sections. As a general control for the barrier function of skin or organotypic samples a highly fluorescent 1mM solution of Lucifer Yellow (LY, Sigma-Aldrich) in PBS was used for parallel topical application.

2.4. Tissue Processing and Sectioning

2.4.1. Preparation of Cryo Sections

Treated skin and organotypic samples were washed in PBS and then submerged in OCT embedding medium (VWR) inside plastic embedding moulds. Sample-containing moulds were then placed directly on dry ice and kept until completely frozen through before being stored at -80°C. A cryotom (Bright OTF5000) was used to prepare 5µm thick full-diameter cross sections of the embedded samples, which were placed on surface-treated microscopy slides (VWR Superfrost plus) and again stored at -80°C until staining.

2.4.2. Preparation of Paraffin Sections

For paraffin embedding, skin and organotypic samples were first washed in PBS before being fixated in 4% paraformaldehyde (PFA) for 2 hours at room temperature (RT). Samples were then transferred into 70% ethanol and kept until further processing (up to 4h). Overnight processing of the samples was performed in a VIP™ 5 Vacuum Infiltration Processor (Tissue-Tek) and involved a series of dehydration steps (Table 8). The following morning, the fixed and dehydrated tissue was taken

from the 60°C paraffin bath and embedded in paraffin blocks via quick freezing. The sample blocks were stored at RT and later on cooled down to 4°C for sectioning. 5µm thick sections were transferred from the microtome (Leica RM2235) unto surface-treated microscopy slides via a 37°C water bath and kept at RT until further usage.

Table 8: Steps for automated tissue processing

Step	**Solution**	**Temperature**	**Time**
1	70% Ethanol	RT	1 hour
2	70% Ethanol	RT	1 hour
3	80% Ethanol	RT	1 hour
4	95% Ethanol	RT	1 hour
5	100% Ethanol	RT	1 hour
6	100% Ethanol	RT	1 hour
7	100% Ethanol	RT	1 hour
8	100% Ethanol	RT	1 hour
9	Xylene	RT	1 hour
10	Xylene	RT	1 hour
11	Paraffin	60°C	1 hour
12	Paraffin	60°C	1 hour
13	Paraffin	60°C	1 hour
14	Paraffin	60°C	until embedding

2.5. Staining Techniques

2.5.1. Histological Staining (Haematoxylin & Eosin)

For haematoxylin & eosin (H&E) staining of paraffin sections, the sections were first de-paraffinised and rehydrated by transferring them through a series of two times xylene, 100% ethanol, 90% ethanol, 70% ethanol and de-ionised water (3 minutes for each step). From the de-ionised water, the sections were then transferred to a

solution of Gill's haematoxylin (Sigma-Aldrich) for 5 minutes before being blued in running tap water for 10 minutes. After the blueing the sections were quickly dipped in de-ionised water and then submerged in eosin Y (Sigma-Aldrich) for 2min. Subsequently, the sections underwent a dehydration series (same steps as before, but in reverse and 1 minute each) before being air dried and mounted in xylene-containing Entellan mounting medium (Millipore).

In the case that cryo sections had to be used instead of paraffin sections, they were first brought to room temperature, washed once with PBS in order to wash of the OCT embedding medium and then fixated with 4% PFA for 30min at RT. The sections were then washed in de-ionised water and transferred to haematoxylin. From there on the protocol was identical to the one for paraffin sections.

2.5.2. Immunocytochemistry (ICC)

In preparation of the eventual staining, monolayer cells were cultured on sterile glass cover slips (VWR) in 12well culture plates. After culturing, and potential treatment, cells on cover slips were first washed once in PBS and then fixated with 4% PFA (10min at RT) while still inside the culture plates. This was followed by three quick washes with PBS and a permeabilisation step in 0.1% Triton X-100 (Sigma-Aldrich), followed by another three PBS washes. After blocking with 4% normal goat serum (NGS; Sigma Aldrich) for 30 minutes at RT, the coverslips were taken out of the culture plate and transferred upside down unto 100µl drops of primary antibody solution which consisted of the respective antibody, or two antibodies in case of co-staining, in 4% NGS (Table 12). The cells were incubated with the primary antibody overnight at 4°C, washed three times with PBS and incubated with secondary antibodies in blocking solution (Table 13) for 2 hours at RT (still as inverted drop setup). After a last set of three PBS washes (the first one containing 0.1 µg/ml DAPI in PBS for 5 minutes) the coverslips were mounted with Shandon Immu-Mount (Thermo Fisher) mounting medium on microscopy slides, air dried at RT and then stored at 4°C until imaging.

In case of imaging cells treated with fluorescent nanopolymers, DAPI got replaced by 10µM DRAQ5 (BioStatus / $Ex\lambda_{max}$= 600nm; $Em\lambda_{max}$= 694nm) as nuclear counterstain in order to avoid overlap with the excitation spectrum of the nanopolymers at around 400nm.

2.5.3. Immunohistochemistry (IHC)

For antibody staining on sections, the initial steps are different depending on whether the sections are cryo or paraffin. Cryo sections were taken from -80°C and brought to RT, before they were hydrated in de-ionised water, fixated with ice-cold Methanol/Acetone (1:1) for 5 minutes and washed three times in PBS. Paraffin sections were de-paraffinised and rehydrated as described above ("Histological Staining") before undergoing an antigen retrieval procedure by being incubated in trypsin-EDTA for 30 minutes at 37°C. The slides were then washed three time in PBS and thereby brought back to RT. The remaining steps were identical for both cryo and paraffin sections. After blocking of the sections with 4% NGS for 2 hours at RT, they were incubated with the primary antibodies (up to two antibodies of different host species together in blocking solution) overnight at 4°C. The sections were washed three times with PBS and then incubated with secondary antibodies (in blocking solution) for 1 hour at RT. The first of the following three PBS washes (5 minutes each) contained 0.1 µg/ml DAPI as nuclear counterstain; subsequent to this step the sections were mounted, covered by glass cover slips and air dried at RT before being stored at 4°C until imaging. Cryo sections of nanopolymer- or LY-treated samples were fixated in the same way as for other stainings and then directly counterstained with 10µM DRAQ5 for 5 minutes at RT before being washed twice in PBS and mounted.

2.6. Imaging

ICC and IHC stainings were imaged using either a Leica DM500B epifluorescence microscope with MetaMorph Basic (Molecular Devices) or Zeiss 710 Z2 laser scanning confocal microscope with ZEN (Zeiss). Images were taken at 100x to 630x magnification using the same acquisition settings for all samples of one set. Post-processing of the images was performed with ImageJ v1.50b (National Institute of Health, USA).

2.6.1. Quantitative Image Analysis of Penetration on Skin and Organotypics

For the quantitation of nanopolymer penetration into treated tissue samples images of nuclear counterstained cryo sections were analysed in ImageJ. In a first step the epidermal area of interest was defined via nuclear staining (discarding outlying fluorescence of stratum corneum and dermis) and the green fluorescent signal isolated. The green signal was then transformed into a binary threshold image (using the same threshold for all the compared images), quantitated via particle analysis and related to the size of the epidermal area of interest (Figure 27).

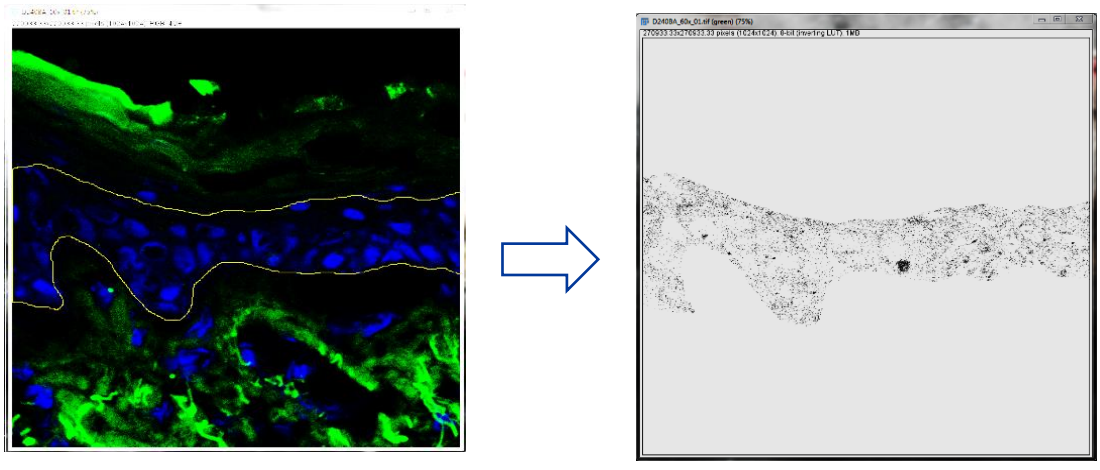

Figure 27: Quantification of green fluorescent signal for polymer penetration in cryo sections.
For the quantification of nanopolymer localisation, first the epidermal area of interest (yellow line) was determined via the blue DRAQ5-staining of keratinocyte nuclei. In this area the green channel was isolated and transformed into a binary threshold image which could then be quantified in relation to the area size.

2.6.2. Quantitative Image Analysis of Colocalisation in Monolayer Cells

Colocalisation analysis of fluorescent nanopolymers with antibody-stained compartments in monolayer keratinocytes was performed in ImageJ by using two specialised plugins: *JACoP* (Bolte and Cordelières 2006) and *Intensity Correlation Analysis* (http://wwwfacilities.uhnresearch.ca/wcif/imagej/colour_analysis.htm). For the analysis, 630x magnified image stacks (8 single images in 0.5µm intervals along the z-axis) were taken on the Zeiss 710 Z2 and underwent analysis in parallel using the same thresholds and parameters for all compared samples.

By using the specialised plugins, several coefficients were generated for the individual images. Pearson Coefficient (PsCo) (Manders et al. 1992) and Li's Intensity Correlation Quotient (Li's ICQ) (Li et al. 2004) are general co-localisation coefficients that correlate intensity spikes in the red and green channel of the image and express the global degree of colocalisation in a single numeric value (-1 to 1 for Pearson and -0.5 to 0.5 for Li, with positive values indicating a degree of colocalisation and negative values exclusion) . Manders Coefficients 1 and 2 break down the fraction of co-localising pixels for each channel individually, allowing for a separate analysis of the two co-localising elements (Manders et al. 1993).

2.7. Western Blotting

In order to perform quantitative protein expression analysis on monolayer cells established western blotting protocols were used. As a first step protein lysates from monolayer cells were acquired by using a specified lysis buffer (Table 9). Culture plates with confluent cells were put on ice and washed twice with ice cold PBS before adding 90 °C hot lysis buffer (100 µl per x cm^2). The cells were scraped off and pipetted with the lysis buffer into eppendorf tubes before aliquoted and stored at -80 °C. Protein concentrations were determined using a Bradford assay kit (Bio-Rad protein assay) according to manufacturer's instructions. Running and stacking gels (Table 10) were sequentially prepared (15wells per gel) and lysates loaded into them at 30µg protein per well. Prior to the loading the lysate aliquots were transferred

directly from -80°C unto a heating block at 95°C and kept at this temperature for 5min for further denaturation of the proteins. The loaded gels were run in running buffer (Table 11) and at 12mA per gel (up to two gels per running tank) until proteins were sufficiently resolved, judged by the co-loaded protein marker (Amersham Rainbow Molecular Weight Marker, GE Healthcare). Proteins were subsequently transferred unto nitrocellulose membranes in transfer buffer (Table 11) at 4°C over night (80mA per transfer tank). Protein-containing membranes were then blocked with 5% milk powder in PBST (PBS + 0.05% Tween-20) before being cut into appropriate segments and incubated with the individual primary antibodies (Table 12) over night at 4°C. After washing the membranes three times with PBST (10 minutes each time) horseradish peroxidase(HRP)-conjugated secondary antibodies (Table 13) were incubated on the membranes for 2 hours at RT, followed by another three washing steps. Stained protein bands were then detected by using Immobilon ECL Substrate (Millipore) and the ChemiDoc MP System (Bio-Rad) according to the manufacturer's instructions. Comparative quantitation of imaged bands was performed via ImageJ (integrated gel analysis tool).

2.8. Statistical Analysis

Where applicable, error bars in graphs denote the standard deviation for three independent measurements as part of one single experiment (i.e. 'technical replicates').

Table 9: Composition of lysis buffer

Ingredient	**Supplier**	**Final concentration**
Tris	Sigma-Aldrich	1 M
Sodium chloride	Sigma-Aldrich	2.5 M
Glycerol	Sigma-Aldrich	10 %
Glycerophosphate	Sigma-Aldrich	0.5 M
Tween-20	Sigma-Aldrich	1 %
Nonidet P40	Sigma-Aldrich	0.5 %
cOmplete ™ Protease inhibitor (EDTA-free)	Sigma-Aldrich	1 tablet per 50 ml

Table 10: Composition of running and stacking gels for SDS PAGE

Ingredient	**Supplier**	**Final concentration (running gel)**	**Final concentration (stacking gel)**
Protogel Acrylamide mix	National Diagnostic	12 %	5 %
Tris-HCl (pH 6.8)	BioVision	---	0.13 M
Tris-HCl (pH 8.8)	BioVision	0.375 M	---
SDS	Sigma-Aldrich	1 %	
Ammonium persulfate	Sigma-Aldrich	1 %	
TEMED	Sigma-Aldrich	0.1 %	

Table 11: Composition of running and transfer buffer

Ingredient	**Supplier**	**Final concentration (running buffer)**	**Final concentration (transfer buffer)**
Tris-HCl (pH 8.9)	Sigma-Aldrich	25 mM	
Glycine	Sigma-Aldrich	190 mM	
SDS	Sigma-Aldrich	0.1 %	---
Methanol	Sigma-Aldrich	---	20 %

Table 12: List of primary antibodies

Marker protein	**Host species**	**Supplier**	**Product no.**	**Concentration (ICC / IHC)**	**Concentration (WB)**
ABCA 1	rabbit	Abcam	ab125064	1:500	1:1000
ABCA 12	rabbit	Abcam	ab98976	1:100	1:1000
ADAM 17	rabbit	Abcam	ab2051	1:100	n/a
Connexin 26 (Cx26)	mouse	Thermo Fisher	13-8100	1:200	n/a
CK10	mouse	Abcam	ab9025	1:200	1:1000
CK14	mouse	CRUK	LL001	1:50	1:1000
CK16	rabbit	Abcam	ab76416	1:200	n/a
EGFR	rabbit	Abcam	ab2430	1:50	n/a
GAPDH	rabbit	Abcam	ab9485	n/a	1:1000
GM130	rabbit	Abcam	ab52649	1:100	n/a
Involucrin	mouse	Abcam	ab68	1:100	1:1000
iRHOM2	rabbit	Sigma-Aldrich	HPA018080	1:200	n/a
Ki67	rabbit	Abcam	ab15580	1:500	n/a
LAMP2	mouse	Abcam	ab25631	1:100	n/a
TGN46	mouse	Abcam	ab2809	1:200	n/a
TGM1	rabbit	Sigma-Aldrich	HPA040171	1:200	1:1000
Vinculin	rabbit	Abcam	ab125064	n/a	1:2000

Table 13: List of secondary antibodies

Target species	**Conjugate**	**Host species**	**Supplier**	**Product no.**	**Concentration (ICC / IHC)**	**Concentration (WB)**
mouse	Alexa 488	goat	life technologies	A21121	1:600	n/a
mouse	HRP	goat	DAKO	P0447	n/a	1:4000
rabbit	Alexa 546	goat	life technologies	A11010	1:600	n/a
rabbit	HRP	goat	DAKO	P0448	n/a	1:4000

3. Results

3.1. Establishment of an Organotypic Keratinocyte Culture Model

3.1.1. Introduction

A first necessary step of the project was the identification of a suitable protocol for the organotypic culture of various immortalised keratinocyte cell lines. Different approaches regarding the supporting matrix were hereby used with the aim of producing a viable skin equivalent, the quality of which was judged through the comparison with explant skin cultures as a gold standard (Figure 28). Since the model has to be suitable for the assessment of topical compound applications, focus was placed on a variety of supra-basally expressed differentiation markers such as CK10, Involucrin and TGM1. In addition, the highly fluorescent, hydrophilic dye Lucifer Yellow was topically applied to samples in order to perform a functional assessment of the permeability barrier, with the dye solution being retained in the stratum corneum of the treated sample in the presence of a functional epidermal permeability barrier. Proliferation markers of the more basal layers such as CK16 and Ki67 were also used to assess the possibility of modelling hyperproliferative skin diseases.

3.1.2. Alvetex-based Model

The first attempt at generating an organotypic keratinocyte culture involved the application of commercially available Alvetex culture inserts: 200µm thick, porous polystyrene scaffold for the seeding and subsequent submerged or airlift culture of cells. Initially, a variety of culture periods were used to generate epidermal (only containing immortalised K17 keratinocytes) and dermal-epidermal (combination of primary human fibroblasts and K17 keratinocytes) equivalents, using histological H&E staining to assess the resulting models (Figure 29). Epidermal equivalents were cultured for one (Figure 29 a), two (Figure 29 b) and three weeks (Figure 29 c) in airlift conditions. A visible onset of an eosinophilic red stratum corneum-like upper layer

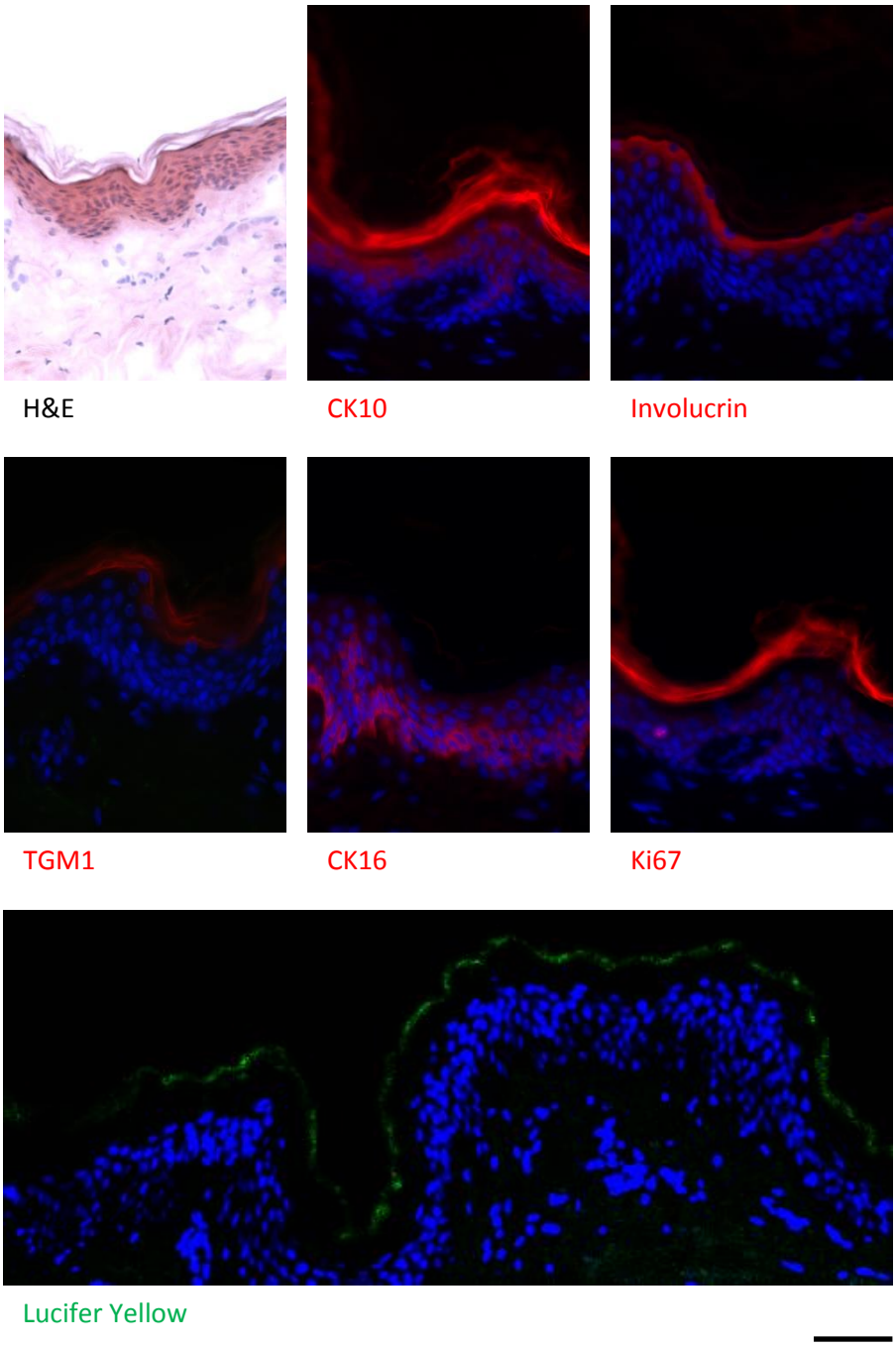

Figure 28: Protein marker expression and barrier function in explant skin

Explant skin that has been kept in a tissue culture incubator (37°C; 5% CO_2; humidified) for up to 48 hours shows a typical expression of marker proteins. Differentiation-associated CK10 and Involucrin are expressed suprabasally and TGM1, as a marker for terminal differentiation, can be found in the uppermost layers of the epidermis. Proliferation markers CK16 and Ki67 are restricted to the lower epidermal layers (disregarding a false background staining of the stratum corneum in case of Ki67). The topically applied green fluorescent dye Lucifer Yellow is entirely retained by the stratum corneum. Scale bar represents 50µm.

was detected after two weeks but no striking signs of layering / stratification of the keratinocytes inside the Alvetex scaffold. Dermal- epidermal models were generated through the initial seeding of fibroblasts in the scaffold followed by the addition of keratinocytes after a set culture period and subsequent culturing of the combined model. The pre-incubation of fibroblast for one week seemed to generally yield viable models with visible incorporation and stratification of added keratinocytes. Whereas the subsequent culture of the combined model for one additional week resulted in an even distribution of keratinocytes across the scaffold and appearance of flattened cells building up an uppermost stratum corneum-like layer (Figure 29 d), the elongation of the combined culture period to three weeks increased this effect: keratinocytes appeared to settle mostly in the upper parts of the scaffold and the uppermost layer was more pronounced and included first signs of shedding as well (Figure 29 e). An initial three week-culture of fibroblast followed by the addition of keratinocytes for another week did not seem to result in a viable equivalent, with minimal signs of incorporated keratinocytes (Figure 29 f).

After narrowing down the culture conditions to a few promising alternatives, one of the combinations (one week of fibroblasts followed of three weeks of combined culture) was further assessed in regards to marker expression and permeability barrier function (Figure 30). The pattern of differentiation-associated protein expression appeared to be tendentially right, with the basal marker CK14 being restricted to the lower parts of the epidermal portion of the organotypic and Involucrin being mostly expressed in the uppermost layers. However, the topically applied Lucifer Yellow though was exclusively found in the bottom part of the organotypic, indicating a diffusion of the dye throughout the organotypic and therefore the absence of a functional permeability barrier in the Alvetex-based model.

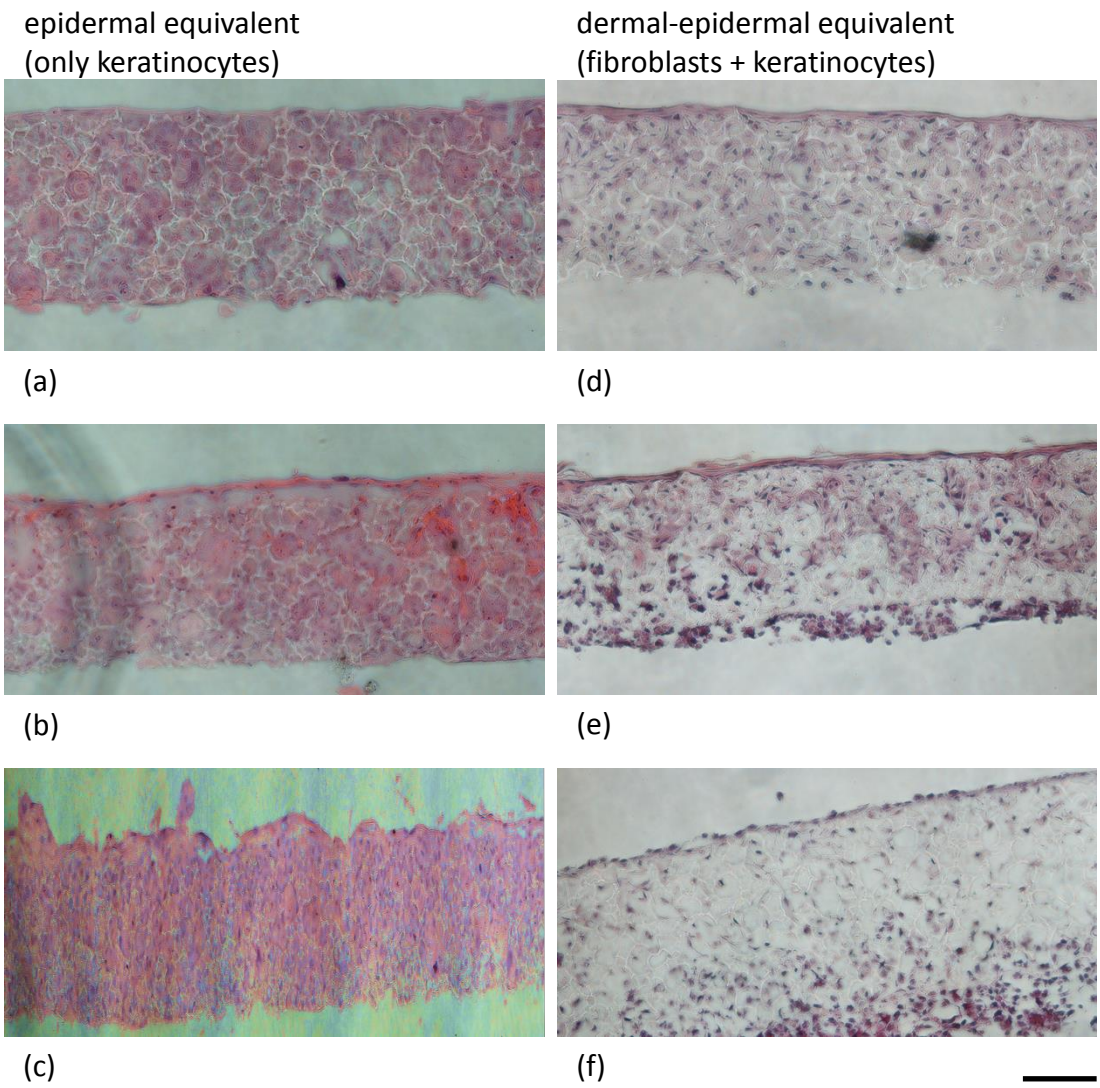

Figure 29: Histology of Alvetex-based organotypic after different incubation times

Epidermal equivalents, containing only keratinocytes, were cultured for one (a), two (b) and three weeks (c) under airlift conditions. H&E staining indicates an increasing degree of stratification in the upper layers over time. Different combinations of dermal-epidermal equivalents were tested: one week of fibroblasts followed by another week after the addition of keratinocytes (d), one week of fibroblasts followed by three weeks after the addition of keratinocytes (e) and three weeks of fibroblasts followed by one week of keratinocytes (f); resulting in vastly different histologies as a result. Scale bar represents 100µm.

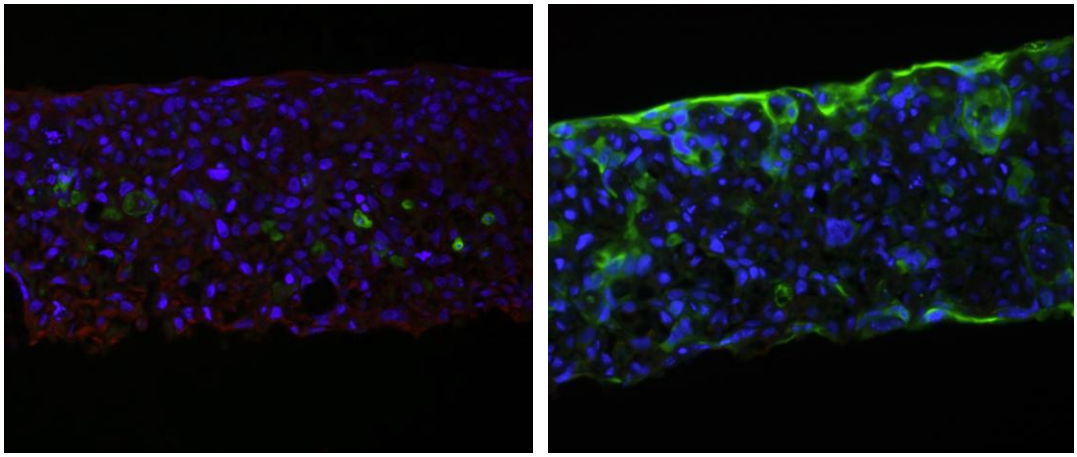

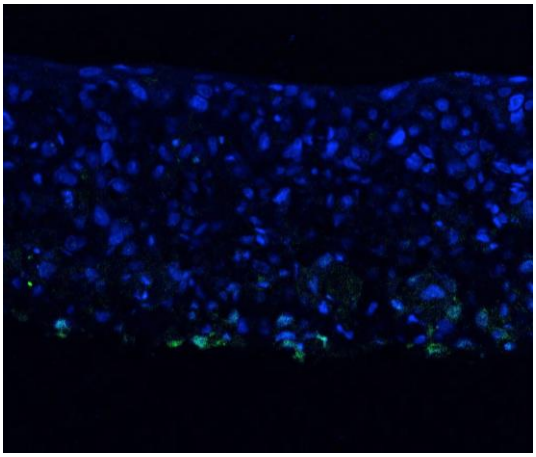

Figure 30: Marker expression and permeability barrier in Alvetex-based organotypics
Alvetex-based epidermal equivalents were cultured for two weeks in airlift conditions and subsequently tested for expression of protein markers and the presence of a permeability barrier. Basal marker CK14 was found in the lower parts of the organotypic and differentiation marker Involucrin mostly restricted to the uppermost layers. Traces of the topically applied dye Lucifer Yellow are found in the lowermost layer of the organotypic. Scale bar represents 100µm.

3.1.3. Collagen-based Model (Normal Phenotype)

Due to the Alvetex-based model not forming a functioning epidermal permeability barrier, another approach using a collagen 1-scaffold with incorporated fibroblasts as dermal equivalent to seed epidermal keratinocytes on was used. Applying this model on the same K17 keratinocytes resulted in a superior organotypic in regard to histology and barrier function (Figure 31). The epidermal portion of the organotypic displayed an epidermis-like arrangement of keratinocytes, with signs of different

layers due to change in orientation of the stacking cells from vertical to horizontal and the build-up of an anucleated, strongly eosinophilic upper layer similar to the stratum corneum in skin explants. Consequently, topically applied Lucifer Yellow was retained in this uppermost layer of the organotypic, again similarly to the retention of the dye in the stratum corneum of explant skin.

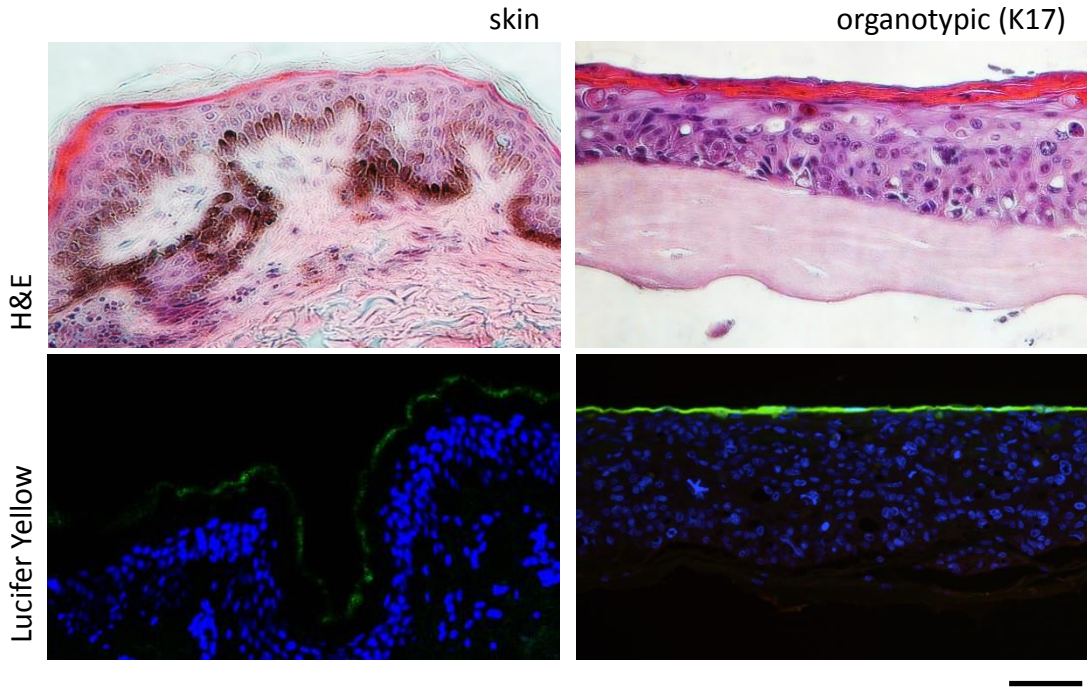

Figure 31: Histology and barrier function in explant skin and normal-phenotype organotypic
Organotypics based on immortalised normal keratinocytes show a layered, stratified arrangement of cells including an eosinophilic, anucleated uppermost layer, similar to the epidermal structure of control skin. Topically applied green fluorescent Lucifer Yellow is retained by the uppermost layer of the organotypic as well as the stratum corneum of explant skin. Scale bar represents 50µm.

Subsequently, the collagen-based model was used in conjunction with a variety of immortalised keratinocyte control cell lines (K17, HaCaT, nTERT, NEB1) as well as primary keratinocytes. The resulting organotypics were very different when it came to general histology of the epidermal portion and expression of selected marker proteins (Figure 32). Regarding the histology of the various organotypics the most striking difference is the degree of invasion of keratinocytes into the underlying dermal collagen part and connected to this the presence of a defined basal layer. Whereas nTERTs show no signs of invasion and display a lowermost layer of cuboidal, vertically oriented keratinocytes, HaCaTs and NEB1s have islets of invading cells in

addition to a fairly defined lowermost layer and primary keratinocytes appear with a more bulk-like invasion including a basal layer inside these bulks. K17 cells on the other hand tended to result in a rather disorganised, invasive phenotype. NEB1s that were grown directly on top of a PET membrane, without the addition of a dermal component, again display a histologically defined basal layer.

Signs of terminal differentiation into a stratum corneum-like uppermost layer also varied between the different organotypics. K17s resulted in a defined, strongly eosinophilic layer on top but this only occured to a lesser degree in primary keratinocytes and NEB1s, though the omission of the dermal component does seem to increase the stratification in the latter. HaCaTs and nTERTs show an onsetting flattening of cells in the uppermost layers. A common feature of all of the organotypic models is the tendency for epidermal thickening to varying degrees, with epidermal portions being comprised of more layers of keratinocytes than is typical for interfollicular skin. In regard to the differentiation-associated marker protein CK10, HaCaTs and NEB1s show an expression throughout the suprabasal layers of the epidermal portion while primary keratinocytes, K17s and NEB1 (without collagen) are more restricted towards the upper layers. Involucrin as another differentiation marker is suprabasally expressed in all the various organotypics. The more terminal differentiation-associated enzyme TGM1 is also expressed in all organotypics but whereas it is mostly restricted to upper layers in primary keratinocytes, K17, nTERT and NEB1 (without collagen) HaCaTs and NEB1s show a strong expression throughout all suprabasal layers. The hyperproliferation marker CK16 is predominantly found in the lower layers of primary keratinocyte, K17, HaCaT and nTERT organotypics.

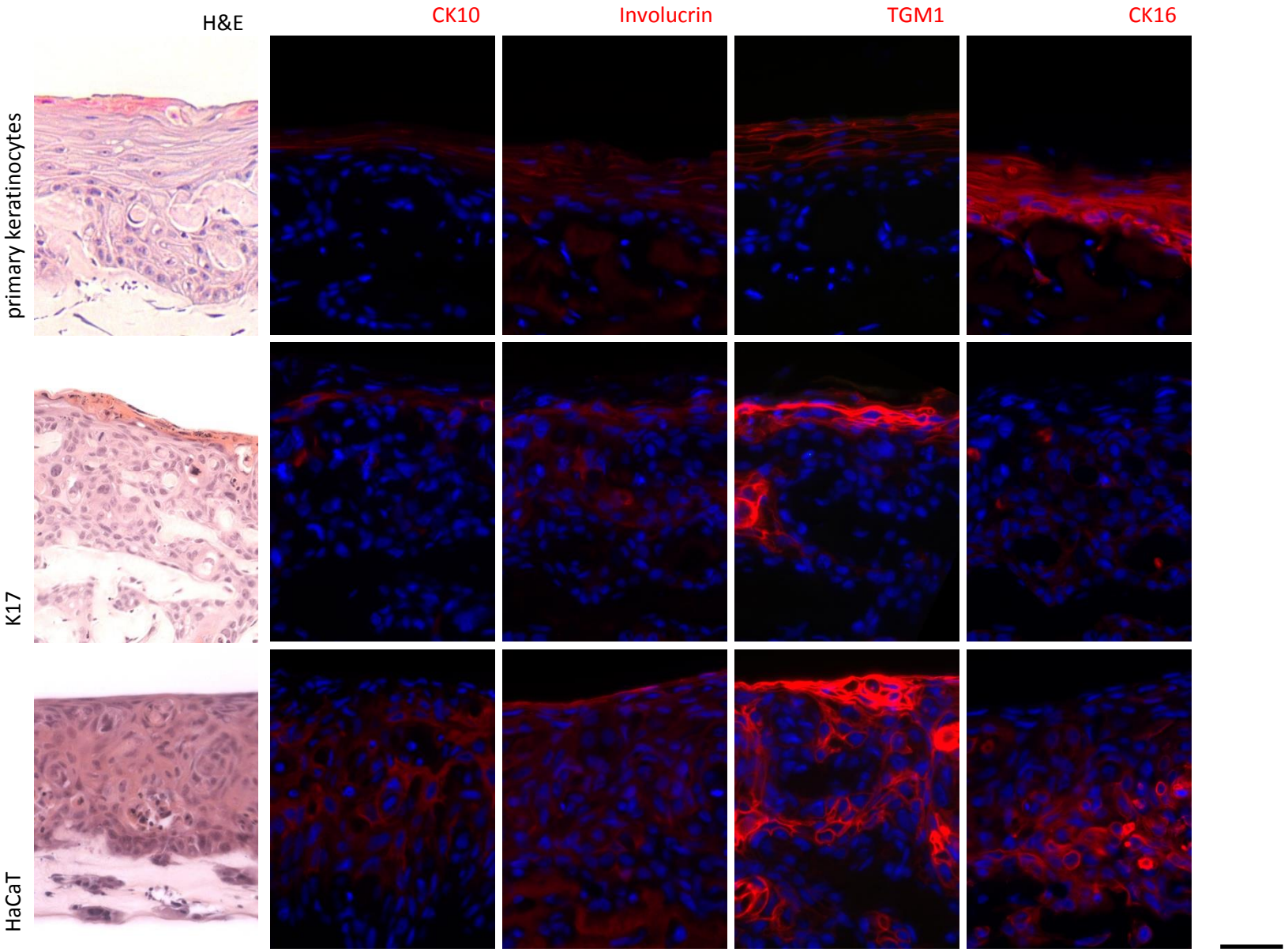
H&E
CK10
Involucrin
TGM1
CK16
primary keratinocytes
K17
HaCaT

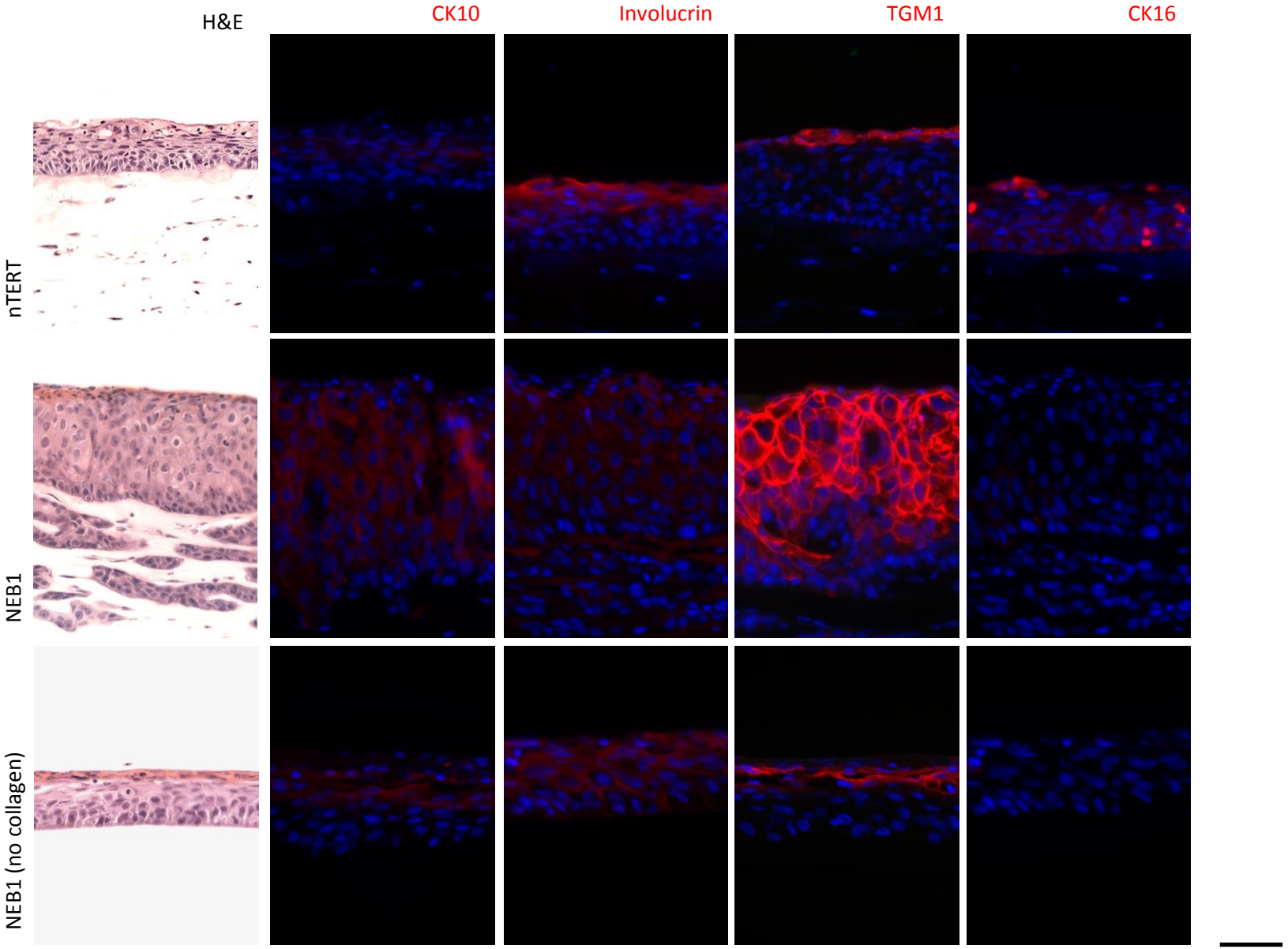
H&E
CK10
Involucrin
TGM1
CK16
nTERT
NEB1
NEB1 (no collagen)

Figure 32: Differences in histology and marker expression between normal-phenotype organotypics
Organotypics based on primary keratinocytes and a variety of normal, immortalised keratinocyte cell lines (K17, HaCaT, nTERT, NEB1) display striking differences in the expression of protein markers for differentiation (CK10, Involucrin, TGM1) and hyperproliferation (CK16). Scale bar represents 50µm.

In addition to comparing different cell lines in the organotypic model, organotypics for selected cell lines (K17, HaCaT, NEB1 with or without collagen scaffold) were cultured for one and two week periods in airlift conditions in order to track and compare the change of histology and differentiation marker expression over time (Figure 33). Histologically all the organotypics appear to develop a thickened epidermal portion in between day 7 and day 14 together with an increased degree of stratification in the upper layers. This is accompanied by a consolidation of differentiation markers CK10 and Involucrin, namely an increase in expression levels and/or spatial shift towards upper layers. TGM1 also displays a general increase in expression over time which in the case of HaCaT, NEB1 and to some degree K17 is combined with a spreading towards lower suprabasal layers. In the NEB1 configuration without a dermal equivalent TGM1 gets more restricted towards the uppermost layer of the organotypic after 14 days. K17 and HaCaT-derived organotypics display an increase in CK16 expression whereas NEB1 organotypics do not express CK16 even after 14 days of culture. Overall, despite general differences in histology and marker expression, all the various organotypics appear to show signs of increased differentiation and stratification when prolonging the culture time from 7 days to 14 days.

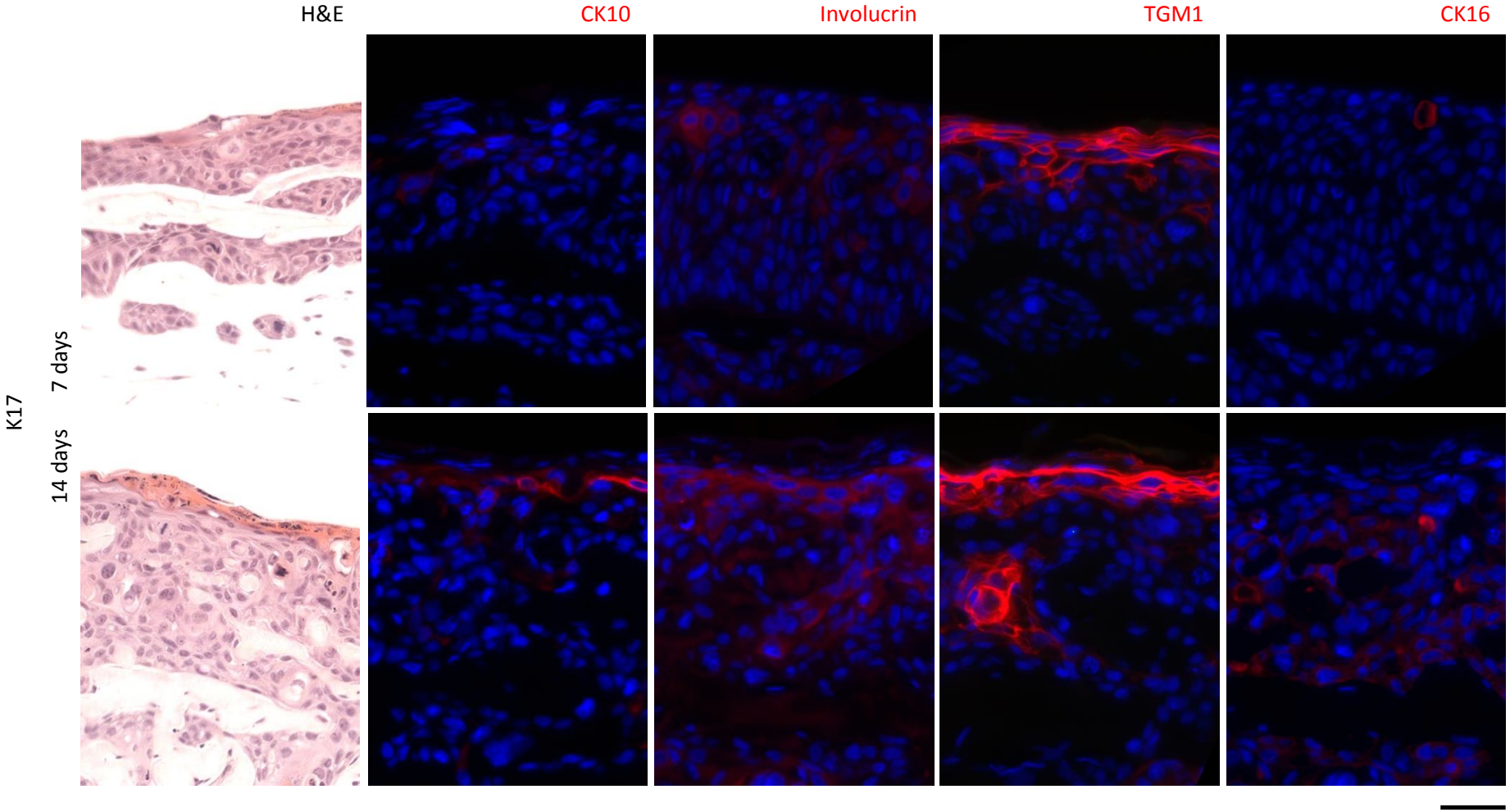
H&E
CK10
Involucrin
TGM1
CK16
K17
7 days
14 days

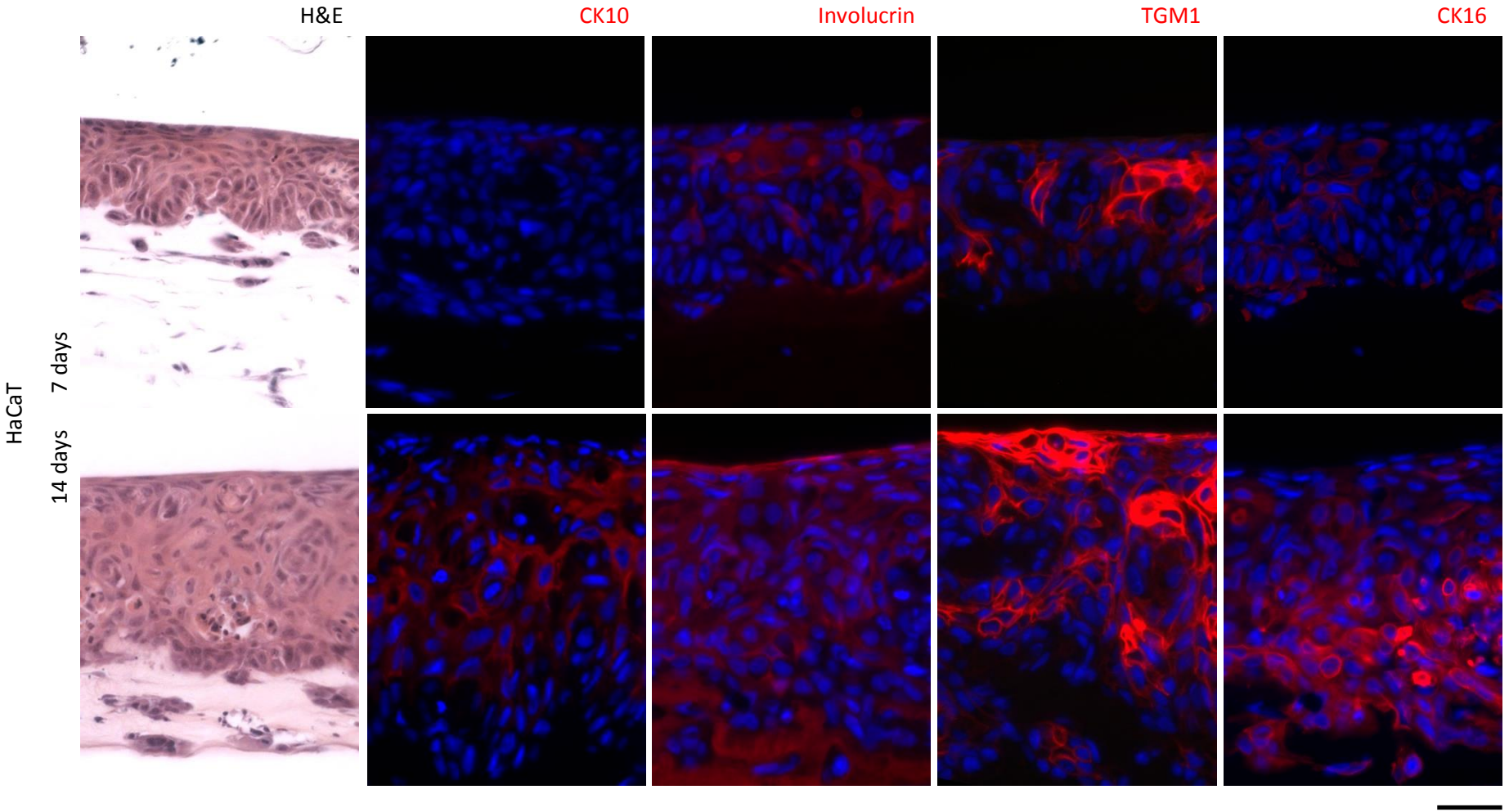
H&E
CK10
Involucrin
TGM1
CK16
HaCaT
7 days
14 days

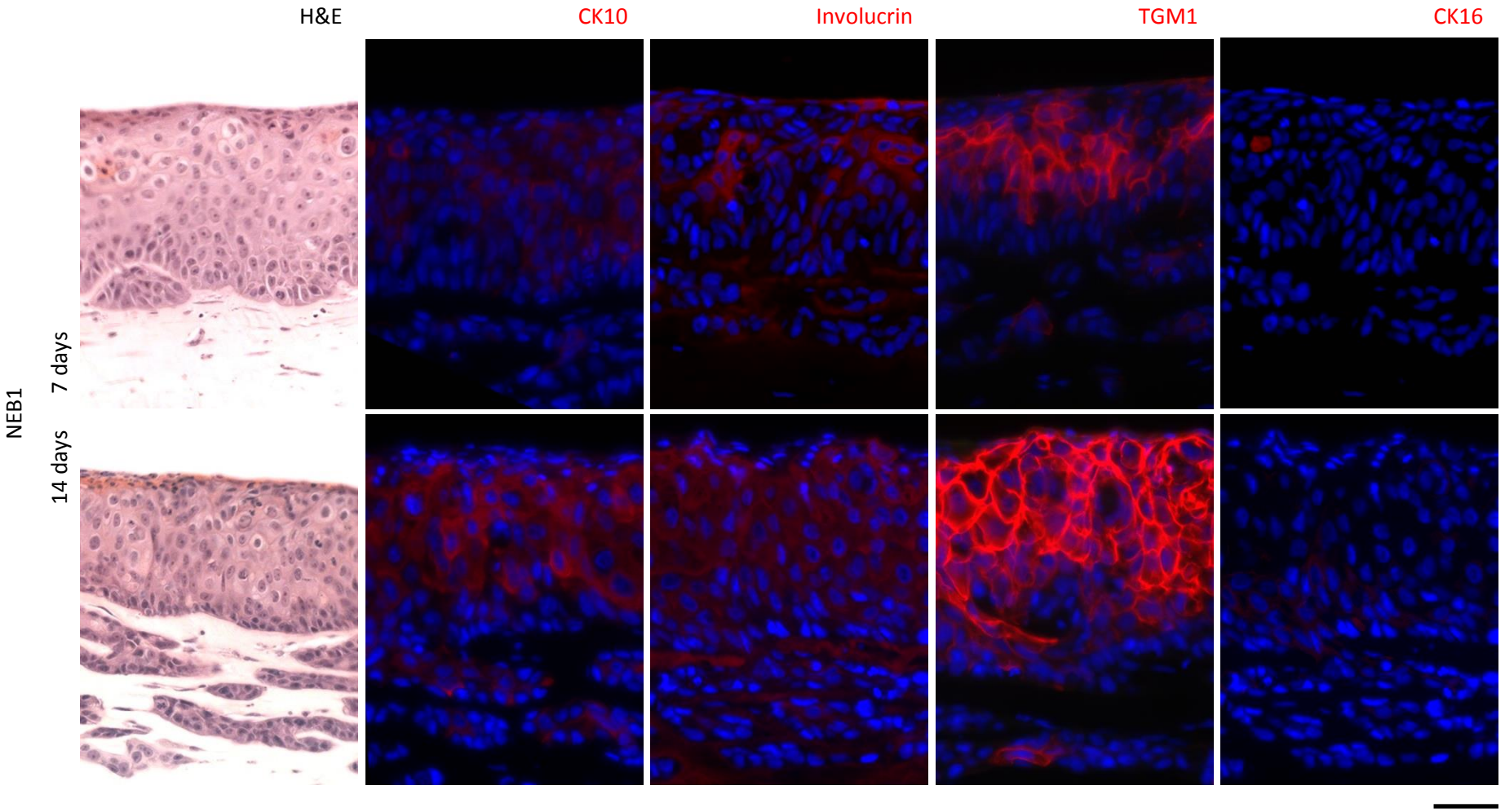
H&E
CK10
Involucrin
TGM1
CK16
NEB1
7 days
14 days

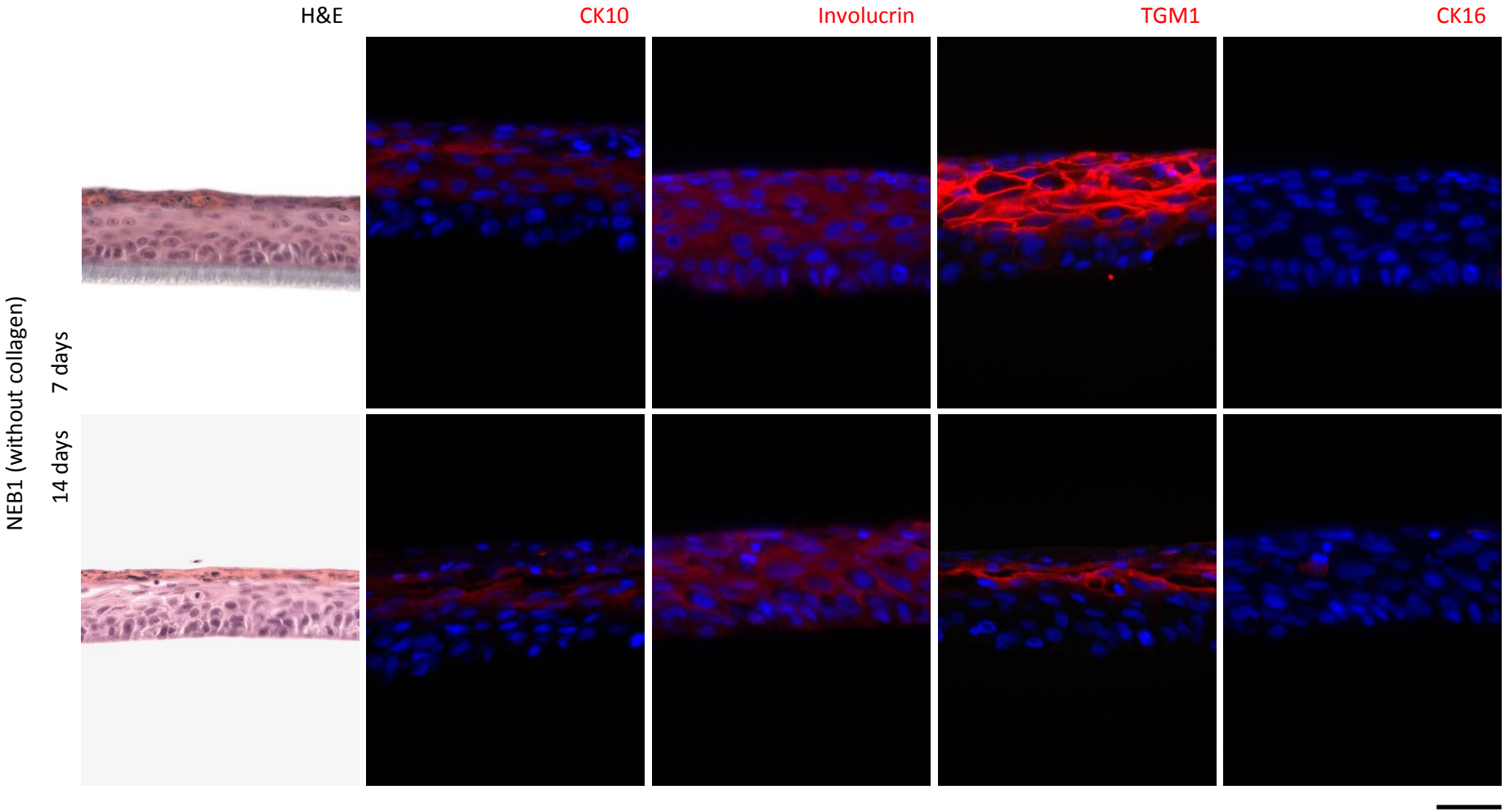
H&E
CK10
Involucrin
TGM1
CK16
NEB1 (without collagen)
7 days
14 days

Figure 33: Changes in protein expression of normal-phenotype organotypics over culture time
All keratinocyte cell line-based organotypics (K17, HaCaT, NEB1) exhibit a general upregulation and/or restriction to suprabasal layers of differentiation-associated markers (CK10, Involucrin, TGM1) in between 7 and 14 days of airlift culture. In the case of K17 and HaCaT this is accompanied by an increased expression of CK16 in the lower parts of the organotypic. All organotypics display signs of increased stratification in histological stainings with culture time. Scale bars represent 50µm.

3.1.4. Characterisation of Monolayer Keratinocytes in different Media

Since the use of different keratinocyte cell lines in the organotypic model yielded very varied results regarding the expression of marker proteins, monolayer cultures for K17, HaCaT, NEB1 and primary keratinocytes were stained for several protein markers and compared while also recapitulating the change from maintenance to differentiation medium which is part of the protocol for the generation of organotypic cultures (Figure 34). Brightfield images revealed similar changes in cell morphology as result of the medium switch: after the switch cells generally show a more flattened shape and presence of granules in the cytoplasm, with a more pronounced effect in primary keratinocytes which already start off in more flattened morphology. In regard to marker expression, K17 cells in maintenance culture have virtually no expression of differentiation markers CK10 and Involucrin, moderate levels of differentiation marker Loricrin and proliferation-associated Ki67 and ubiquitous expression of basal marker CK14 and hyperproliferation marker CK16. During the switch to differentiation medium this changes with a slight increase in the number of Ki67-positive cells, a stronger restriction of CK14 to the edge of colonies and the appearance of single Involucrin-positive cells. In the case of HaCaT cells there appears to be an increase in Loricrin and Involucrin-positive cells through the medium switch accompanied to a similar redistribution of CK14 expression as seen in K17 cells. NEB1 cultures displayed an increase in the number of CK10 positive cells whereas Involucrin and Loricrin seems mostly unaffected. Ki67 is more abundant after the medium switch while CK14 is absent before or after. Similarly, CK16 levels are very low compared to the other two cell lines. In primary keratinocyte cultures the switch to differentiation medium seems to induce a reduction in Ki67-positive cells and an increase in Involucrin expression.

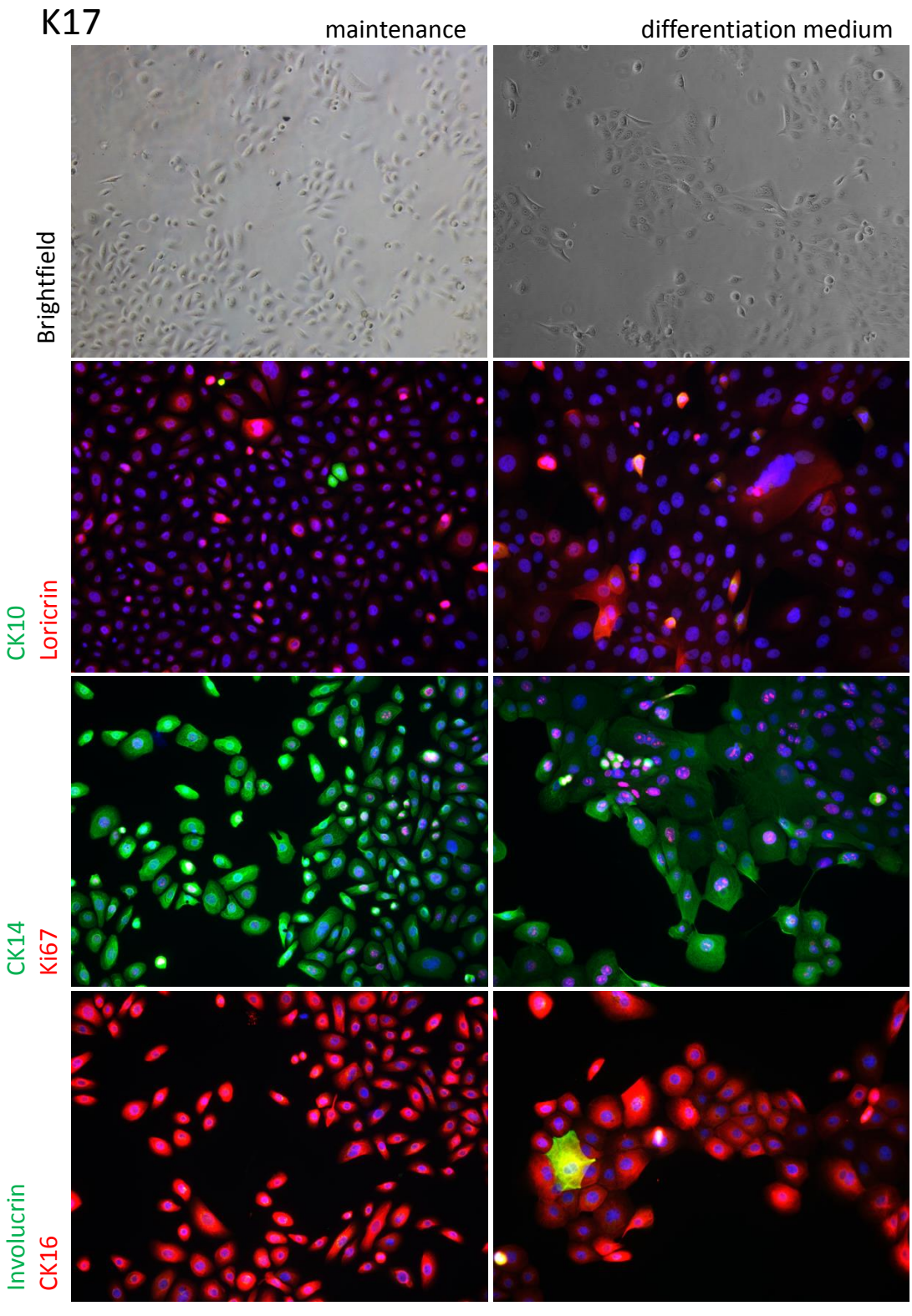
K17
maintenance
differentiation medium
Brightfield
CK10
Loricrin
CK14
Ki67
Involucrin
CK16

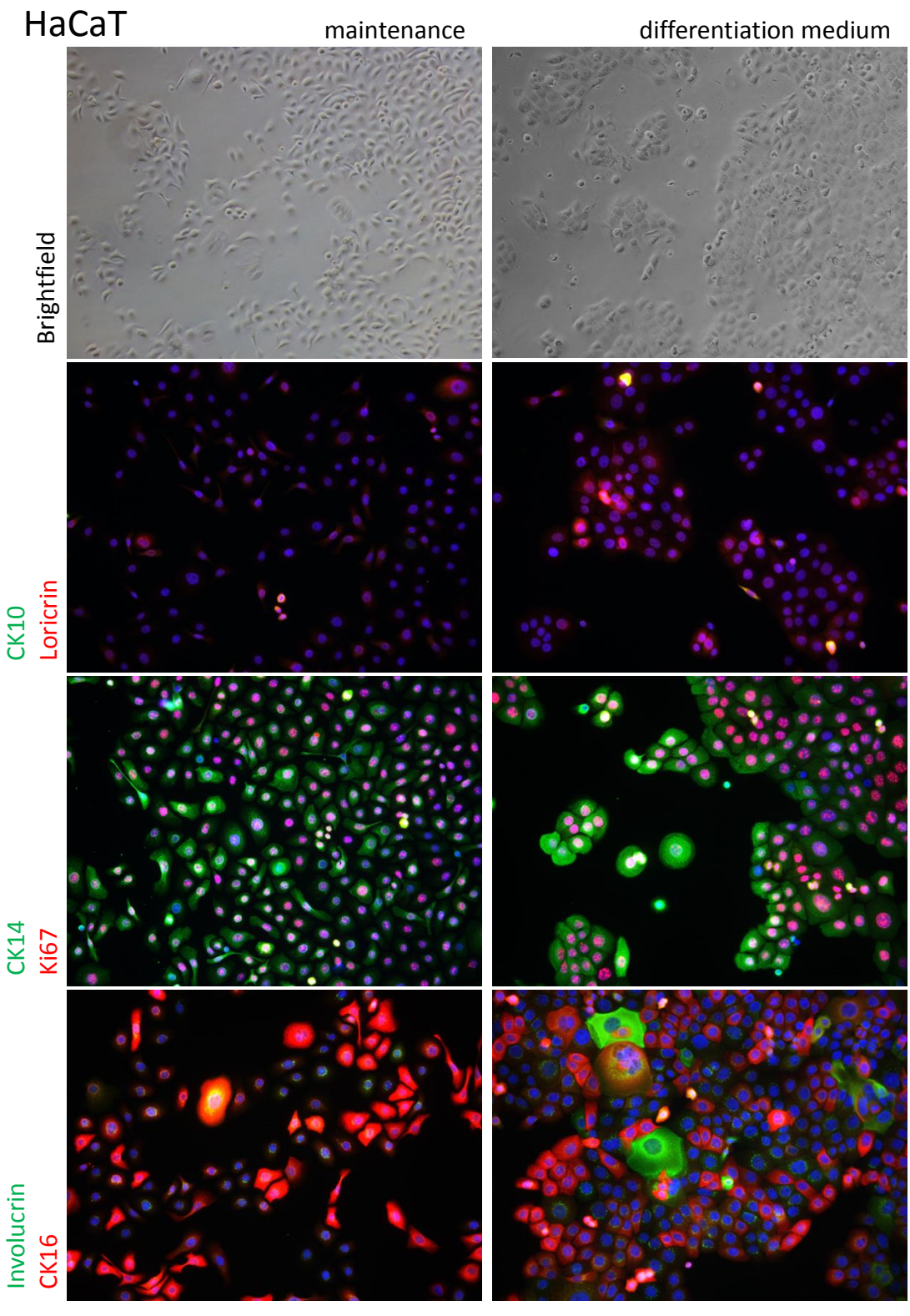
HaCaT
maintenance
differentiation medium
Brightfield
CK10
Loricrin
CK14
Ki67
Involucrin
CK16

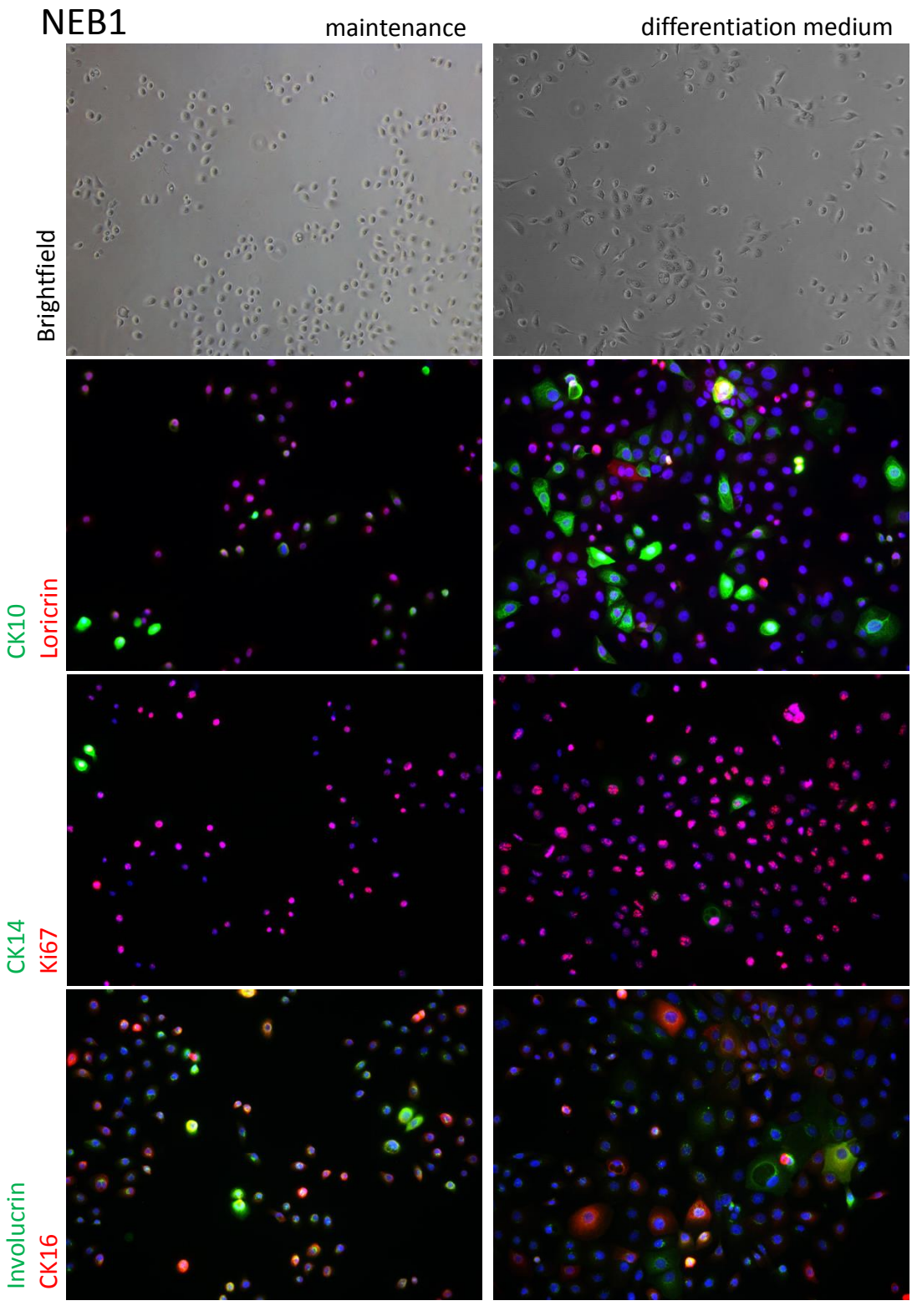
NEB1
maintenance
differentiation medium
Brightfield
CK10
Loricrin
CK14
Ki67
Involucrin
CK16

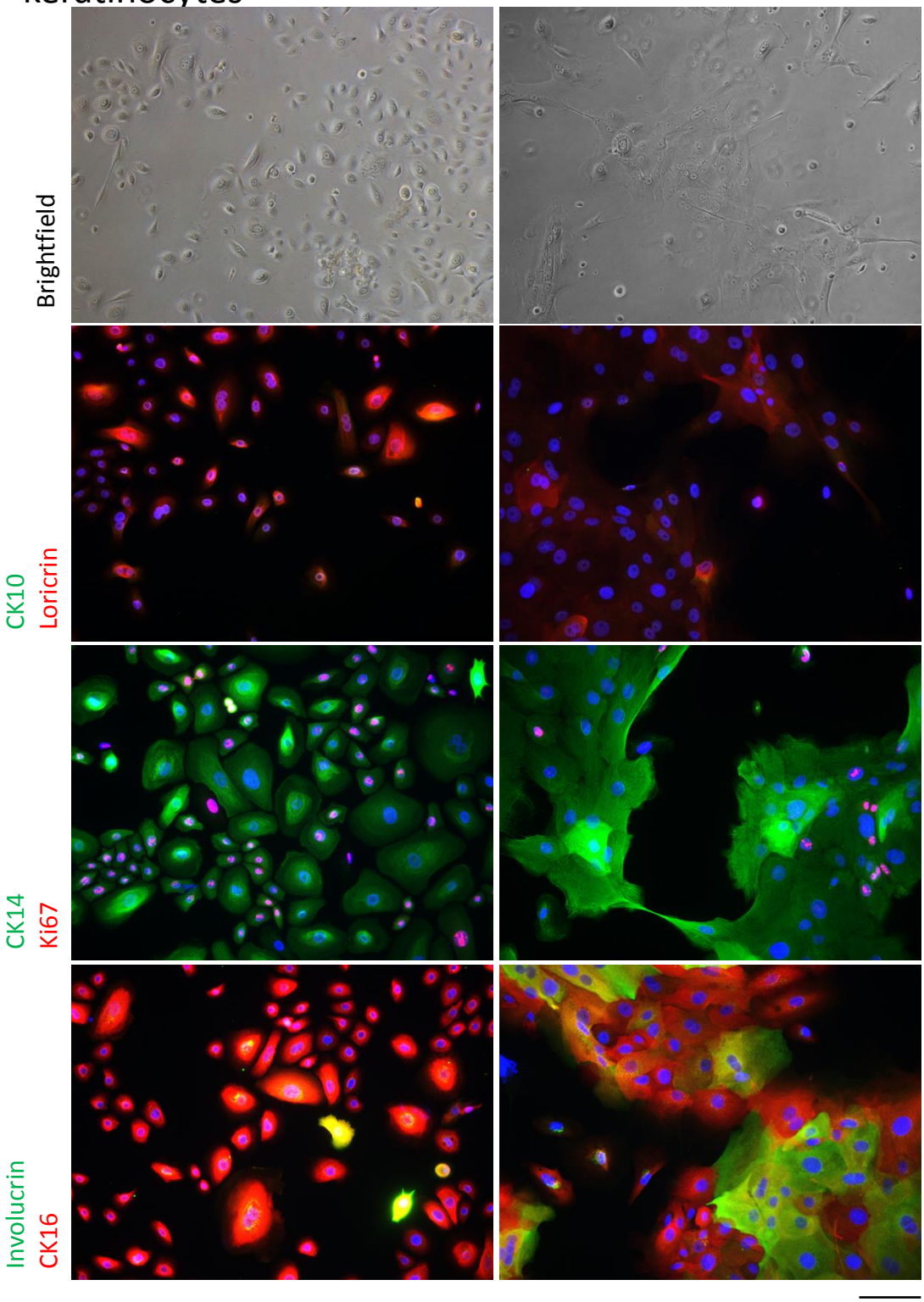
primary keratinocytes
maintenance
differentiation medium
Brightfield
CK10
Loricrin
CK14
Ki67
Involucrin
CK16

Figure 34: Medium-dependant changes in protein expression of monolayer keratinocytes
After switching from maintenance medium to differentiation medium for 48 hours, monolayer keratinocytes show similar trends in regard to changes in protein expression: one or more differentiation markers (CK10, Loricrin, Involucrin) are mostly upregulated and CK14 is slightly restricted to the proliferative edges of colonies. Proliferation markers Ki67 and CK16 seem mostly unaffected by the medium switch. Scale bars represent 100µm.

Already high levels of CK14 and CK16 during maintenance culture appear to be mostly unaffected by the medium switch, which also applies to the moderate levels of Loricrin expression. Overall, while all the keratinocyte cultures have strikingly different protein expression patterns in general, there does appear to be a common trend towards a more differentiation-associated phenotype as a result of the medium switch.

3.1.4. Summary and Discussion

Two different scaffold-based systems were applied in this project with the aim to establish a viable *in vitro* skin equivalent using organotypic cultures of immortalised keratinocytes. In an initial approach the commercially available Alvetex polystyrene scaffold was used. While this model has been published in a variety of tissue engineering applications (Liu et al. 2013; Caiazza et al. 2015; Li et al. 2015; Smith et al. 2015) there is only singular evidence for its use as an epidermal model, while using only early-passage primary keratinocytes in this case (Sharma et al. 2013; Hill et al. 2015). Several combinations of co-culturing fibroblasts and keratinocytes as well as culturing keratinocytes on their own were therefore attempted in order to narrow down an optimised protocol for the generation of skin equivalents with in this system. Even though the best combinations yielded a degree of layering and stratification in the epidermal portion, both visible in the histology as well as the expression of marker proteins CK14 and Involucrin, the likeness to actual skin explants was still sub-optimal. Furthermore, none of the generated organotypics resulted in the retention of a topically applied aqueous Lucifer Yellow solution, a widely used method for the assessment of a functional epidermal permeability

barrier (Blaydon et al. 2011; Frankart et al. 2012; Bachelor et al. 2014; Pendaries et al. 2014). Apart from insufficient terminal differentiation of keratinocytes in this specific model, this might also be due to the presence of the non-degradable polystyrene fibres as essential constituent of the Alvetex scaffold. Epidermal barrier function is strictly dependant on the tight physical connection of the corneocytes and keratinocytes in the upper layers of the epidermis (i.e. stratum corneum and upper stratum granulosum), both through intercellular contacts such as tight junctions and extracellular lipid and protein envelopes (Proksch et al. 2008; Brandner et al. 2010; Kirschner et al. 2010). It is therefore feasible to assume that the polystyrene fibres interrupt these connections and provide a way for aqueous solutions to diffuse throughout the organotypic. Since a functional permeability barrier was essential for the model in regard for its later application (see Chapter 3.4), this finding was enough to exclude the Alvetex-based system from further applications. Consequently, collagen-based culture models were approached as an alternative since their application as skin equivalents and for the *in vitro* modelling of skin diseases has been widely established (Mildner et al. 2006; Alnasif et al. 2014; Eckl et al. 2014).

In the context of this project several keratinocyte cell lines from different origins have been applied in the collagen-based model: HaCaT is a spontaneously immortalised cell line (Boukamp et al. 1988), nTERT cells are based on the induced overexpression of telomerase reverse transcriptase (Lee et al. 2004) and K17 / NEB1 were generated through transfections with HPV16 E6/7 genes (Storey et al. 1988). Even though the majority of published applications is based on using primary keratinocytes (Mildner et al. 2010; Bogaard et al. 2013; Gschwandtner et al. 2013; Alnasif et al. 2014) there are also cases of immortalised keratinocytes being used, though with varying success possibly due to the different cell lines being used (Boelsma et al. 1999; Schoop et al. 1999; Allen-Hoffmann et al. 2000; Skazik et al. 2014; Reijnders et al. 2015). The application of immortalised cell lines in the attempt of recapitulating physiological features *in vitro* can potentially be problematic since different approaches of immortalisation can result in distinct genomic and phenotypic changes. While hTERT cells have been repeatedly used in the generation of normal looking skin equivalents (Dickson et al. 2000; Man et al. 2007; Reijnders et al. 2015), HaCaT cells on the other hand were shown to display deficits in regard to (terminal) differentiation and

hyperproliferation characteristics (Schurer et al. 1993; Boelsma et al. 1999; Schoop et al. 1999; Micallef et al. 2009). Furthermore, expression of HPV16 E6/7 genes in keratinocytes has been widely associated with hyperproliferation, invasion and an overall disordered, premalignant phenotypes in organotypic models (Blanton et al. 1991; Boxman et al. 2001; Delvenne et al. 2001; Pickard et al. 2015; Srivastava et al. 2015). These previous studies seem to mostly correspond with the results of the different cell line-derived organotypics. In addition, a prolonged overall culture life-time which is the case in all keratinocyte cell lines and even in high-passage primary keratinocytes, such as the ones that have been used as controls in the establishment of the organotypic protocol, can also lead to wide-ranging genomic changes and aberrant cell behaviour which might further add to the problematic (Maitra et al. 2005; Binato et al. 2013; Bentivegna et al. 2016). Consequently, when using a variety of cell lines as well as high-passage primary cells in the established organotypic model, the results were strikingly different in regard to protein expression, invasion and stratification. Even before the application in the more complex three-dimensional model, monolayer cultures already showed diverse protein expression patterns, underlining the phenotypic differences between the various cells (which could potentially be compared in more detail by quantitation of cells positive for proliferation or differentiation marker across the different cell lines and conditions). Even though low-passage primary cells are generally preferable for the generation of skin equivalents, there are still distinct advantages in using immortalised cell lines, especially when it comes to the prolonged availability of rare patient-derived and therefore disease-relevant cell material (Thomas et al. 2009; Blaydon et al. 2013; Brooke et al. 2014). Furthermore, all applied cells successfully recapitulated epidermis-like features in the organotypic culture model (including the presence of a functional permeability barrier) and displayed common reactions to changes in the culture protocol, such as the increased differentiation phenotype due to medium switch and prolonged culture time.

Therefore, the possibility of using immortalised keratinocytes for *in vitro* skin equivalents is still justifiable as long as the distinct characteristics of each cell line are taken into consideration when choosing a suitable model for a specific application, such as the ability to build a viable permeability barrier for the assessment of topical

polymer delivery (Chapter 3.4) or a similar genetic background due to same immortalisation protocol when comparing normal and disease-related phenotypes (Chapter 3.2).

3.2. Modelling and Manipulation of Disease Phenotypes

3.2.1. Introduction

After establishing a model for the generation of normal-phenotype *in vitro* skin equivalents through organotypic keratinocyte culture on collagen scaffolds, the next step of the project involved the application of patient-derived keratinocyte cell lines in order to recapitulate disease phenotypes in the *in vitro* model. For this purpose, cell lines for two hereditary skin disorders were used: Harlequin Ichthyosis (Chapter 1.2.1) and Tylosis (Chapter 1.2.2). Since those two cell lines were immortalised using HPV16 E6/7 genes, K17 was used as a normal-phenotype control, having been immortalised around the same time, in the same lab and with the same protocol (Storey et al. 1988). After having successfully established a distinct disease phenotype for each model, by comparing with known and published features for each disorder, it was then attempted to manipulate these phenotypes through shRNA interference or specific small-molecular compounds aimed at disease-relevant pathways. Successful application of TOC-specific compounds was then replicated in another disease model for Pachyonychia congenita (Chapter 1.2.3), since this disorder is caused by dominant mutations in the gene for CK16 which is implicated to be functionally connected to the TOC-relevant iRHOM2-ADAM17-EGFR pathway (Maruthappu et al. 2016).

3.2.2. Characterisation of Cutaneous Disease Models

Striking histological differences were found in the skin equivalents based on HI and TOC keratinocytes in comparison to the normal-phenotype K17-derived organotypic (Figure 35). While K17-based organotypics show a normal skin-like histology, HI organotypics display signs of hyper- and parakeratosis: the uppermost, stratum corneum-like layer is severely thickened in comparison to the normal model and seems to contain a higher amount of nuclei. TOC organotypics also show signs of parakeratosis, in addition to having a highly disorganised and abnormally thickened, hyperproliferative epidermal portion.

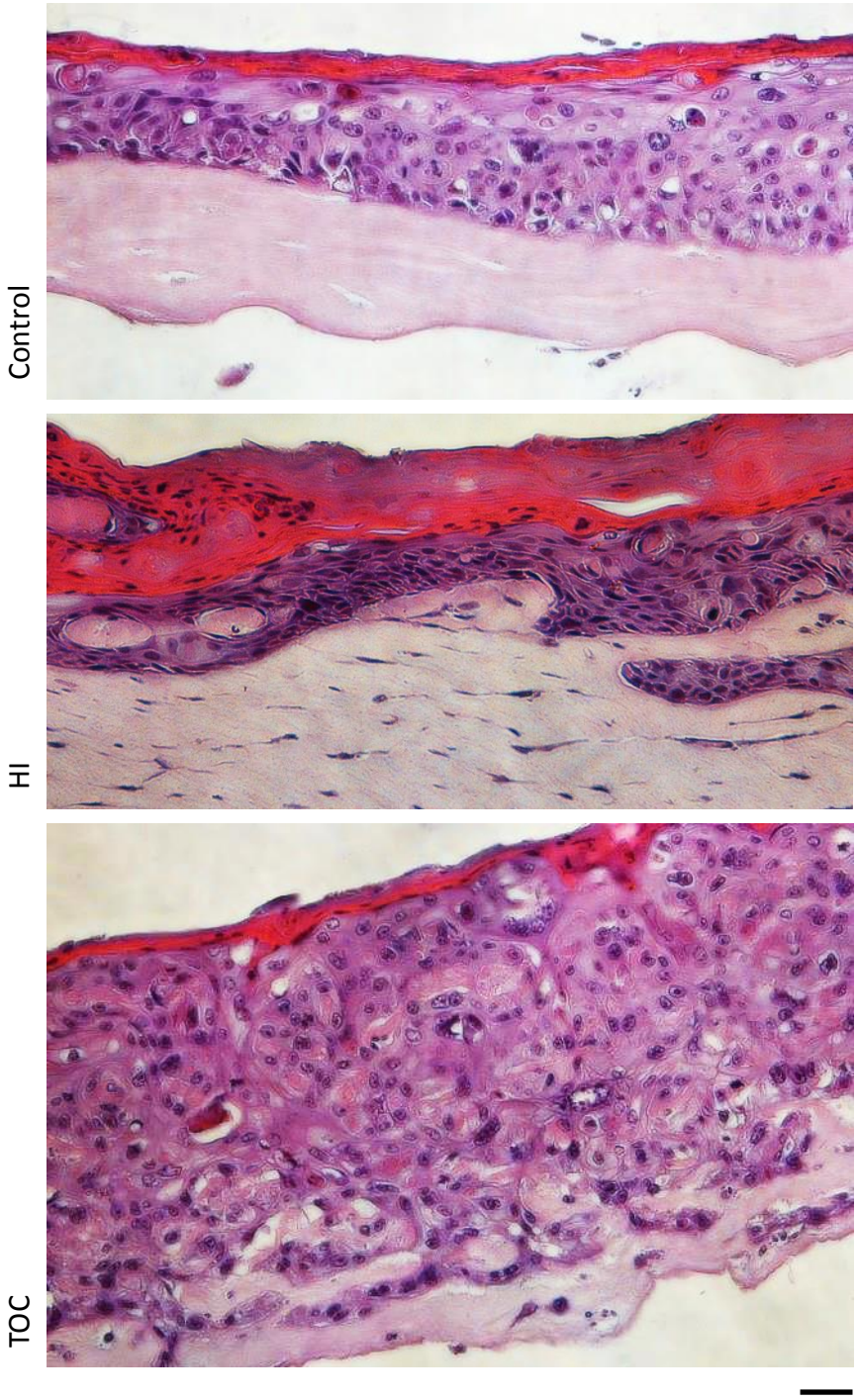

Figure 35: Histological differences in between normal and disease organotypics
Organotypics based on normal as well as patient-derived keratinocytes were cultured for two weeks in airlift conditions and subsequently compared in their histology, displaying distinct differences. HI organotypics exhibit a thickened, nucleated stratum corneum, whereas TOC organotypics show a hyperkeratotic, disorganised arrangement of the epidermal portion in comparison to the normal-phenotype control organotypic. Scale bar represents 50µm.

Subsequently, when examining the hyperproliferation-associated protein marker CK16, further differences can be seen in between the normal and disease models (Figure 36). Whereas the K17-based organotypics show a slight expression of CK16 in the more basal layers of the epidermal portion, this expression is distinctly upregulated in the HI model and even more so in the TOC organotypic. Additionally, in case of TOC the expression of CK16 seems to be found throughout all suprabasal layers of the epidermal portion.

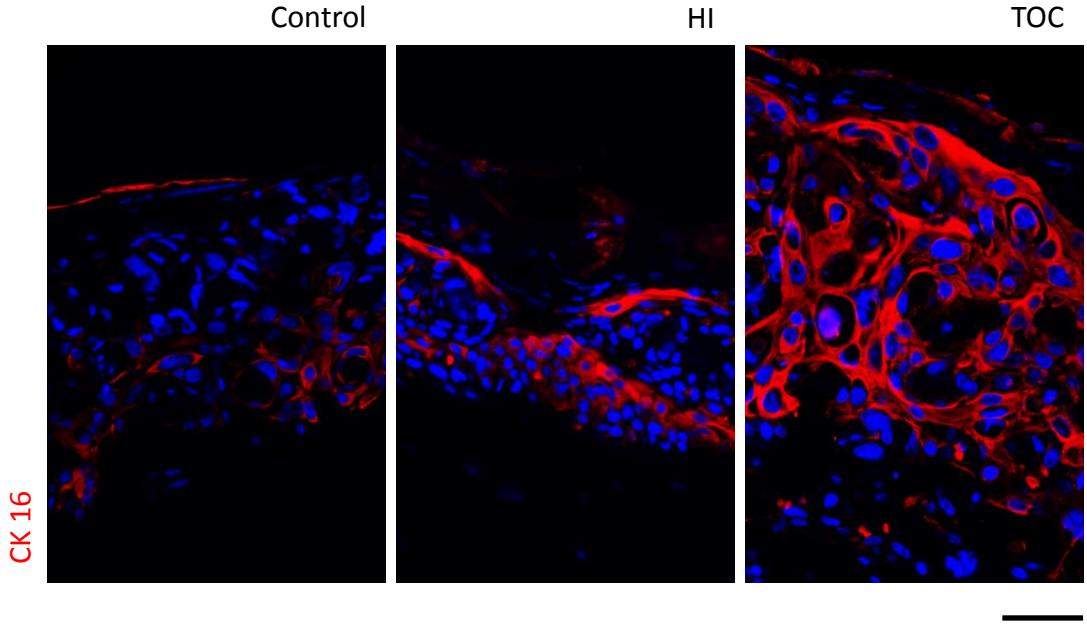

Figure 36: Different hyperproliferation phenotype in normal and disease organotypics
Organotypics for Harlequin ichthyosis and Tylosis show a strongly increased suprabasal expression of hyperproliferation-associated CK16, compared to normal-phenotype organotypics. Scale bar represents 50µm.

When looking into more detail for the individual disease models, the HI-based organotypic displays a reduction of the membrane transporter ABCA12 and an upregulation / earlier onset of the differentiation marker Involucrin (Figure 37 a). Nile Red staining though shows no visible imbalance of polar (red) and non-polar (green) lipids when compared to the normal phenotype organotypic, which can also be confirmed in matched patient skin sections (Figure 37 b).
In case of the TOC model, immunohistochemistry reveals a strong upregulation of inactive rhomboid protease iRHOM2 across suprabasal layers in comparison to the normal model and a similarly increased expression for the EGFR (Figure 38).

(a)

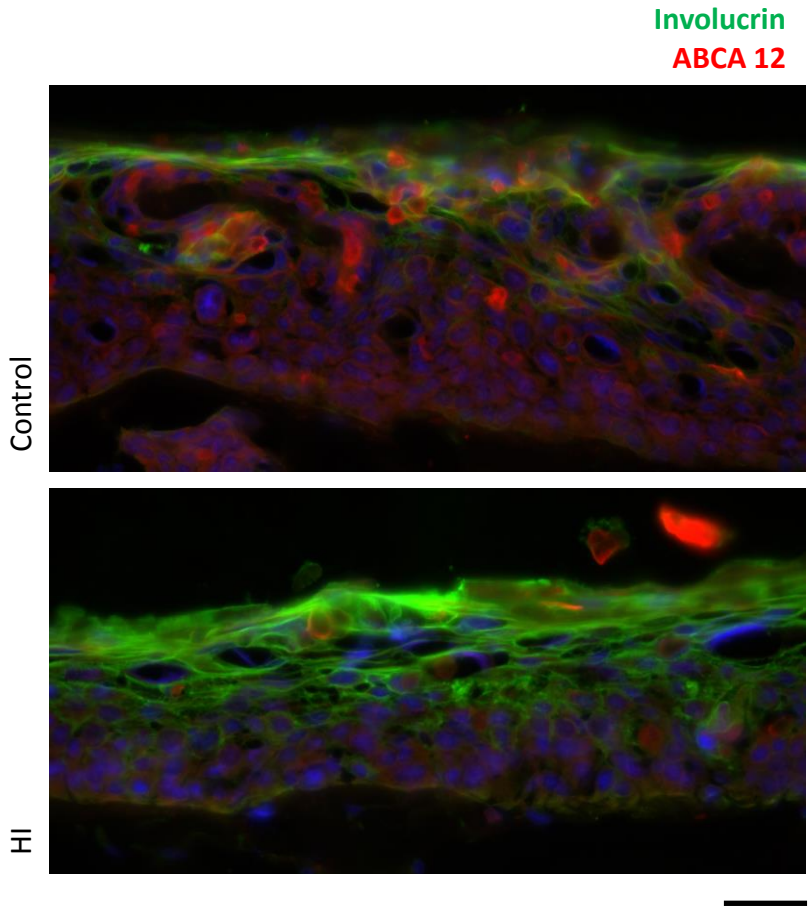
Involucrin
ABCA 12
Control
HI

(b)

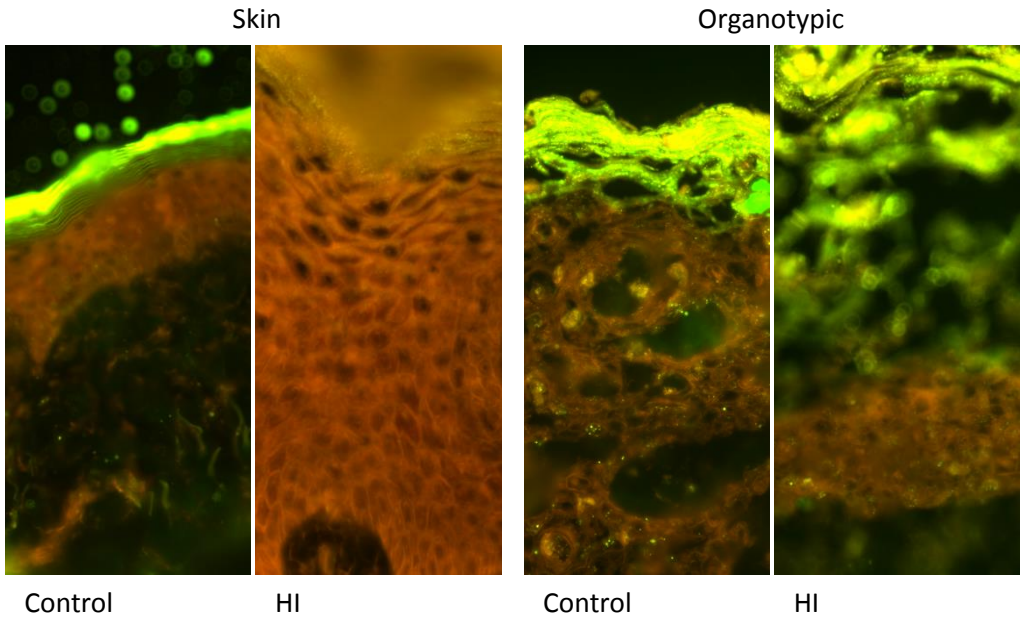
Skin
Organotypic
Control
HI
Control
HI

Figure 37: Phenotypical features of HI organotypics

Organotypics based on keratinocytes from patients with HI display an overall reduction in the expression of membrane transporter ABCA12 accompanied by an upregulation of differentiation marker Involucrin (a) compared to organotypics from normal keratinocytes. Nile red staining on the other hand reveals a similar lipid profile between normal and HI, without the typical absence of non-polar lipids (green) in the case of HI. Parallel staining of the corresponding patient skin sample reproduces this finding (b). Scale bar represents 50µm.

3.2.3. Manipulation of a Harlequin Ichthyosis Model

After establishing a distinctly different disease phenotype for the HI model, two small-molecular PPARδ and LXR agonists (GW0742 and TO901317 respectively) were applied in order to try to counteract disease-specific mechanisms through upregulation of ABCA1. As first step the compounds were used on monolayer HI keratinocytes in order to verify the intended effect. Both compounds result hereby in similar changes for the treated cultures, first in general upregulation of membrane transporter ABCA1 and trans-Golgi marker TGN46 (staining lamellar granules) and then in the decrease of Involucrin-positive cells (Figure 39).

Subsequent to characterising the effect of both compounds in monolayer cells, they were then applied to HI organotypics by supplying them via the culture medium for the last 10 days of airlift culture, treating control HI and K17 organotypics with equal doses of the DMSO solvent. Both compounds showed hereby distinct effects on histology and protein expression of the HI organotypics (Figure 40). While the untreated HI sample displayed expected features, such as hyper- and parakeratosis, upregulation of Involucrin and downregulation of ABCA1 and ABCA12, treatment with GW0742 lead to a reduced disease phenotype and features more resembling the ones seen in the K17-based control organotypic: the stratum corneum was slightly reduced in thickness and with less retained nuclei and Involucrin slightly less expressed.

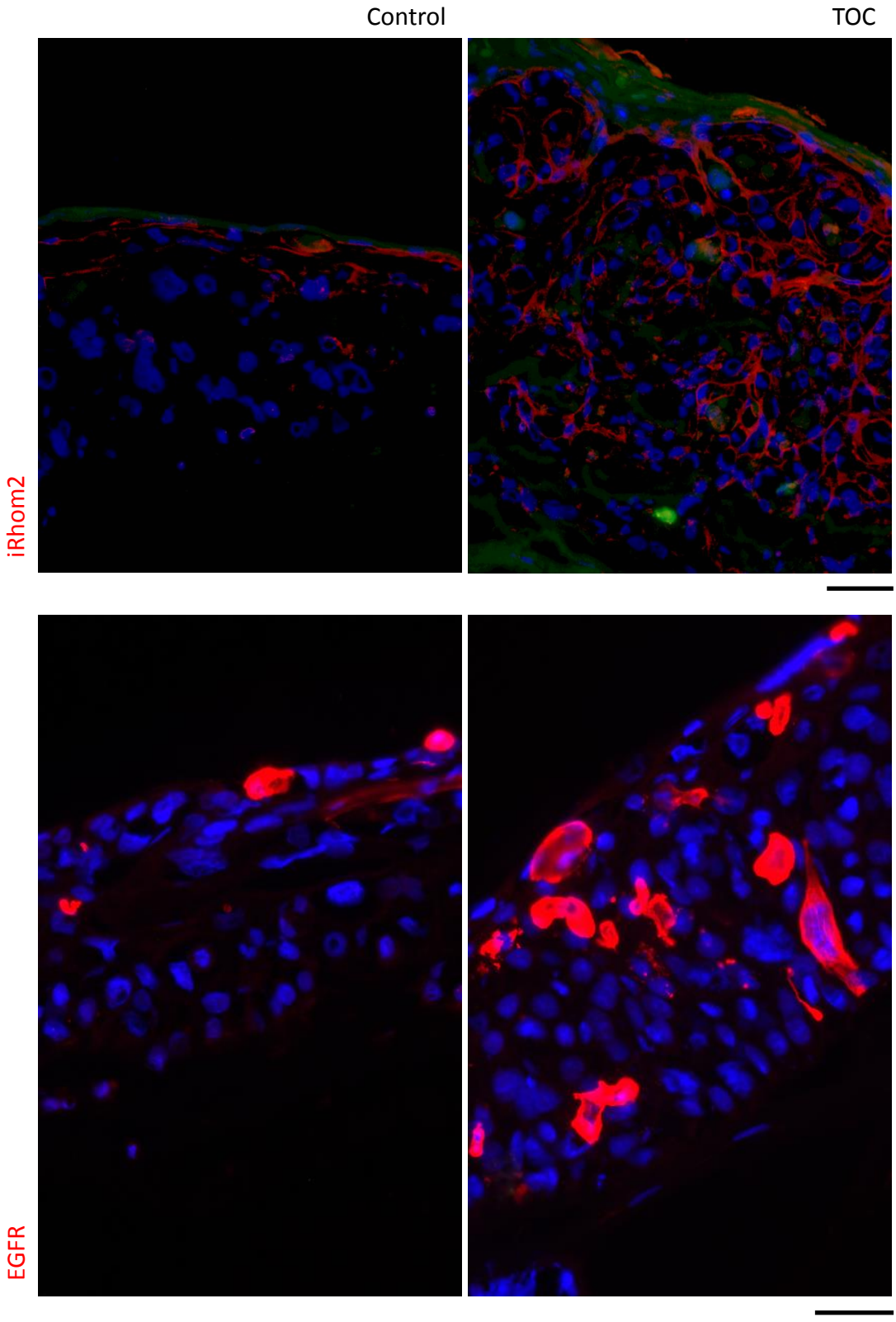

Figure 38: Differential protein expression in normal and TOC organotypics

Two-week old organotypics from TOC keratinocytes show a strong upregulation of iRHOM2 and EGFR compared to the corresponding normal-phenotype organotypics. Scale bar represents 50µm.

The expression of ABCA1 was increased similar again to levels in the K17 sample whereas the reduction in ABCA12 appeared unchanged. In regard to the TO901317-treated sample, the epidermal portion appeared to be severely disrupted and ABCA1 drastically upregulated both in comparison to the HI as well as the K17 sample. Involucrin seemed to be slightly higher in expression and ABCA12 again mostly unchanged.

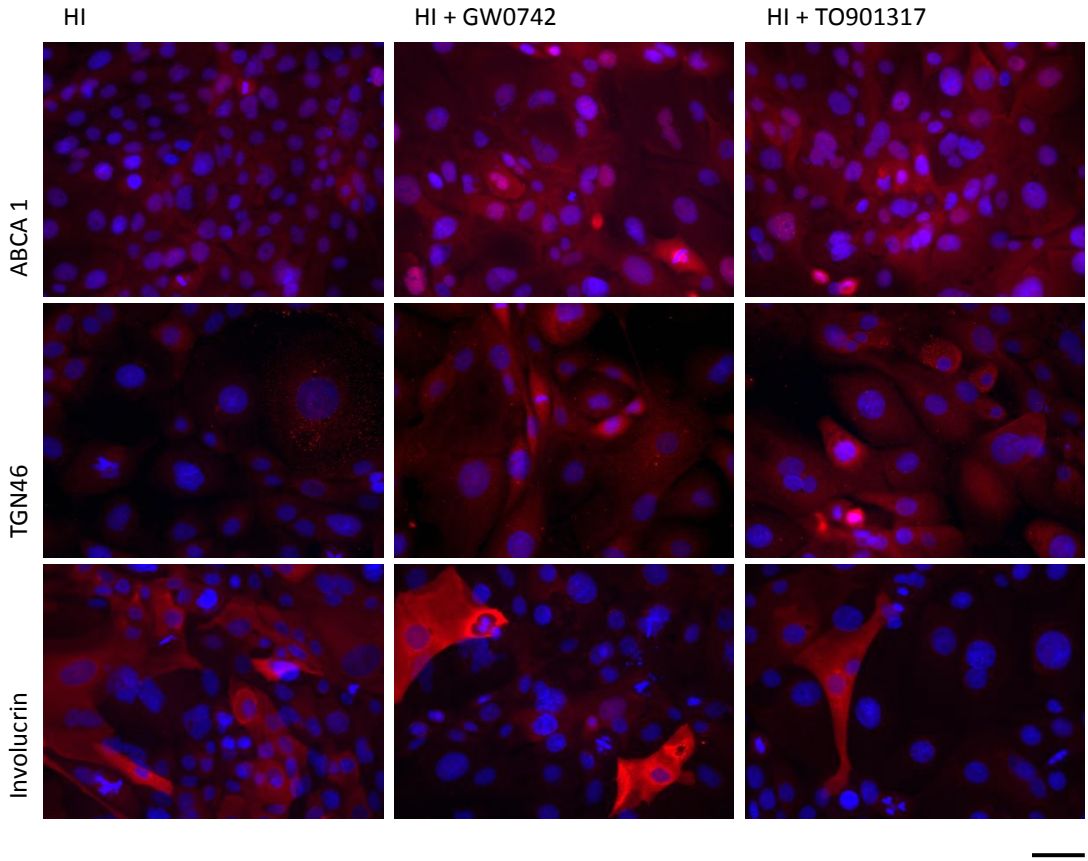

Figure 39: Compound-driven modulation of HI-specific features in monolayer cells

Patient-derived keratinocytes were cultured in monolayer, treated for two days with small molecular compounds and then stained for HI-specific protein markers. Both compounds, PPARϑ-agonist GW0742 (10µM) and LXR-agonist TO901317 (8µM), resulted in an upregulation of membrane transporter ABCA1 and trans-Golgi component TGN46, whereas differentiation-associated Involucrin seemed less expressed with the treatment. Scale bar represents 50µm.

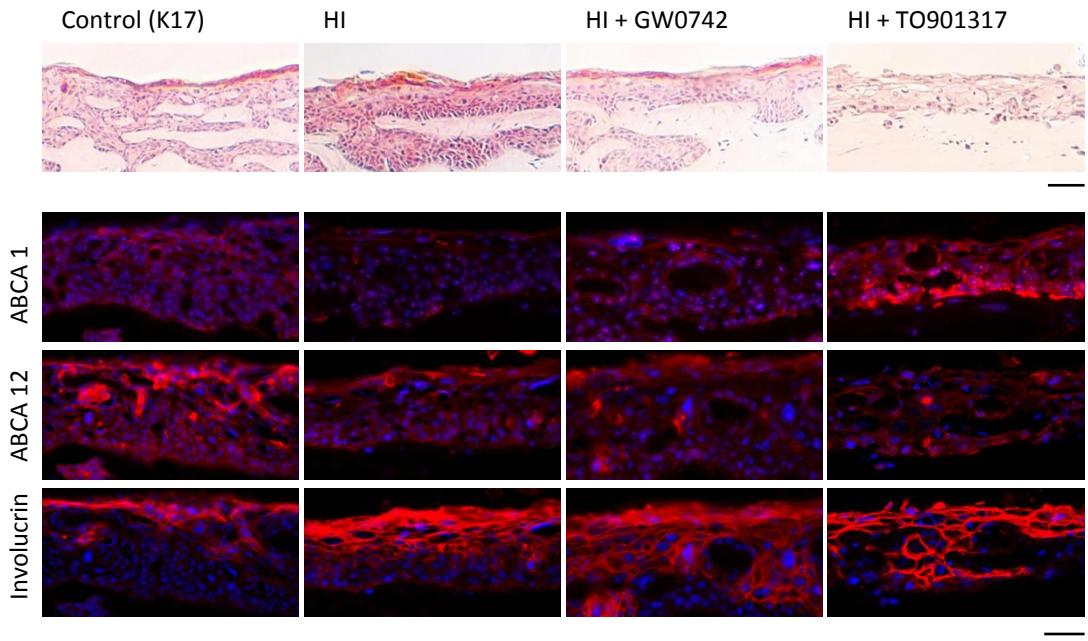

Figure 40: Compound-driven modulation of HI-specific features in organotypics

HI organotypics were treated with two small-molecular compounds, PPARð-agonist GW0742 (10µM) and LXR-agonist TO901317 (8µM), while grown in parallel to K17 organotypics as normal-phenotype control. GW0742 appears hereby to partially shift the aberrant HI phenotype towards the phenotype of the K17 control: the uppermost stratum corneum seems slightly reduced and less parakeratotic, ABCA1, which was strikingly reduced in the HI organotypic, was upregulated to similar levels as in K17 and the HI-specifically overexpressed Involucrin seems to be slightly downregulated. ABCA12, being naturally less expressed in HI, does not appear to be affected by the treatment with GW0742. In case of TO901317, ABCA1 expression was drastically increased and the overall structure of the epidermal portion seemingly disrupted. ABCA12 expression again appears mostly unaffected and Involucrin slightly upregulated. Scale bars represent 50µm.

3.2.4. Manipulation of a Tylosis Model via shRNA-knockdown of iRHOM2

One possible way of counteracting the TOC-related phenotype in cells and organotypics, due to the dominant iRHOM2 mutation, was approached via introduction of a stable shRNA-based knockdown of iRHOM2 (this and the resulting experiments were done in cooperation with Dr Thiviyani Maruthappu and Dr Anissa Chikh, Blizard Institute, QMUL). The knockdown led to a stable 57% reduction of iRHOM2 protein in TOC keratinocytes (Figure 41 a) and a concomitantly reduced iRHOM2 staining in organotypics derived from these cells. This was accompanied by

a general reduction in thickness of the treated organotypic samples (Figure 41 b). The difference in iRHOM2 expression between control TOC organotypics and knockdown organotypics was similar in appearance to the different expression levels that can be found in TOC and healthy normal skin. In addition to generating organotypics the knockdown cells were further tested for hyperproliferation features in monolayer. Growth curves over 7 days showed a strikingly decreased reduction in proliferation of treated keratinocytes (Figure 41 c) and scratch assays also verified a reduction in migration with only a partial scratch closure after 18 hours (Figure 41 d). Since CK16 as hyperproliferation-associated keratin is indicated to be regulated by its interaction with iRHOM2, expression levels were also checked both in monolayer and organotypics. The iRHOM2 knockdown resulted in a 47% reduction of CK16 expression in comparison to control TOC cells (Figure 41 e). The reduction was also present in the derived organotypics and once again mirrored differences between TOC and normal skin (Figure 41 f).

3.2.5. Manipulation of a Tylosis Model via compounds

In addition to applying iRHOM2-targeting shRNA in order to manipulate the TOC phenotype in organotypics, another approach was based on the use of inhibitory compounds specific to components of the TOC-relevant iRHOM2-ADAM17-EGFR pathway. For this the EGFR-specific therapeutic antibody Cetuximab and the small-molecular ADAM17 inhibitor TMI-005 were added to the medium supply of one-week pre-cultured TOC organotypics and continuously supplied for the remaining 7 days of airlift culture. The two treatment options had hereby differing effects on TOC features in the organotypic model (Figure 42). Whereas Cetuximab-treated organotypics did not display any obvious difference in regard to histology and expression of CK16, the TMI-005 treatment appeared to slightly alter the phenotypical features of TOC. H&E staining revealed a slight reduction in para- and hyperkeratosis in conjunction with a slight overall reduction in thickness for the epidermal portion.

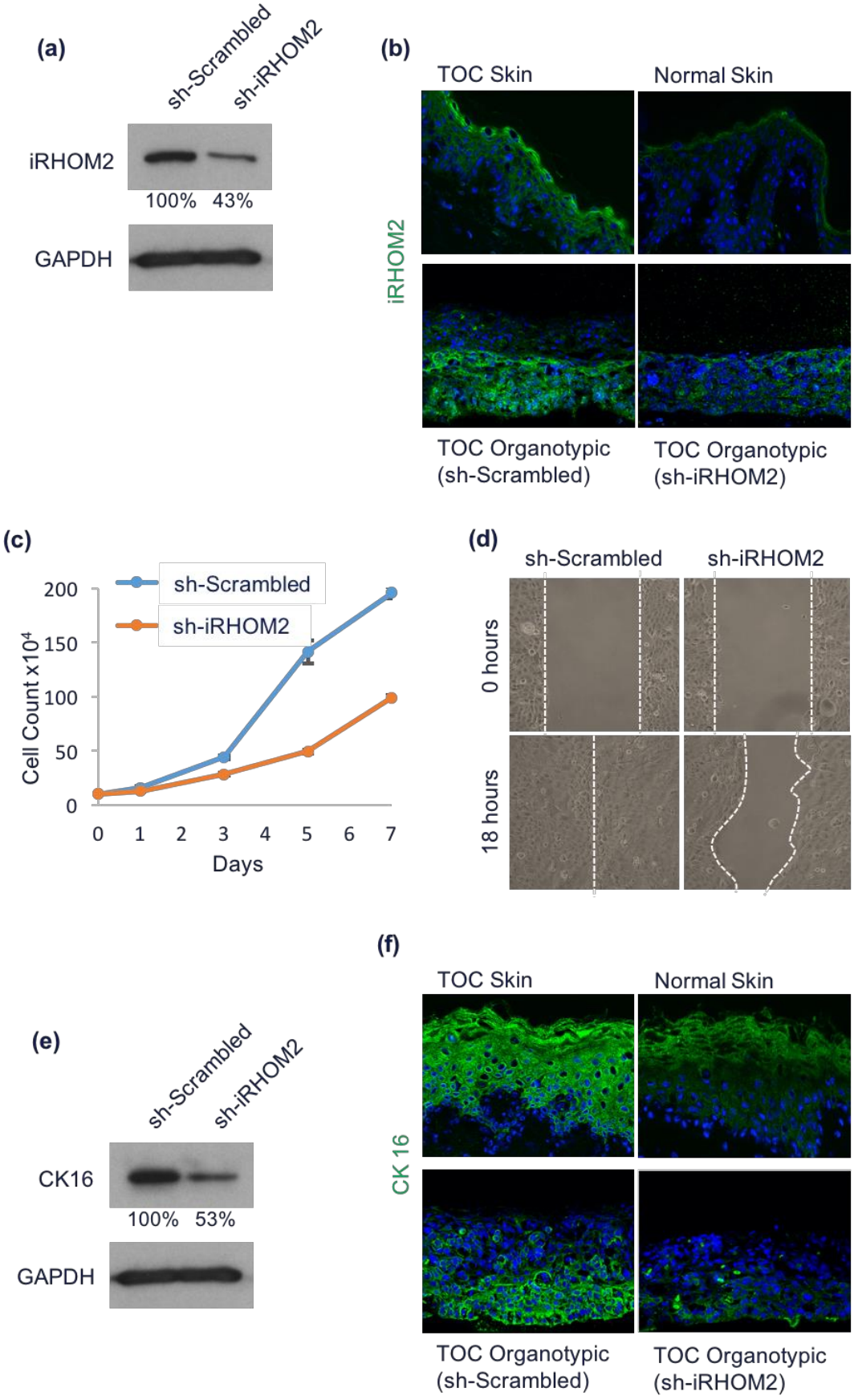
(a)
sh-Scrambled
sh-iRHOM2
iRHOM2
100% 43%
GAPDH
(b)
TOC Skin
Normal Skin
iRHOM2
TOC Organotypic (sh-Scrambled)
TOC Organotypic (sh-iRHOM2)
(c)
sh-Scrambled
sh-iRHOM2
Cell Count x10⁴
200
150
100
50
0
0 1 2 3 4 5 6 7
Days
(d)
sh-Scrambled
sh-iRHOM2
0 hours
18 hours
(e)
sh-Scrambled
sh-iRHOM2
CK16
100% 53%
GAPDH
(f)
TOC Skin
Normal Skin
CK 16
TOC Organotypic (sh-Scrambled)
TOC Organotypic (sh-iRHOM2)

Figure 41: Effect of shRNA-mediated iRHOM2 knockdown on TOC keratinocytes
shRNA-mediated stable knockdown led to a strong decrease (57%) of iRHOM2 expression in Tylosis keratinocytes (a). The knockdown was still present in organotypics after two weeks of airlift culture, mimicking the difference in iRHOM2 expression between tylotic and healthy skin (b). In monolayer cultures the loss of iRHOM2 also resulted in a distinct decrease in proliferation (c) and migration (d) of knockdown cells. Furthermore, the iRHOM2 knockdown led to a subsequent reduction in expression of hyperproliferation-associated CK16 both in monolayer (e) and organotypics (f), where it again mirrors the differential expression in healthy and tylotic skin.

Furthermore, CK16 expression was downregulated and spatially restricted towards the more basal layers of the organotypic in comparison to the control and Cetuximab-treated samples.

3.2.6. Manipulation of a Pachyonychia Congenita Model

After the application of the ADAM17 inhibitor TMI-005 in TOC organotypics, the treatment approach was subsequently extended to another disease model based on keratinocytes from patients with Pachyonychia Congenita. The PC organotypics were hereby pre-cultured for two days in airlift culture before application of the compound via the medium supply for the remaining 12 days, resulting in a striking difference in regard to histology and protein expression of treated samples. While the histology for the untreated and DMSO control samples appeared disorganised and only moderately stratified, the inhibitor-treated organotypic was strikingly thinner, with a more distinguished basal layer and stronger stratification in the upper layers (Figure 43).
Staining for protein markers in the PC control and TMI-005 samples further supported this initial observation through distinct changes in protein expression (Figure 44). In the treated sample both ADAM17 and iRHOM2 were severely reduced which was also accompanied by a decrease in Ki67-positive cells. In addition, CK16 staining was slightly reduced and Involucrin slightly upregulated.

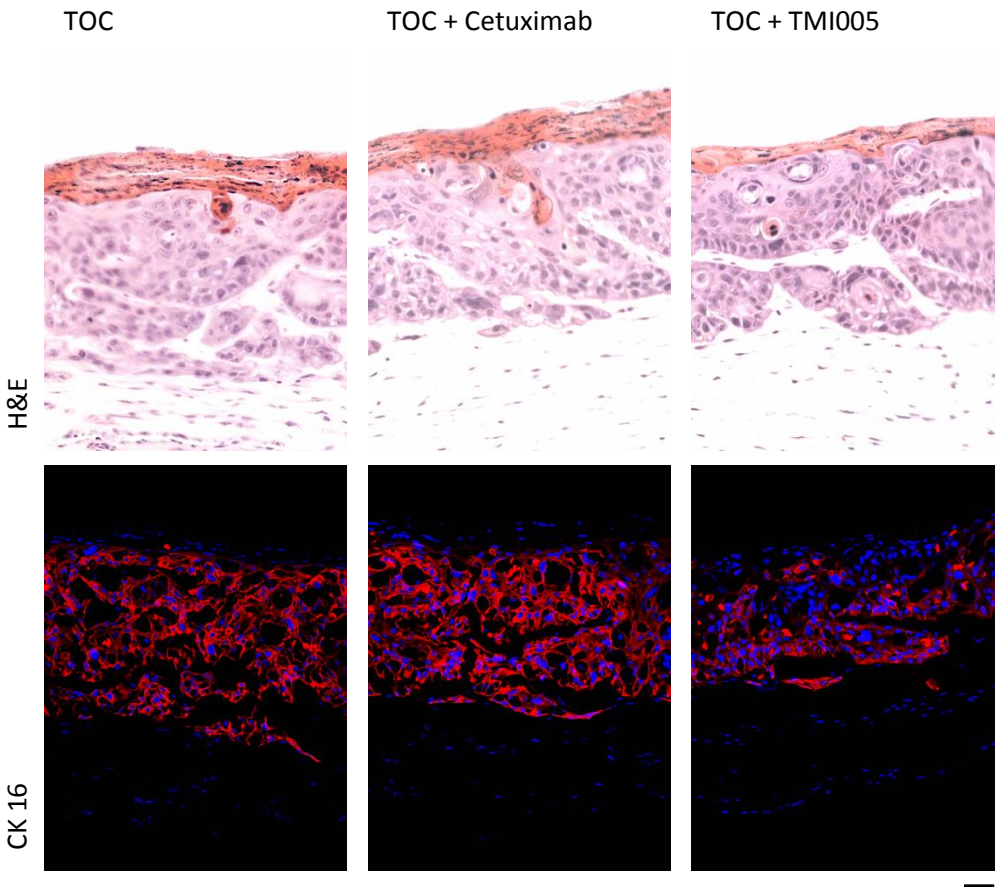

Figure 42: Inhibitor-treatment of TOC organotypics

TOC organotypics were pre-cultured in airlift for one week before being supplied via the culture medium with inhibitors for EGFR (Cetuximab, 1µg/ml) and ADAM17 (TMI-005, 500nm) for the remaining 7 days. Organotypics treated with the therapeutic antibody Cetuximab showed hereby no visible effect on histology and expression of hyperproliferation marker CK16. The small-molecular inhibitor TMI-005 on the other hand seems to lead to a slight reduction in hyperkeratosis and restriction of CK16 to more basal layers. Scale bar represents 50 µm.

3.2.7. Summary and Discussion

Subsequent to establishing an organotypic culture model for immortalised normal-phenotype keratinocytes, patient-derived cell lines were applied to the developed protocol in order to recapitulate disease phenotypes *in vitro*. While similar organotypic disease models have been done for a variety of disorders using primary keratinocytes derived directly from patients, optionally via the reprogramming of

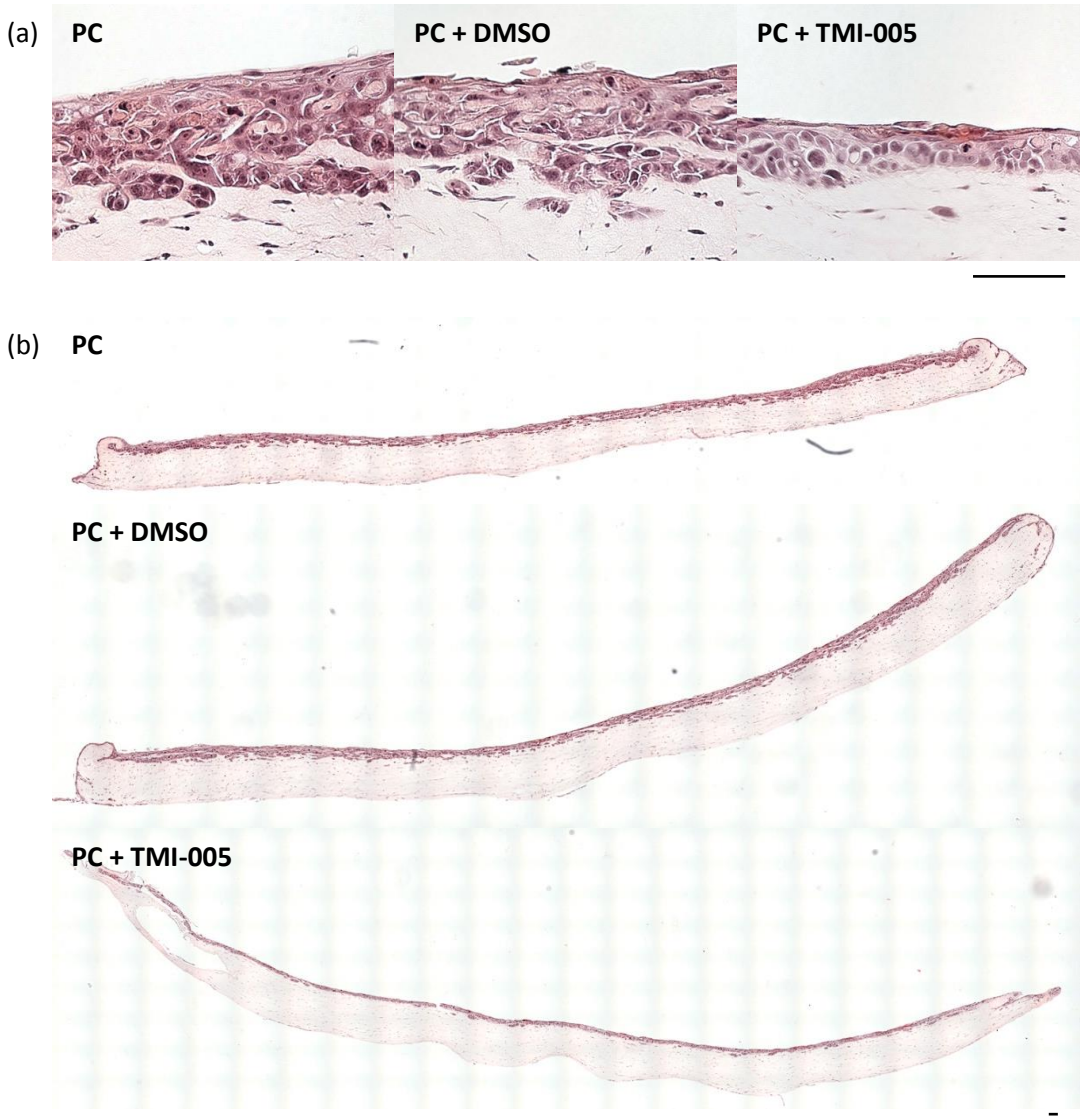

Figure 43: Histological changes in PC organotypics after application of ADAM17 inhibitor

After culturing organotypics based on PC keratinocytes in the presence of ADAM17 inhibitor TMI-005 for 10 days (first application at day 4 after airlift at 500nM) striking changes in the histology of the epidermal portion in comparison to the control and DMSO vehicle-treated samples can be seen (a): a visible reduction in thickness of the epidermal part is accompanied by a decreased invasion of keratinocytes into the collagen gel and a generally more structured arrangement of cells. This is in addition to a more prevalent eosin-stained uppermost layer, indicating a stronger terminal differentiation of the treated keratinocytes. Those changes can be observed throughout the whole diameter cross section of the organotypics (b). Scale bars represent 50µm.

iPS cells (Barker et al. 2004; Jean et al. 2009; Bogaard et al. 2013; Umegaki-arao et al. 2014), or by using cells treated with siRNA/shRNA to simulate disease-relevant loss-of-function mutations (Mildner et al. 2006; Thomas et al. 2009; Eckl et al. 2011; Pendaries et al. 2014), the application of immortalised patient cell lines is a so far

lesser explored option. Using immortalised cells would provide certain advantages by making patient-specific cells, carrying (potentially dominant gain-of-function) disease mutations, available for long-term experimental series. Consequently, for this project, two different inflammatory disorders have been initially chosen in order to test the capacity of the model to mimic epidermal disease characteristics: Harlequin ichthyosis (Kelsell et al. 2005) and Tylosis with oesophageal cancer (Blaydon et al. 2012). The limited availability of rare disease material had hereby the consequence that a direct comparison of the modelled phenotype with patient skin was only possible in a few instances and had otherwise to be replaced by an assessment based on what has been previously described in the literature. In both disease models the combination of the organotypic model with patient-derived keratinocytes resulted in distinct changes in the histology and expression of hyperproliferation marker CK16. HI organotypics, although slightly variable in between batches as is the case for most of the cell-line based skin equivalents, generally showed pronounced signs of hyper- and parakeratosis, both typical features of HI (Rajpopat et al. 2011). A closer look at differentiation marker Involucrin further revealed the premature terminal differentiation phenotype which has already been described for HI (Thomas et al. 2009) and could be further investigated in the established model by using additional differentiation markers, e.g. Kallikreins. Despite these positive results though, other features were not reproducible in the model. Expression of ABCA12 was still present in the organotypics, although in reduced levels compared to controls, whereas HI skin classically shows a complete ablation of the protein (Akiyama 2005). This might be dependent on the specific type of mutation in the ABCA12 gene though and the loss-of-function mutation for this patient-derived cell line has been previously confirmed by Dr Philip Bland (Blizard Institute, QMUL) to be a splice site mutation that still produces a (non-functional) shortened protein. The observed reduction in expression might consequently be the result of a negative feedback loop mechanism (Scott et al. 2013). Another atypical feature of the disease organotypics was the presence of polar as well as non-polar lipids. Whereas HI skin should typically display a visible loss of non-polar ceramides as a result of the faulty packaging of lamellar granules via ABCA12 (Hovnanian 2005), the HI organotypics showed a balance of lipids similar to controls, which could

furthermore be also seen in the patient-matched skin sample. It was previously shown that HI patients undergo an improvement in their clinical features with age, towards a less severe, congenital ichthyosiform erythroderma-like phenotype (Rajpopat et al. 2011). Furthermore, a culture time-dependent self-improvement of HI keratinocytes *in vitro*, which also included a normalisation of their lipid profile, has been demonstrated before (Yanagi et al. 2010). It is therefore feasible to assume that the Nile Red results are due to the age of the (adult) donor as well as the prolonged overall culture of the derived keratinocytes.

Even though the model did not reproduce all the features typical for HI skin, based on the features that could be replicated it was still deemed sufficient in assessing the effect of potential therapeutically relevant compounds. The activation of nuclear hormone receptors PPARδ and LXR was hypothesised to improve HI-specific features by counteracting lipid imbalance in the upper suprabasal layers through enhanced cholesterol transport and subsequent secretion via membrane transporter ABCA1 as well as enhanced lamellar granule formation induced by AP-1 (Chawla et al. 2001; Schmuth et al. 2004a, 2004b; Jiang et al. 2006; Demerjian et al. 2009; Ouvrier et al. 2009; Feingold and Jiang 2011). Consequently, two commercially available agonists for PPARδ and LXR were applied to the HI model. Initial use in monolayer HI keratinocytes verified the intended effect by upregulating ABCA1 expression as well as increasing the presence of TGN46-positive lamellar granules. Additionally, Involucrin-staining showed a de-differentiating effect of the compound treatment which might be beneficial in regard to the pre-mature terminal differentiation phenotype that was already shown in the organotypic model. The subsequent application of the two compounds in the 3D model resulted in a visible disruption of the epidermal portion in case of the LXR agonist, possibly due to dose-dependent toxic side effects that did not became apparent in the monolayer culture (Götz et al. 2012a, 2012b), and only subtle changes for the PPARδ-specific compound despite the visible upregulation of ABCA1. This might be explained by the already discussed compensation of lipid imbalance by culture-time dependent mechanisms which would mask the effect of an increased ABCA1-induced cholesterol efflux in the upper layers.

TOC phenotypic features are based on gain-of-function mutations in the RHBDF2 gene, encoding for the inactive rhomboid protease iRHOM2, and the resulting downstream upregulation of the EGFR pathway via increased ADAM17-dependent shedding (Brooke et al. 2014). A first approach in regard to trying to regulate these features included therefore the stable shRNA-mediated knockdown of iRHOM2 in TOC keratinocytes, the rational being that a partial loss in protein would counteract the gain of function (Maruthappu et al. 2016). Correspondingly, a stable knockdown in the monolayer cells translated in a still visible loss of expression in the organotypic culture after two weeks, accompanied by a striking loss in epidermal thickness. This finding was further supported by the striking reduction of migration and proliferation in treated monolayer cultures, which implies an overall loss in hyperproliferation features. Recently, a functional link between iRHOM2 and CK16 has been established by Maruthappu et al., with the stress- and hyperproliferation-associated CK16 being directly regulated by iRHOM2. The iRHOM2 knockdown-dependent downregulation of CK16 could hereby be also shown in both monolayer cells and the organotypic culture. Interestingly, knockdown-based changes in the organotypic model mirrored the general difference in expression of those proteins in between TOC and normal interfollicular skin, thereby implying the validity of the iRHOM2-ADAM17-EGFR axis as potential therapeutic target for this kind of hyperproliferative skin disorder. Based on these findings ADAM17 and EGFR, as therapeutically relevant targets, were blocked in their function by applying specific inhibitors to the TOC model. For the inhibition of ADAM17 the small-molecular inhibitor TMI-005 was chosen due to its previously published applications as specific and potent inhibitor for ADAM17 (Thabet and Huizinga 2006; Shu et al. 2011; Maney et al. 2015). In parallel, the FDA-approved EGFR-inhibitory antibody Cetuximab was used in order to assess the option of preventing the increasingly shed EGFR ligands from taking effect by blocking the corresponding receptor (Harding and Burtness 2005; Vincenzi et al. 2010). After applying both inhibitors to the differentiating organotypics for one week, the Cetuximab treatment showed hereby no visible effect on histology or CK16 expression, even though it had a visible effect when applied in equivalent dosage on monolayer (as verified internally by Kelsell group members).

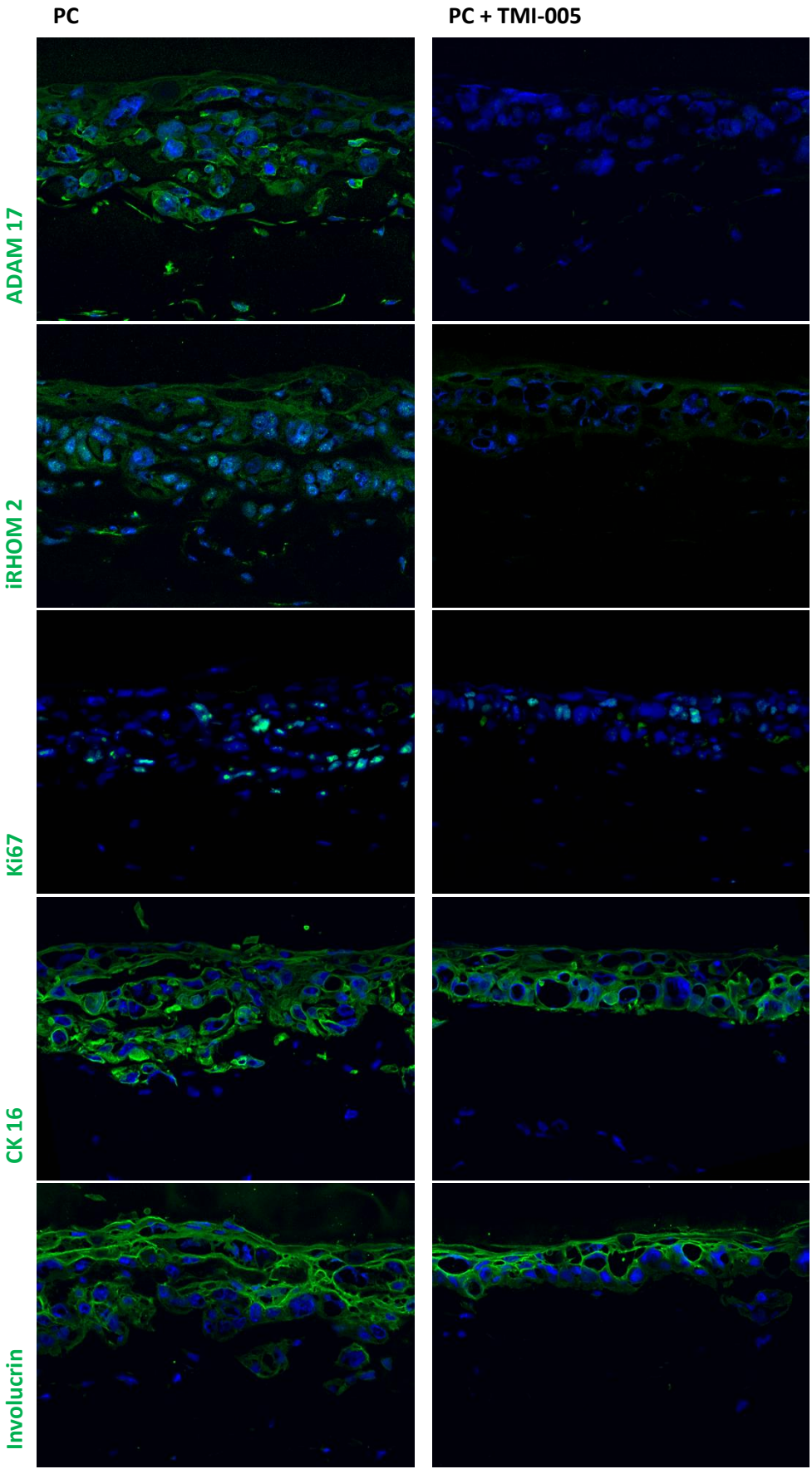
PC
PC + TMI-005
ADAM 17
iRHOM 2
Ki67
CK 16
Involucrin

Figure 44: Differential protein expression in PC organotypics through inhibitor treatment
PC organotypics that were cultured in the presence of ADAM17 inhibitor TMI-005 (500nM) for 10 days show distinct changes in protein expression pattern: inhibitor treatment leads to a complete loss of ADAM17 expression and strong reduction in iRHOM2 and Ki67 throughout the organotypic. CK16 seems slightly down- and Involucrin slightly upregulated. Scale bar represents 50μm.

One likely explanation for this might be the supply mode via the medium, which would require the presumably unlikely upwards diffusion of the comparatively big antibody (molecular weight of circa 145 kDa) through the collagen matrix and underlying PET membrane. In contrast, the far smaller inhibitor TMI-005 (around 0.4 kDa) was found to have a visible effect on epidermal thickness, hyperkeratosis and CK16 expression. This effect was still relatively subtle though, compared to the internal TOC control, and might be increasable through a prolonged treatment period.

Subsequently, a longer treatment was used for a similar application of TMI-005 on an organotypic model for Pachyonychia congenita. PC is generally caused by mutations in Keratins 6a, 16 or 17, with the patient from which the keratinocytes for this model were derived from displaying a dominant mutation in the 1A-helical domain of CK16 (Terrinoni et al. 2001). Approaches for the treatment of PC via mTOR-mediated transcriptional silencing of the affected keratin have already been published (Hickerson et al. 2009). Based on the established interaction of the iRHOM2-ADAM17 axis with CK16, it was therefore hypothesised that the ADAM17 inhibitor might have a beneficial effect on the PC organotypic model, in addition to the general effect on hyperproliferation (and inflammation) that can be expected from the downregulation of ADAM17-mediated TNFα shedding. Consequently, a prolonged treatment with TMI-005 did result in a drastic improvement on the phenotype of the control PC samples, which did not necessarily reflect a typical hyperkeratotic disease phenotype (Leachman et al. 2005) due to the age and quality of the used cell line. The concomitant effect on the invasion of cells into the collagen gel could hereby also be caused by the inhibitory effect of TMI-005 on matrix metalloproteases 1 and 13 , which are known to be involved in the breakdown of collagen 1 (Johansson et al. 2000; Hu et al. 2007). In addition to the performed

analysis phosphoEGFR-specific antibody staining and ELISA for ADAM17-shedded growth factors could be used to further assess the inhibitory effect of applied compounds in more detail.

Overall, the established organotypic keratinocyte culture system could be used in first proof-of-principle experiments to model and modulate disease phenotypical features to varying degrees for three different inflammatory skin disorders (Table 14). Further replication and extended analysis (e.g. via Western Blotting in addition to the predominantly qualitative IHC readout) have to be done though in order to validate these initial results and account for the underlying aspect of batch-to-batch variability of *in vitro* reconstituted tissue models, which is also partially emerging in the applied model.

Table 14: Summary of results for in vitro skin disease modelling

	HI	**TOC**	**PC**
disease cause	recessive mutation for ABCA12 (p.Glu2264X)	dominant mutation for iRHOM2 (p.Ile186Thr)	dominant mutation for CK16 (p.Leu128Glu)
modelled phenotype	hyperkeratosis, parakeratosis, premature differentiation	thickened and disorganised epidermis , parakeratosis, CK16 upregulation	disorganised epidermis, keratinocyte invasion
missing features	loss of ABCA12, lipid imbalance	---	hyperkeratosis, pronounced hyperproliferation
treatment approach	PPARð / LXR agonists	shRNA(iRHOM2), ADAM17 inhibitor	ADAM17 inhibitor
treatment effects	slightly less ABCA 1 and hyperkeratosis	reduction in thickness, CK16 and hyperproliferation	thinner, more organised epidermis and less invasion

3.3. Organotypic Wound Model

3.3.1. Introduction

Cutaneous wound healing is a complicated process dependent on a multitude of components from epidermis, dermis, vasculature and immune system (Singer and Clark 1999; Baum and Arpey 2005). Modelling it in order to investigate underlying mechanisms therefore classically involves *in vivo* animal studies (Gallucci et al. 2000; Galiano et al. 2004), the short-term use of explant skin (Bhora et al. 1995; Xu et al. 2012) or the breaking down of the multi-layered biological system into simple *in vitro* approximations, such as the widely used monolayer scratch assay (Rodriguez et al. 2005; Liang et al. 2007). Recently, several approaches have been made to use advances in tissue engineering by applying more complex 3D culture systems (El Ghalbzouri et al. 2004; Breetveld et al. 2006; Safferling et al. 2013). Similarly, using the already established organotypic culture system, the possibility of a simplified *in vitro* cutaneous wound healing model including epidermal and dermal components in a three-dimensional arrangement was investigated, applying three different keratinocyte cell lines in order to account for the already demonstrated cell line-dependent phenotypic variance of normal-phenotype organotypics. The established wound protocol was then combined with the TOC model to further recapitulate and modulate disease-specific wound healing features.

3.3.2. Establishing an in vitro Epidermal Wound Phenotype

For the process of modelling cutaneous wound healing in vitro, a normal-phenotype organotypic based on K17 keratinocytes was cultured for two weeks in order to achieve a full differentiation and stratification of the epidermal portion before applying a punch wound and culturing it for another two days on an underlying collagen layer. After 48 hours of culturing in this arrangement, signs of re-epithelialisation could be found in the organotypic (Figure 45). Across the full wound area (indicated by the absence of the underlying PET membrane which was excised as part of the full-thickness wound) keratinocytes were found on top of the wound

collagen in a layered and partially stratified arrangement. In addition, immunofluorescence staining revealed a distinct expression of marker proteins. The differentiation marker CK10, suprabasally expressed in the unaffected parts of the organotypic distant to the wound edge, was completely absent from the wound area. In contrast, hyperproliferation-associated CK16, proliferation marker Ki67 and the wound-specific gap junction protein Cx26 were all upregulated across the whole wound area.

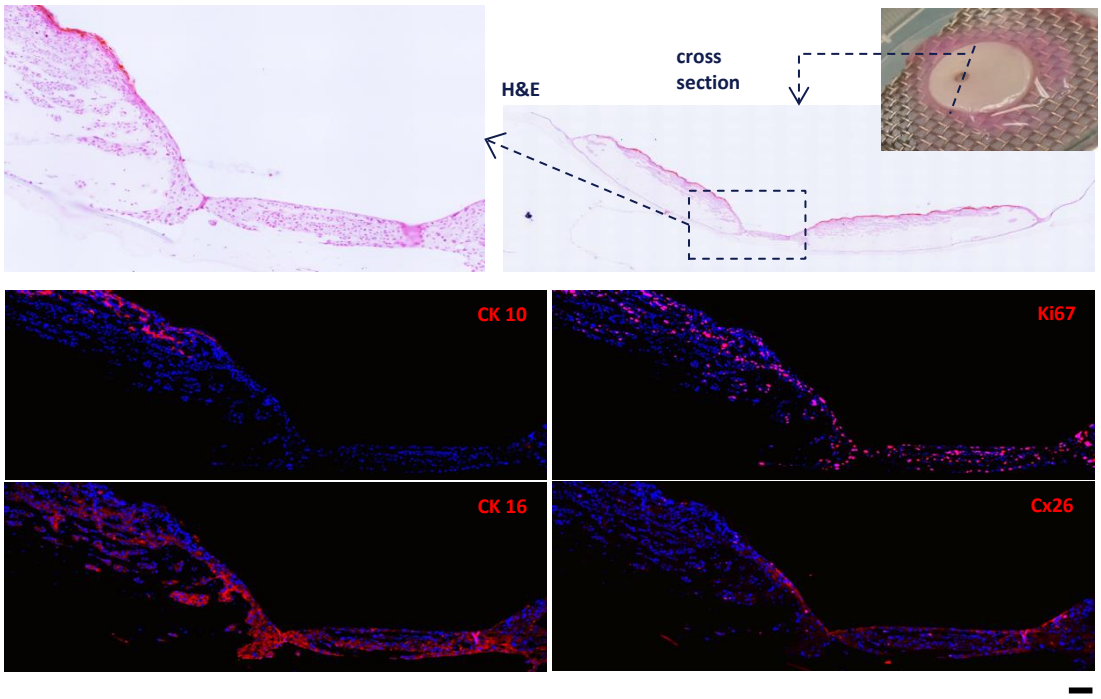

Figure 45: Generation of an dermal-epidermal wound model

Immortalised K17 keratinocytes were seeded unto a primary, dermal fibroblast-containing collagen 1-scaffold and cultured in airlift condition for two weeks. The by then fully stratified skin equivalent was treated with a full thickness 3mm punch wound and transferred on a fresh collagen scaffold to culture for an additional two days in airlift. After two days, H&E staining of the full-diameter cross section showed signs of 're-epithelialisation' with keratinocytes being present in the wound area in several layers. Immunofluorescence staining displayed a wound-specific marker expression, with CK10 being absent and, conversely, hyperproliferation and wound specific markers Ki67, CK16 and Cx26 being upregulated in the regenerating area. Scale bar represents 100µm.

3.3.3. Changes in Wound Phenotype over Time

The progression of the wound-specific features over time was investigated by wounding fully differentiated NEB1 organotypics and harvesting them at one, three and five days after wounding for comparison (Figure 46). Histological changes displayed hereby an advancement of the epidermal portion from the unaffected parts of the organotypic unto the wound collagen matrix. One day after wounding a short and thinning epithelial tongue was present, while after two additional days the whole wound area was covered by a bi-layered epidermal portion which by day 5 after wounding was further thickened and beginning to stratify. Interestingly, the upper layers of the unaffected parts of the organotypic started to detach over time, with first signs holes appearing at day 3 after wounding and an almost complete detachment after day 5. CK16 upregulation was limited to the wound edge one day after wounding and spread first retrograde into the unaffected organotypic and subsequently into the wound area over the following days. Similarly, Ki67 expression was first increased around the wound edge, which was followed by an even upregulation in both directions of the edge. Cx26 on the other hand was strikingly upregulated across the wound edge as well as the whole epidermal tongue after the first 24 hours and then decreased again over the following four days.

3.3.4. Changes in Wound Phenotype in Dependence on Scaffold

In addition to investigating the wound phenotype over time it was further attempted to modify wound healing features through environmental manipulation, specifically via changes in the wound collagen composition. Using fully differentiated HaCaT-derived organotypics, several collagen gels (with or without fibroblasts and with the optional addition of EGF) were used as underlying wound scaffold to assess the potential effect on the wound closure (Figure 47). The collagen gel with any addition of cells or growth factors showed hereby minimal progression of the epidermal portion into the wound area. The fibroblast-containing wound scaffold was uniformly covered by a single layer of keratinocytes whereas the scaffold containing EGF

seemed to have caused a strong progression of the epidermal portion into the wound area, with a multi-layered and stratified arrangement of keratinocytes advancing approximately 300µm past the initial wound edge before thinning into a single layer of cells. Correspondingly, the EGF-treated sample displayed a strongly increased CK16 staining across the wound edge compared to the other samples which was further accompanied by an apparently increased expression of CK10 in the suprabasal layers of the wound edge. Combining EGF and fibroblasts seems to negate this effect, resulting in a wound healing phenotype very similar in histology and marker expression to the sample with only fibroblasts.

3.3.5. Wound Model for TOC

The final step in the *in vitro* modelling of cutaneous wound healing was aimed at combining the organotypic wound model with the previously established TOC disease phenotype and its manipulation via stable RNA interference (Chapter 3.2.4). For this TOC organotypics, with or without shRNA-mediated knockdown for iRHOM2, were cultured for two weeks, wounded and then cultured for an additional 24 hours on a fibroblast-containing collagen wound scaffold (Figure 48). The control samples that were treated with scrambled shRNA displayed constitutive wound healing phenotypical features, with CK16 and Cx26 being evenly expressed through even unaffected parts of the organotypic and only slight relative upregulation at the wound edge. In case of the sh(iRHOM2)-treated samples striking changes in protein expression were visible. iRHOM2 was mostly absent in the organotypic, with only minimal expression directly at the wound edge. Similarly, CK16 and Cx26 were visibly downregulated in the unaffected parts of the organotypic and consequently mostly limited in expression to the wound edge.

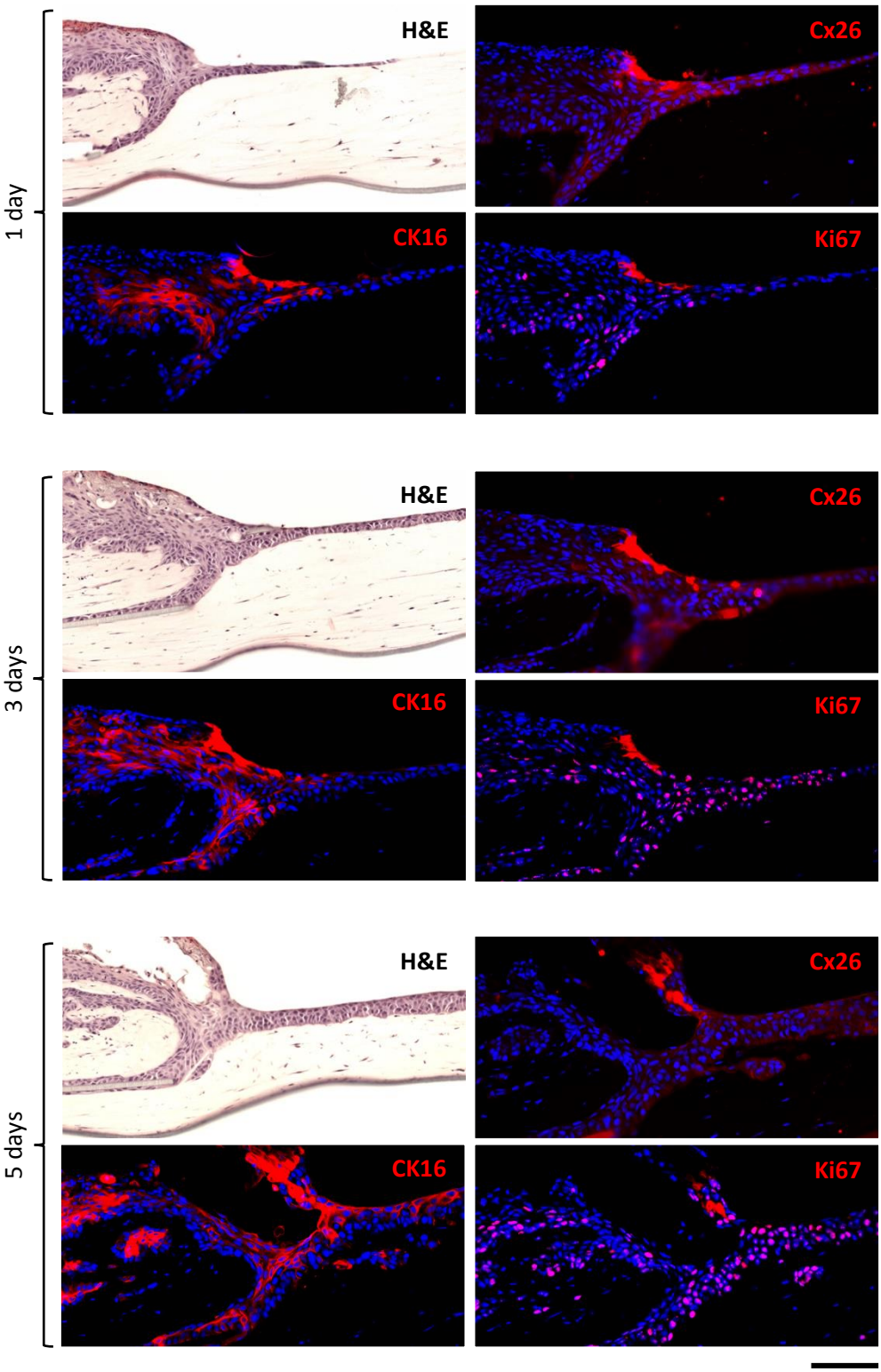
1 day
H&E
Cx26
CK16
Ki67
3 days
H&E
Cx26
CK16
Ki67
5 days
H&E
Cx26
CK16
Ki67

Figure 46: Organotypic wound healing over time

Fully differentiated NEB1-based organotypics were wounded and cultured for up to an additional 5 days. Histological stainings of the resulting cross sections reveal hereby a progressive advancing of the epidermal keratinocytes unto the wound scaffold, resulting in an increasingly stratified re-epidermalised layer. This is accompanied by a change in protein expression from the initial wound healing marker Cx26 towards the proliferation markers CK16 and Ki67 over time. Scale bar represents 100µm.

3.3.6. Summary and Discussion

Cutaneous wound healing is a complex process and can be negatively impacted by a variety of factors, e.g. systemic diseases such as diabetes mellitus can lead to severely impaired healing and chronic wounds (Gurtner et al. 2008; Guo and Dipietro 2010) or, in contrast, upregulated healing mechanisms can result in hypertrophic scarring and the formation of keloids (Robles and Berg 2007; van der Veer et al. 2009). Underlying mechanisms are not thoroughly understood and comprehensive models can help towards elucidating the causes of dysregulated wound healing and assess potential therapeutic approaches (Sherratt and Murray 1990; van den Broek et al. 2012). While *in vivo* animal models are the most representative option in terms of multi-compartmental complexity, they do come with disadvantages in term of species-specific biological variations and general regulatory, logistic and ethical aspects in regard to animal experiments (Davidson 1998; Dorsett-Martin 2004; Jansen 2004; Nordgren 2004). *In vitro* models on the other hand tend to still be limited in their scope of recreating the full complexity of the native biological system, with many epidermal wound models being limited to keratinocyte scratch assays (Rodriguez et al. 2005). As a consequence, recent developments were aimed at translating advances in the generation of 3D *in vitro* skin models towards the recapitulation of wound healing in a suitable *in vitro* model (El Ghalbzouri et al. 2004; Vaughan et al. 2004; Safferling et al. 2013).

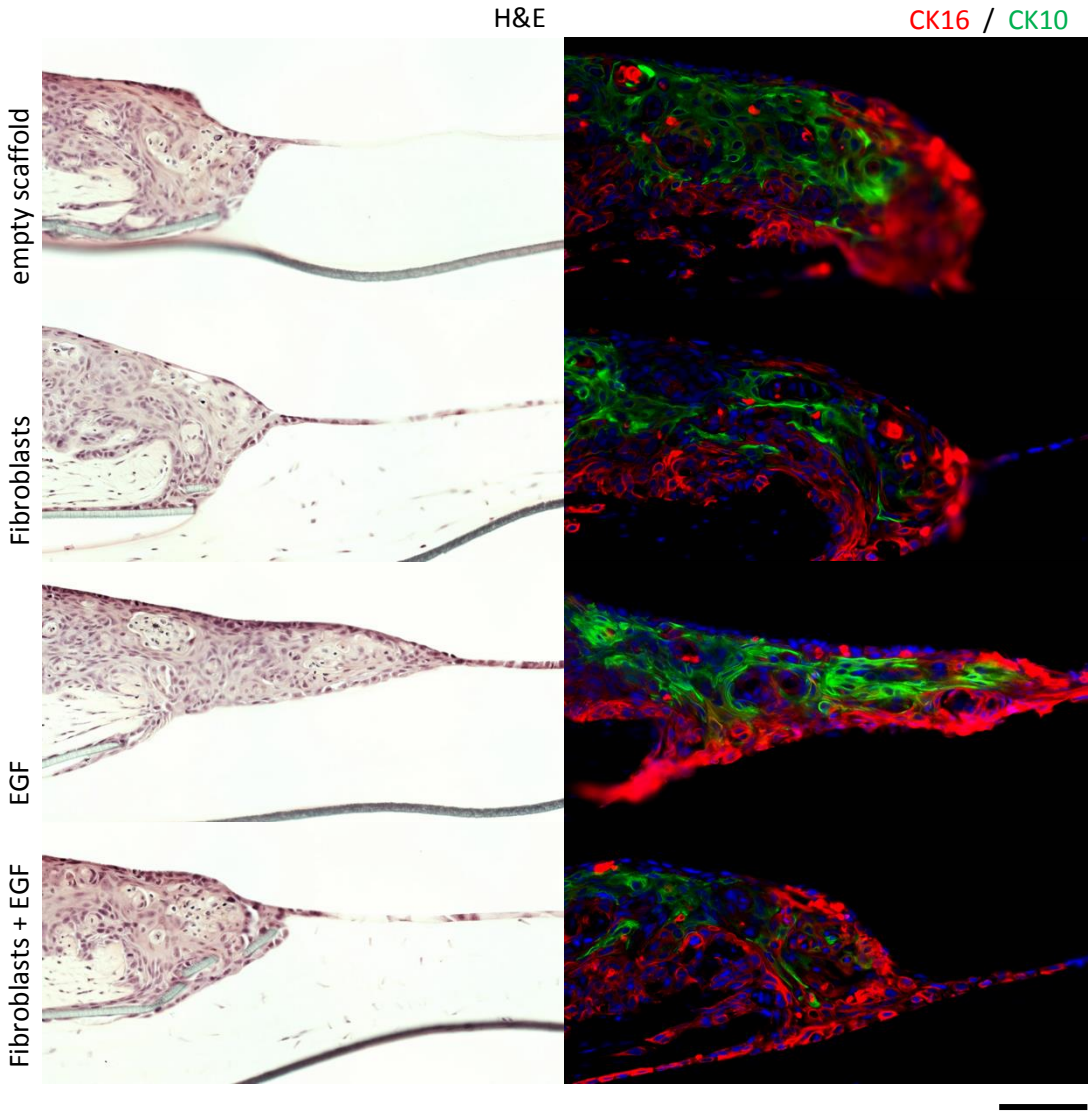

Figure 47: Effect of different scaffolds on organotypic wound healing

Fully-differentiated HaCaT organotypics were wounded and grown for additional 48 hours on scaffolds with only collagen (first row), collagen with fibroblasts (second row), collagen with EGF (third row) or collagen with fibroblasts and EGF (last row). Histological staining of the cross-sections reveals hereby minimal wound closure on the empty scaffold, a keratinocyte monolayer on the fibroblast and fibroblast + EGF samples and a strong advancement of the epidermal portion unto the EGF-containing scaffold. Furthermore, immunofluorescence staining shows a higher expression of hyperproliferation-associated CK16 along the wound edge of the EGF-treated sample, followed by a stronger progression of differentiation marker CK10 in comparison to the other samples. Scale bar represents 100µm.

Employing a similar protocol, slightly adapted to the specifics of the pre-established organotypic model, it was now tried to model and modulate epidermal wound healing features using immortalised keratinocyte cell lines. The use of a full-thickness punch wound, as opposed to for example (superficial) burn or freeze wounds (El Ghalbzouri et al. 2004; Breetveld et al. 2006), was hereby chosen for the advantage of setting a very clearly defined wound edge (which could later one be traced back in cross section stainings via the absence of the easily visible PET membrane in between the two collagen layers) and reliably removing all epidermal cells inside the newly created wound area. In addition, subsequent wound healing experiments were undertaken by using different normal-phenotype keratinocyte cell lines (K17, HaCaT, NEB1), in order to assess the adaptability and validity of the experimental setup in context of the already established phenotypical variance of the different cell lines (Chapter 3.1.3).

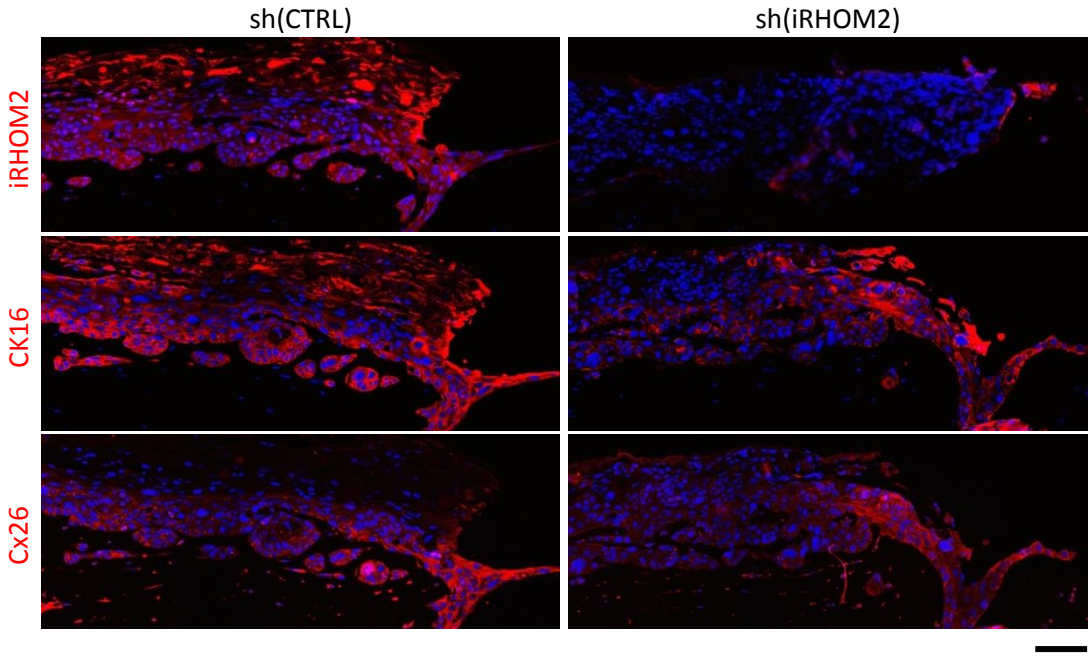

Figure 48: Modelling and correction of a TOC-specific wound healing phenotype

Fully differentiated organotypics based on Tylosis keratinocytes, with or without stable knockdown for iRHOM2, were wounded and cultured for additional 48 hours. Non-knockdown samples display an expression of hyperproliferation (CK16) and wound healing (Cx26) markers throughout even the unwounded parts of the organotypic (left side of each picture), whereas the knockdown of iRHOM2 leads to a restriction of expression to the actual wound edge (right side of each picture). Scale bar represents 100µm.

A first application of the protocol in organotypics using the K17 cell line did consequently result in a clear display of wound healing features. A newly present multi-layer arrangement of keratinocytes on top of the wound collagen scaffold was the likely result of re-epithelisation involving probably migration and certainly proliferation of keratinocytes along the wound edge. This was further supported by protein marker expression patterns typical for cutaneous wound healing. Keratin-reorganisation plays an important role in the re-epithelisation after acute skin injury and especially Keratin 16, and its type 2 binding partner Keratin 6a, are described as essential component in this process (Brody 1988; Paladini et al. 1996; Wojcik et al. 2000; Safer et al. 2004). The concomitant downregulation of differentiation-associated Keratin 10 is hereby further indication for an actual remodelling of keratins in the organotypic wound and accompanying de-differentiation and proliferation of wound edge keratinocytes, which is also apparent through the increased Ki67 expression in the wound area (Betz et al. 1993; Safferling et al. 2013). Interestingly, overly abundant expression of Ki67 inside the epithelial tongue has previously also been associated with chronic ulcerous wound healing, which could in this case be connected to the use of immortalised, hyperproliferative keratinocytes (Usui et al. 2008). Connexin 26 is a wound-specific gap junction protein and is thought to be especially expressed by hyperproliferative keratinocytes in the leading edge of spontaneous wounds (Kretz et al. 2003; Brandner et al. 2004). The expression of it in the wound area and especially at the actual wound edge of the organotypic can therefore be seen as further validation of the *in vitro*-generated wound healing features. Additional gap junctions could be stained for though to further confirm the phenotype, e.g. Connexin 30 which is expressed together with Connexin 26 or Connexin 43 which is constitutively expressed in healthy epidermis and subsequently downregulated during wound healing (Coutinho 2003; Becker et al. 2012).

After verifying a general wound phenotype in the model, the next step involved a time-dependent investigation of phenotypical features in order to assess re-epithelisation and changes in protein expression over a timeframe of up to five days after wounding. Histology stainings could hereby indeed show the advancing of an epidermal tongue from the wound edge unto the collagen scaffold of the wound area, followed by proliferation-based layering of keratinocytes and the onset of

stratification into a horizontally flattened upper layer. A re-emergence of differentiation markers such as Keratin 10 or Involucrin in the re-epithelised parts could not be detected though (data not shown), which might be due to the limited time frame of the model not allowing for later-stage differentiation of the newly formed epidermal portion. Corresponding to the expansion of the epithelial tongue, proliferation markers CK16 and Ki67 were shown to spread in upregulation from the initial wound edge and along the leading edge into the re-epithelised wound area. The additional retrograde increase for both of the markers into the unaffected parts of the organotypic past the wound edge was hereby similar to the retrograde spreading of wound healing markers described before and is likely attributed to increased cytokine and growth factor secretion at the wound edge affecting those parts of the epidermal portion (Brandner et al. 2004). Contrasting the temporal pattern of the proliferation markers, Connexin 26 was found to be maximally expressed at the wound edge early on and subsequently downregulated again over the following days. This generally corresponds with earlier findings in skin (Brandner et al. 2004), although the process seems to be accelerated in comparison which might be a consequence of the general hyperproliferation-phenotype and subsequently higher turn-over of the organotypic cell culture. In this regard, the changes over time in the non-wounded parts of the organotypic are of interest as well. The apparent disintegration and subsequent separation of the upper suprabasal layers of the epidermal portion has not be seen in previous experiments and might be connected to the overall prolonged culture time of the organotypic (up to 19 days instead of 14) which might possibly allow the continuously proliferative epidermal portion to grow to a degree where the upper layers can no longer be sufficiently supplied with nutrients from the basal medium reservoir. This essential nutrient diffusion might also be hampered by the additional layers of the wound model and it is furthermore feasible to assume that the existing hyperproliferation might be increased by the already described retrograde wound effect and therefore enhances this problem in addition to the prolonged culture time.

One important aspect in the setup of the wound models was its modular nature, achieved through the separate preparation / pre-culture of the organotypic and wound scaffold. This allows for an easy combinatorial approach in regard to different

conditions, for example the composition of the collagen mixture that comprises the wound scaffold. Subsequently, it was tested if the addition or omission of different components in the dermal equivalent would have an effect on the epidermal wound healing features. Dermal fibroblasts are shown to have a strong paracrine effect on proliferation and migration of epidermal keratinocytes, which is even more enhanced in an acute wound healing setting, through the secretion of several interleukins and growth factors (Werner et al. 2007). It is therefore a feasible assumption that a cell-free collagen scaffold would result in a reduced epithelialisation in the model. This hypothesis seemed to be verified by the experimental findings which showed a stunted advancement of the epidermal portion unto the fibroblast-free scaffold. Interestingly, this was accompanied by an apparent absence of CK10-reduction which might imply a delayed de-differentiation of the wound edge keratinocytes, possibly due to the absence of keratinocyte growth factor (KGF) which can be secreted by dermal fibroblasts and has been described to have a potentially beneficial effect on keratinocyte re-differentiation (Staiano-Coico et al. 1993; Werner et al. 1994). Similarly, epidermal growth factor is known for its supportive effect on wound healing, primarily via the upregulation of migration and proliferation of wound edge keratinocytes (Nanney and King 1988; Bodnar 2013; Kuroyanagi et al. 2014). Correspondingly, an EGF-supplemented wound scaffold seemed to have a strikingly positive effect on wound closure in the organotypic model, as has already been shown before for different full-thickness wound models (El Ghalbzouri et al. 2004). A visible upregulation of CK16 in keratinocytes along the leading edge further supports the assumption that this is actually a direct result of the EGF treatment, since the growth factor is known to upregulate CK16 expression (Jiang et al. 1993; Wang and Chang 2003). Upregulation of CK10 via EGF on the other hand has not been described so far, the visible increase in expression might therefore be more indicative of a generally more advanced wound healing and subsequent maturation of the re-epithelised areas. Combining EGF-treatment with the presence of fibroblasts in the wound scaffold seems to mostly negate the EGF-derived effect and results in a phenotype similar to the fibroblasts-only sample. Fibroblasts are known to express EGF receptors and to furthermore exhibit a reduced responsiveness to EGF stimulation with age (Shiraha et al. 2000; Cao et al. 2006;

Simpson et al. 2010), the ineffectual binding of EGF to the embedded (high-passage) fibroblasts might therefore be a likely explanation for this observation. Overall though, the modulation of the underlying the wound scaffold in order to influence the epidermal wound healing phenotype has been verified to be a viable option, which opens up a variety of possibilities to advance the wound model into a more *in vivo*-like setting. Two examples would be the addition of a simple capillary system by incorporating HUVEC endothelial or even adipose-derived stem cells in the collagen scaffold before adding it to the wound model (Black et al. 1998; Auxenfans et al. 2012) or the inclusion of an immune system component through the embedding of macrophages or even tissue-resident T cells (Bechetoille et al. 2011; Linde et al. 2012; Van Den Bogaard et al. 2014). An even simpler method would be the alteration of the scaffold composition itself by replacing collagen 1 with a defined mixture of collagen 3, fibronectin and hyaluronan in order to mimic early stage granulation tissue (Häkkinen et al. 2011). In addition to making the wound model more *in vivo*-like in general, dermal components could also be used to model more aberrant healing mechanisms, for example by recapitulating hypertrophic scarring through the application of disease-specific fibroblasts (van den Broek et al. 2012, 2014).

The combination with a previously established disease phenotype was a logical next step in the establishment of the organotypic wound model, since epidermal disorders can influence acute wound healing, for example through alteration of cytokine secretion and alteration of signalling pathways (Werner et al. 2007; Guo and Dipietro 2010). TOC is hereby an interesting candidate due to the specific, EGFR-based constitutive wound healing phenotype (Brooke et al. 2014; Ellis et al. 2015). Consequently, untreated control TOC organotypics displayed an expression of CK16 and Cx26 throughout even the unaffected parts of the parts of the epidermal portion, far beyond the wound edge. Employing the partial shRNA-mediated knockdown of iRHOM2, which has already been described to downregulate wound healing features such as proliferation and migration in monolayer cultures (Chapter 3.2.4), could subsequently be restricted to the area close to the wound edge and by that normalise the wound healing phenotype in the TOC model. In conclusion, this proof-of-principle experiment demonstrates the valid option of using the model to recapitulate disease-specific wound healing features and the subsequent effect of potential

therapeutic strategies on those. Building up on these findings, it would now be interesting to test the possibility of using external stimuli to achieve similar effects, for example through the application small-molecular compounds directly into the wound area (Galiano et al. 2004).

Overall, the principle of using the organotypic culture system in order to simulate cutaneous wound healing could be shown to be viable for a variety of normal- and disease-phenotype keratinocyte cell lines, even though continuous optimisation can and has to be undertaken. Practical aspects, such as the right method of tissue processing in order to avoid processing artefacts especially along the more fragile wound edge, or optimisation of the culture protocol are an important factor to consider for future development. Adding to the complexity of the model is another option that could be followed up. So far, only epidermal and dermal components are included but it is feasible to assume that the incorporation of vascularisation and inflammation, both vital components in the case of in vivo wound healing (Singer and Clark 1999; Gurtner et al. 2008), could be achieved through relatively easy means. Another interesting alternative would be the introduction of bacterial cultures to the wound model in order to investigate the interplay of microbiota and cutaneous wound healing (Edwards and Harding 2004; Scales and Huffnagle 2013). For example, a suitable pathogen for this would be Staphylococcus aureus, which is a common skin pathogen and has been shown to have a negative effect on wound healing (Haisma et al. 2014; Popov et al. 2014).

3.4. Organotypic Model for the Assessment of Nanopolymer Application

3.4.1. Introduction

In parallel to using the organotypic keratinocyte culture system to model disease phenotypes and investigate potential therapeutic targets, another intended application was the assessment of nanopolymer-based topical delivery approaches. Any external application of a formulation on the skin has to take into account the native permeability barrier function of the upper epidermal layers, which can be crossed through several mechanisms / pathways in order to deliver the drug to the intended area of effect (Prausnitz et al. 2004; Cevc and Vierl 2010). Providing a suitable (and scalable) model of the epidermal permeability barrier would therefore be a distinct advantage in the early development stages of any skin delivery system, providing the means of assessing and optimising the application of the formulation *in vitro* (Jepps et al. 2013; Mathes et al. 2014; Flaten et al. 2015) before proceeding into more complex and elaborate systems such as animal models (GODIN and TOUITOU 2007).Thermo-responsive, PolyNIPAm-based nanogels have recently become a focus of ongoing research since their unique chemical properties make them interesting candidates for controlled drug delivery (Bhuchar et al. 2012; Bergueiro and Calderõn 2015). Shrinking in volume and consequently expelling their cargo at a threshold temperature around 35°C, these nanopolymers would be ideal for the controlled release of compounds into the lower layers of the epidermis after topical application (Samah et al. 2010; Singka et al. 2010; Witting et al. 2015).

Subsequently, fluorescently labelled PolyNIPAm-based nanopolymers were obtained from Prof Marina Resmini (School of Biological and Chemical Sciences, QMUL) and applied on the organotypic model (in comparison to explant skin) after assessing their general interaction with epidermal keratinocytes in monolayer cultures. After verifying the successful epidermal localisation of the nanopolymers as a result of optimised application protocols, the actual delivery and release of a model drug (FFA) into the artificial tissue was analysed.

3.4.2. Nanopolymer Internalisation in Keratinocytes and Effect on Viability

Negatively and neutrally charged nanopolymers were incubated in various concentrations on K17 keratinocytes for 24 and 48 hours before being assessed in regard to their cell internalisation and effect on cell viability (Figure 49). The negatively charged polymers displayed hereby a concentration-dependent increase in internalisation, visible through cytoplasmic green fluorescent signal and the appearance of cytoplasmic vesicles, which further increased with additional incubation time. In contrast, the neutrally charged nanopolymers showed only minimal signs of internalisation but instead formed floating, spherical aggregates which again were dependent in their size on concentration and incubation time. Correspondingly, fluorescent readouts for the Alamar Blue viability assay display only a slight decrease with higher concentrations after 48 hours in case of the neutrally charged polymers. The negatively charged nanopolymers on the other hand resulted in a mostly linear decrease with higher concentrations, with overall higher fluorescence levels (due to an increase in cell number) and a steeper decline after an additional 24 hours, resulting in an almost 50% decrease in viability for the highest concentration of 1 mg/ml in comparison to the untreated control.

In-depth analysis of the internalised negatively charged nanopolymers was subsequently done by incubating at the highest concentration (1mg/ml) for 24 / 48 hours and correlating the internalised green polymer signal with subcellular compartments stained via ICC in red, resulting in a colocalisation of the polymer signal with markers for cis-Golgi (GM130), trans-Golgi (TGN46) and endolysosomes (LAMP2). In order to gain more detailed information about the nanopolymer internalisation, image analysis was performed on the colocalisation pictures and the correlation of green and red signal quantified and compared (Figure 50). The general correlation coefficients PsCo and Li's ICQ display hereby a similar trend as the Manders 1 coefficient which denotes the colocalising fraction of green pixels: a comparatively large decrease for GM130 in between 24 and 48 hours with a moderate decrease for LAMP2 and a relatively slight one in case of TGN46. The red signal-specific Manders 2 coefficient displays a different pattern with slight increases for GM130 and LAMP2 and a minimal decrease for TGN46.

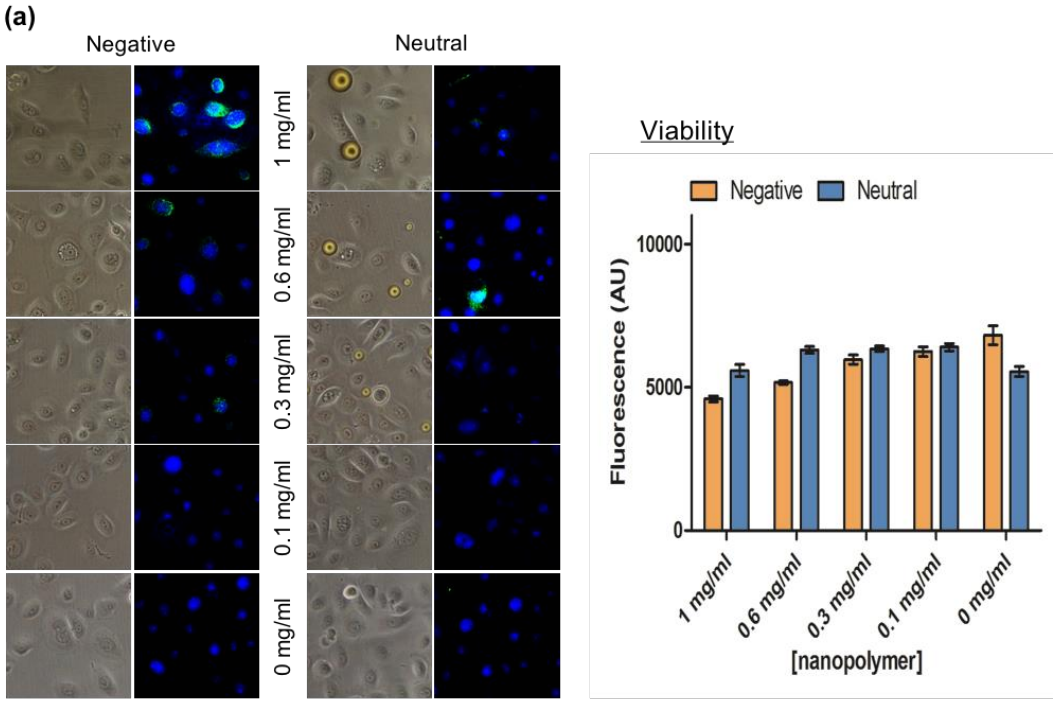
(a)
Negative
Neutral
1 mg/ml
0.6 mg/ml
0.3 mg/ml
0.1 mg/ml
0 mg/ml
Viability
Negative
Neutral
Fluorescence (AU)
10000
5000
0
1 mg/ml
0.6 mg/ml
0.3 mg/ml
0.1 mg/ml
0 mg/ml
[nanopolymer]

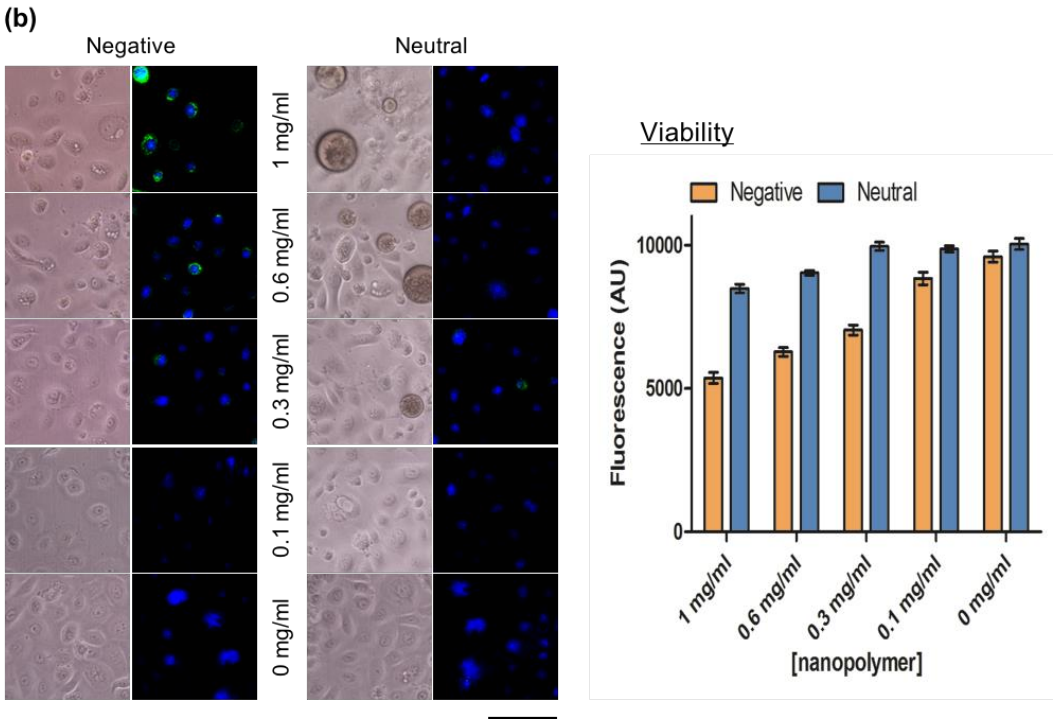
(b)
Negative
Neutral
1 mg/ml
0.6 mg/ml
0.3 mg/ml
0.1 mg/ml
0 mg/ml
Viability
Negative
Neutral
Fluorescence (AU)
10000
5000
0
1 mg/ml
0.6 mg/ml
0.3 mg/ml
0.1 mg/ml
0 mg/ml
[nanopolymer]

Figure 49: Internalisation of nanopolymers in keratinocytes and effect on viability
Negatively and neutrally charged nanopolymers were added to pre-cultured monolayer keratinocytes in concentrations ranging from 0 to 1 mg/ml and incubated together for 24 hours (a) and 48 hours (b). Negatively charged nanopolymers internalise into the cells in a concentration- and time-dependant manner, visible through cytoplasmic green polymer signals and the appearance of internalisation-associated vesicles inside the cells. Neutrally charged nanopolymers only show minimal internalisation but instead tend to form aggregates, visible as yellow floating spheres the diameter of which seems to be concentration and time-dependant as well. Correspondingly to the internalisation data an Alamar Blue assay verified a negative effect of nanopolymers on cell viability which increased with time and concentration and is not visible for neutrally charged nanopolymers.

3.4.3. Topical Application of Nanopolymers on Skin and Organotypics

Subsequent to assessing the interaction of the nanopolymers with keratinocytes in monolayer cultures, polymer solutions were topically applied to explant skin and K17 normal-phenotype organotypics. The aim in this was the investigation of a possible penetration of the nanopolymers across the permeability barrier in the upper epidermal layers and subsequent localisation in the epidermis. Consequently, cross sections of treated skin and organotypic samples were checked for the presence of green fluorescent nanopolymer signals (Figure 51). Correlating the green fluorescence with the brightfield image, and a nuclear counterstain later on for better contrast and resolution, it became apparent that the polymers predominantly stayed on top of the stratum corneum of the skin or the equivalent uppermost layer of the organotypic respectively. Another observation was the strong, inherent autofluorescence of the dermal parts of the explant skin, visible in both the treated as well as the control samples. In consequence to the initially unsuccessful topical application of the negatively charged nanopolymers a more advanced attempt was undertaken, employing both the negatively and neutrally charged polymers in conjunction with two chemical penetration enhancers (DMSO or BA) and using quantitative image analysis for generating an easily comparable readout (Figure 52).

(a)

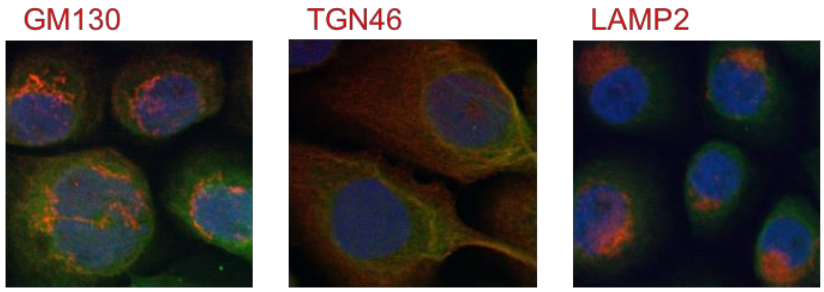

(b)

	GM130		*TGN46*		*LAMP2*	
	24 h	*48 h*	*24 h*	*48 h*	*24 h*	*48 h*
PsCo	0.348	0.167	0.267	0.259	0.291	0.185
Li's ICQ	0.205	0.132	0.153	0.137	0.184	0.154
Manders 1	0.213	0.053	0.317	0.218	0.114	0.055
Manders 2	0.321	0.340	0.151	0.146	0.295	0.332

(c)

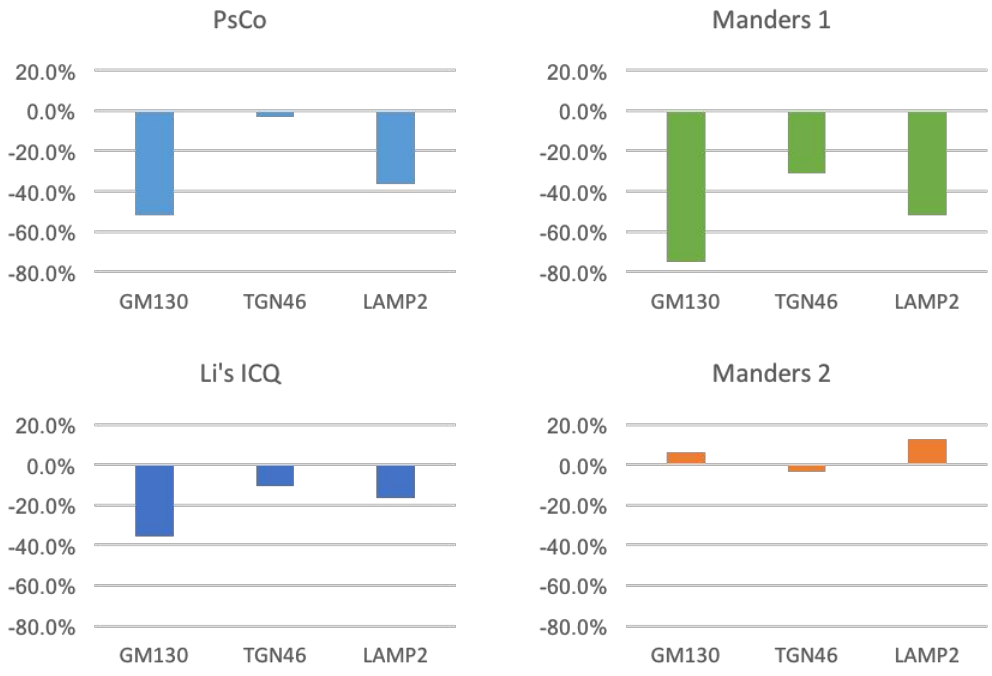

Figure 50: Colocalisation of nanopolymers with subcellular compartments
Image stacks for nanopolymer-subcellular compartment co-stainings (sample images shown in (a) with the compartments in red and nanopolymers in green) were quantified through using to general co-localisation coefficients with PsCo and Li's ICQ as well as channel-specific Manders coefficients, with Manders 1 indicating the fraction of colocalising green nanopolymer signals and Manders 2 showing the fraction of colocalising red department signals. Absolute values for each time point (b) were put into relation to display the relative changes over 24 hours (c). Pearson, Li's ICQ and Manders 1 show hereby similar changes with a strong decrease in colocalisation for GM130 (cis-Golgi), moderate decrease for LAMP2 (endolysosome) and comparatively slight decrease in the case of TGN46 (trans-Golgi). Nanopolymer-based Manders 2 displays a different trend with only a slight decrease in TGN46 and actual increases in colocalisation for GM130 and LAMP2.

Looking at the localisation of both types of polymers in the epidermal area of interest of explant skin samples (Figure 52 a), it was found that in case of the negatively charged polymer both enhancers resulted in an increased epidermal localisation, with a slightly stronger effect for BA. The neutrally charged nanopolymers on the other hand seemed to display a slightly higher localisation on their own, which decreased in combination with BA and increased with DMSO, but was generally more variable, evident through higher error bars. Replicating the application of the negatively charged polymers on normal-phenotype organotypics resulted in similar results to the skin application (Figure 52 b). Even though overall levels of localisation were lower than in the skin the enhancer-dependent increase followed similar a pattern. Correspondingly, when comparing the enhancer-induced fold change in localisation in between skin and organotypic application (Figure 52 c), the results were very comparable (with the organotypic application displaying slightly lower error bars).

After assessing the potential of the negatively charged nanopolymers to cross the epidermal permeability barrier, the next step involved their application as delivery system for the model drug FFA. For this, FFA-loaded polymers were topically applied on organotypics under various conditions, the released FFA extracted from the treated tissue and measured via HPLC (Figure 53).

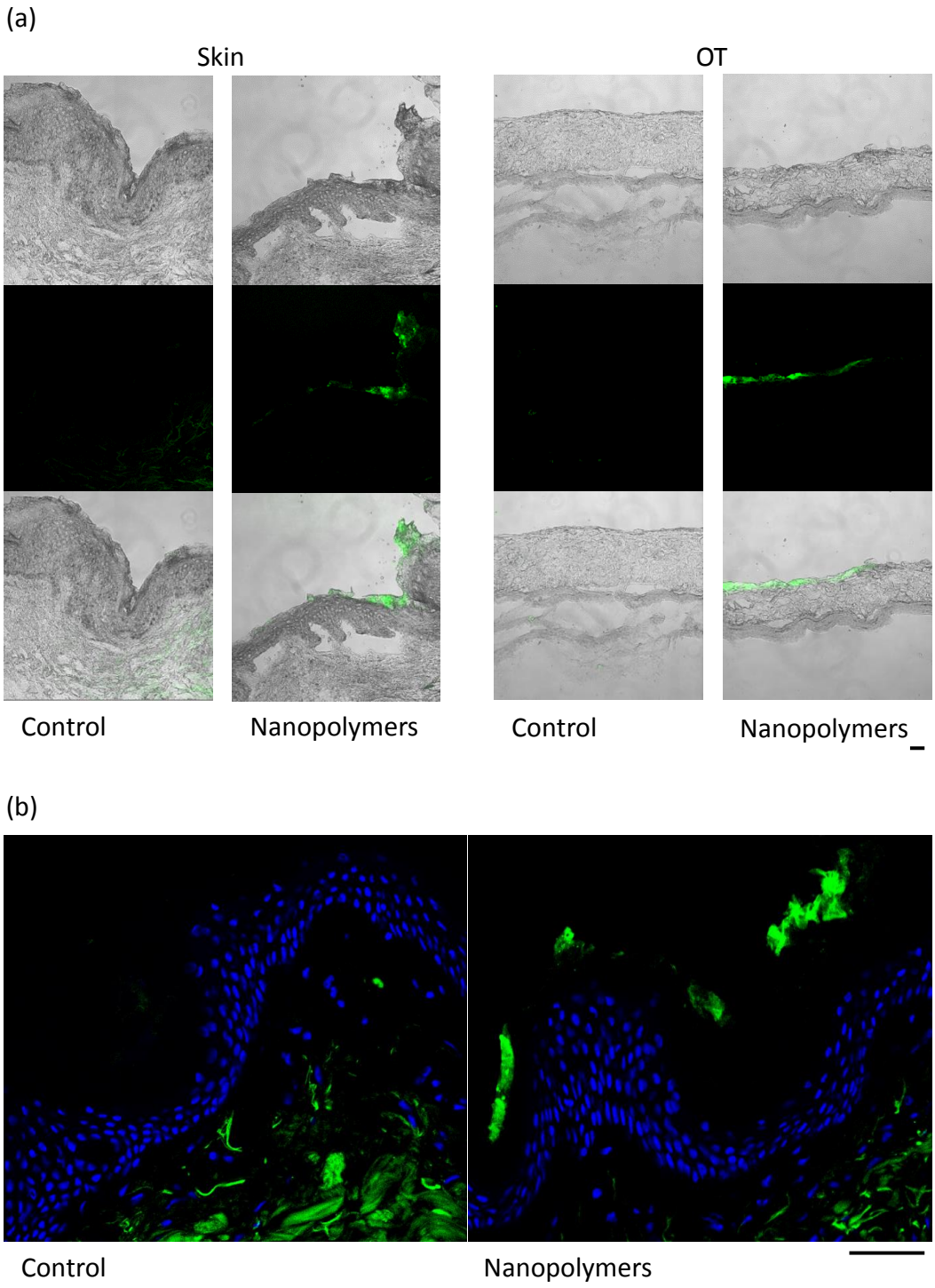

Figure 51: Visualisation of topically applied nanopolymers on skin and organotypic

Green fluorescent nanopolymers were topically applied on explant skin and normal-phenotype organotypics for 24 hours and their retention in the uppermost layers initially visualised in the context of brightfield images (a). Later on, DRAQ5 nuclear counterstaining and high-resolution confocal imaging were used to confirm these findings (b). Scale bar represents 25µm.

Using a commercially available FFA formulation as gold standard, FFA release into the organotypic tissue could be seen to increase slightly over time and more pronounced with an increase in temperature.

A similar trend could be detected for the nanopolymer applications (without the addition of penetration enhancer), albeit with some differences. While the FFA release a room temperature is comparable to the commercial formulation for both time points, the increase at 35°C was strikingly delayed and far more pronounced with almost 25% more recovered FFA after 24 hours than at 12 hours, slightly surpassing the release value for the gold standard at this point. The combination of the FFA-loaded nanopolymers with BA appeared to result in a slight decrease in recovered FFA over time, for both the RT-incubated samples as well as the samples at 35°C which displayed generally higher FFA release rates in comparison. Overall, the three different formulations showed similar release levels at RT, with no major difference in between 12 and 24 hours, and distinctly different changes over time at 35°C, with a slight decrease for the BA-combined polymer sample, a slight increase for the commercial formulation and a drastic increase for the pure nanopolymers.

3.4.4. Summary and Discussion

Due to progressively more restrictive legislation and waning public acceptance, there is an increasing need for the pharmaceutical and especially cosmetic industry to move away from the use of animal models and adopt suitable *in vitro* assays for early development stages of new drugs and delivery systems (Mathes et al. 2014). Complex organotypic *in vitro* assays have to fulfil several requirements in order to be able to sufficiently replace *in vivo* animal experiments (Flaten et al. 2015): besides scalability and reproducibility, which are of importance for large-scale testing series, the faithful modelling of biological parameters in the *in vitro* system is a crucial factor for the viability of any given model (Lotte et al. 2002; Götz et al. 2012a, 2012b). In regard to skin models for the assessment of (trans-)dermal compound applications the presence of a properly functioning permeability barrier is consequently essential (Thakoersing et al. 2012; Andrews et al. 2013; Jepps et al. 2013). The barrier function

of the fully differentiated, normal-phenotype organotypics has already been demonstrated by using a Lucifer Yellow permeation assay (Chapter 3.1.3) but a more thorough follow-up assessment of therapeutically relevant applications in comparison with explant skin was still to be undertaken. For this, thermo-responsive poly-NIPAm-based nanogels were used since their conformational properties makes them ideal candidates for targeted drug carriers (Bhuchar et al. 2012; Bergueiro and Calderõn 2015).

In initial preparation of the actual application, the basic interaction of the nanopolymers with keratinocytes was tested in monolayer cultures. Since surface charge is known to influence skin penetration and cellular uptake of particles, neutrally and negatively charged polymers were therefore tested in parallel (Cho et al. 2009; Gillet et al. 2011; Yang et al. 2012). Positively charged polymers were hereby already dismissed in earlier stages of chemical characterisation due to unfavourable release characteristics. It has been shown that negatively charged polymers internalise to a higher degree than neutrally charged ones but less than particles with a positive charge, which is likely connected to the overall negative charge of the plasma membrane (Jiang et al. 2011; Fröhlich 2012; Kralj et al. 2012). The same trend could be seen in the internalisation experiment, though further enhanced by the unique property of the neutrally charged polymers to form inert aggregates, possibly due to hydrophobic interactions in the aqueous solution. In contrast, the negatively charged polymers readily internalised into the keratinocytes and showed only moderately negative effects on the viability of the cells at the applied concentration range. Viability was hereby measured via an Alamar Blue assay, which has been widely published in the assessment of potentially toxic compounds and is based on the reducing conditions in the cytoplasm of living cells (Rampersad 2012). Subsequently, this initial viability measurement could be complimented by more detailed assessments of plasma membrane integrity , cell proliferation or essential cellular components such as mitochondria, all of which are described as potential mediators of nanopolymer-mediated cytotoxicity (Marquis et al. 2009; Fröhlich 2012).

(a)

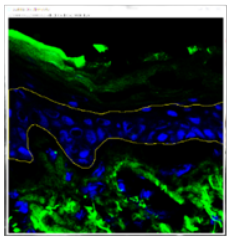

Skin

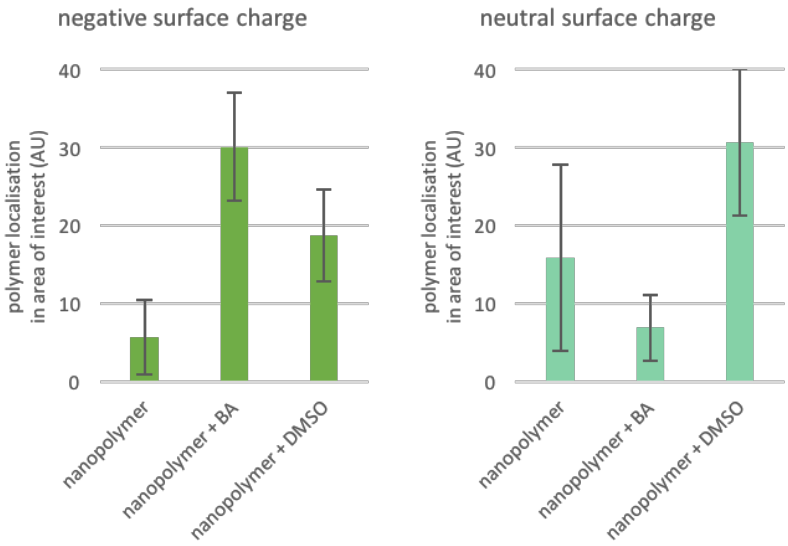
negative surface charge
neutral surface charge
polymer localisation in area of interest (AU)
40
30
20
10
0
nanopolymer
nanopolymer + BA
nanopolymer + DMSO

(b)

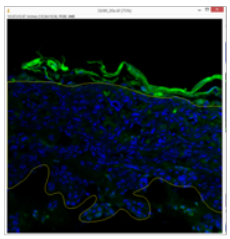

OT

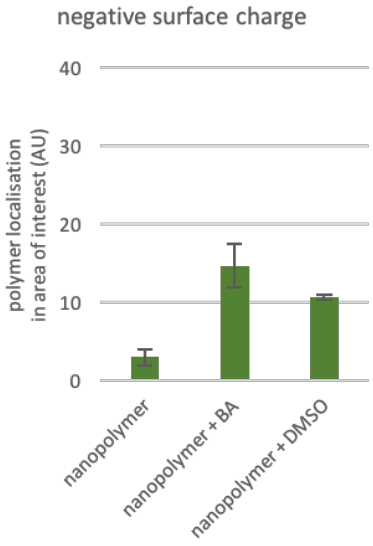
negative surface charge
polymer localisation in area of interest (AU)
40
30
20
10
0
nanopolymer
nanopolymer + BA
nanopolymer + DMSO

(c)

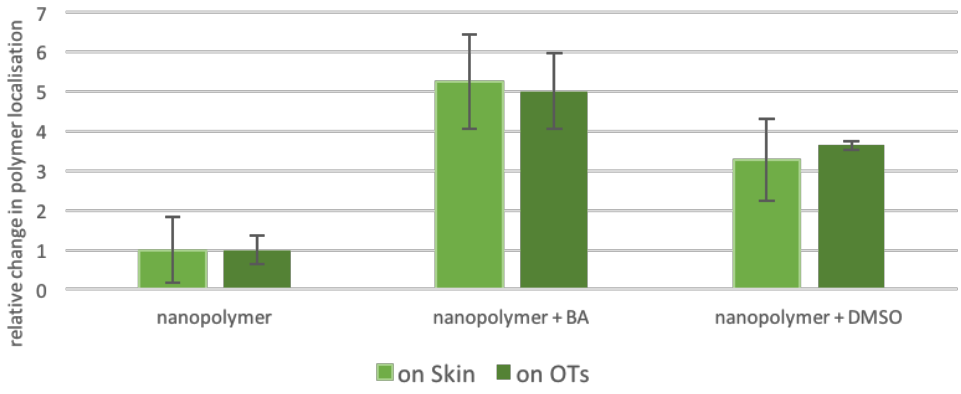
relative change in polymer localisation
7
6
5
4
3
2
1
0
nanopolymer
nanopolymer + BA
nanopolymer + DMSO
on Skin
on OTs

Figure 52: Quantification of epidermal nanopolymer localisation in skin and organotypic
Green-fluorescent nanopolymers (both with negative or neutral surface charge) were topically applied for 24 hours on explant skin, alternatively in conjunction with DMSO or BA as penetration enhancer, and the resulting sample sections analysed for epidermal localisation of the nanopolymers (a). The negatively charged polymers show hereby a strongly increased localisation in the epidermal area of interest with BA and a slightly less increased localisation with DMSO. The neutrally charged polymers show a decrease in localisation with BA and strong increase with DMSO. Parallel application of the negatively charged nanopolymers on normal-phenotype organotypics results in a similar, though generally lower-levelled, pattern as in skin (b). Normalising the values to the pure polymer application reveals very similar enhancer-dependant changes of localisation in both skin and organotypic areas of interest (c).

In conclusion to the general verification of negative polymers internalising into keratinocytes, a more detailed look at internalised polymers in relation to subcellular compartments was undertaken. A first finding was hereby that the polymers appeared to co-localise with components of the endolysosomal pathway, namely late endolysosomes marked by LAMP2 (Winchester 2001; Eskelinen 2006). This seems to indicate an active vesicular uptake of the polymers via endocytosis as opposed to passive plasma membrane penetrance, which seems to be a rare internalisation route mostly connected to cationic gold particles (Lin et al. 2010; Taylor et al. 2010). Correspondingly, clathrin-dependent endocytosis has already been described as possible internalisation route for a variety of negatively charged nanoparticles (Rejman et al. 2004; Jiang et al. 2011; Zaki et al. 2011). Alternatively, other evidence suggests a clathrin-independent endocytosis for small-enough anionic particles, which would be the case for the 10nm-wide negatively charged polymer, outside the endolysosomal pathway (Harush-Frenkel et al. 2007; LAI et al. 2007). To which degree this specific nanopolymer is dependent on clathrin-mediated endocytosis could consequently be clarified with relative ease though by blocking assembly of the clathrin complex through compound treatment or RNA interference (Huang et al. 2004; Gratton et al. 2008). Other compartments found to co-localise with internalised polymers were the cis- and trans-Golgi, which would point to an

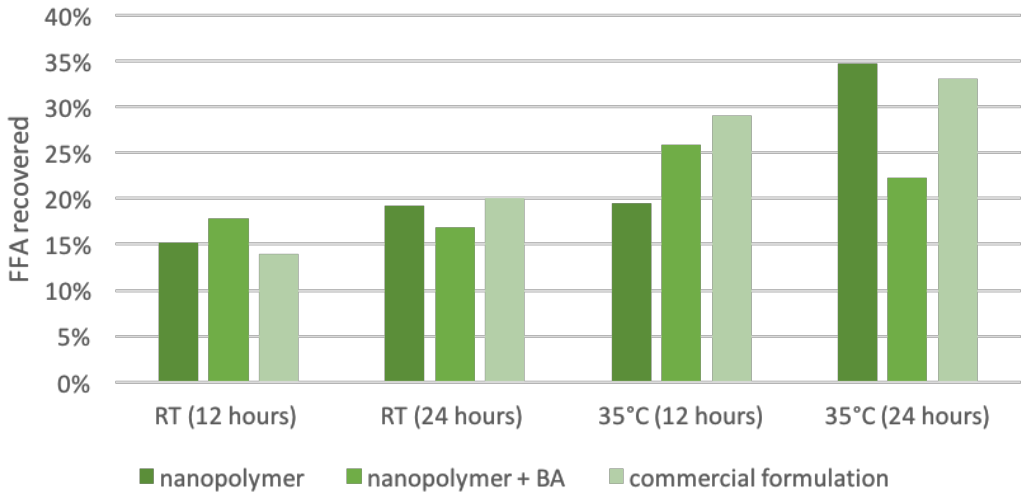
40%
35%
30%
25%
20%
15%
10%
5%
0%
FFA recovered
RT (12 hours)
RT (24 hours)
35°C (12 hours)
35°C (24 hours)
nanopolymer
nanopolymer + BA
commercial formulation

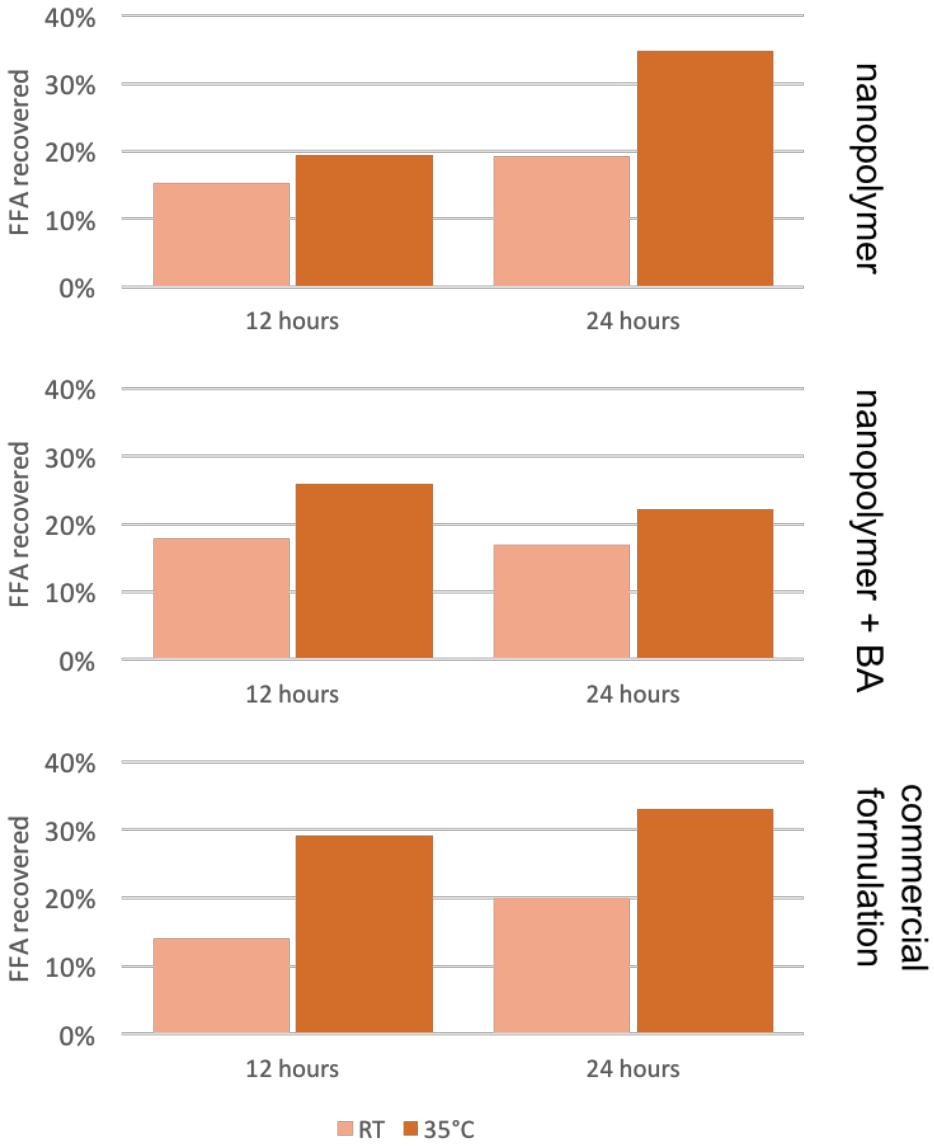
40%
30%
20%
10%
0%
FFA recovered
12 hours
24 hours
nanopolymer
nanopolymer + BA
commercial formulation
RT
35°C

Figure 53: Quantification of nanopolymer-mediated delivery of FFA in organotypics
FFA-loaded nanopolymers, as well as a commercial FFA formulation as gold standard, were topically applied on normal-phenotype organotypics for up to 24 hours at RT and 35°C. Subsequently, the FFA that was released inside the organotypics was retrieved, quantitated via HPLC and related to the initially loaded amount. The commercial formulation shows hereby a steady increase in recovered FFA over time and with higher temperature. Nanopolymer-loaded samples only show a slight increase in released FFA after an additional 12 hours or at 35°C but a drastic rise after 24 hours at the higher temperature. The combination of nanopolymers and BA seems to lead to slightly higher release of FFA at higher temperature but an overall decrease of retrievable FFA after 24 hours.

alternative intracellular transport route from the endosomal compartment retrograde via the trans-Golgi towards cis-Golgi and possibly also ER, potentially followed by subsequent exocytosis (Jiang et al. 2010; Sahay et al. 2010; Kafshgari et al. 2015). Interestingly, GM130-staining for the cis-Golgi seemed to show signs of structural disintegration of the cis-Golgi apparatus, possibly due to enrichment of the polymers followed by a concentration-driven cytoplasmic escape and concomitant disruption of the Golgi cisterns (Domozych 1999; Bantel-schaal et al. 2002; Strobel et al. 2015). Overall the Manders 2 coefficient, which illustrates the involvement of the respectively stained compartment, seemed to indicate an accumulation of the polymers in both the endolysosomal and cis-Golgi compartments whereas the trans-Golgi displayed a slight decrease in polymer co-localisation. This could be explained by the trans-Golgi's role as an intermediate compartment which does not retain polymers but transports them either further towards the ER or alternatively unto an exocytotic route via exosome vesicles (Sakhtianchi et al. 2013; Kafshgari et al. 2015; Strobel et al. 2015). This would also correspond with the comparatively mild changes in Manders 1 and Pearson coefficient as well as Li's ICQ for TGN46, even though changes in these three parameters are mostly driven by the cytoplasmic enrichment of the green-fluorescent polymers, which does not apply to Manders 2, and therefore less reliable in this specific case.

After verifying a typical internalisation pattern and acceptable degree of cytotoxicity for the chosen nanopolymers they were subsequently taken forward to a topical application on explant skin and organotypics, similar in execution and analysis to experiments undertaken before by other groups (Alnasif et al. 2014; Witting et al.

2015). For the topical application the highest used concentration from the monolayer experiments (1 mg/ml) was chosen after initial results showed a strong retention of polymers in the uppermost layers of the skin and organotypics. The rational was hereby that even though the polymer concentration in the topically applied solution resulted in moderate toxicity and possibly detrimental effects on intracellular compartments, the actual concentration in the tissue would be considerably lower due to the limited penetrance and therefore in a range with no negative effect on the surrounding keratinocytes. Furthermore, since penetrance of the nanopolymers by themselves was negligible the two FDA-approved penetration enhancers DMSO and Benzylic alcohol were added to the polymer solutions in subsequent experiments (Sand et al. 2007; Marren 2011).

Consequently, both negatively and neutrally charged polymers showed distinct changes in the application on explant skin with or without the penetration enhancers. The neutral polymers seemed to penetrate slightly better on their own but were generally very variable, even more so than the negatively charged ones, and showed a tendentially reduced penetration with BA, which would imply unfavourable interactions of the neutral polymer with the alcohol. These findings in combination with the results of the monolayer experiments led to the discontinuation of the neutral polymer for further applications. In contrast, the negatively charged polymers displayed a promising pattern of enhanced penetration with slightly less variations and were therefore subsequently applied to the normal-phenotype organotypics as well, resulting in a very similar enhancer-dependent pattern albeit with lower variation in between samples.

Results of the penetration assessments based on image analysis have to be regarded in relation to the inherent limitations of the system. Dermal autofluorescence around the same wavelength as the polymer emission and the inability to account for polymers that might have penetrated all throughout the organotypic sample limit the assessment to the localisation of polymers inside the epidermal portion. As a consequence, it is impossible to tell how much the different results for various enhanced polymer solutions are due to over-penetration of polymers across the epidermis and into non-detectable areas of the tissue. This might be sufficient for carrier systems aimed at the delivery of compounds to epidermal keratinocytes,

which would for example be the case for inflammatory skin diseases, but does not account for the possibility of assessing transdermal delivery of systemically active drugs. Furthermore, even for locally active compounds the information of systemic entry is of importance in regard to pharmacokinetic and toxicological studies (Shah et al. 2014). The existing model would therefore have to be expanded by the addition of a Franz diffusion cell, which would make it possible to detect the fraction of polymers that diffuse through and out of the (organotypic) tissue and thereby complete the assessment (Samah et al. 2010; Witting et al. 2015). Nonetheless, the strikingly similar, though limited, readout for both the application on explant skin as well as organotypic seems to verify the possibility of recreating a functionally equivalent permeability barrier function in the model which has been described as a critical and mostly lacking point in the development of organotypic skin models before, especially when based on immortalised keratinocyte lines (Petrova et al. 2014).

In conclusion to ascertaining the possibility of re-creating a functional permeability barrier in the normal-phenotype organotypic, the model was then taken one step further towards a therapeutically relevant application by assessing the actual drug release from topically applied nanopolymers. For this proof-of-principle experiment, flufenamic acid (FFA) was chosen as a model drug which has already been used in this context by various groups (Luengo et al. 2006; Santander-Ortega et al. 2010). Negatively charged, FFA-loaded polymers were therefore applied to the organotypic model with or without the addition of BA as penetration enhancer and compared to equivalent dose of a commercially available FFA-containing gel formulation (Mobilisin®) as gold standard. In order to achieve a more sensitive, quantifiable readout HPLC analysis was hereby performed on extracts from whole tissue lysates by the School for Biological and Chemical Sciences at Queen Mary University London. The resulting preliminary data seems to indicate a temperature-dependent increase in drug release over time with the nanopolymers, which would correspond with their thermo-responsive properties, and generally similar levels of tissue-released FFA for the polymer- and formulation-treated samples. A slight decrease in recovered FFA over time for the BA-containing sample might again be based on an over-enhanced penetration of polymers and compound through the organotypic into the underlying

culture dish. Overall though, repeated experiments would have to be done in order to account for inherent variability of the model and application and validate the observed preliminary differences. Furthermore, the actual mode of action for the release of FFA from the polymers into the organotypic tissue would have to be studied in more detail in order be able to differentiate between for example an intracellular release of the drug by phagocytosed polymers versus the possibility of polymers being retained in the upper epidermal layers and acting as reservoirs for a sustained extracellular release of compounds and subsequent cellular uptake (Witting et al. 2015). The combination of different fluorophores, one covalently linked to the polymers and one loaded as releasable cargo, and higher-resolution imaging should hereby be suitable to provide more information in this regard (Pappinen et al. 2012).

After performing a series of preliminary experiments in order to investigate the potential of applying the organotypic culture model for the assessment of topical drug delivery the results appear promising but in need of further optimisation. It was possible to generate an epidermal barrier function that displays skin-similar characteristic changes in polymer permeation in reaction to different conditions but in order to account for the penetration of topically applied substances throughout the organotypic further enhancements, for example in form of a Franz cell system, have to be made. In addition to the possibility of a systemic entry of the drug via dermal capillaries, another important aspect of skin drug delivery is the interaction of compounds and carriers with dermally located parts of the immune system; the incorporation of macrophages and other tissue-resident lymphocytes would therefore be a distinct advantage for the overall viability of the model (Bechetoille et al. 2011; Linde et al. 2012; Van Den Bogaard et al. 2014). Since skin appendages present an important route for the (trans-)dermal delivery of drug, it would furthermore be an intriguing option to include pre-cultured or artificially generated sweat glands or hair follicles into the organotypic (Michel et al. 1999; Huang et al. 2010, 2012; Lindner et al. 2011). Subsequent to optimising the normal-phenotype model for the assessment of topical delivery it would also be interesting to then perform the same assessment in the established disease phenotypes (Chapter 3.2), since both HI and TOC are known to manifest in barrier dysregulation (Thomas et al.

2009; Brooke et al. 2014). Additionally, the delivery of already tested compounds, for example the ADAM17-inhibitor TMI-005 for TOC, would allow for a simple and therapeutically relevant readout for the successful application, similarly to an already published delivery of TGM-1 to disease organotypics and the subsequent alleviation of the specific phenotype (Witting et al. 2015). In parallel to the disease models, the organotypic wound model (Chapter 3.3.) also presents an interesting opportunity for the application and assessment of several nanomaterials which have already been described in their positive effect on epidermal wound healing (Leu et al. 2012; Rigo et al. 2013; Krausz et al. 2015).

4. Final Discussion

4.1. Summary of the Results

The overall aim of this thesis project was the establishment of a modifiable organotypic keratinocyte culture system and its application in modelling of cutaneous disease phenotypes and epidermal wound healing as well as the assessment of topical drug delivery via nanopolymeric carrier systems.

A collagen-based organotypic cell culture protocol was established and used to generate skin equivalents for a variety of immortalised cell lines (HaCaT, nTERT, K17, NEB1). While very variable and with a more or less pronounced tendency towards hyperproliferation (dependent on the individual cell line), all of them resulted in skin-like phenotypes, showing mostly appropriate protein expression patterns and epidermal barrier function (which further included a stratum corneum-like uppermost layer, visible in histological stainings).

The culture system was then expanded to include several disease models based on patient-derived keratinocyte cell lines for Harlequin ichthyosis, Tylosis and Pachyonychia congenita. The HI model, possessing a recessive loss-of-function mutation in the ABCA12 gene, displayed various disease-specific phenotypical features in regard to histology (hyper- and parakeratosis) and protein expression (upregulation of CK16 and Involucrin). Other features, such as an expected absence of non-polar lipids, were not present, which might be explained by the extended culture time of the immortalised cells and a connected self-improvement mechanism. Nonetheless, in an attempt to alleviate the presented disease features two agonistic compounds for LXR and PPARδ were applied to the model, resulting in the intended upregulation of ABCA1 and consequently a slight improvement in regard to the histological features and Involucrin expression. The TOC model showed a hyperproliferation phenotype, corresponding to the disease-causing gain-of-function mutation in iRHOM2 and the resulting ADAM17-dependent upregulation of

EGFR signalling, which manifested itself in a thickened, disordered epidermal portion and upregulated expression of iRHOM2, CK16 and EGFR. Epidermal thickening and CK16 overexpression were subsequently counteracted via two independent approaches: shRNA-mediated (partial) knockdown of iRHOM2 and application of the ADAM17 inhibitor TMI-005. The successful application of TMI-005 was consequently extended to the PC model, on the basis of the general anti-hyperproliferative effect of TMI-005 and the demonstrated functional connection between CK16, which harbours the PC-causing gain-of-function mutation, and the iRHOM2-ADAM17-EGFR axis. Using the ADAM17 inhibitor in the PC model resulted in comparable results to the one from the TOC model: hyperproliferation-associated markers were slightly down- and differentiation marker slightly upregulated, in addition to an improvement to the initially disordered histology.

In parallel to the various disease phenotypes, a full-thickness dermal-epidermal wound healing model was established. Showing a progressive re-epithelialisation and spatially appropriate expression of wound healing markers such as CK16 and Cx26 over time, it could further be positively or negatively modulated though variations in the underlying wound matrix (e.g. via the omission of fibroblast or the addition of EGF). Furthermore, the model was used to recapitulate a TOC-typical “constitutive wound healing” phenotype and alleviate it subsequently via RNA interference for iRHOM2.

Based on the presence of a functional permeability barrier, the normal-phenotype model was then used for the assessment of topically applied fluorescent nanopolymers. Subsequently to verifying a typical internalisation pattern and lack of overly cytotoxic effect on monolayer keratinocytes, negatively charged polymers were applied on top of explant skin and fully stratified organotypics in order to test for permeation across the uppermost layer and into the epidermis. After displaying a negligible penetrance of the polymers by themselves, they were applied in conjunction with penetration enhancers DMSO and BA, resulting in very similar enhancer-dependent changes for the epidermal localisation of the polymers on skin and organotypics. With the suitability of the model therefore being demonstrated it

was then taken one step further towards a relevant application by successfully trying to detect and quantify the delivery and release of FFA inside the tissue. Subsequently, further work could be undertaken by employing additional analysis methods (e.g. Franz cell diffusion chamber) or widening the application of the model to the assessment of other carrier systems.

4.2. Limitations of the Organotypic Model

In the course of establishing the culture model and its several applications, various shortcomings and limitations became apparent. While (minor) technical issues, such as the necessary analysis of transdermal polymer penetrance via Franz cells, the expansion of the wound model through additional components or the optimisation of compound applications, are comparatively easy to be addressed, the problematic of the immortalised cell lines is more elaborate. The application of immortalised patient-derived cell lines has undisputable advantages when it comes to the virtually unlimited availability of rare disease-specific material and the modelling of more complex and/or dominant gain-of-function mutations (Thomas et al. 2009; Blaydon et al. 2013; Brooke et al. 2014). But the tendency of HPV16 E6/7-immortalised cell lines to present hyperproliferative and even premalignant characteristics (especially in 3D skin equivalents) is well documented (Blanton et al. 1991; Delvenne et al. 2001; Pickard et al. 2015; Srivastava et al. 2015) and also apparent in the context of this project. As a result, skin equivalents show a comparatively high degree of variability (in between different cell lines of the same origin as well as in between batches of the same cell line) and a general hyperproliferation / invasion phenotype which potentially poses a problem in the modelling of hyperproliferative, inflammatory diseases.

4.3. Potential Improvements for the Organotypic Model

A straightforward solution for future applications would be the switch to a more preferable protocol for the generation of patient-derived cells. Different immortalisation methods have been shown to result in cell lines more suitable for complex modelling: hTERT-based immortalised cells have already been used in the

setup of relatively healthy skin equivalents (Dickson et al. 2000; Man et al. 2007; Reijnders et al. 2015) and the manipulation of the Rho/ROCK signalling pathway has recently emerged as a promising alternative to classic immortalisation protocols (McMullan et al. 2003). Using the specific ROCK inhibitor Y-27632 on primary keratinocytes results in a reversible transition into an effectively immortalised state with greatly increased proliferative capacity, while forgoing the introduction of exogenous genes (Chapman et al. 2010; Liu et al. 2012). Consequently, treated keratinocytes retain primary cell characteristics, revert back to normal senescence after treatment stop and are capable of forming very skin-like equivalents (van den Bogaard et al. 2012; Chapman et al. 2014). Alternatively, the induced pluripotency of patient-derived primary cells and subsequent reprogramming into keratinocyte suitable for high-quality skin equivalents is a well-established method (Itoh et al. 2011; Petrova et al. 2014; Umegaki-arao et al. 2014). Another distinct advantage would hereby be the possibility of differentiating one iPSC line into different cell types and create complex tissue models from the same (mutated) genetic source, e.g. a dermal-epidermal model for dystrophic epidermolysis bullosa with fibroblast and keratinocytes being based on the same patient-derived iPSC culture (Itoh et al. 2013).

Since these approaches are not applicable to the existing (and irreplaceable) patient cell lines, another aim has to be the optimisation of the organotypic culture for already immortalised cell lines. One possible solution has already been implied in the course of this project: ADAM17-inhibitor TMI-005 has been demonstrated to reduce hyperproliferation and invasion in TOC and PC disease models. A preliminary attempt at translating these findings to a normal-phenotype skin equivalent resulted in the strikingly improved histology and expression of differentiation marker Involucrin in HaCaT organotypics (Figure 54).

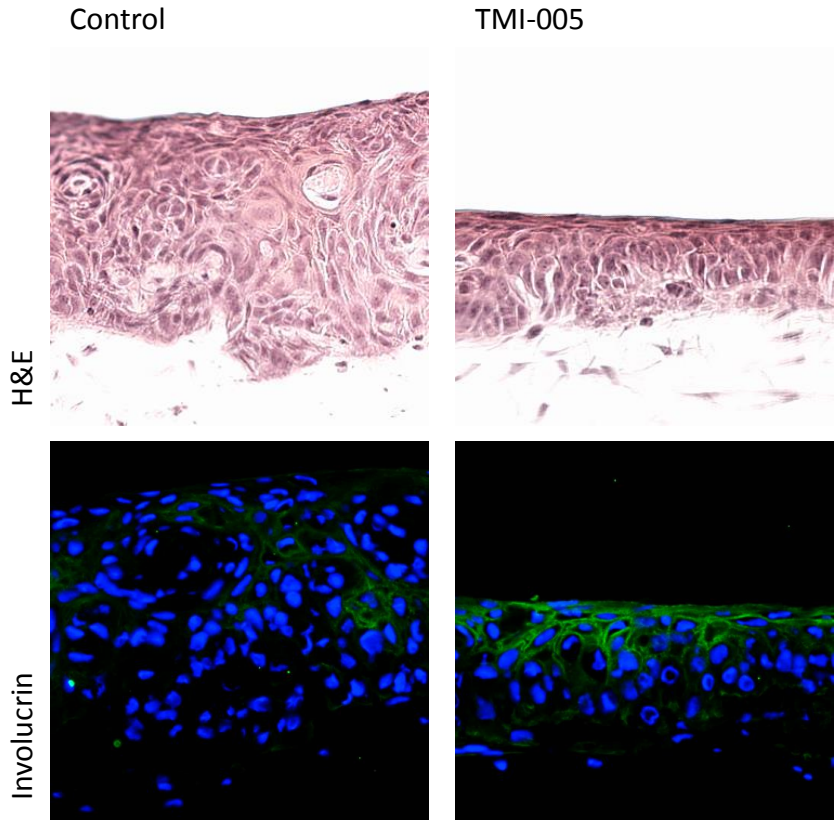

Figure 54: Effect of TMI-005 on HaCaT organotypics

After culturing HaCaT organotypics for 10 days with the ADAM17 inhibitor TMI-005 (or DMSO for the control), striking differences in regard to histology and differentiation can be seen. The epidermal portion is less hyperproliferative and disordered but more stratified instead; suprabasal expression of differentiation marker Involucrin is concomitantly upregulated.

Variability in between cell lines immortalised with the same HPV-based protocol is another issue that became apparent in the early stage of this project. Since this variability cannot be excluded in the context of disease and control cell lines either and would potentially dampen disease-related differences (especially in regard to hyperproliferation-associated features), certain adjustments would be advantageous. The CRISPR/Cas9 system can be used to either introduce specific (disease-causing) mutations into healthy cells or perform genomic correction on disease cell lines (Li et al. 2016; Paquet et al. 2016), thereby providing the perfect tool to generate isogenic control-disease cell line pairs derived from a single immortalised cell line (Kim et al. 2014; Marthaler et al. 2016) and disregard the inherent variability in between different cell lines.

In addition to the variability in between cell lines, the inter-batch variability for each individual cell line in the context of complex organotypic culture systems has to be taken into consideration when interpreting results derived in this context. Therefore, thorough repetition for certain experiments would have to be undertaken in order to account for this variability and confirm (quantifiable) results.

4.4. Conclusion

Even though the established model system and applications are still in need of further optimisation (some of which is already in progress) and preliminary results have to be repeated and confirmed, it was so far possible to model several inflammatory disease phenotypes to some degree, recreate dermal wound healing features in vitro and use a functional epidermal barrier function in the organotypic to assess the application novel drug delivery systems.

Consequently, the potential to advance this proof-of-principle project into a relevant tool for the investigation of cutaneous disease / wound models and possible therapeutic strategies is present and warrants a continued development.

References

Ackermann, K, Lombardi Borgia, S, Korting, HC, *et al.* (2010). The Phenion full-thickness skin model for percutaneous absorption testing. *Skin Pharmacol Physiol* 23: 105–12.

Adebowale, AS, Choonara, YE, Kumar, P, *et al.* (2015). Functionalized Nanocarriers for Enhanced Bioactive Delivery to Squamous Cell Carcinomas: Targeting Approaches and Related Biopharmaceutical Aspects. *Curr Pharm Des* 21: 3167–80.

Adrain, C, Freeman, M (2012). New lives for old: evolution of pseudoenzyme function illustrated by iRhoms. *Nat Rev Mol Cell Biol* 13: 489–98.

Agar, N, Young, AR (2005). Melanogenesis: a photoprotective response to DNA damage? *Mutat Res* 571: 121–32.

Akiyama, M (2005). Mutations in lipid transporter ABCA12 in harlequin ichthyosis and functional recovery by corrective gene transfer. *J Clin Invest* 115: 1777–84.

Alexander, A, Dwivedi, S, Ajazuddin, *et al.* (2012). Approaches for breaking the barriers of drug permeation through transdermal drug delivery. *J Control Release*.

Allen-Hoffmann, BL, Schlosser, SJ, Ivarie, CA, *et al.* (2000). Normal growth and differentiation in a spontaneously immortalized near-diploid human keratinocyte cell line, NIKS. *J Invest Dermatol* 114: 444–55.

Alnasif, N, Zoschke, C, Fleige, E, *et al.* (2014). Penetration of normal, damaged and diseased skin--an in vitro study on dendritic core-multishell nanotransporters. *J Control Release* 185: 45–50.

Amagai, M, Klaus-Kovtun, V, Stanley, JR (1991). Autoantibodies against a novel epithelial cadherin in pemphigus vulgaris, a disease of cell adhesion. *Cell* 67: 869–77.

Andrei, G, Duraffour, S, Van den Oord, J, *et al.* (2010). Epithelial raft cultures for investigations of virus growth, pathogenesis and efficacy of antiviral agents. *Antiviral Res* 85: 431–49.

Andrews, SN, Jeong, E, Prausnitz, MR (2013). Transdermal delivery of molecules is

limited by full epidermis, not just stratum corneum. *Pharm Res* 30: 1099–109.

Anigbogu, ANC, Williams, AC, Barry, BW, *et al.* (1995). Fourier transform raman spectroscopy of interactions between the penetration enhancer dimethyl sulfoxide and human stratum corneum. *Int J Pharm* 125: 265–82.

Antonio, JR, Antonio, CR, Cardeal, ILS, *et al.* (2014). Nanotechnology in dermatology. *An Bras Dermatol*.

Arif, T, Nisa, N, Amin, SS, *et al.* (2015). Therapeutic and Diagnostic Applications of Nanotechnology in Dermatology and Cosmetics. *J Nanomedine Biotherapeutic Discov* 5.

Arribas, J, Esselens, C (2009). ADAM17 as a therapeutic target in multiple diseases. *Curr Pharm Des* 15: 2319–35.

Astashkina, A, Mann, B, Grainger, D (2012). A critical evaluation of in vitro cell culture models for high-throughput drug screening and toxicity. *Pharmacol Ther* 134: 82–106.

Auxenfans, C, Lequeux, C, Perrusel, E, *et al.* (2012). Adipose-derived stem cells (ASCs) as a source of endothelial cells in the reconstruction of endothelialized skin equivalents. *J Tissue Eng Regen Med* 6: 512–8.

Azagury, A, Khoury, L, Enden, G, *et al.* (2014). Ultrasound mediated transdermal drug delivery. *Adv Drug Deliv Rev*.

Bachelor, M, Binder, RL, Cambron, RT, *et al.* (2014). Transcriptional profiling of epidermal barrier formation in vitro. *J Dermatol Sci* 73: 187–97.

Bannasch, H, Momeni, A, Knam, F, *et al.* (2010). Tissue engineering of skin substitutes. *Burns* 36: 450–60.

Bantel-schaal, U, Hub, B, Kartenbeck, J (2002). Endocytosis of Adeno-Associated Virus Type 5 Leads to Accumulation of Virus Particles in the Golgi Compartment Endocytosis of Adeno-Associated Virus Type 5 Leads to Accumulation of Virus Particles in the Golgi Compartment. *Society* 76: 2340–9.

Barker, CL, McHale, MT, Gillies, AK, *et al.* (2004). The development and characterization of an in vitro model of psoriasis. *J Invest Dermatol* 123: 892–901.

Baroli, B (2010). Penetration of Nanoparticles and Nanomaterials in the Skin : Fiction or Reality ? *J Pharm Sci* 99: 21–50.

Barry, B (1983). Dermatological Formulations: Percutaneous Absorption. *Inf Heal Care* 18.

Baum, CL, Arpey, CJ (2005). Normal cutaneous wound healing: clinical correlation with cellular and molecular events. *Dermatologic Surg* 31: 674–86; discussion 686.

Bechetoille, N, Vachon, H, Gaydon, A, *et al.* (2011). A new organotypic model containing dermal-type macrophages. *Exp Dermatol* 20: 1035–7.

Becker, DL, Thrasivoulou, C, Phillips, ARJ (2012). Connexins in wound healing; perspectives in diabetic patients. *Biochim Biophys Acta - Biomembr* 1818: 2068–75.

Becker, RA, Borgert, CJ, Webb, S, *et al.* (2006). Report of an ISRTP Workshop: Progress and barriers to incorporating alternative toxicological methods in the U.S. *Regul Toxicol Pharmacol* 46: 18–22.

Bentivegna, A, Roversi, G, Riva, G, *et al.* (2016). The effect of culture on human bone marrow mesenchymal stem cells: Focus on DNA methylation profiles. *Stem Cells Int* 2016: 5656701.

Bergueiro, J, Calderõn, M (2015). Thermoresponsive nanodevices in biomedical applications. *Macromol Biosci* 15: 183–99.

Berner, B, Mazzenga, GC, Otte, JH, *et al.* (1989). Ethanol: water mutually enhanced transdermal therapeutic system II: skin permeation of ethanol and nitroglycerin. *J Pharm Sci* 78: 402–7.

Betz, P, Nerlich, A, Wilske, J, *et al.* (1993). The time-dependent localization of Ki67 antigen-positive cells in human skin wounds. *Int J Legal Med* 106: 35–40.

Bhora, FY, Dunkin, BJ, Batzri, S, *et al.* (1995). Effect of growth factors on cell proliferation and epithelialization in human skin. *J Surg Res* 59: 236–44.

Bhuchar, N, Sunasee, R, Ishihara, K, *et al.* (2012). Degradable Thermoresponsive Nanogels for Protein Encapsulation and Controlled Release. *Bioconjug Chem* 23: 75–83.

Binato, R, de Souza Fernandez, T, Lazzarotto-Silva, C, *et al.* (2013). Stability of human mesenchymal stem cells during in vitro culture: Considerations for cell therapy. *Cell Prolif* 46: 10–22.

Black, AF, Berthod, F, L'heureux, N, *et al.* (1998). In vitro reconstruction of a human

capillary-like network in a tissue-engineered skin equivalent. *FASEB J* 12: 1331–40.

Blank, IH, Scheuplein, RJ, Macfarlane, DJ (1967). Mechanism of Percutaneous Absorption. *J Invest Dermatol* 49: 582–9.

Blanpain, C, Fuchs, E (2009). Epidermal homeostasis: a balancing act of stem cells in the skin. *Nat Rev Mol Cell Biol* 10: 207–17.

Blanton, RA, Perez-Reyes, N, Merrick, DT, *et al.* (1991). Epithelial cells immortalized by human papillomaviruses have premalignant characteristics in organotypic culture. *Am J Pathol* 138: 673–85.

Blaydon, D, Etheridge, S, Risk, J, *et al.* (2012). RHBDF2 mutations are associated with tylosis, a familial esophageal cancer syndrome. *Am J Hum Genet* 90: 340–6.

Blaydon, D, Lind, L, Plagnol, V, *et al.* (2013). Mutations in AQP5, encoding a water-channel protein, cause autosomal-dominant diffuse nonepidermolytic palmoplantar keratoderma. *Am J Hum Genet* 93: 330–5.

Blaydon, DC, Nitoiu, D, Eckl, K-M, *et al.* (2011). Mutations in CSTA, encoding Cystatin A, underlie exfoliative ichthyosis and reveal a role for this protease inhibitor in cell-cell adhesion. *Am J Hum Genet* 89: 564–71.

Bodnar, RJ (2013). Epidermal Growth Factor and Epidermal Growth Factor Receptor: The Yin and Yang in the Treatment of Cutaneous Wounds and Cancer. *Adv wound care* 2: 24–9.

Boelsma, E, Verhoeven, M, Ponec, M (1999). Reconstruction of a Human Skin Equivalent Using a Spontaneously Transformed Keratinocyte Cell Line (HaCaT). *Soc Invest Dermatol* 112: 489–98.

Bogaard, E van den, Bergboer, J, Vonk-Bergers, M (2013). Coal tar induces AHR-dependent skin barrier repair in atopic dermatitis. *J Clin Invest* 1–11.

van den Bogaard, EH, Rodijk-Olthuis, D, Jansen, PAM, *et al.* (2012). Rho Kinase Inhibitor Y-27632 Prolongs the Life Span of Adult Human Keratinocytes, Enhances Skin Equivalent Development, and Facilitates Lentiviral Transduction. *Tissue Eng Part A* 18: 1827–36.

Van Den Bogaard, EH, Tjabringa, GS, Joosten, I, *et al.* (2014). Crosstalk between Keratinocytes and T Cells in a 3D Microenvironment: A Model to Study

Inflammatory Skin Diseases. *J Invest Dermatol* 134: 719–27.

Bolte, S, Cordelières, FP (2006). A guided tour into subcellular colocalization analysis in light microscopy. *J Microsc* 224: 213–32.

Bonifas, JM, Rothman, AL, Epstein, EH (1991). Epidermolysis bullosa simplex: evidence in two families for keratin gene abnormalities. *Science* 254: 1202–5.

Boukamp, P, Petrussevska, RTT, Breitkreutz, D, *et al.* (1988). Normal Keratinization in a Spontaneously Immortalized Aneuploid Human Keratinocyte Cell Line. *J Cell Biol* 106: 761–71.

Bowden, PE, Haley, JL, Kansky, A, *et al.* (1995). Mutation of a type II keratin gene (K6a) in pachyonychia congenita. *Nat Genet* 10: 363–5.

Boxman, ILA, Mulder, LHC, Noya, F, *et al.* (2001). Transduction of the E6 and E7 Genes of Epidermodysplasia-Verruciformis-Associated Human Papillomaviruses Alters Human Keratinocyte Growth and Differentiation in Organotypic Cultures. *J Invest Dermatol* 117: 1397–404.

Brandner, J, Haftek, M, Niessen, C (2010). Adherens Junctions , Desmosomes and Tight Junctions in Epidermal Barrier Function. *Open Dermatol J* 4: 14–20.

Brandner, JM, Houdek, P, Hüsing, B, *et al.* (2004). Connexins 26, 30, and 43: Differences among spontaneous, chronic, and accelerated human wound healing. *J Invest Dermatol* 122: 1310–20.

Breetveld, M, Richters, CD, Rustemeyer, T, *et al.* (2006). Comparison of wound closure after burn and cold injury in human skin equivalents. *J Invest Dermatol* 126: 1918–21.

Brody, I (1988). Changes in Keratinocyte Maturation during Wound Healing. *J Invest Dermatol* 90: 770.

van den Broek, LJ, Limandjaja, GC, Niessen, FB, *et al.* (2014). Human hypertrophic and keloid scar models: Principles, limitations and future challenges from a tissue engineering perspective. *Exp Dermatol* 23: 382–6.

van den Broek, LJ, Niessen, FB, Scheper, RJ, *et al.* (2012). Development, validation and testing of a human tissue engineered hypertrophic scar model. *ALTEX* 29: 389–402.

Brooke, MA, Etheridge, SL, Kaplan, N, *et al.* (2014). iRHOM2-dependent regulation of ADAM17 in cutaneous disease and epidermal barrier function. *Hum Mol*

Genet 23: 4064–76.

Burns, D, Breathnach, S, Cox, N, *et al.* (2008). *Rook's Textbook of Dermatology.* 7th edn. Blackwell Science.

Buzea, C, Pacheco, II, Robbie, K (2007). Nanomaterials and nanoparticles: sources and toxicity. *Biointerphases* 2: MR17-R71.

Cai, M, Yang, Y (2014). Targeted Genome Editing Tools for Disease Modeling and Gene Therapy. *Curr Gene Ther* 14: 2–9.

Caiazza, F, McGowan, PM, Mullooly, M, *et al.* (2015). Targeting ADAM-17 with an inhibitory monoclonal antibody has antitumour effects in triple-negative breast cancer cells. *Br J Cancer* 112: 1895–903.

Campbell, CSJ, Contreras-Rojas, LR, Delgado-Charro, MB, *et al.* (2012). Objective assessment of nanoparticle disposition in mammalian skin after topical exposure. *J Control Release* 162: 201–7.

Candi, E, Schmidt, R, Melino, G (2005). The cornified envelope: a model of cell death in the skin. *Nat Rev Mol Cell Biol* 6: 328–40.

Cao, C, Sun, Y, Healey, S, *et al.* (2006). EGFR-mediated expression of aquaporin-3 is involved in human skin fibroblast migration. *Biochem J* 400: 225–34.

Caubet, C, Jonca, N, Brattsand, M, *et al.* (2004). Degradation of corneodesmosome proteins by two serine proteases of the kallikrein family, SCTE/KLK5/hK5 and SCCE/KLK7/hK7. *J Invest Dermatol* 122: 1235–44.

Cevc, G (2004). Lipid vesicles and other colloids as drug carriers on the skin. *Adv Drug Deliv Rev* 56: 675–711.

Cevc, G, Vierl, U (2010). Nanotechnology and the transdermal route. A state of the art review and critical appraisal. *J Control Release*.

Chapman, S, Liu, X, Meyers, C, *et al.* (2010). Human keratinocytes are efficiently immortalized by a Rho kinase inhibitor. *J Clin Invest* 120: 2619–26.

Chapman, S, McDermott, DH, Shen, K, *et al.* (2014). The effect of Rho kinase inhibition on long-term keratinocyte proliferation is rapid and conditional. *Stem Cell Res Ther* 5: 60.

Charoo, N a, Rahman, Z, Repka, M a, *et al.* (2010). Electroporation: an avenue for transdermal drug delivery. *Curr Drug Deliv* 7: 125–36.

Chawla, A, Boisvert, WA, Lee, CH, *et al.* (2001). A PPAR gamma-LXR-ABCA1 pathway

in macrophages is involved in cholesterol efflux and atherogenesis. *Mol Cell* 7: 161–71.

Chen, B, Wei, J, Iliescu, C (2010). Sonophoretic enhanced microneedles array (SEMA)—Improving the efficiency of transdermal drug delivery. *Sensors Actuators B Chem* 145: 54–60.

Cheng, R, Meng, F, Deng, C, *et al.* (2013). Dual and multi-stimuli responsive polymeric nanoparticles for programmed site-specific drug delivery. *Biomaterials* 34: 3647–57.

Cho, EC, Xie, J, Wurm, PA, *et al.* (2009). Understanding the Role of Surface Charges in Cellular Adsorption versus Internalization by Selectively Removing Gold Nanoparticles on the Cell Surface with a I_2/KI Etchant. *Nano Lett* 9: 1080–4.

Cho, K, Wang, X, Nie, S, *et al.* (2008). Therapeutic nanoparticles for drug delivery in cancer. *Clin Cancer Res* 14: 1310–6.

Clark, RAF, Nielsen, LD, Welch, MP, *et al.* (1995). Collagen matrices attenuate the collagen-synthetic response of cultured fibroblasts to TGF-β. *J Cell Sci* 108: 1251–61.

Clausen, B, Kel, J (2010). Langerhans cells: critical regulators of skin immunity? *Immunol Cell Biol* 88: 351–60.

Cong, L, Ran, FA, Cox, D, *et al.* (2013). Multiplex genome engineering using CRISPR/Cas systems. *Science* 339: 819–23.

Contado, C (2015). Nanomaterials in consumer products: a challenging analytical problem. *Front Chem* 3: 48.

Cotsarelis, G (2006). Epithelial Stem Cells: A Folliculocentric View. *J Invest Dermatol* 126: 1459–68.

Coutinho, P (2003). Dynamic changes in connexin expression correlate with key events in the wound healing process. *Cell Biol Int* 27: 525–41.

Cuggino, JC, Alvarez I., CI, Strumia, MC, *et al.* (2011). Thermosensitive nanogels based on dendritic polyglycerol and N-isopropylacrylamide for biomedical applications. *Soft Matter* 7: 11259.

Cvetkovska, B, Islam, N, Goulet, F, *et al.* (2009). Identification of functional markers in a self-assembled skin substitute in vitro. *Vitr Cell Dev Biol - Anim* 44: 444–50.

Dai, N-T, Williamson, MR, Khammo, N, *et al.* (2004). Composite cell support

membranes based on collagen and polycaprolactone for tissue engineering of skin. *Biomaterials* 25: 4263–71.

Dale, B, Presland, R (1997). Transient expression of epidermal filaggrin in cultured cells causes collapse of intermediate filament networks with alteration of cell shape and nuclear integrity. *J Invest Dermatol* 108: 179–87.

Davidson, JM (1998). Animal models for wound repair. *Arch Dermatol Res* 290: S1–11.

Delouise, LA (2012). Applications of Nanotechnology in Dermatology. *J Invest Dermatol* 132: 964–75.

Delvenne, P, Al-Saleh, W, Gilles, C, *et al.* (1995). Inhibition of growth of normal and human papillomavirus-transformed keratinocytes in monolayer and organotypic cultures by interferon-gamma and tumor necrosis factor-alpha. *Am J Pathol* 146: 589–98.

Delvenne, P, Hubert, P, Jacobs, N, *et al.* (2001). The organotypic culture of HPV-transformed keratinocytes: an effective in vitro model for the development of new immunotherapeutic approaches for mucosal (pre)neoplastic lesions. *Vaccine* 19: 2557–64.

Demerjian, M, Choi, EH, Man, MQ, *et al.* (2009). Activators of PPARs and LXR decrease the adverse effects of exogenous glucocorticoids on the epidermis. *Exp Dermatol* 18: 643–9.

Desmoulière, A, Redard, M, Darby, I, *et al.* (1995). Apoptosis mediates the decrease in cellularity during the transition between granulation tissue and scar. *Am J Pathol* 146: 56–66.

Dhote, V, Bhatnagar, P, Mishra, PK, *et al.* (2012). Iontophoresis: A potential emergence of a transdermal drug delivery system. *Sci Pharm*.

Dickson, MA, Hahn, WC, Ino, Y, *et al.* (2000). Human keratinocytes that express hTERT and also bypass a p16(INK4a)-enforced mechanism that limits life span become immortal yet retain normal growth and differentiation characteristics. *Mol Cell Biol* 20: 1436–47.

Domozych, D (1999). Disruption of the Golgi apparatus and secretory mechanism in the desmid, Closterium acerosum by brefeldin A. *J Exp Bot* 50: 1323–30.

Dorsett-Martin, WA (2004). Rat models of skin wound healing: A review. *Wound*

Repair Regen.

Dowling, a, Clift, R, Grobert, N, *et al.* (2004). Nanoscience and nanotechnologies : opportunities and uncertainties. *London R Soc R Acad Eng Rep* 46: 618–618.

van Drongelen, V, Danso, MO, Mulder, A, *et al.* (2014). Barrier properties of an N/TERT-based human skin equivalent. *Tissue Eng Part A* 20: 3041–9.

Duval, C, Chagnoleau, C, Pouradier, F, *et al.* (2012). Human Skin Model Containing Melanocytes: Essential Role of Keratinocyte Growth Factor for Constitutive Pigmentation—Functional Response to α-Melanocyte Stimulating Hormone and Forskolin. *Tissue Eng Part C Methods* 18.

Eckl, K, Alef, T, Torres, S, *et al.* (2011). Full-thickness human skin models for congenital ichthyosis and related keratinization disorders. *J Invest Dermatol* 131: 1938–42.

Eckl, K, Weindl, G, Ackermann, K, *et al.* (2014). Increased cutaneous absorption reflects impaired barrier function of reconstructed skin models mimicking keratinisation disorders. *Exp Dermatol* 23: 286–8.

Edwards, R, Harding, K (2004). Bacteria and Wound Healing. *Curr Opin Infect Dis* 17: 91–5.

Eichner, R, Sun, T, Aebi, U (1986). The Role of keratin subfamilies and keratin pairs in the formation of Human Epidermal Intermediate Filaments. *J Cell Biol* 102: 1767–77.

Elias, P, Choi, E (2005). Interactions among stratum corneum defensive functions. *Exp Dermatol* 14: 719–26.

Ellis, A, Field, J, Field, E, *et al.* (1994). Tylosis associated with carcinoma of the oesophagus and oral leukoplakia in a large Liverpool family--a review of six generations. *Eur J Cancer B Oral Oncol* 30B: 102–12.

Ellis, A, Risk, JM, Maruthappu, T, *et al.* (2015). Tylosis with oesophageal cancer: Diagnosis, management and molecular mechanisms. *Orphanet J Rare Dis* 10: 126.

Elsholz, F, Harteneck, C, Muller, W, *et al.* (2014). Calcium - A central regulator of keratinocyte differentiation in health and disease. *Eur J Dermatology* 24: 650–61.

Engelbrecht, TN, Demé, B, Dobner, B, *et al.* (2012). Study of the influence of the

penetration enhancer isopropyl myristate on the nanostructure of stratum corneum lipid model membranes using neutron diffraction and deuterium labelling. *Skin Pharmacol Physiol* 25: 200–7.

Engelhart, K, El Hindi, T, Biesalski, HK, *et al.* (2005). In vitro reproduction of clinical hallmarks of eczematous dermatitis in organotypic skin models. *Arch Dermatol Res* 297: 1–9.

Eskelinen, E-L (2006). Roles of LAMP-1 and LAMP-2 in lysosome biogenesis and autophagy. *Mol Aspects Med* 27: 495–502.

Estrach, S, Cordes, R, Hozumi, K, *et al.* (2008). Role of the Notch Ligand Delta1 in Embryonic and Adult Mouse Epidermis. *J Invest Dermatol* 128: 825–32.

Falke, LL, van Vuuren, SH, Kazazi-Hyseni, F, *et al.* (2015). Local therapeutic efficacy with reduced systemic side effects by rapamycin-loaded subcapsular microspheres. *Biomaterials* 42: 151–60.

Fang, C-L, Aljuffali, IA, Li, Y-C, *et al.* (2014). Delivery and targeting of nanoparticles into hair follicles. *Ther Deliv* 5: 991–1006.

Feely, MA, Smith, BL, Weinberg, JM (2015). Novel psoriasis therapies and patient outcomes, part 1: topical treatments. *Cutis* 95: 282–90.

Feingold, K (2012). Lamellar bodies: the key to cutaneous barrier function. *J Invest Dermatol* 132: 1951–3.

Feingold, K, Elias, P (2014). Role of lipids in the formation and maintenance of the cutaneous permeability barrier. *Biochim Biophys Acta* 1841: 280–94.

Feingold, KR, Jiang, YJ (2011). The mechanisms by which lipids coordinately regulate the formation of the protein and lipid domains of the stratum corneum: Role of fatty acids, oxysterols, cholesterol sulfate and ceramides as signaling molecules. *Dermatoendocrinol*.

Ferguson, MWJ, O'Kane, S, O 'kane, S (2004). Scar-free healing: from embryonic mechanisms to adult therapeutic intervention. *Phil Trans R Soc Lond B* 359: 839–50.

Flaten, GEGE, Palac, Z, Engesland, AA, *et al.* (2015). In vitro skin models as a tool in optimization of drug formulation. *Eur J Pharm Sci* 75: 10–24.

Forrester, AR, Elias, MS, Woodward, EL, *et al.* (2014). Induction of a chloracne phenotype in an epidermal equivalent model by 2,3,7,8-tetrachlorodibenzo-p-

dioxin (TCDD) is dependent on aryl hydrocarbon receptor activation and is not reproduced by aryl hydrocarbon receptor knock down. *J Dermatol Sci* 73: 10–22.

Frankart, A, Malaisse, J, De Vuyst, E, *et al.* (2012). Epidermal morphogenesis during progressive in vitro 3D reconstruction at the air-liquid interface. *Exp Dermatol* 21: 871–5.

Freinkel, R, Woodley, D (2001). *The Biology of the Skin*. 1st edn. CRC Press.

Fröhlich, E (2012). The role of surface charge in cellular uptake and cytotoxicity of medical nanoparticles. *Int J Nanomedicine* 7: 5577–91.

Fuchs, E (1990). Mini-Review Epidermal Differentiation : The Bare Essentials. *J Cell Biol* 111: 2807–14.

Fuchs, E (2008). Skin stem cells: Rising to the surface. *J Cell Biol* 180: 273–84.

Fuchs, E, Cleveland, DW (1998). A structural scaffolding of intermediate filaments in health and disease. *Science (80-)* 279: 514–9.

Gabbanini, S, Lucchi, E, Carli, M, *et al.* (2009). In vitro evaluation of the permeation through reconstructed human epidermis of essentials oils from cosmetic formulations. *J Pharm Biomed Anal* 50: 370–6.

Gaj, T, Gersbach, C, Barbas, C (2013). ZFN, TALEN, and CRISPR/Cas-based methods for genome engineering. *Trends Biotech* 31: 397–405.

Galiano, RD, Tepper, OM, Pelo, CR, *et al.* (2004). Topical vascular endothelial growth factor accelerates diabetic wound healing through increased angiogenesis and by mobilizing and recruiting bone marrow-derived cells. *Am J Pathol* 164: 1935–47.

Gallucci, RM, Simeonova, PP, Matheson, JM, *et al.* (2000). Impaired cutaneous wound healing in interleukin-6-deficient and immunosuppressed mice. *FASEB J* 14: 2525–31.

El Ghalbzouri, A, Hensbergen, P, Gibbs, S, *et al.* (2004). Fibroblasts facilitate re-epithelialization in wounded human skin equivalents. *Lab Invest* 84: 102–12.

Gillet, A, Compère, P, Lecomte, F, *et al.* (2011). Liposome surface charge influence on skin penetration behaviour. *Int J Pharm* 411: 223–31.

GODIN, B, TOUITOU, E (2007). Transdermal skin delivery: Predictions for humans from in vivo, ex vivo and animal models☆. *Adv Drug Deliv Rev* 59: 1152–61.

Gollnick, HPM (1996). Oral retinoids - Efficacy and toxicity in psoriasis. *Br J Dermatology, Suppl* 135: 6–17.

Gonzalez-Gonzalez, E, Speaker, T, Hickerson, R, *et al.* (2010). Silencing of reporter gene expression in skin using siRNAs and expression of plasmid DNA delivered by a soluble protrusion array device (PAD). *Mol Ther* 18: 1667–74.

Götz, C, Pfeiffer, R, Tigges, J, *et al.* (2012a). Xenobiotic metabolism capacities of human skin in comparison with a 3D-epidermis model and keratinocyte-based cell culture as in vitro alternatives for chemical testing: phase II enzymes. *Exp Dermatol* 21: 364–9.

Götz, C, Pfeiffer, R, Tigges, J, *et al.* (2012b). Xenobiotic metabolism capacities of human skin in comparison with a 3D epidermis model and keratinocyte-based cell culture as in vitro alternatives for chemical testing: activating enzymes (Phase I). *Exp Dermatol* 21: 358–63.

Gratton, SEA, Ropp, PA, Pohlhaus, PD, *et al.* (2008). The effect of particle design on cellular internalization pathways. *Proc Natl Acad Sci* 105: 11613–8.

Groeber, F, Holeiter, M, Hampel, M, *et al.* (2011). Skin tissue engineering--in vivo and in vitro applications. *Adv Drug Deliv Rev* 63: 352–66.

Gschwandtner, M, Mildner, M, Mlitz, V, *et al.* (2013). Histamine suppresses epidermal keratinocyte differentiation and impairs skin barrier function in a human skin model. *Allergy* 68: 37–47.

Guo, S, Dipietro, LA (2010). Factors affecting wound healing. *J Dent Res* 89: 219–29.

Gurtner, G, Werner, S, Barrandon, Y, *et al.* (2008). Wound repair and regeneration. *Nature* 453: 314–21.

Haisma, EM, De Breij, A, Chan, H, *et al.* (2014). LL-37-derived peptides eradicate multidrug-resistant Staphylococcus aureus from thermally wounded human skin equivalents. *Antimicrob Agents Chemother* 58: 4411–9.

Häkkinen, L, Larjava, H, Koivisto, L (2011). Granulation tissue formation and remodeling. *Endod Top* 24: 94–129.

Halata, Z, Grim, M, Bauman, KI (2003). Friedrich Sigmund Merkel and his “Merkel cell”, morphology, development, and physiology: review and new results. *Anat Rec A Discov Mol Cell Evol Biol* 271: 225–39.

Harding, J, Burtness, B (2005). Cetuximab: An epidermal growth factor receptor

chimeric human-murine monoclonal antibody. *Drugs of Today*.

Harush-Frenkel, O, Debotton, N, Benita, S, *et al.* (2007). Targeting of nanoparticles to the clathrin-mediated endocytic pathway. *Biochem Biophys Res Commun* 353: 26–32.

Hickerson, RP, Leake, D, Pho, LN, *et al.* (2009). Rapamycin selectively inhibits expression of an inducible keratin (K6a) in human keratinocytes and improves symptoms in pachyonychia congenita patients. *J Dermatol Sci* 56: 82–8.

Hill, DS, Robinson, NDP, Caley, MP, *et al.* (2015). A Novel Fully Humanized 3D Skin Equivalent to Model Early Melanoma Invasion. *Mol Cancer Ther* 14: 2665–73.

Hitomi, K (2005). Transglutaminases in skin epidermis. *Eur J Dermatology*.

Hogan, NC, Taberner, AJ, Jones, LA, *et al.* (2015). Needle-free delivery of macromolecules through the skin using controllable jet injectors. *Expert Opin Drug Deliv* 5247: 1–12.

Hovnanian, A (2005). Harlequin ichthyosis unmasked: a defect of lipid transport. *J Clin Invest* 115.

Hu, J, Van den Steen, PE, Sang, Q-XA, *et al.* (2007). Matrix metalloproteinase inhibitors as therapy for inflammatory and vascular diseases. *Nat Rev Drug Discov* 6: 480–98.

Huang, F, Khvorova, A, Marshall, W, *et al.* (2004). Analysis of clathrin-mediated endocytosis of epidermal growth factor receptor by RNA interference. *J Biol Chem* 279: 16657–61.

Huang, S, Lu, G, Wu, Y, *et al.* (2012). Mesenchymal stem cells delivered in a microsphere-based engineered skin contribute to cutaneous wound healing and sweat gland repair. *J Dermatol Sci* 66: 29–36.

Huang, S, Xu, Y, Wu, C, *et al.* (2010). In vitro constitution and in vivo implantation of engineered skin constructs with sweat glands. *Biomaterials* 31: 5520–5.

Iliev, D, Hinnen, U, Elsner, P (1997). Skin roughness is negatively correlated to irritation with DMSO, but not with NaOH and SLS. *Exp Dermatol* 6: 157–60.

Irvine, AD, Mclean, WHI (1999). Human keratin diseases: the increasing spectrum of disease and subtlety of the phenotype-genotype correlation. *Br J Dermatol* 140: 815–28.

Ishida-Yamamoto, A, Kishibe, M (2011). Involvement of corneodesmosome

degradation and lamellar granule transportation in the desquamation process. *Med Mol Morphol* 44: 1–6.

Ishida-Yamamoto, A, Simon, M, Kishibe, M, *et al.* (2004). Epidermal lamellar granules transport different cargoes as distinct aggregates. *J Invest Dermatol* 122: 1137–44.

Ita, K (2016). Perspectives on transdermal electroporation. *Pharmaceutics* 8.

Itoh, M, Kiuru, M, Cairo, MS, *et al.* (2011). Generation of keratinocytes from normal and recessive dystrophic epidermolysis bullosa-induced pluripotent stem cells. *Proc Natl Acad Sci U S A* 108: 8797–802.

Itoh, M, Umegaki-Arao, N, Guo, Z, *et al.* (2013). Generation of 3D Skin Equivalents Fully Reconstituted from Human Induced Pluripotent Stem Cells (iPSCs). *PLoS One* 8.

Jakubovic, H, Ackerman, A (1992). Structure and Function of Skin: Development, Morphology and Physiology. *Dermatology* 3: 3–79.

Jannasch, M, Groeber, F, Brattig, NW, *et al.* (2015). Development and application of three-dimensional skin equivalents for the investigation of percutaneous worm invasion. *Exp Parasitol* 150: 22–30.

Jansen, JA (2004). Special Issue: *Biomaterials* 25: 1461.

Jean, J, Lapointe, M, Soucy, J, *et al.* (2009). Development of an in vitro psoriatic skin model by tissue engineering. *J Dermatol Sci* 53: 19–25.

Jepps, OG, Dancik, Y, Anissimov, YG, *et al.* (2013). Modeling the human skin barrier--towards a better understanding of dermal absorption. *Adv Drug Deliv Rev* 65: 152–68.

Jiang, CK, Magnaldo, T, Ohtsuki, M, *et al.* (1993). Epidermal growth factor and transforming growth factor alpha specifically induce the activation- and hyperproliferation-associated keratins 6 and 16. *Proc Natl Acad Sci U S A* 90: 6786–90.

Jiang, SJ, Zhou, XJ (2003). Examination of the mechanism of oleic acid-induced percutaneous penetration enhancement: an ultrastructural study. *Biol Pharm Bull* 26: 66–8.

Jiang, X, Musyanovych, A, Röcker, C, *et al.* (2011). Specific effects of surface carboxyl groups on anionic polystyrene particles in their interactions with

mesenchymal stem cells. *Nanoscale* 3: 2028–35.

Jiang, X, Röcker, C, Hafner, M, *et al.* (2010). Endo- and exocytosis of zwitterionic quantum dot nanoparticles by live hela cells. *ACS Nano* 4: 6787–97.

Jiang, YJ, Lu, B, Kim, P, *et al.* (2006). Regulation of ABCA1 expression in human keratinocytes and murine epidermis. *J Lipid Res* 47: 2248–58.

Johansson, N, Ahonen, M, Kähäri, VM (2000). Matrix metalloproteinases in tumor invasion. *Cell Mol Life Sci*.

Kafshgari, MH, Harding, FJ, Voelcker, NH (2015). Insights into Cellular Uptake of Nanoparticles. *Curr Drug Deliv* 63–77.

Kalia, YN, Naik, A, Garrison, J, *et al.* (2004). Iontophoretic drug delivery. *Adv Drug Deliv Rev* 56: 619–58.

Karimi, M, Ghasemi, A, Sahandi Zangabad, P, *et al.* (2016). *Smart micro/nanoparticles in stimulus-responsive drug/gene delivery systems*. *Chem Soc Rev*. Royal Society of Chemistry.

Kelsell, D, Norgett, E, Unsworth, H, *et al.* (2005). Mutations in ABCA12 underlie the severe congenital skin disease harlequin ichthyosis. *Am J Hum Genet* 76: 794–803.

Kennedy, IM (2014). Nanotechnology and toxicology. *Rev Environ Health* 29: 101–3.

van de Kerkhof, PCM (2015). An Update on Topical Therapies for Mild-Moderate Psoriasis. *Dermatol Clin* 33: 73–7.

Kim, HS, Bernitz, JM, Lee, D-F, *et al.* (2014). Genomic editing tools to model human diseases with isogenic pluripotent stem cells. *Stem Cells Dev* 23: 2673–86.

Kirschner, N, Houdek, P, Fromm, M, *et al.* (2010). Tight junctions form a barrier in human epidermis. *Eur J Cell Biol* 89: 839–42.

Kligman, AM (1965). Topical Pharmacology and Toxicology of Dimethyl Sulfoxide. 1. *J Am Med Assoc* 193: 796–804.

Kolditz, F, Krausze, J, Heinz, D, *et al.* (2014). Wound healing potential of a dimeric InlB variant analyzed by in vitro experiments on re-epithelialization of human skin models. *Eur J Pharm Biopharm* 86: 277–83.

Krajewska, E, Lewis, C, Staton, C, *et al.* (2011). New insights into induction of early-stage neovascularization in an improved tissue-engineered model of psoriasis. *J Tissue Eng Regen Med* 5: 363–74.

Kralj, S, Rojnik, M, Romih, R, *et al.* (2012). Effect of surface charge on the cellular uptake of fluorescent magnetic nanoparticles. *J Nanoparticle Res* 14: 1151.

Krausz, AE, Adler, BL, Cabral, V, *et al.* (2015). Curcumin-encapsulated nanoparticles as innovative antimicrobial and wound healing agent. *Nanomedicine Nanotechnology, Biol Med* 11: 195–206.

Kretz, M, Euwens, C, Hombach, S, *et al.* (2003). Altered connexin expression and wound healing in the epidermis of connexin-deficient mice. *J Cell Sci* 116: 3443–52.

Kuroyanagi, M, Yamamoto, A, Shimizu, N, *et al.* (2014). Development of cultured dermal substitute composed of hyaluronic acid and collagen spongy sheet containing fibroblasts and epidermal growth factor. *J Biomater Sci Polym Ed* 25: 1133–43.

Lademann, J, Richter, H, Meinke, MC, *et al.* (2013). Drug delivery with topically applied nanoparticles: Science fiction or reality? *Skin Pharmacol Physiol* 26: 227–33.

Lademann, J, Richter, H, Teichmann, A, *et al.* (2007). Nanoparticles – An efficient carrier for drug delivery into the hair follicles. *Eur J Pharm Biopharm* 66: 159–64.

LAI, S, HIDA, K, MAN, S, *et al.* (2007). Privileged delivery of polymer nanoparticles to the perinuclear region of live cells via a non-clathrin, non-degradative pathway. *Biomaterials* 28: 2876–84.

Lamartine, J, Munhoz Essenfelder, G, Kibar, Z, *et al.* (2000). Mutations in GJB6 cause hidrotic ectodermal dysplasia. *Nat Genet* 26: 142–4.

Lane, ME (2013). Skin penetration enhancers. *Int J Pharm* 447: 12–21.

Langerhans, P (1868). Ueber die Nerven der menschlichen Haut. *Arch für Pathol Anat und Physiol und für Klin Med* 44: 325–37.

Larese Filon, F, Mauro, M, Adami, G, *et al.* (2015). Nanoparticles skin absorption: New aspects for a safety profile evaluation. *Regul Toxicol Pharmacol* 72: 310–22.

Larjava, H, Salo, T, Haapasalmi, K, *et al.* (1993). Expression of integrins and basement membrane components by wound keratinocytes. *J Clin Invest* 92: 1425–35.

Leachman, SA, Kaspar, RL, Fleckman, P, *et al.* (2005). Clinical and pathological features of pachyonychia congenita. *J Invest Dermatol* 10: 3–17.

Lechler, T, Fuchs, E (2005). Asymmetric cell divisions promote stratification and differentiation of mammalian skin. *Nature* 437: 275–80.

Lee, KM, Choi, KH, Ouellette, MM (2004). Use of exogenous hTERT to immortalize primary human cells. *Cytotechnology* 45: 33–8.

Lee, SH, Elias, PM, Proksch, E, *et al.* (1992). Calcium and Potassium Are Important Regulators of Barrier Homeostasis in Murine Epidermis. *J Clin Invest* 89: 530–8.

Leu, J-G, Chen, S-A, Chen, H-M, *et al.* (2012). The effects of gold nanoparticles in wound healing with antioxidant epigallocatechin gallate and α-lipoic acid. *Nanomedicine Nanotechnology, Biol Med* 8: 767–75.

Li, HL, Gee, P, Ishida, K, *et al.* (2016). Efficient genomic correction methods in human iPS cells using CRISPR-Cas9 system. *Methods*.

Li, Q, Morris, T, Guo, L, *et al.* (2004). A Syntaxin 1, G o, and N-Type Calcium Channel Complex at a Presynaptic Nerve Terminal: Analysis by Quantitative Immunocolocalization. *J Neurosci* 24: 4070–81.

Li, S, Sengers, BG, Oreffo, ROC, *et al.* (2015). Chondrogenic potential of human articular chondrocytes and skeletal stem cells: a comparative study. *J Biomater Appl* 29: 824–36.

Liang, C-C, Park, AY, Guan, J-L (2007). In vitro scratch assay: a convenient and inexpensive method for analysis of cell migration in vitro. *Nat Protoc* 2: 329–33.

Lieschke, GJ, Currie, PD (2007). Animal models of human disease: zebrafish swim into view. *Nat Rev Genet* 8: 353–67.

Lin, J, Zhang, H, Chen, Z, *et al.* (2010). Penetration of lipid membranes by gold nanoparticles: Insights into cellular uptake, cytotoxicity, and their relationship. *ACS Nano* 4: 5421–9.

Lindberg, K, Badylak, SF (2015). Porcine small intestinal submucosa (SIS): a bioscaffold supporting in vitro primary human epidermal cell differentiation and synthesis of basement membrane proteins. *Burns* 27: 254–66.

Linde, N, Gutschalk, CM, Hoffmann, C, *et al.* (2012). Integrating macrophages into organotypic co-cultures: a 3D in vitro model to study tumor-associated

macrophages. *PLoS One* 7: e40058.

Lindner, G, Horland, R, Wagner, I, *et al.* (2011). De novo formation and ultra-structural characterization of a fiber-producing human hair follicle equivalent in vitro. *J Biotechnol* 152: 108–12.

Liu, B, Zhang, J, Liao, J, *et al.* (2014). Aptamer-functionalized nanoparticles for drug delivery. *J Biomed Nanotechnol* 10: 3189–203.

Liu, FF, Peng, C, Escher, BI, *et al.* (2013). Hanging drop: An in vitro air toxic exposure model using human lung cells in 2D and 3D structures. *J Hazard Mater* 261: 701–10.

Liu, X, Ory, V, Chapman, S, *et al.* (2012). ROCK inhibitor and feeder cells induce the conditional reprogramming of epithelial cells. *Am J Pathol* 180: 599–607.

Lotte, C, Patouillet, C, Zanini, M, *et al.* (2002). Permeation and skin absorption: reproducibility of various industrial reconstructed human skin models. *Ski Pharmacol Appl Ski Physiol* 15 Suppl 1: 18–30.

Luengo, J, Weiss, B, Schneider, M, *et al.* (2006). Influence of nanoencapsulation on human skin transport of flufenamic acid. *Skin Pharmacol Physiol* 19: 190–7.

Lutolf, MP, Hubbell, JA (2005). Synthetic biomaterials as instructive extracellular microenvironments for morphogenesis in tissue engineering. *Nat Biotechnol* 23: 47–55.

Maitra, A, Arking, DE, Shivapurkar, N, *et al.* (2005). Genomic alterations in cultured human embryonic stem cells. *Nat Genet* 37: 1099–103.

Man, YKS, Trolove, C, Tattersall, D, *et al.* (2007). A deafness-associated mutant human connexin 26 improves the epithelial barrier in vitro. *J Membr Biol* 218: 29–37.

Manders, EMM, Stap, J, Brakenhoff, GJ, *et al.* (1992). Dynamics of three-dimensional replication patterns during the S-phase, analysed by double labelling of DNA and confocal microscopy. *J Cell Sci* 103 (Pt 3: 857–62.

Manders, EMM, Verbeek, FJ, Ate, JA (1993). Measurement of co-localisation of objects in dual-colour confocal images. *J Microsc*.

Maney, SK, McIlwain, DR, Polz, R, *et al.* (2015). Deletions in the cytoplasmic domain of iRhom1 and iRhom2 promote shedding of the TNF receptor by the protease ADAM17. *Sci Signal* 8: ra109.

Margadant, C, Charafeddine, R, Sonnenberg, A (2010). Unique and redundant functions of integrins in the epidermis. *FASEB J* 24: 4133–52.

Maricich, SM, Wellnitz, SA, Nelson, AM, *et al.* (2009). Merkel cells are essential for light-touch responses. *Science (80-)* 324: 1580–2.

Marquis, BJ, Love, SA, Braun, KL, *et al.* (2009). Analytical methods to assess nanoparticle toxicity. *Analyst* 134: 425–39.

Marren, K (2011). Dimethyl sulfoxide: an effective penetration enhancer for topical administration of NSAIDs. *Phys Sport* 39: 75–82.

Marthaler, AG, Tubsuwan, A, Schmid, B, *et al.* (2016). Generation of an isogenic, gene-corrected control cell line of the spinocerebellar ataxia type 2 patient-derived iPSC line H266. *Stem Cell Res* 16: 202–5.

Martignoni, M, Groothuis, G, de Kanter, R (2006). Species differences between mouse, rat, dog, monkey and human CYP-mediated drug metabolism, inhibition and induction. *Exp Opin Drug Metab Toxicol* 2: 875–94.

Martin, P, Leibovich, SJ (2005). Inflammatory cells during wound repair: The good, the bad and the ugly. *Trends Cell Biol*.

Maruthappu, T, Chikh, A, Fell, B, *et al.* (2016). iRHOM2 Regulates Keratin 16, a Major Cytoskeletal Stress Keratin. *Nat Commun* in Revisio.

Mathes, SH, Ruffner, H, Graf-Hausner, U (2014). The use of skin models in drug development. *Adv Drug Deliv Rev* 69–70: 81–102.

Matoušková, E, Mestak, O (2014). The effect of different biologic and biosynthetic wound covers on keratinocyte growth, stratification and differentiation in vitro. *J Tissue Eng* 5: 2041731414554966.

McKay, I a, Leigh, IM (1991). Epidermal cytokines and their roles in cutaneous wound healing. *Br J Dermatol* 124: 513–8.

McLean, WH, Rugg, EL, Lunny, DP, *et al.* (1995). Keratin 16 and keratin 17 mutations cause pachyonychia congenita. *Nat Genet* 9: 273–8.

Mcmillan, JR, Haftek, M, Akiyama, M, *et al.* (2003). Alterations in Desmosome Size and Number Coincide with the Loss of Keratinocyte Cohesion in Skin with Homozygous and Heterozygous Defects in the Desmosomal Protein Plakophilin 1. *J Invest Dermatol* 121: 96–103.

McMullan, R, Lax, S, Robertson, VH, *et al.* (2003). *Keratinocyte Differentiation Is*

Regulated by the Rho and ROCK Signaling Pathway. *Curr Biol*.

Menon, GK, Elias, PM, Lee, SH, *et al.* (1992). Localization of calcium in murine epidermis following disruption and repair of the permeability barrier. *Cell Tissue Res* 270: 503–12.

Micallef, L, Belaubre, F, Pinon, A, *et al.* (2009). Effects of extracellular calcium on the growth-differentiation switch in immortalized keratinocyte HaCaT cells compared with normal human keratinocytes. *Exp Dermatol* 18: 143–51.

Michel, M, L'Heureux, N, Pouliot, R, *et al.* (1999). Characterization of a new tissue-engineered human skin equivalent with hair. *In Vitro Cell Dev Biol Anim* 35: 318–26.

Mildner, M, Ballaun, C, Stichenwirth, M, *et al.* (2006). Gene silencing in a human organotypic skin model. *Biochem Biophys Res Comm* 348: 76–82.

Mildner, M, Jin, J, Eckhart, L, *et al.* (2010). Knockdown of filaggrin impairs diffusion barrier function and increases UV sensitivity in a human skin model. *J Invest Dermatol* 130: 2286–94.

Misra, SK, Mohn, D, Brunner, TJ, *et al.* (2008). Comparison of nanoscale and microscale bioactive glass on the properties of P(3HB)/Bioglass® composites. *Biomaterials* 29: 1750–61.

Molina, M, Giulbudagian, M, Calder??n, M (2014). Positively charged thermoresponsive nanogels for anticancer drug delivery. *Macromol Chem Phys* 215: 2414–9.

Montagna, W (2012). *The Structure and Function of Skin*. 3rd edn. Elsevier.

Nanayakkara, G, Bartlett, A, Forbes, B, *et al.* (2005). The effect of unsaturated fatty acids in benzyl alcohol on the percutaneous permeation of three model penetrants. *Int J Pharm* 301: 129–39.

Nanney, LB, King, LE (1988). Epidermal Growth Factor and Transforming Growth Factor-α. *In*: *Mol. Cell. Biol. Wound Repair*. Springer US: Boston, MA, 171–94.

Nel, A, Xia, T, Mädler, L, *et al.* (2006). Toxic potential of materials at the nanolevel. *Science* 311: 622–7.

Nguyen, BC, Lefort, K, Mandinova, A, *et al.* (2006). Cross-regulation between Notch and p63 in keratinocyte commitment to differentiation. *Genes Dev* 20: 1028–42.

Nguyen, T, Zuniga, R (2013). Skin conditions: new drugs for managing skin disorders. *FP Essent* 407: 11–6.

Nicholas, MN, Jeschke, MG, Amini-Nik, S (2016). Methodologies in creating skin substitutes. *Cell Mol Life Sci* Online.

Nissan, X, Larribere, L, Saidani, M, *et al.* (2011). Functional melanocytes derived from human pluripotent stem cells engraft into pluristratified epidermis. *Proc Natl Acad Sci* 108: 17856–17856.

Nordgren, A (2004). Moral imagination in tissue engineering research on animal models. *Biomaterials* 25: 1723–34.

Norgett, EE, Hatsell, SJ, Carvajal-Huerta, L, *et al.* (2000). Recessive mutation in desmoplakin disrupts desmoplakin-intermediate filament interactions and causes dilated cardiomyopathy, woolly hair and keratoderma. *Hum Mol Genet* 9: 2761–6.

Orgill, D, Blanco, C (2009). *Biomaterials for Treating Skin Loss*. 1st edn. Elsevier.

Ouvrier, A, Cadet, R, Vernet, P, *et al.* (2009). LXR and ABCA1 control cholesterol homeostasis in the proximal mouse epididymis in a cell-specific manner. *J Lipid Res* 50: 1766–75.

Ouwehand, K, Spiekstra, SW, Waaijman, T, *et al.* (2012). CCL5 and CCL20 mediate immigration of Langerhans cells into the epidermis of full thickness human skin equivalents. *Eur J Cell Biol* 91: 765–73.

Padmanabhan, P, Kumar, A, Kumar, S, *et al.* (2016). Nanoparticles in Practice for Molecular-Imaging Applications: An Overview. *Acta Biomater* 41: 1–16.

Paladini, RD, Takahashi, K, Bravo, NS, *et al.* (1996). Onset of re-epithelialization after skin injury correlates with a reorganization of keratin filaments in wound edge keratinocytes: defining a potential role for keratin 16. *J Cell Biol* 132: 381–97.

Palma, SD, Maletto, B, Lo Nostro, P, *et al.* (2006). Potential use of ascorbic acid-based surfactants as skin penetration enhancers. *Drug Dev Ind Pharm* 32: 821–7.

Pappinen, S, Pryazhnikov, E, Khiroug, L, *et al.* (2012). Organotypic cell cultures and two-photon imaging: tools for in vitro and in vivo assessment of percutaneous drug delivery and skin toxicity. *J Control Release* 161: 656–67.

Paquet, D, Kwart, D, Chen, A, *et al.* (2016). Efficient introduction of specific homozygous and heterozygous mutations using CRISPR/Cas9. *Nature* 533: 1–18.

Park, D, Park, H, Seo, J, *et al.* (2014). Sonophoresis in transdermal drug deliverys. *Ultrasonics*.

Paulsson, M (1992). Basement membrane proteins: structure, assembly, and cellular interactions. *Crit Rev Biochem Mol Biol* 27: 93–127.

Pendaries, V, Malaisse, J, Pellerin, L, *et al.* (2014). Knockdown of Filaggrin in a Three-Dimensional Reconstructed Human Epidermis Impairs Keratinocyte Differentiation. *J Invest Dermatol*.

Petrova, A, Celli, A, Jacquet, L, *et al.* (2014). 3D In Vitro Model of a Functional Epidermal Permeability Barrier from Human Embryonic Stem Cells and Induced Pluripotent Stem Cells. *Stem Cell Reports* 2: 675–89.

Phillips, L, Steinberg, M, Maibach, HI, *et al.* (1972). A comparison of rabbit and human skin response to certain irritants. *Toxicol Appl Pharmacol* 21: 369–82.

Pickard, A, McDade, SS, McFarland, M, *et al.* (2015). HPV16 Down-Regulates the Insulin-Like Growth Factor Binding Protein 2 to Promote Epithelial Invasion in Organotypic Cultures. *PLOS Pathog* 11: e1004988.

Pilcher, BK, Dumin, JA, Sudbeck, BD, *et al.* (1997). The activity of collagenase-1 is required for keratinocyte migration on a type I collagen matrix. *J Cell Biol* 137: 1445–57.

Platt, RJ, Chen, S, Zhou, Y, *et al.* (2014). CRISPR-Cas9 Knockin Mice for Genome Editing and Cancer Modeling. *Cell* 159: 440–55.

Ponec, M (2002). Skin constructs for replacement of skin tissues for in vitro testing. *Adv Drug Deliv Rev* 54: S19-30.

Popov, L, Kovalski, J, Grandi, G, *et al.* (2014). Three-dimensional human skin models to understand Staphylococcus aureus skin colonization and infection. *Front Immunol* 5: 41.

Pouillot, A, Dayan, N, Polla, A, *et al.* (2008). The stratum corneum : a double paradox. *J Cosmet Dermatol* 7: 143–8.

Poumay, Y, Coquette, A (2007). Modelling the human epidermis in vitro: tools for basic and applied research. *Arch Dermatol Rev* 298: 361–9.

Prausnitz, M, Langer, R (2008). Transdermal drug delivery. *Nat Biotech* 26: 1261–8.

Prausnitz, M, Mitragotri, S, Langer, R (2004). Current Status and Future Potential of Transdermal Drug Delivery. *Nat Rev Drug Discov* 3: 115–24.

Prausnitz, MR (2004). Microneedles for transdermal drug delivery. *Adv Drug Deliv Rev* 56: 581–7.

Proksch, E, Brandner, J, Jensen, J (2008). The skin: an indispensable barrier. *Exp Dermatol* 17: 1063–72.

Prow, T, Grice, J, Lin, L, *et al.* (2011). Nanoparticles and microparticles for skin drug delivery. *Adv Drug Deliv Rev* 63: 470–91.

Pulkkinen, L, Christiano, AM, Airenne, T, *et al.* (1994). Mutations in the gamma 2 chain gene (LAMC2) of kalinin/laminin 5 in the junctional forms of epidermolysis bullosa. *Nat Genet* 6: 293–7.

Rajpopat, S, Moss, C, Mellerio, J, *et al.* (2011). Harlequin ichthyosis: a review of clinical and molecular findings in 45 cases. *Arch Dermatol* 147: 681–6.

Rammler, D (1967). Biological Implications of Dmso Based on a Review of Its Chemical Properties*. *Ann New York Acad* 141: 13–23.

Rampersad, SN (2012). Multiple applications of alamar blue as an indicator of metabolic function and cellular health in cell viability bioassays. *Sensors (Switzerland)* 12: 12347–60.

Raphael, AP, Wright, ORL, Benson, HA, *et al.* (2015). Recent advances in physical delivery enhancement of topical drugs. *Curr Pharm Des* 21: 2830–47.

Reijnders, CMA, van Lier, A, Roffel, S, *et al.* (2015). Development of a Full-Thickness Human Skin Equivalent In Vitro Model Derived from TERT-Immortalized Keratinocytes and Fibroblasts. *Tissue Eng Part A* 21: 2448–59.

Rejman, J, Oberle, V, Zuhorn, IS, *et al.* (2004). Size-dependent internalization of particles via the pathways of clathrin- and caveolae-mediated endocytosis. *Biochem J* 377: 159–69.

Rennekampff, HO, Hansbrough, JF, Kiessig, V, *et al.* (2000). Bioactive interleukin-8 is expressed in wounds and enhances wound healing. *J Surg Res* 93: 41–54.

Richard, G, Rouan, F, Willoughby, CE, *et al.* (2002). Report Missense Mutations in GJB2 Encoding Connexin-26 Cause the Ectodermal Dysplasia Keratitis-Ichthyosis-Deafness Syndrome. *Am J Hum Genet* 70: 1341–8.

Rigo, C, Ferroni, L, Tocco, I, *et al.* (2013). Active silver nanoparticles for wound healing. *Int J Mol Sci* 14: 4817–40.

Van Rijt, SH, Bein, T, Meiners, S (2014). Medical nanoparticles for next generation drug delivery to the lungs. *Eur Respir J*.

Rimann, M, Graf-Hausner, U (2012). Synthetic 3D multicellular systems for drug development. *Curr Opion Biotech* 23: 803–9.

Roberts, MS, Walters, KA (2008). *Dermal absorption and toxicity assessment*. *Drugs Pharm Sci*. 2nd edn. CRC Press.

Robin, JD, Wright, WE, Zou, Y, *et al.* (2015). Isolation and immortalization of patient-derived cell lines from muscle biopsy for disease modeling. *J Vis Exp* 52307.

Robles, DT, Berg, D (2007). Abnormal wound healing: keloids. *Clin Dermatol* 25: 26–32.

Rodriguez, LG, Wu, X, Guan, J-L (2005). Wound-healing assay. *Methods Mol Biol* 294: 23–9.

Rossant, J, McKerlie, C (2001). Mouse-based phenogenomics for modelling human disease. *Trends Mol Med* 7: 502–7.

Rudramurthy, GR, Swamy, MK, Sinniah, UR, *et al.* (2016). Nanoparticles: Alternatives Against Drug-Resistant Pathogenic Microbes. *Molecules* 21: 836.

Russell, LJ, DiGiovanna, JJ, Rogers, GR, *et al.* (1995). Mutations in the gene for transglutaminase 1 in autosomal recessive lamellar ichthyosis. *Nat Genet* 9: 279–83.

Safer, JD, Crawford, TM, Holick, MF (2004). A Role for Thyroid Hormone in Wound Healing through Keratin Gene Expression. *Endocrinology* 145: 2357–61.

Safferling, K, Sütterlin, T, Westphal, K, *et al.* (2013). Wound healing revised: a novel reepithelialization mechanism revealed by in vitro and in silico models. *J Cell Biol* 203: 691–709.

Sahay, G, Alakhova, DY, Kabanov, A V (2010). Endocytosis of nanomedicines. *J Control Release*.

Sakhtianchi, R, Minchin, RF, Lee, K-B, *et al.* (2013). Exocytosis of nanoparticles from cells: Role in cellular retention and toxicity. *Adv Colloid Interface Sci* 201–202: 18–29.

Salmon, AB (2015). About-face on the metabolic side effects of rapamycin. *Oncotarget* 6: 2585–6.

Samah, NA, Williams, N, Heard, CM (2010). Nanogel particulates located within diffusion cell receptor phases following topical application demonstrates uptake into and migration across skin. *Int J Pharm* 401: 72–8.

Sand, BJ, Babich, M, Haghighi, AZ (2007). Transdermal drug delivery and topical compositions comprising at least two permeation enhancers, such as benzyl alcohol and lecithin for application on the skin. *PCT Int Appl*.

Santander-Ortega, MJ, Stauner, T, Loretz, B, *et al.* (2010). Nanoparticles made from novel starch derivatives for transdermal drug delivery. *J Control Release* 141: 85–92.

Sarpotdar, P p., Zatz, JL (1986). Percutaneous Absorption Enhancement by Nonionic Surfactants. *Drug Dev Ind Pharm* 12.

Sayes, C, Reed, K, Warheit, D (2007). Assessing Toxicity of Fine and Nanoparticles : Comparing In Vitro Measurements to In Vivo Pulmonary Toxicity Profiles. *Toxicol Sci* 97: 163–80.

Scales, BS, Huffnagle, GB (2013). The microbiome in wound repair and tissue fibrosis. *J Pathol* 229: 323–31.

Schaefer, H, Lademann, J (2001). The role of follicular penetration: A differential view. *Skin Pharmacol Appl Skin Physiol* 14: 23–7.

Schaller, M, Mailhammer, R, Korting, HC (2002). Cytokine expression induced by Candida albicans in a model of cutaneous candidosis based on reconstituted human epidermis. *J Med Microbiol* 51: 672–6.

Schechtman, LM (2002). Implementation of the 3Rs (refinement, reduction, and replacement): validation and regulatory acceptance considerations for alternative toxicological test methods. *ILAR J* 43 Suppl: S85-94.

Scheller, J, Chalaris, A, Garbers, C, *et al.* (2011). ADAM17: a molecular switch to control inflammation and tissue regeneration. *Trends Immunol* 32: 380–7.

Schmieder, S, Patel, P, Krishnamurthy, K (2015). Research Techniques Made Simple: Drug Delivery Techniques, Part 1: Concepts in Transepidermal Penetration and Absorption. *J Invest Dermatol* 135: 1–5.

Schmuth, M, Elias, PM, Hanley, K, *et al.* (2004a). The effect of LXR activators on AP-

1 proteins in keratinocytes. *J Invest Dermatol* 123: 41–8.

Schmuth, M, Haqq, CM, Cairns, WJ, *et al.* (2004b). Peroxisome proliferator-activated receptor (PPAR)-β/δ stimulates differentiation and lipid accumulation in keratinocytes. *J Invest Dermatol* 122: 971–83.

Schoop, V, Mirancea, N, Fusenig, N (1999). Epidermal Organisation and Differentiation of HaCaT Keratinocytes in Organotypic Coculture with Human Fibroblasts. *J Invest Dermatol* 12: 343–53.

Schurer, N, Kohne, A, Schliep, V, *et al.* (1993). Lipid composition and synthesis of HaCaT cells, an immortalized human keratinocyte line, in comparison with normal human adult keratinocytes. *Exp Dermatol* 2: 179–85.

Schwank, G, Koo, B-K, Sasselli, V, *et al.* (2013). *Functional Repair of CFTR by CRISPR/Cas9 in Intestinal Stem Cell Organoids of Cystic Fibrosis Patients*. *Cell Stem Cell*.

Scott, C, Rajpopat, S, Di, W (2013). Harlequin ichthyosis: ABCA12 mutations underlie defective lipid transport, reduced protease regulation and skin-barrier dysfunction. *Cell Tissue Res* 351: 281–8.

Senoo, M, Pinto, F, Crum, CP, *et al.* (2007). p63 Is Essential for the Proliferative Potential of Stem Cells in Stratified Epithelia. *Cell* 129: 523–36.

Shah, VP, Maibach, HI, Jenner, J (2014). Topical Drug Bioavailability, Bioequivalence and Penetration. *Springer Verlag* 402.

Shahrokhi, S, Arno, A, Jeschke, MG (2014). The use of dermal substitutes in burn surgery: Acute phase. *Wound Repair Regen*.

Sharma, R, Barakzai, SZ, Taylor, SE, *et al.* (2013). Epidermal-like architecture obtained from equine keratinocytes in three-dimensional cultures. *J Tissue Eng Regen Med* n/a-n/a.

Sherratt, J a, Murray, JD (1990). Models of epidermal wound healing. *Proc Biol Sci* 241: 29–36.

Shiraha, H, Gupta, K, Drabik, K, *et al.* (2000). Aging fibroblasts present reduced epidermal growth factor (EGF) responsiveness due to preferential loss of EGF receptors. *J Biol Chem* 275: 19343–51.

Shu, C, Zhou, H, Afsharvand, M, *et al.* (2011). Pharmacokinetic-pharmacodynamic modeling of apratastat: a population-based approach. *J Clin Pharmacol* 51:

472–81.

Simpson, C, Patel, D, Green, K (2011). Deconstructing the skin: cytoarchitectural determinants of epidermal morphogenesis. *Nat Rev Mol Cell Biol* 12: 565–80.

Simpson, RML, Wells, A, Thomas, D, *et al.* (2010). Aging fibroblasts resist phenotypic maturation because of impaired hyaluronan-dependent CD44/epidermal growth factor receptor signaling. *Am J Pathol* 176: 1215–28.

Singer, AJ, Clark, R a F (1999). Cutaneous Wound Healing. *N Engl J Med* 341: 738–46.

Singka, GSL, Samah, NA, Zulfakar, MH, *et al.* (2010). Enhanced topical delivery and anti-inflammatory activity of methotrexate from an activated nanogel. *Eur J Pharm Biopharm* 76: 275–81.

Sinico, C, Fadda, AM (2009). Vesicular carriers for dermal drug delivery. *Expert Opin Drug Deliv* 6: 813–25.

Skazik, C, Amann, P, Heise, R, *et al.* (2014). Downregulation of STRA6 expression in epidermal keratinocytes leads to hyperproliferation-associated differentiation in both in vitro and in vivo skin models. *J Invest Dermatol* 134: 1579–88.

Smijs, TGM, Bouwstra, JA (2010). Focus on skin as a possible port of entry for solid nanoparticles and the toxicological impact. *J Biomed Nanotechnol*.

Smith, FJD, Hansen, CD, Hull, PR, *et al.* (1993). Pachyonychia Congenita. *In*: *GeneReviews(®)*. University of Washington, Seattle.

Smith, I, Silveirinha, V, Stein, JL, *et al.* (2015). Human neural stem cell-derived cultures in three-dimensional substrates form spontaneously functional neuronal networks. *J Tissue Eng Regen Med* n/a-n/a.

Soldner, F, Jaenisch, R (2012). iPSC disease modeling. *Science (80-)* 338: 1155–6.

Srivastava, K, Pickard, A, McDade, S, *et al.* (2015). p63 drives invasion in keratinocytes expressing HPV16 E6/E7 genes through regulation of Src-FAK signalling. *Oncotarget*.

Staiano-Coico, L, Krueger, JG, Rubin, JS, *et al.* (1993). Human Keratinocyte Growth Factor Effects in a Porcine Model of Epidermal Wound Healing. *J Exp Med* 178.

Storey, A, Pim, D, Murray, A, *et al.* (1988). Comparison of the in vitro transforming activities of human papillomavirus types. *EMBO J* 7: 1815–20.

Stoughton, R, McClure, W (1983). Azone: a new non-toxic enhancer of cutaneous

penetration. *Drug Dev Ind Pharm* 9: 725–44.

Strachan, LR, Ghadially, R (2008). Tiers of clonal organization in the epidermis: the epidermal proliferation unit revisited. *Stem Cell Rev* 4: 149–57.

Strobel, C, Oehring, H, Herrmann, R, *et al.* (2015). Fate of cerium dioxide nanoparticles in endothelial cells: exocytosis. *J Nanoparticle Res* 17: 206.

Stücker, M, Struk, A, Altmeyer, P, *et al.* (2002). The cutaneous uptake of atmospheric oxygen contributes significantly to the oxygen supply of human dermis and epidermis. *J Physiol* 538: 985–94.

Sun, T, Jackson, S, Haycock, JW, *et al.* (2006). Culture of skin cells in 3D rather than 2D improves their ability to survive exposure to cytotoxic agents. *J Biotechnol* 122: 372–81.

Sun, T, Mai, S, Norton, D, *et al.* (2005). Self-Organization of Skin Cells in Three-Dimensional Electrospun Polystyrene Scaffolds. *Tissue Eng* 11: 1023–33.

Taylor, U, Klein, S, Petersen, S, *et al.* (2010). Nonendosomal cellular uptake of ligand-free, positively charged gold nanoparticles. *Cytom Part A* 77: 439–46.

Terrinoni, A, Smith, FJD, Didona, B, *et al.* (2001). Novel and Recurrent Mutations in the Genes Encoding Keratins K6a, K16 and K17 in 13 Cases of Pachyonychia Congenita. *J Invest Dermatol* 117: 1391–6.

Thabet, MM, Huizinga, TWJ (2006). Drug evaluation: Apratastat, a novel TACE/MMP inhibitor for rheumatoid arthritis. *Curr Opin Investig Drugs* 7: 1014–9.

Thakoersing, VS, Gooris, GS, Mulder, A, *et al.* (2012). Unraveling Barrier Properties of Three Different In-House Human Skin Equivalents. *Tissue Eng Part C Methods* 18: 1–11.

Thomas, A, Tattersall, D, Norgett, E, *et al.* (2009). Premature terminal differentiation and a reduction in specific proteases associated with loss of ABCA12 in Harlequin ichthyosis. *Am J Path* 174: 970–8.

Tiscornia, G, Vivas, EL, Belmonte, JCI (2011). Diseases in a dish: modeling human genetic disorders using induced pluripotent cells. *Nat Med* 17: 1570–6.

Tjabringa, G, Bergers, M, van Rens, D, *et al.* (2008). Development and validation of human psoriatic skin equivalents. *Am J Path* 173: 815–23.

Tokumoto, S, Higo, N, Sugibayashi, K (2006). Effect of electroporation and pH on the iontophoretic transdermal delivery of human insulin. *Int J Pharm* 326: 13–9.

Trommer, H, Neubert, RHH (2006). Overcoming the stratum corneum: the modulation of skin penetration. A review. *Skin Pharmacol Physiol* 19: 106–21.

Tsuji, J, Maynard, A, Howard, P, *et al.* (2006). Research Strategies for Safety Evaluation of Nanomaterials , Part IV : Risk Assessment of Nanoparticles. *Toxicol Sci* 89: 42–50.

Umegaki-arao, N, Pasmooij, AMG, Itoh, M, *et al.* (2014). Induced pluripotent stem cells from human revertant keratinocytes for the treatment of epidermolysis bullosa. *Sci Transl Med* 6.

Usui, ML, Mansbridge, JN, Carter, WG, *et al.* (2008). Keratinocyte migration, proliferation, and differentiation in chronic ulcers from patients with diabetes and normal wounds. *J Histochem Cytochem* 56: 687–96.

Vaughan, MB, Ramirez, RD, Brown, SA, *et al.* (2004). A reproducible laser-wounded skin equivalent model to study the effects of aging in vitro. *Rejuvenation Res* 7: 99–110.

van der Veer, WM, Bloemen, MCT, Ulrich, MMMMW, *et al.* (2009). Potential cellular and molecular causes of hypertrophic scar formation. *Burns* 35: 15–29.

Vellonen, K, Malinen, M, Mannermaa, E, *et al.* (2014). A Critical Assessment of In Vitro Tissue Models for ADME and Drug Delivery. *J Control Release* 190: 94–114.

Vincenzi, B, Zoccoli, A, Pantano, F, *et al.* (2010). Cetuximab: from bench to bedside. *Curr Cancer Drug Targets* 10: 80–95.

Wang, YN, Chang, WC (2003). Induction of Disease-associated Keratin 16 Gene Expression by Epidermal Growth Factor Is Regulated through Cooperation of Transcription Factors Sp1 and c-Jun. *J Biol Chem* 278: 45848–57.

Warren, EW, Khanderia, U (1989). Use of retinoids in the treatment of psoriasis. *Clin Pharm* 8: 344–51.

Watkinson, AC, Bunge, AL, Hadgraft, J, *et al.* (2013). Nanoparticles do not penetrate human skin - A theoretical perspective. *Pharm Res*.

Watt, F (1983). Involucrin and other markers of keratinocyte terminal differentiation. *J Invest Dermatol* 81: 100s–3s.

Wei, C, Liu, J, Yu, Z, *et al.* (2013). TALEN or Cas9 - rapid, efficient and specific choices for genome modifications. *J Genet Genom* 40: 281–9.

Werner, S, Krieg, T, Smola, H (2007). Keratinocyte-fibroblast interactions in wound healing. *J Invest Dermatol* 127: 998–1008.

Werner, S, Smola, H, Liao, X, *et al.* (1994). The function of KGF in morphogenesis of epithelium and reepithelialization of wounds. *Science* 266: 819–22.

Williams, AC, Barry, BW (2012). Penetration enhancers. *Adv Drug Deliv Rev* 64: 128–37.

Williams, S, Ratliff, L, Postiglione, M, *et al.* (2014). Par3-mInsc and Gαi3 cooperate to promote oriented epidermal cell divisions through LGN. *Nat Cell Biol* 16: 758–69.

Winchester, BG (2001). Lysosomal membrane proteins. *Eur J Paediatr Neurol* 5 Suppl A: 11–9.

Witte, MB, Barbul, A (2002). Role of nitric oxide in wound repair. *Am J Surg* 183: 406–12.

Witting, M, Molina, M, Obst, K, *et al.* (2015). Thermosensitive dendritic polyglycerol-based nanogels for cutaneous delivery of biomacromolecules. *Nanomedicine* 11: 1179–87.

Wojcik, SM, Bundman, DS, Roop, DR (2000). Delayed Wound Healing in Keratin 6a Knockout Mice. *Mol Cell Biol* 20: 5248–55.

Wong, TW (2014). Electrical, magnetic, photomechanical and cavitational waves to overcome skin barrier for transdermal drug delivery. *J Control Release*.

Xu, W, Jong Hong, S, Jia, S, *et al.* (2012). Application of a partial-thickness human ex vivo skin culture model in cutaneous wound healing study. *Lab Investig* 92: 584–99.

Yan, H, Tsujii, K (2005). Potential application of poly(N-isopropylacrylamide) gel containing polymeric micelles to drug delivery systems. *Colloids Surfaces B Biointerfaces* 46: 142–6.

Yanagi, T, Akiyama, M, Nishihara, H, *et al.* (2010). Self-improvement of keratinocyte differentiation defects during skin maturation in ABCA12-deficient harlequin ichthyosis model mice. *Am J Pathol* 177: 106–18.

Yang, Y, Sunoqrot, S, Stowell, C, *et al.* (2012). Effect of size, surface charge, and hydrophobicity of poly(amidoamine) dendrimers on their skin penetration. *Biomacromolecules* 13: 2154–62.

Zaki, NM, Nasti, A, Tirelli, N (2011). Nanocarriers for cytoplasmic delivery: cellular uptake and intracellular fate of chitosan and hyaluronic acid-coated chitosan nanoparticles in a phagocytic cell model. *Macromol Biosci* 11: 1747–60.

Zegers, MMP, Forget, MA, Chernoff, J, *et al.* (2003). Pak1 and PIX regulate contact inhibition during epithelial wound healing. *EMBO J* 22: 4155–65.

Zhang, P, Hu, C, Ran, W, *et al.* (2016). Recent Progress in Light-Triggered Nanotheranostics for Cancer Treatment. *Theranostics* 6: 948–68.

Van Zyl, L, Du Preez, J, Gerber, M, *et al.* (2016). Essential Fatty Acids as Transdermal Penetration Enhancers. *J Pharm Sci* 105: 188–93.